

Biomaterials Translational

CONTENTS Quarterly Established in December 2020. Volume 4, Issue 4 December 28, 2023

EDITORIAL

- 197 **Converging technologies in biomaterial translational research**
Long Bai, Jiacan Su

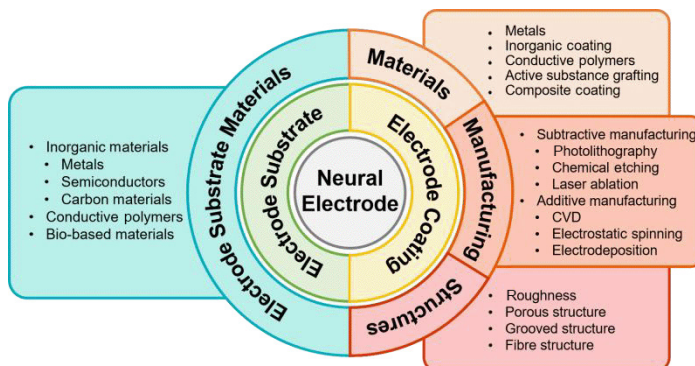
REVIEWS

- 199 **Organoid extracellular vesicle-based therapeutic strategies for bone therapy**
Han Liu, Jiacan Su



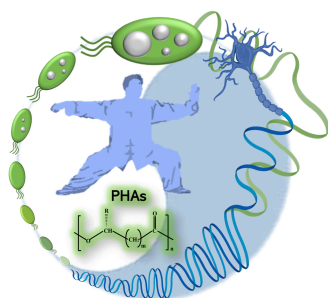
Organoid extracellular vesicles (OEVs) have emerging as promising cell-free nanocarriers for bone therapy due to their vigorous physiological effects, significant biological functions, stable loading capacity, and great biocompatibility.

- 213 **Advances in electrode interface materials and modification technologies for brain-computer interfaces**
Yunke Jiao, Miao Lei, Jianwei Zhu, Ronghang Chang, Xue Qu



This review provides a comprehensive materials-based overview of the last 5 years in neuroelectrode substrate materials and coating-modified materials for brain-computer interfaces, with additional emphasis on the importance of coating modification techniques and coating structure design.

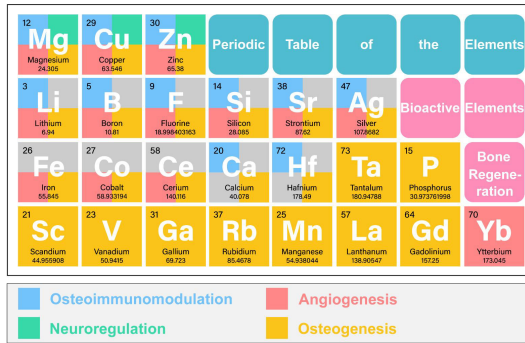
- 234 **Recent advances of medical polyhydroxyalkanoates in musculoskeletal system**
Chen-Hui Mi, Xin-Ya Qi, Yan-Wen Ding, Jing Zhou, Jin-Wei Dao, Dai-Xu Wei



This review reviews highlights the outstanding performance of polyhydroxyalkanoates (PHAs) as excellent biosynthetic materials, focusing on the role of PHAs and their composites in the musculoskeletal system in recent years. They not only contribute to the recovery and reconstruction of bone, joint, cartilage, blood vessel, etc., but also serve as drug carriers to assist in the recovery of related tissues. At the same time, the unique role of PHA degradation products is also elaborated.

248 Bioactive elements manipulate bone regeneration

Long Bai, Peiran Song, Jiacan Su

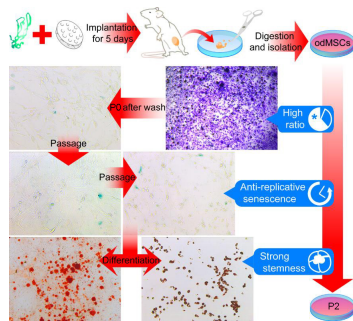


The significance of bioactive elements in bone repair is increasingly recognised. These elements play a pivotal role in promoting bone regeneration, offering innovative solutions for addressing bone-related injuries and diseases. This review meticulously delineates the impact of bioactive elements during various stages of bone regeneration, elucidating their mechanisms in osteoimmunomodulation, orchestrating neuroregulation, stimulating angiogenesis, and promoting osteogenesis, spotlight the therapeutic benefits and enhanced stability of elements such as magnesium, strontium, zinc, and silicon.

RESEARCH ARTICLES

270 Harvest of functional mesenchymal stem cells derived from *in vivo* osteo-organoids

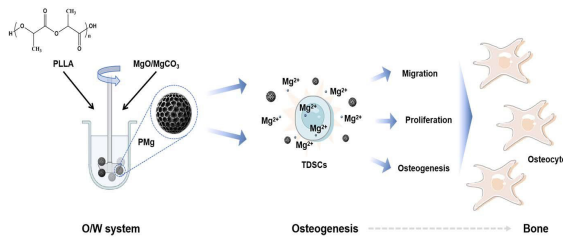
Shunshu Deng, Fuwei Zhu, Kai Dai, Jing Wang, Changsheng Liu



Recombinant human bone morphogenetic protein 2-loaded gelatin sponge scaffolds were used to construct *in vivo* osteo-organoids, and then osteo-organoid-derived mesenchymal stem cells (odMSCs) were isolated and cultured from passage 0 (P0) to passage 2 (P2). Owing to the highlights of odMSCs, this strategy can be translated into autologous stem cell transplantation protocols.

280 Fabrication of magnesium-doped porous polylactic acid microsphere for bone regeneration

Ziwei Tao, Ziyang Yuan, Dong Zhou, Lang Qin, Lan Xiao, Shihao Zhang, Changsheng Liu, Jinzhong Zhao, Yulin Li



Magnesium oxide (MgO)/magnesium carbonate (MgCO₃)-loaded polylactic acid porous microspheres (PMg) were prepared by solvent evaporation method, and the release of Mg²⁺ could promote the migration, proliferation, and osteogenesis of tendon-derived stem cells (TDSCs), thus PMg has potential prospects for osteogenic transformation.

COMMENTARIES

291 AI accelerated discovery of self-assembling peptides

Yejiao Shi, Honggang Hu

294 Early immunomodulation by magnesium ion: catalyst for superior osteogenesis

Bo Li

297 Comments on Innovative design of minimal invasive biodegradable poly(glycerol-dodecanoate) nucleus pulposus scaffold with function regeneration

Hao Zhou, Aimin Wu

Converging technologies in biomaterial translational research

Long Bai^{1,2,3}, Jiacan Su^{1,2,3,*}

In the realm of scientific innovation, the study of biomaterials emerges as a field of profound significance, bridging the gap between theoretical exploration and translational application.¹ The essence of biomaterial research lies not only in understanding the intricate relationships between biological systems and materials but more importantly, in the translational potential these materials hold.² The true value of this research unfolds in its application - from regenerative medicine to bioengineered solutions, where these materials become pivotal in addressing some of the most pressing clinical challenges. Meanwhile, the necessity for translating laboratory research into real-world applications has become increasingly urgent, as global ageing intensifies and public attention to health concerns grows.

With the rapid evolution of technology, a new paradigm in biomaterial research has emerged, characterised by the convergence of multiple disciplines.³ This multidisciplinary approach has broken the traditional boundaries of the field, a convergence of insights from nanotechnology, biotechnology, information technology, and cognitive science. This interdisciplinary convergence not only expands the horizon of biomaterial research, but also poses unique challenges and unprecedented opportunities, driving innovation on an unprecedented scale.

In this issue, we present a collection of papers from different fields of translational biomaterials research. There are four review articles: the first, by Han Liu and co-authors,⁴ discusses the therapeutic potential of organoid extracellular vesicles in bone therapy, emphasising their physiological effects, biological functions, and biocompatibility; the second, by Yunke Jiao and co-authors,⁵ focuses on the advancements in neuroelectrode materials and technologies for brain-computer interfaces, emphasising the critical aspects of biocompatibility, signal quality, and durability for improved system performance; the third, by Chen-Hui Mi and co-authors,⁶

reviews the use of polyhydroxyalkanoates in musculoskeletal system applications, discussing their biocompatibility, biodegradability, and potential in tissue engineering and regeneration; the fourth, by Long Bai and co-authors,⁷ examines the role of bioactive elements like zinc, magnesium, and silicon in bone regeneration, focusing on their impacts on osteoimmunomodulation, neuroregulation, and angiogenesis, highlights their integration into biomaterials as a promising approach in bone tissue engineering.

Additionally, this issue presents two original research articles, including the development of a rapid method for harvesting mesenchymal stem cells from osteo-organoids, resulting in a high yield of mesenchymal stem cells with enhanced stemness and anti-senescence properties, marking a significant advancement in regenerative medicine;⁸ a comprehensive investigation on magnesium-doped polylactic acid microspheres for bone regeneration, highlighting their enhanced biocompatibility, osteogenic activity, and anti-inflammatory properties.⁹ Moreover, three commentaries shed light on the most advanced research techniques shaping the field today. Among the highlights are explorations into artificial intelligence accelerated discovery of self-assembling peptides, early immunomodulation by magnesium ion: catalyst for superior osteogenesis and exploration of minimal invasive biodegradable poly(glycerol-dodecanoate) nucleus pulposus scaffold with function regeneration.¹⁰⁻¹² The convergence of these technologies symbolises the rapidly evolving landscape of aforementioned four major scientific domains and represents a technological revolution in biomaterials.

At the forefront of this transformative era, the landscape of biomaterials in translational research presents both thrilling prospects and formidable challenges. The converging technologies in biomaterials translational signal a shift towards more innovative and effective solutions in

1 Organoid Research Center, Institute of Translational Medicine, Shanghai University, Shanghai, China; 2 Department of Orthopedics, Xinhua Hospital Affiliated to Shanghai Jiao Tong University School of Medicine, Shanghai, China; 3 National Center for Translational Medicine (Shanghai) SHU Branch, Shanghai University, Shanghai, China

*Corresponding author:
Jiacan Su,
drsujiacan@163.com.

<http://doi.org/10.12336/biomatertransl.2023.04.001>

How to cite this article:
Bai, L.; Su, J. Converging technologies in biomaterial translational research. *Biomater Transl.* 2023, 4(4), 197-198.



clinical treatment, through enhancing drug delivery systems, improving tissue engineering methodologies, and more responsive biosensors. Nevertheless, these advancements also bring intricate ethical considerations regarding patient safety and privacy, rigorous regulatory landscapes that ensure product efficacy and safety, and the need for extensive interdisciplinary collaboration to navigate the complexities of these innovations effectively. This scenario calls for a harmonious blend of scientific expertise, ethical understanding, and global cooperation.

In conclusion, as *Biomaterials Translational* embarks on its new journey at Shanghai University, China, the development of the journal is entering its new phase. Our dedication to the founding principles of the journal remains unwavering. We are committed to delivering the latest research findings and in-depth academic insights to our esteemed readers, continuing our legacy of interdisciplinary collaboration in the field of biomaterials science and translational research. Our goal is to provide an exceptional platform for the exchange and exploration of ideas in biomaterials translation, fostering a bridge between scientific discoveries and practical applications, and collectively advancing the ongoing development and innovation in this dynamic field.

-
1. Huebsch, N.; Mooney, D. J. Inspiration and application in the evolution of biomaterials. *Nature*. **2009**, *462*, 426-432.
 2. Sadtler, K.; Singh, A.; Wolf, M. T.; Wang, X.; Pardoll, D. M.; Elisseeff, J. H. Design, clinical translation and immunological response of biomaterials in regenerative medicine. *Nat Rev Mater*. **2016**, *1*, 16040.
 3. Fong, E. L.; Watson, B. M.; Kasper, F. K.; Mikos, A. G. Building bridges: leveraging interdisciplinary collaborations in the development of biomaterials to meet clinical needs. *Adv Mater*. **2012**, *24*, 4995-5013.
 4. Liu, H.; Su, J. Organoid extracellular vesicle-based therapeutic strategies for bone therapy. *Biomater Transl*. **2023**, *4*, 199-212.
 5. Jiao, Y.; Lei, M.; Zhu, J.; Chang, R.; Qu, X. Advances in electrode interface materials and modification technologies for brain-computer interfaces. *Biomater Transl*. **2023**, *4*, 213-233.
 6. Mi, C. H.; Qi, X. Y.; Ding, Y. W.; Zhou, J.; Dao, J. W.; Wei, D. X. Recent advances of medical polyhydroxyalkanoates in musculoskeletal system. *Biomater Transl*. **2023**, *4*, 234-247.
 7. Bai, L.; Song, P.; Su, J. Bioactive elements manipulate bone regeneration. *Biomater Transl*. **2023**, *4*, 248-269.
 8. Deng, S.; Zhu, F.; Dai, K.; Wang, J.; Liu, C. Harvest of functional mesenchymal stem cells derived from in vivo osteo-organoids. *Biomater Transl*. **2023**, *4*, 270-279.
 9. Tao, Z.; Yuan, Z.; Zhou, D.; Qin, L.; Xiao, L.; Zhang, S.; Liu, C.; Zhao, J.; Li, Y. Fabrication of magnesium-doped porous polylactic acid microsphere for bone regeneration. *Biomater Transl*. **2023**, *4*, 280-290.
 10. Shi, Y.; Hu, H. AI accelerated discovery of self-assembling peptides. *Biomater Transl*. **2023**, *4*, 291-293.
 11. Li, B. Early immunomodulation by magnesium ion: catalyst for superior osteogenesis. *Biomater Transl*. **2023**, *4*, 294-296.
 12. Zhou, H.; Wu, A. Comments on Innovative design of minimal invasive biodegradable poly(glycerol-dodecanoate) nucleus pulposus scaffold with function regeneration. *Biomater Transl*. **2023**, *4*, 297-298.

Organoid extracellular vesicle-based therapeutic strategies for bone therapy

Han Liu^{1,2,3,4}, Jiacan Su^{1,2,3,4,*}

Key Words:

bone therapy; engineering modifications; extracellular vesicles; nanotechnology; organoid extracellular vesicles

From the Contents

Introduction	199
Overview of Organoid Extracellular Vesicles	200
The Differences between Organoid Extracellular Vesicles and traditional Extracellular Vesicles	203
Applications of Organoid Extracellular Vesicles	203
Engineering Methods for Modifying Organoid Extracellular Vesicles	204
The Potential Role of Organoid Extracellular Vesicles in Bone Therapy	207
Advantages and Challenges	207
Conclusions and Perspectives	208

ABSTRACT

With the rapid development of population ageing, bone-related diseases seriously affecting the life of the elderly. Over the past few years, organoids, cell clusters with specific functions and structures that are self-induced from stem cells after three-dimensional culture in vitro, have been widely used for bone therapy. Moreover, organoid extracellular vesicles (OEVs) have emerging as promising cell-free nanocarriers due to their vigorous physiological effects, significant biological functions, stable loading capacity, and great biocompatibility. In this review, we first provide a comprehensive overview of biogenesis, internalisation, isolation, and characterisation of OEVs. We then comprehensively highlight the differences between OEVs and traditional EVs. Subsequently, we present the applications of natural OEVs in disease treatment. We also summarise the engineering modifications of OEVs, including engineering parental cells and engineering OEVs after isolation. Moreover, we provide an outlook on the potential of natural and engineered OEVs in bone-related diseases. Finally, we critically discuss the advantages and challenges of OEVs in the treatment of bone diseases. We believe that a comprehensive discussion of OEVs will provide more innovative and efficient solutions for complex bone diseases.

*Corresponding author:

Jiacan Su,
drsujiacan@163.com.

<http://doi.org/10.12336/biomatertransl.2023.04.002>

How to cite this article:

Liu, H.; Su, J. Organoid extracellular vesicle-based therapeutic strategies for bone therapy. *Biomater Transl.* 2023, 4(4), 199-212.

Introduction

The most significant issue arising from population ageing is the gradual decline in the function of tissues and cells as age advances. Various degenerative diseases continue to develop, affecting multiple tissues and organs within the body, and this process is largely irreversible.^{1, 2} The skeletal system, a component of the human musculoskeletal system, undergoes numerous physiological changes as the body ages. The deterioration of physiological functions leads to conditions such as osteoporosis, osteoarthritis, and osteoporotic fractures due to the fragile bone microstructure, resulting in diminished bone strength and susceptibility to fractures.^{3, 4} Additionally, the ageing of cartilage cells reduces lubrication, cartilage degeneration, and subchondral bone sclerosis leading to joint discomfort and even pain during movement. Overall, ageing has adverse effects

on the musculoskeletal system.⁵⁻⁷ Currently, effective treatment options for conditions like osteoporosis and osteoarthritis caused by ageing are lacking. Long-term use of anti-osteoporosis drugs and non-steroidal anti-inflammatory drugs places a substantial burden on the body and carries severe side effects.⁸⁻¹⁰

Extracellular vesicles (EVs) have emerged as a focal point in biomedical research in recent years due to their nanoscale structure, low immunogenicity, favourable biocompatibility, and drug delivery potential.¹¹⁻¹⁴ Moreover, EVs have been shown to effectively improve the progression of osteoporosis and osteoarthritis,¹⁵⁻²¹ and have also been shown to accelerate the healing of osteoporotic fracture.²²⁻²⁵ Although EVs have shown great advantages in bone ageing diseases, their inherent limitations, such as low yield and low therapeutic efficiency, hinder their further development.



With the advancement of stem cell technology, a three-dimensional (3D) model of organ-like structures that closely mimic native tissue architecture and physiological functions has emerged. Organoids are cell clusters with specific functions and structures that are self-induced from human adult stem cells or pluripotent stem cells after 3D culture *in vitro*.^{26, 27} Moreover, organoid EVs (OEVs) have also received much attention. Compared with traditional EVs, OEVs contain more quantity, better biological properties, and better therapeutic effects.²⁸ We innovatively propose the concept that not only organoids but also OEVs can be used for the treatment of complex diseases.²⁹ The discovery of OEVs might yield unexpected benefits for the improvement of age-related bone diseases. It is firmly believed that OEVs represent a novel

research paradigm, harboring immense scientific exploration and clinical utility²⁵.

Here, a comprehensive overview of biogenesis, internalisation, isolation, and characterisation of OEVs was provided. Then, the differences between OEVs and traditional EVs were comprehensively highlighted. Subsequently, the applications of natural OEVs in disease treatment were presented. Furthermore, the engineering modifications of OEVs were summarised. Moreover, an outlook on the potential of natural and engineered OEVs in bone-related diseases was provided. Finally, the advantages and challenges of OEVs in the treatment of bone diseases were discussed. We hope that a full understanding of OEVs will promote progress in the field of biomedical field and provide new strategies for the treatment of complex bone diseases (**Figure 1**).



Figure 1. Schematic illustration of organoid extracellular vesicle (OEV)-based bone disease treatment strategy. OEVs have emerging as promising cell-free nanocarriers for bone therapy due to their vigorous physiological effects, significant biological functions, stable loading capacity, and great biocompatibility. Created with BioRender.com.

Overview of Organoid Extracellular Vesicles

Organoids are cell clusters constructed through *in vitro* 3D cultivation using stem cells, recapitulating the spatial architecture and physiological functions of the source tissue.³⁰⁻³² As 3D models composed of living cells, they are also capable of secreting OEVs, which exhibit significant advantages in quantity and physiological function compared with traditional two-dimensional (2D) cultured EVs.³³ Currently, organoid research is in its infancy, where extensive investigation on the OEV biogenesis is limited. However, traditional EVs and OEVs are essentially derived from mammalian cells.^{13, 34} The general principles underlying the biogenesis of these two types of EVs are similar. Therefore, we exploited the biogenesis, internalisation, and isolation of mammalian EVs (MEVs) to characterise OEVs. Although the biogenesis of OEVs may be

similar to that of EVs, the unique properties of the organoids may introduce subtle differences to OEVs. As OEVs continue to advance, it is expected that the biogenesis of OEVs will be further elucidated.

Biogenesis and internalisation of organoid extracellular vesicles

Here, the biogenesis of OEVs is summarised (**Figure 2**). The cellular plasma membrane undergoes invagination to absorb cell surface proteins and soluble proteins from the extracellular environment, resulting in the formation of early sorting endosomes (ESEs), sometimes synthesised in conjunction with pre-existing ESEs; ESEs engages in cargo exchange with the endoplasmic reticulum and Golgi apparatus, maturing into late sorting endosomes, ultimately giving rise

1 Institute of Translational Medicine, Shanghai University, Shanghai, China; 2 Organoid Research Center, Shanghai University, Shanghai, China; 3 National Center for Translational Medicine (Shanghai) SHU Branch, Shanghai University, Shanghai, China; 4 Department of Orthopedics, Xinhua Hospital, Shanghai Jiao Tong University School of Medicine, Shanghai, China

Organoid extracellular vesicles

to multivesicular bodies. The multivesicular body membrane undergoes secondary invagination to form intraluminal vesicles, subsequently guided by relevant proteins, the multivesicular body elects either to merge with lysosomes for degradation or to fuse with the cell plasma membrane to release intraluminal vesicles into the extracellular space, thereby releasing OEVs.^{25, 35-37}

Released EVs primarily function in maintaining intercellular communication and can be absorbed by recipient cells through three modes: membrane fusion, receptor-ligand binding, and endocytosis (Figure 2). Benefiting from the fact that both OEVs and recipient cells possess phospholipid bilayer membrane structures, when they can overcome the instability of phospholipid bilayer interactions and the high activation energy barrier, membrane fusion between the two becomes plausible.³⁸ During membrane fusion, a partially fused connecting segment forms between two adjacent distinct phospholipid bilayer membranes. As they draw closer, this

connecting segment expands, evolving into a semi-fused double-layered membrane structure that progressively enlarges until OEVs fuse with recipient cells.³⁹ On the other hand, the ligand-receptor binding pathway heavily relies on the presence of lectins, polysaccharides, integrins, and other cell adhesion molecules.⁴⁰ The presence or absence of these substances significantly impacts the internalisation of OEVs through this pathway, although the specific mechanisms remain indeterminate in current research.⁴¹ Some studies indicate that protein-coated internalisation is a typical route for OEV uptake, and inhibiting the coating proteins can notably diminish cellular uptake of OEVs.^{42, 43} Moreover, owing to the distinctive 3D structure of organoids, the efficiency of OEVs internalisation is enhanced. The intricate cellular interactions and spatial arrangement within organoids create a unique microenvironment that facilitates efficient uptake of OEVs by neighbouring cells.⁴⁴

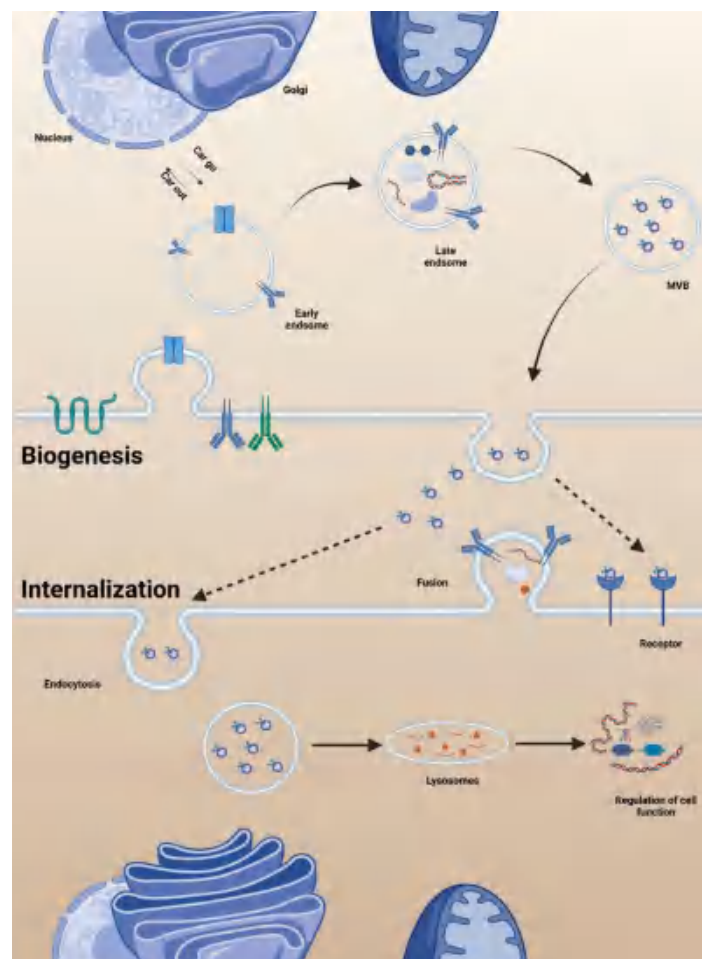


Figure 2. Biogenesis and internalisation of organoid extracellular vesicles (OEVs). The early endosome was formed by the absorption of extracellular proteins by the plasma membrane through endocytosis. The early endosome gradually matured into the late endosome by exchanging goods with the endoplasmic reticulum and Golgi apparatus. In the late endosomes, a second plasma membrane invasion occurs to form multivesicular body (MVB), which is finally selected to fuse with the plasma membrane of the cell to release OEVs or to fuse with lysosomes with the participation of sorting proteins. The free OEVs arrive at the recipient cell and are absorbed by endocytosis or receptor ligand binding. Created with BioRender.com.

Isolation and characterisation of organoid extracellular vesicles

Currently, methods for the isolation of EVs primarily encompass density gradient centrifugation, differential centrifugation, size-exclusion chromatography, and kit-based extraction. Each approach possesses its distinct advantages and limitations. Here, we summarised extraction methodology for OEVs (**Figure 3**). First, the separation of organoids and matrix gel is achieved by subjecting the mixture to low-speed centrifugation at $1,000 \times g$ for 5 minutes at 4°C . Subsequently, the supernatant is subjected to a low speed centrifugation at

$10,000 \times g$ for 10 minutes at 4°C , followed by filtration through a $0.22 \mu\text{m}$ sterile filter. Then, employing ultracentrifugation at $150,000 \times g$ for 90 minutes at 4°C , the sediment at the bottom is identified as OEVs, which are subsequently resuspended in sterile phosphate buffered saline. For purification, a repeat ultracentrifugation at $150,000 \times g$ for 90 minutes at 4°C is conducted, yielding the purified OEVs as the sediment at the bottom. Sterile phosphate buffered saline is employed to resuspend the collected purified OEVs, which are then stored at -80°C for future use.^{14, 45-47} Other OEVs extraction schemes are shown in **Table 1**.⁴⁸⁻⁵²

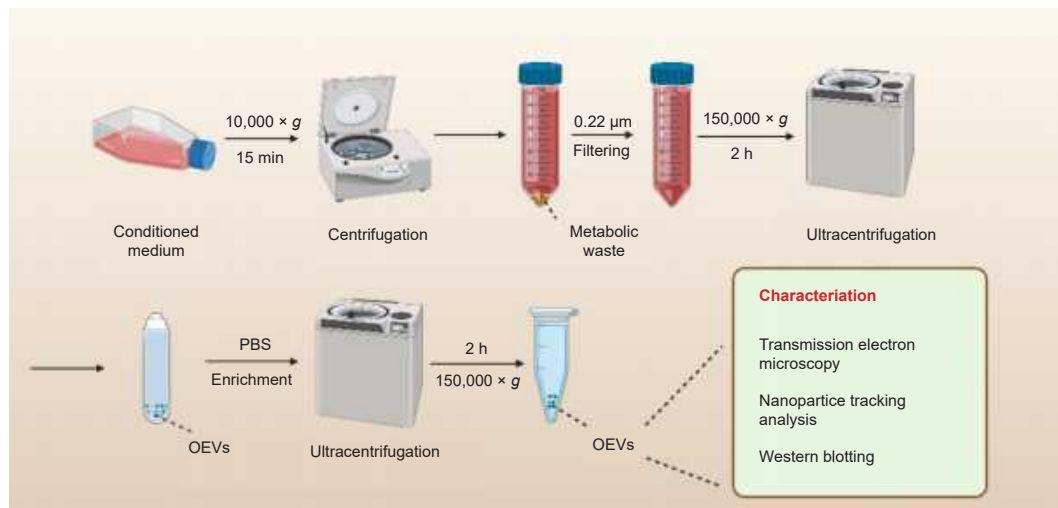


Figure 3. Isolation of organoid extracellular vesicles (OEVs). After three-dimensional (3D) cultivation, the organoid culture is collected and centrifuged at $10,000 \times g$ for 15 minutes at 4°C . The supernatant is then filtered by $0.22 \mu\text{m}$ sterile filter to remove impurities. Subsequently, OEVs precipitate are collected by the ultracentrifugation for 2 hours at $150,000 \times g$. The collected OEVs are purified with phosphate buffered saline (PBS) and ultracentrifuged at $150,000 \times g$ for 2 hours. The obtained OEVs can be characterised and verified using nanoparticle tracking analysis, transmission electron microscopy, and Western blotting to represent the size, shape, concentration, and specific markers of OEVs. The collected OEVs are used immediately or stored at -80°C until use. Created with BioRender.com.

Table 1. The extraction methods of organoid extracellular vesicles

Method	Principle	Advantage	Disadvantage	Reference
Gradient ultrafast centrifugation	Different settlement coefficient	High purity; Separable subgroup	Time-consuming; High equipment requirements	48
Volume exclusion chromatography	Different particle size	High purity; Fast preparation	Expensive; Low output	49
Immunoaffinity capture	Specific binding	High purity; Specific exosomes	Expensive; Need to optimise ligand; Low yield	50
Microfluidic technology	Immunoaffinity, particle size and density	High efficiency; No chemical pollution	Low yield; Expensive	51
EVs extraction kit	Immune magnetic bead capture	Simple method	Low output; Expensive	–
Sucrose density gradient centrifugation method	Centrifugal force	High purity	Low output; Long time; Tedious process	52

After the isolation of OEVs, transmission electron microscopy, nanoparticle tracking analysis, and Western blotting are the most used characterisation methods.^{16, 53, 54} Generally, transmission electron microscopy and nanoparticle tracking

analysis are used to represent the size, shape, and concentration of OEVs. In addition, Western blotting is used to characterise specific markers such as transmembrane proteins CD9, CD63, CD81, and tumour susceptibility gene 101^{55, 56} (**Figure 3**).

In summary, this isolation and characterisation protocol provides a clear procedure to obtain pure OEVs suitable for subsequent research. As organoid technology matures and more people realise the existence and ability of OEVs, it is necessary to propose a standardised set of guidelines for the isolation and characterisation of OEVs.

The Differences between Organoid Extracellular Vesicles and traditional Extracellular Vesicles

In contrast to 2D monolayer cell culture models within culture dishes, organoids exhibit advanced 3D physiological structures, facilitating intricate intercellular communication.^{50,57} A study investigated EVs released by gastric cancer cells from the same source cultured in both 2D and 3D conditions.^{58,59} Subsequent observations revealed a substantial advantage in the quantity of EVs collected under 3D conditions. Furthermore, a decrease in adenosine diphosphate-ribosylation factor 6 expression and an overall elevation in microRNA expression were detected within EVs collected from 3D conditions.^{58,59} A recent study on 3D EVs has shown that, unlike 2D EVs, many miRNAs choose to be highly expressed in 3D EVs rather than in 2D EVs.⁶⁰ In addition, when stimulated by amyloid- β 42, 3D EVs showed stronger anti-inflammatory effects, while 2D EVs

showed reduced pro-inflammatory factors.⁶⁰

Additionally, studies explored the transplantation of mesenchymal stem cell derivatives cultured in 2D and 3D conditions into mice with brain injuries.⁶¹⁻⁶³ Mice injected with derivatives from 3D culture exhibited superior improvements in angiogenesis and neural recovery. This potentially arises from the more natural physiological structure of cells from 3D culture, leading to the secretion of EVs with advantages in both quantity and physiological functionality. At present, many preclinical and clinical studies have demonstrated the therapeutic effect, drug delivery capacity and diagnostic potential of EVs, but the production and clinical conversion technology of EVs are the main challenges limiting the application of EVs.^{48,64-66} Monolayer cell culture mode leads to reduced cell-cell interaction, which seriously affects the production and function of EVs. Fortunately, OEVs from 3D solved these problems perfectly. 3D culture not only preserves the cell phenotype, but also brings more high-yield and efficient OEVs.

Overall, OEVs derived from 3D culture conditions surpass traditional EVs in terms of quantity and physiological effects, rendering them more suitable for therapeutic applications in disease treatment⁶⁷ (Figure 4).

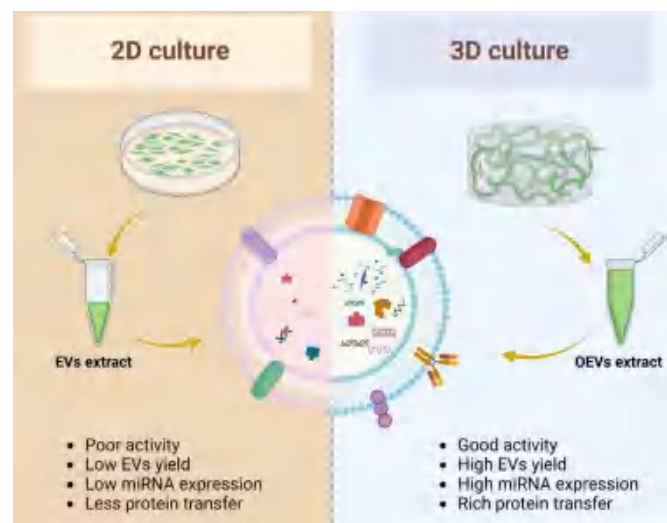


Figure 4. The differences between organoid extracellular vesicles (OEVs) and traditional extracellular vesicles (EVs). Two-dimensional (2D) cultured cells produced fewer EVs, poor bioactivity, and less protein and nucleic acid (left), while three-dimensional (3D) cultured cells produced more OEVs, more active, and more protein and nucleic acid (right). Created with BioRender.com. miRNA: microRNA.

Applications of Organoid Extracellular Vesicles

Currently, the literature related to OEVs is very scarce.^{55,68} However, existing research results show that OEVs have significant therapeutic effects, which makes scientists and clinicians full of interest and confidence in the huge therapeutic potential of OEVs.⁶⁹ In addition to disease treatment, it is foreseeable that OEVs will prosper in fields such as liquid biopsy, pharmacological testing, toxicity testing, drug testing,

and genetic research (Figure 5). Here, we summarise the applications of OEVs in immunomodulation and epithelial repair.

Organoid extracellular vesicles for immunomodulation

Many studies have shown that EVs are effective mediators of intercellular communication between intestinal cells and immune cells.^{70,71} Current studies show that EVs derived from human intestinal organoids can modulate the

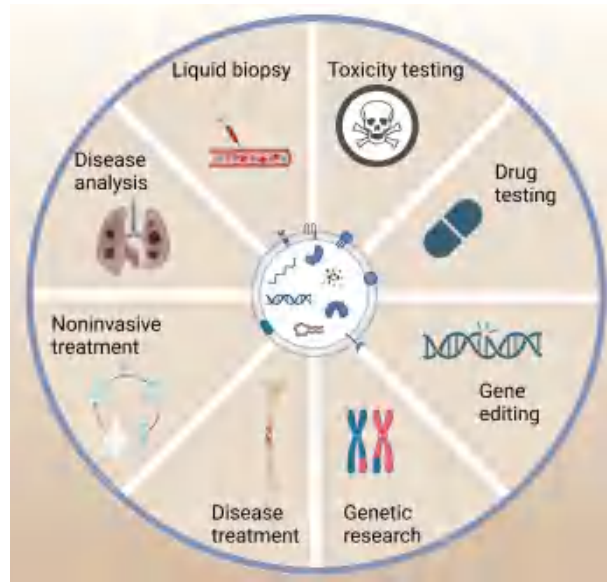


Figure 5. The application diagram of organoid extracellular vesicles (OEVs). OEVs have a wide range of applications, including liquid biopsy, pharmacological testing, toxicity testing, disease treatment, customised personalised medicine, genetic research. Created with BioRender.com.

inflammatory response of multiple immune cells.⁷² OEVs from organoids derived from murine intestinal crypt stem cells exhibit pronounced immunomodulatory capabilities (**Figure 6A**). Notably, OEVs inhibit lipopolysaccharide-triggered cytokine production in immune cells. However, this immunomodulatory function is susceptible to suppression by opiate drugs. Specifically, upon intervention with opioid analgesics on intestinal organoids, the immunomodulatory prowess of OEVs becomes nullified.^{73,74} Through microarray analysis, a multitude of microRNAs, particularly Let-7 (an inflammation-regulating factor), were found to regulate OEVs-mediated immune regulation.

In *in vivo* experiments, Zhang et al.⁷² found that injection of EVs derived from intestinal organoids significantly reduced lipopolysaccharide-induced systemic inflammation and improved the symptoms of dextran sulfate sodium-induced colitis. Similarly, EVs derived from intestinal organoids under morphine treatment failed to suppress immune responses. Intestinal organoids are essential *in vitro* tools that bring new research opportunities to intestinal stem cell research. Watanabe et al.⁷⁵ used intestinal organoids to treat inflammatory bowel disease. The medical team at Tokyo Medical and Dental University in Japan announced that they successfully completed a colon transplant by using tissue taken from the patient's intestine to create organoids to treat inflammatory bowel disease.⁷⁶ This is the first time in the world that organoid technology has been used to perform transplantation for patients with the refractory disease ulcerative colitis. We have reason to believe that EVs derived from intestinal organoids will also be a powerful weapon in the treatment of inflammatory bowel disease. In the future, the combination of organoids and EVs derived from intestinal organoids may achieve better therapeutic effects.

Organoid extracellular vesicles for epithelial repair

Radiation therapy can cause significant damage to the salivary glands (SGs).^{76,77} Stem cell technology stands as a prospective strategy for repairing SG injuries. Adine et al.⁷⁸ has employed a magnetic 3D bio-assembly platform to construct SG-like organs (SGOs), aiming to introduce novel therapeutic approaches for SG injury restoration. However, subsequent experiments revealed suboptimal reparative outcomes of SGOs, achieving only 25% efficacy.

In addition, during the cultivation of SGOs, it was observed that conditioned media obtained by continuous centrifugation of the cultures could yield oligodendrocyte-derived EVs derived from SGOs (**Figure 6B**). These EVs derived from SGOs were validated through nanoparticle tracking analysis, transmission electron microscopy, and Western blot analysis. Chansaenroj et al.⁷⁹ found that EVs derived from SGOs had significant effects on SG injury, specifically stimulating SG epithelial cell mitosis and promoting the growth of associated neurons with an efficacy of 60% (**Figure 6B**). To a certain extent, the therapeutic potential of OEVs greatly surpasses that of organoids.

Engineering Methods for Modifying Organoid Extracellular Vesicles

Although OEVs have better physiological effects than EVs, OEVs still have limitations, such as lack of organ targeting.⁸⁰⁻⁸² Currently, numerous articles have reported that modified EVs can endow them with more powerful functions.⁸³⁻⁸⁶ Given the similarities between OEVs and EVs, engineering strategies can also be used on OEVs to enhance their functionality and achieve specific goals. Here, we summarise different engineering approaches including engineering parental cells to create therapeutic OEVs and engineering OEVs after isolation (**Figure 7 and Table 2**).^{11, 53, 87-90}

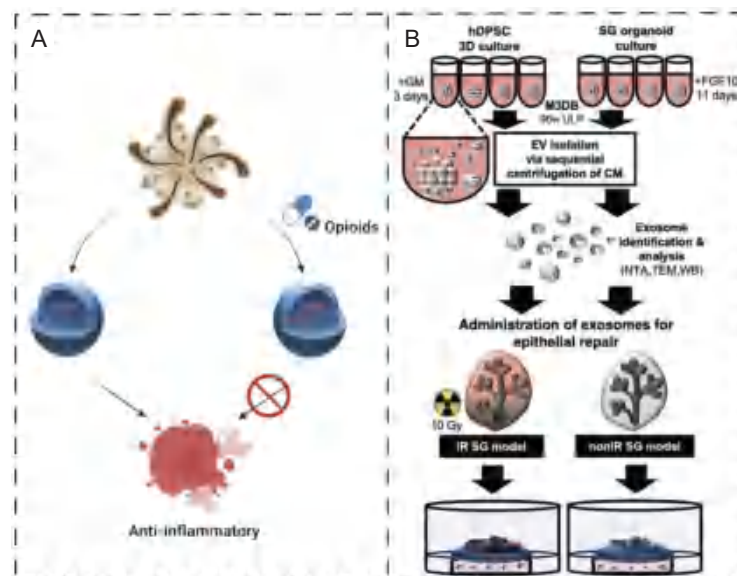


Figure 6. Organoid extracellular vesicles (OEVs) for disease treatment. (A) OEVs secreted by intestinal organoids can exert anti-inflammatory effects, while the anti-inflammatory effects of secreted OEVs are lost after the use of opioids acting on organoids. Created with BioRender.com. (B) Cultivation and collection of SG-like organ (SGO) by magnetic 3D bio-assembly (M3DB) system for the treatment of radiation-induced epithelial damage. Reprinted from Chansaenroj et al.⁷⁹ 3D: three-dimensional; 96w ULP: 96-well ultra-low attachment plate; CM: conditioned media; EV: extracellular vesicle; FGF10: fibroblast growth factor 10; GM: growth media; hDPSC: human dental pulp stem cell; IR: irradiated; NTA: nanoparticle tracking analysis; SG: salivary gland; TEM: transmission electron microscopy; WB: Western blotting.

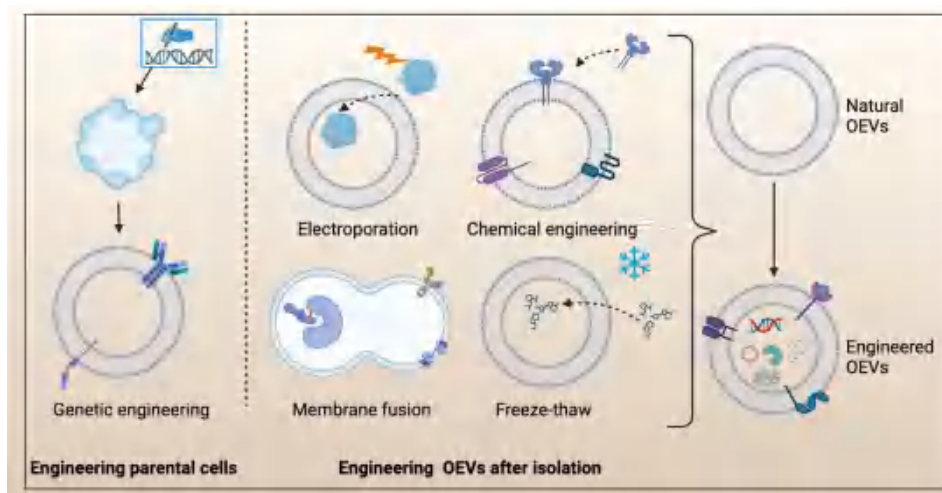


Figure 7. The engineering approaches for modifying organoid extracellular vesicles (OEVs), including the engineering parental cells and engineering OEVs after isolation. Engineering parental cells, such as using clustered regularly interspaced short palindromic repeats–CRISPR-associated protein 9 (CRISPR–Cas9) to modify cells to obtain engineered organoids. Engineering OEVs after isolation are mainly Electroporation, chemical engineering, membrane fusion, and freeze thaw. Created with BioRender.com.

Engineering parental cells

When parental cells are genetically engineered to overexpress proteins, secreted EVs can also carry such proteins. For example, Hu et al.⁵³ genetically engineered NIH-3T3 cells to generate engineered MEVs with C-X-C motif chemokine receptor 4 (CXCR4) on their surface (Figure 8A). Moreover, Liu et al.¹¹ used synthetic biology methods to construct

probiotic *Escherichia coli* Nissle 1917 (ECN) containing recombinant plasmid pClyA-CXCR4 (ClyA, a bacterial surface protein,^{91, 92} thereby obtaining a large number of engineered bacterial EVs (BEVs) displaying CXCR4 on the membrane surface (Figure 8B). In addition, organoid can also be genetically modified to generate engineered OEVs with powerful functions.

Table 2. Engineered retrofit solutions for organoid extracellular vesicles

Engineering approach	Strategy	Method	Purpose	Reference
Engineering parental cells	Genetic engineering	Direct modification of parent cells	The protein was displayed on the surface of extracellular vesicles to enrich its physiological function	53
	Synthetic biology	Shuttle plasmid	Giving new functionality to bacterial extracellular vesicles	11
Engineering after isolation	Membrane fusion	Co-incubation	Loading of exogenous cargo into the membrane	87
	Chemical engineering	Non-covalent reaction	Increased extracellular vesicles targeting	88
	Chemical engineering	Click chemistry	Loading of azides onto the membrane surface	89
	Freeze-thaw	Freeze-thaw cycle	Loading extracellular vesicles with exogenous substances and ensuring normal morphology	90
	Electroporation technique	High voltage electric field	Transfer of DNA, or/and RNA into extracellular vesicles	11

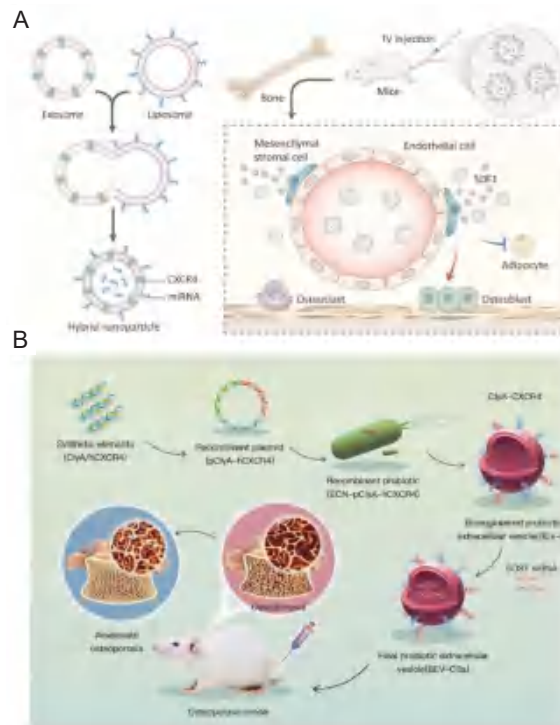


Figure 8. Engineering parental cells to endow their extracellular vesicles (EVs) with powerful functions. (A) Schematic illustration of exosome-guided microRNA (miRNA) blocking. Reprinted from Hu et al.⁵³ (B) Schematic illustration of the construction of bioengineered bacterial EVs (BEVs). Reprinted from Liu et al.¹¹ Copyright 2023, with permission from Elsevier. BEV: bacterial extracellular vesicle; BEV-C: BEVs-hCXCR4; BEV-CS: BEVs-hCXCR4-SOST siRNA; ClyA: A bacterial surface protein; CXCR4: C-X-C motif chemokine receptor 4; ECN: construct probiotic *Escherichia coli* Nissle 1917; hCXCR4: human C-X-C motif chemokine receptor 4; IV: intravenous; p: plasmid; SDF1: stromal cell-derived factor 1; siRNA: small interfering RNA; SOST: sclerostin.

Engineering organoid extracellular vesicles after isolation

Membrane fusion

OEVs with a phospholipid bilayer structure can spontaneously fuse with other phospholipid bilayer materials, thereby endowing OEVs with new functions.^{87, 93, 94} In general, EVs can fuse with liposomes after 12 hours of incubation at 37°C.⁸⁷ Moreover, polyethylene glycol can accelerate the

fusion of EVs and functionalised liposomes.⁹⁵ Chen et al.⁹⁶ used membrane fusion technology to construct BEVs-cancer EVs hybrid membranes and achieved tumor targeting and immunogenicity. Lin et al.⁸⁷ constructed hybrid nanoparticles for delivering the CRISPR-Cas9 system to MSCs by incubating fused MEVs and liposomes. The same principle can be applied to induce fusion between OEVs and liposomes, thereby augmenting the functions of OEVs.

Chemical engineering

Covalent and non-covalent reactions are commonly employed techniques to modify the membrane surface of EVs.^{97,98} This modification strategy is equally applicable to OEVs. For instance, direct co-incubation utilizing hydration forces can integrate targeting peptides into the phospholipid bilayer of OEVs, enhancing their targeting capabilities.⁸⁸ Furthermore, the amine properties on the membrane of OEVs can be modified with alkyne groups and click chemistry can be employed for surface modification of OEVs. When alkyne groups label the amines on the OEVs' membrane, copper-catalysed azide-alkyne cycloaddition reactions can impart new properties to the EVs' membrane by orthogonal reaction with azide compounds.⁸⁹

Freeze thawing

The freeze thawing approach is a straightforward method for loading exogenous substances into OEVs. For example, Haney et al.⁹⁹ constructed a new MEVs-based delivery system to treat Parkinson's disease. Catalase was loaded into MEVs *ex vivo* using incubation, freeze-thaw cycles, sonication, or extrusion. In addition, Hajipour et al.¹⁰⁰ isolated MEVs from uterine fluid and loaded human chorionic gonadotropin by freeze-thaw cycle and sonication methods. Shi et al.⁹⁰ have evaluated six drug loading methods, including incubation, sonication, extrusion, freeze-thaw cycles, saponin-assisted, and electroporation method, for milk derived MEVs drug delivery. Drug-loaded MEVs obtained through freeze-thaw cycles showed minimal morphological changes.

Electroporation technique

The electroporation technique involves applying high-intensity electric fields to transiently enhance the permeability of the phospholipid bilayer, facilitating the uptake of exogenous substances from the surroundings.¹⁰¹ Hence, electroporation technique enables the introduction of DNA, RNA, proteins, and more into the membrane of OEVs. An advantage of electroporation lies in its ability to preserve the physical characteristics of small interfering RNA during the transfer process.¹⁰² Alvarez-Erviti et al.¹⁰² loaded exogenous small interfering RNA into brain-targeted MEVs (Lamp2b-MEVs) through electroporation for the treatment of brain diseases, such as Alzheimer's disease. Moreover, Liu et al.¹¹ also used electroporation to load exogenous small interfering RNA into bone-targeted BEVs (BEVs-CXCR4) for the treatment of bone diseases such as osteoporosis.

The Potential Role of Organoid Extracellular Vesicles in Bone Therapy

Due to the limited development of organoids and OEVs, the therapeutic applications of OEV (especially OEV-derived from bone organoids) in the treatment of bone diseases still need to be further explored. However, the existing research on MEVs and BEVs in the treatment of bone diseases has laid the foundation for the treatment of OEVs in bone diseases.^{54,103-105} Importantly, OEVs have surpassed traditional MEVs in

quantity and physiological effects, making them more suitable for therapeutic applications in disease treatment.⁵⁶ Therefore, OEV-based bone therapies, including the natural OEVs and engineered OEVs, have huge potentials.

The nanoscale size of OEVs as well as their cell-free properties and high safety make them excellent nanocarriers.^{85,106} Natural OEVs have been shown to have promising therapeutic effects against complex diseases.^{68,79,107,108} In addition, engineering natural OEVs can endow them with specific organ targeting and stronger therapeutic effects. For example, loading targeting elements on the membrane surface of OEVs can enhance specific targeting. In addition, encapsulating therapeutic agents in OEVs not only enhances drug stability and extends half-life *in vivo* but also reduces the risk of adverse effects.

However, realising the applications of OEVs for bone disorder treatment presents challenges that need to be surmounted, such as organoid preparation, OEV isolation, engineering modifications, drug loading, and release mechanisms. As advances in organoids and OEVs continue, we can foresee that the use of OEVs to treat bone diseases will lead to more effective and personalised treatment options, ultimately improving bone health and improving overall quality of life.^{109,110}

Advantages and Challenges

OEVs represent a novel technological branch that extends from the development of organoid technology. Conceptually aligned with MEVs, BEVs, and plant derived EVs, OEVs are nanoscale vesicles released by living cells into the extracellular environment. Particularly, the similarities between OEVs and MEVs in terms of biological mechanisms are striking. However, the advantages of organoids (similar spatial structure to human tissue) compared to MEVs endow OEVs huge advantages in terms of yield and functionality.^{69,111,112} Moreover, OEVs inherit the low immunogenicity and efficient crossing of biological barriers of MEVs, thereby showing broad prospects in medical applications and drug delivery vehicles. Furthermore, OEVs have the potential to be engineered to enhance their targeting specificity and confer complementary physiological functions, thus enhancing their potential applications.

Nevertheless, OEVs still face several obstacles in moving them from lab to clinic. The biggest obstacle to bring OEVs from lab to clinic is the construction of organoid. As organoid models are still in their nascent stages, currently generated organoids predominantly exhibit singular functions and lack comprehensive functional integration. For example, currently reported bone organoids mainly represent isolated bone functions, such as bone formation, resorption, or haematopoiesis, rather than integrated multifunctional bone organ systems.^{26,113} These divergences prevent OEVs from perfectly replicating the diversity of human cells. Furthermore, while OEVs possess a pronounced production advantage over MEVs, they still cannot meet the demands of research and clinical applications. In addition, OEV extraction methods lack standardised standards, and their mechanism of action remains unclear. Here, we summarise the advantages and challenges of OEVs (Figure 9).



Figure 9. Advantages and challenges of organoid extracellular vesicles (OEVs). OEVs have the advantages of strong physiological function, high yield, low immunogenicity, cell-free system, and good delivery potential. At the same time, OEVs also have several obstacles, including unknown functional mechanism, lack of source, need engineering transformation, single function, and lack of standardised extraction course. Created with BioRender.com.

Conclusions and Perspectives

OEVs and traditional EVs are essentially derived from mammalian cells. Therefore, the biogenesis, internalisation, isolation, and characterisation of OEVs are similar with that of MEVs. However, OEVs exceed traditional MEVs in terms of quantity and physiological effects. Therefore, OEVs are more suitable for therapeutic applications in disease treatment. Subsequently, the applications of natural OEVs in disease treatment, such as immunomodulation and epithelial repair, have been summarised. Although OEVs have better physiological effects than EVs, OEVs still faces several obstacles. We then summarise the engineering modifications of OEVs, including engineering parental cells and engineering OEVs after isolation (membrane fusion, chemical engineering, freeze thawing, and electroporation technique). Furthermore, the potential of natural and engineered OEVs in bone-related diseases is prospected. Finally, the advantages of OEVs (including strong physiological function, high yield, low immunogenicity, cell-free system, and good delivery potential) and challenges of OEVs (including unknown functional mechanism, lack of source, need engineering transformation, single function, and lack of standardised extraction course) have been critically discussed. The comprehensive discussion of OEVs will provide more innovative and efficient solutions for complex bone diseases (**Figure 1**).

Although the research on organoids is very hot, there are only few studies on OEVs, and there are almost no applications of OEVs in diseases, especially bone-related diseases. In essence, we hope that this review can propose a novel concept, where OEVs constitute a powerful new paradigm in the field of biomedical research and provide new therapeutic avenues for a variety of complex diseases, especially bone diseases. With the continuous improvement of organoid technology and the construction of multifunctional integrated organoids, we will be able to highly simulate the physiological environment and functions of the human body *in vitro*. This will also help extract more effective OEVs to meet the needs of disease treatment.

There is no doubt that the potential of OEVs will be further demonstrated in the future to benefit patients. Despite ongoing challenges, the field of organoids and OEVs have significant progress in recent years, driving the realisation of clinical applications.

Author contributions

HL conceptualised the review and drafted the manuscript; JS checked and revised the manuscript. Both authors reviewed and approved the final version of the manuscript.

Financial support

This work was supported by the National Natural Science Foundation of China, No. 82202344; Integrated Project of Major Research Plan of National Natural Science Foundation of China, No. 92249303; Shanghai Committee of Science and Technology Laboratory Animal Research Project, No. 23141900600; Foundation of National Center for Translational Medicine (Shanghai) SHU Branch, Nos. SUTIM-202303, SUTIM-2023006.

Acknowledgement

None.

Conflicts of interest statement

The authors declare no conflict of interest.

Editor note: Jiacan Su is an Editorial Board member of *Biomaterials Translational*. He was blinded from reviewing or making decisions on the manuscript. The article was subject to the journal's standard procedures, with peer review handled independently of this Editorial Board member and his research group.

Open access statement

This is an open access journal, and articles are distributed under the terms of the Creative Commons Attribution-NonCommercial-ShareAlike 4.0 License, which allows others to remix, tweak, and build upon the work non-commercially, as long as appropriate credit is given and the new creations are licensed under the identical terms.

1. Farr, J. N.; Khosla, S. Cellular senescence in bone. *Bone*. **2019**, *121*, 121-133.
2. Metavarayuth, K.; Villarreal, E.; Wang, H.; Wang, Q. Surface topography and free energy regulate osteogenesis of stem cells: effects of shape-controlled gold nanoparticles. *Biomater Transl.* **2021**, *2*, 165-173.
3. Wang, T.; Huang, S.; He, C. Senescent cells: a therapeutic target for osteoporosis. *Cell Prolif.* **2022**, *55*, e13323.

Organoid extracellular vesicles

4. Brown, C. Osteoporosis: staying strong. *Nature*. **2017**, *550*, S15-S17.
5. Coryell, P. R.; Diekman, B. O.; Loeser, R. F. Mechanisms and therapeutic implications of cellular senescence in osteoarthritis. *Nat Rev Rheumatol*. **2021**, *17*, 47-57.
6. Loeser, R. F.; Collins, J. A.; Diekman, B. O. Ageing and the pathogenesis of osteoarthritis. *Nat Rev Rheumatol*. **2016**, *12*, 412-420.
7. Yuan, J.; Maturavongsadit, P.; Zhou, Z.; Lv, B.; Lin, Y.; Yang, J.; Luckanagul, J. A. Hyaluronic acid-based hydrogels with tobacco mosaic virus containing cell adhesive peptide induce bone repair in normal and osteoporotic rats. *Biomater Transl*. **2020**, *1*, 89-98.
8. Day, R. O.; Graham, G. G. Non-steroidal anti-inflammatory drugs (NSAIDs). *BMJ*. **2013**, *346*, f3195.
9. Katz, J. N.; Arant, K. R.; Loeser, R. F. Diagnosis and treatment of hip and knee osteoarthritis: a review. *JAMA*. **2021**, *325*, 568-578.
10. Arora, D.; Robey, P. G. Recent updates on the biological basis of heterogeneity in bone marrow stromal cells/skeletal stem cells. *Biomater Transl*. **2022**, *3*, 3-16.
11. Liu, H.; Zhang, H.; Wang, S.; Cui, J.; Weng, W.; Liu, X.; Tang, H.; Hu, Y.; Li, X.; Zhang, K.; Zhou, F.; Jing, Y.; Su, J. Bone-targeted bioengineered bacterial extracellular vesicles delivering siRNA to ameliorate osteoporosis. *Compos B Eng*. **2023**, *255*, 110610.
12. Liu, H.; Li, M.; Zhang, T.; Liu, X.; Zhang, H.; Geng, Z.; Su, J. Engineered bacterial extracellular vesicles for osteoporosis therapy. *Chem Eng J*. **2022**, *450*, 138309.
13. Liu, H.; Geng, Z.; Su, J. Engineered mammalian and bacterial extracellular vesicles as promising nanocarriers for targeted therapy. *Extracell Vesicles Circ Nucleic Acids*. **2022**, *3*, 63-86.
14. Liu, H.; Zhang, H.; Han, Y.; Hu, Y.; Geng, Z.; Su, J. Bacterial extracellular vesicles-based therapeutic strategies for bone and soft tissue tumors therapy. *Theranostics*. **2022**, *12*, 6576-6594.
15. Guo, J.; Wang, F.; Hu, Y.; Luo, Y.; Wei, Y.; Xu, K.; Zhang, H.; Liu, H.; Bo, L.; Lv, S.; Sheng, S.; Zhuang, X.; Zhang, T.; Xu, C.; Chen, X.; Su, J. Exosome-based bone-targeting drug delivery alleviates impaired osteoblastic bone formation and bone loss in inflammatory bowel diseases. *Cell Rep Med*. **2023**, *4*, 100881.
16. Song, H.; Li, X.; Zhao, Z.; Qian, J.; Wang, Y.; Cui, J.; Weng, W.; Cao, L.; Chen, X.; Hu, Y.; Su, J. Reversal of osteoporotic activity by endothelial cell-secreted bone targeting and biocompatible exosomes. *Nano Lett*. **2019**, *19*, 3040-3048.
17. Wang, J.; Li, X.; Wang, S.; Cui, J.; Ren, X.; Su, J. Bone-targeted exosomes: strategies and applications. *Adv Healthc Mater*. **2023**, *12*, e2203361.
18. Pang, L.; Jin, H.; Lu, Z.; Xie, F.; Shen, H.; Li, X.; Zhang, X.; Jiang, X.; Wu, L.; Zhang, M.; Zhang, T.; Zhai, Y.; Zhang, Y.; Guan, H.; Su, J.; Li, M.; Gao, J. Treatment with mesenchymal stem cell-derived nanovesicle-containing gelatin methacryloyl hydrogels alleviates osteoarthritis by modulating chondrogenesis and macrophage polarization. *Adv Healthc Mater*. **2023**, *12*, e2300315.
19. Liu, H.; Zhang, Q.; Wang, S.; Weng, W.; Jing, Y.; Su, J. Bacterial extracellular vesicles as bioactive nanocarriers for drug delivery: Advances and perspectives. *Bioact Mater*. **2022**, *14*, 169-181.
20. Wang, Z. X.; Luo, Z. W.; Li, F. X.; Cao, J.; Rao, S. S.; Liu, Y. W.; Wang, Y. Y.; Zhu, G. Q.; Gong, J. S.; Zou, J. T.; Wang, Q.; Tan, Y. J.; Zhang, Y.; Hu, Y.; Li, Y. Y.; Yin, H.; Wang, X. K.; He, Z. H.; Ren, L.; Liu, Z. Z.; Hu, X. K.; Yuan, L. Q.; Xu, R.; Chen, C. Y.; Xie, H. Aged bone matrix-derived extracellular vesicles as a messenger for calcification paradox. *Nat Commun*. **2022**, *13*, 1453.
21. Jiang, Y.; Li, J.; Xue, X.; Yin, Z.; Xu, K.; Su, J. Engineered extracellular vesicles for bone therapy. *Nano Today*. **2022**, *44*, 101487.
22. Liu, J. H.; Yue, T.; Luo, Z. W.; Cao, J.; Yan, Z. Q.; Jin, L.; Wan, T. F.; Shuai, C. J.; Wang, Z. G.; Zhou, Y.; Xu, R.; Xie, H. Akkermansia muciniphila promotes type H vessel formation and bone fracture healing by reducing gut permeability and inflammation. *Dis Model Mech*. **2020**, *13*, dmm043620.
23. Shan, S. K.; Lin, X.; Li, F.; Xu, F.; Zhong, J. Y.; Guo, B.; Wang, Y.; Zheng, M. H.; Wu, F.; Yuan, L. Q. Exosomes and bone disease. *Curr Pharm Des*. **2019**, *25*, 4536-4549.
24. Mi, B.; Chen, L.; Xiong, Y.; Yang, Y.; Panayi, A. C.; Xue, H.; Hu, Y.; Yan, C.; Hu, L.; Xie, X.; Lin, Z.; Zhou, W.; Cao, F.; Xiao, X.; Feng, Q.; Liu, G. Osteoblast/osteoclast and immune cocktail therapy of an exosome/drug delivery multifunctional hydrogel accelerates fracture repair. *ACS Nano*. **2022**, *16*, 771-782.
25. Zeng, Z. L.; Xie, H. Mesenchymal stem cell-derived extracellular vesicles: a possible therapeutic strategy for orthopaedic diseases: a narrative review. *Biomater Transl*. **2022**, *3*, 175-187.
26. Chen, S.; Chen, X.; Geng, Z.; Su, J. The horizon of bone organoid: a perspective on construction and application. *Bioact Mater*. **2022**, *18*, 15-25.
27. Keshara, R.; Kim, Y. H.; Grapin-Botton, A. Organoid imaging: seeing development and function. *Annu Rev Cell Dev Biol*. **2022**, *38*, 447-466.
28. Liu, H.; Sun, J.; Wang, M.; Wang, S.; Su, J.; Xu, C. Intestinal organoids and organoids extracellular vesicles for inflammatory bowel disease treatment. *Chem Eng J*. **2023**, *465*, 142842.
29. Liu, H.; Su, J. Organoid and organoid extracellular vesicles for osteoporotic fractures therapy: current status and future perspectives. *Interdiscip Med*. **2023**, *1*, e20230011.
30. Bock, C.; Boutros, M.; Camp, J. G.; Clarke, L.; Clevers, H.; Knoblich, J. A.; Liberali, P.; Regev, A.; Rios, A. C.; Stegle, O.; Stunnenberg, H. G.; Teichmann, S. A.; Treutlein, B.; Vries, R. G. J.; Human cell atlas 'biological network' organoids. The organoid cell atlas. *Nat Biotechnol*. **2021**, *39*, 13-17.
31. Garreta, E.; Kamm, R. D.; Chuva de Sousa Lopes, S. M.; Lancaster, M. A.; Weiss, R.; Treppe, X.; Hyun, I.; Montserrat, N. Rethinking organoid technology through bioengineering. *Nat Mater*. **2021**, *20*, 145-155.
32. Brandenburg, N.; Hoehnel, S.; Kuttler, F.; Homicsko, K.; Ceroni, C.; Ringel, T.; Gjorevski, N.; Schwank, G.; Coukos, G.; Turcatti, G.; Lutolf, M. P. High-throughput automated organoid culture via stem-cell aggregation in microcavity arrays. *Nat Biomed Eng*. **2020**, *4*, 863-874.
33. Lancaster, M. A.; Knoblich, J. A. Organogenesis in a dish: modeling development and disease using organoid technologies. *Science*. **2014**, *345*, 1247125.
34. Zha, Q. B.; Yao, Y. F.; Ren, Z. J.; Li, X. J.; Tang, J. H. Extracellular vesicles: an overview of biogenesis, function, and role in breast cancer. *Tumour Biol*. **2017**, *39*, 1010428317691182.
35. van Niel, G.; D'Angelo, G.; Raposo, G. Shedding light on the cell biology of extracellular vesicles. *Nat Rev Mol Cell Biol*. **2018**, *19*, 213-228.
36. Mathieu, M.; Martin-Jaular, L.; Lavieu, G.; Théry, C. Specificities of secretion and uptake of exosomes and other extracellular vesicles for cell-to-cell communication. *Nat Cell Biol*. **2019**, *21*, 9-17.
37. Jin, S.; Wang, Y.; Wu, X.; Li, Z.; Zhu, L.; Niu, Y.; Zhou, Y.; Liu, Y. Young exosome bio-nanoparticles restore aging-impaired tendon stem/progenitor cell function and reparative capacity. *Adv Mater*. **2023**, *35*, e2211602.
38. Record, M.; Carayon, K.; Poirot, M.; Silvente-Poirot, S. Exosomes as new vesicular lipid transporters involved in cell-cell communication and various pathophysiological processes. *Biochim Biophys Acta*. **2014**, *1841*, 108-

- 120.
39. Nguyen, A.; Yaffe, M. B. Proteomics and systems biology approaches to signal transduction in sepsis. *Crit Care Med.* **2003**, *31*, S1-6.
 40. Murphy, D. E.; de Jong, O. G.; Brouwer, M.; Wood, M. J.; Lavieu, G.; Schiffelers, R. M.; Vader, P. Extracellular vesicle-based therapeutics: natural versus engineered targeting and trafficking. *Exp Mol Med.* **2019**, *51*, 1-12.
 41. Pegtel, D. M.; Gould, S. J. Exosomes. *Annu Rev Biochem.* **2019**, *88*, 487-514.
 42. Zhang, Q.; Wang, L.; Wang, S.; Cheng, H.; Xu, L.; Pei, G.; Wang, Y.; Fu, C.; Jiang, Y.; He, C.; Wei, Q. Signaling pathways and targeted therapy for myocardial infarction. *Signal Transduct Target Ther.* **2022**, *7*, 78.
 43. Zhong, L.; Liao, D.; Li, J.; Liu, W.; Wang, J.; Zeng, C.; Wang, X.; Cao, Z.; Zhang, R.; Li, M.; Jiang, K.; Zeng, Y. X.; Sui, J.; Kang, T. Rab22a-Neof1 fusion protein promotes osteosarcoma lung metastasis through its secretion into exosomes. *Signal Transduct Target Ther.* **2021**, *6*, 59.
 44. Dutta, D.; Heo, I.; Clevers, H. Disease modeling in stem cell-derived 3D organoid systems. *Trends Mol Med.* **2017**, *23*, 393-410.
 45. Shao, H.; Im, H.; Castro, C. M.; Breakefield, X.; Weissleder, R.; Lee, H. New technologies for analysis of extracellular vesicles. *Chem Rev.* **2018**, *118*, 1917-1950.
 46. Rong, Y.; Wang, Z.; Tang, P.; Wang, J.; Ji, C.; Chang, J.; Zhu, Y.; Ye, W.; Bai, J.; Liu, W.; Yin, G.; Yu, L.; Zhou, X.; Cai, W. Engineered extracellular vesicles for delivery of siRNA promoting targeted repair of traumatic spinal cord injury. *Bioact Mater.* **2023**, *23*, 328-342.
 47. Zhang, Q.; Jeppesen, D. K.; Higginbotham, J. N.; Franklin, J. L.; Coffey, R. J. Comprehensive isolation of extracellular vesicles and nanoparticles. *Nat Protoc.* **2023**, *18*, 1462-1487.
 48. Lai, J. J.; Chau, Z. L.; Chen, S. Y.; Hill, J. J.; Korpany, K. V.; Liang, N. W.; Lin, L. H.; Lin, Y. H.; Liu, J. K.; Liu, Y. C.; Lunde, R.; Shen, W. T. Exosome processing and characterization approaches for research and technology development. *Adv Sci (Weinh).* **2022**, *9*, e2103222.
 49. Takov, K.; Yellon, D. M.; Davidson, S. M. Comparison of small extracellular vesicles isolated from plasma by ultracentrifugation or size-exclusion chromatography: yield, purity and functional potential. *J Extracell Vesicles.* **2019**, *8*, 1560809.
 50. Chattrairat, K.; Yasui, T.; Suzuki, S.; Natsume, A.; Nagashima, K.; Iida, M.; Zhang, M.; Shimada, T.; Kato, A.; Aoki, K.; Ohka, F.; Yamazaki, S.; Yanagida, T.; Baba, Y. All-in-one nanowire assay system for capture and analysis of extracellular vesicles from an ex vivo brain tumor model. *ACS Nano.* **2023**, *17*, 2235-2244.
 51. Dong, L.; Zieren, R. C.; Horie, K.; Kim, C. J.; Mallick, E.; Jing, Y.; Feng, M.; Kuczler, M. D.; Green, J.; Amend, S. R.; Witwer, K. W.; de Reijke, T. M.; Cho, Y. K.; Pienta, K. J.; Xue, W. Comprehensive evaluation of methods for small extracellular vesicles separation from human plasma, urine and cell culture medium. *J Extracell Vesicles.* **2020**, *10*, e12044.
 52. Foers, A. D.; Chatfield, S.; Dagley, L. F.; Scicluna, B. J.; Webb, A. I.; Cheng, L.; Hill, A. F.; Wicks, I. P.; Pang, K. C. Enrichment of extracellular vesicles from human synovial fluid using size exclusion chromatography. *J Extracell Vesicles.* **2018**, *7*, 1490145.
 53. Hu, Y.; Li, X.; Zhang, Q.; Gu, Z.; Luo, Y.; Guo, J.; Wang, X.; Jing, Y.; Chen, X.; Su, J. Exosome-guided bone targeted delivery of Antagomir-188 as an anabolic therapy for bone loss. *Bioact Mater.* **2021**, *6*, 2905-2913.
 54. Xu, X.; Liang, Y.; Li, X.; Ouyang, K.; Wang, M.; Cao, T.; Li, W.; Liu, J.; Xiong, J.; Li, B.; Xia, J.; Wang, D.; Duan, L. Exosome-mediated delivery of kartogenin for chondrogenesis of synovial fluid-derived mesenchymal stem cells and cartilage regeneration. *Biomaterials.* **2021**, *269*, 120539.
 55. Szvicsek, Z.; Oszvald, Á.; Szabó, L.; Sándor, G. O.; Kelemen, A.; Soós, A.; Pálóczi, K.; Harsányi, L.; Tölgyes, T.; Dede, K.; Bursics, A.; Buzás, E. I.; Zeöld, A.; Wiener, Z. Extracellular vesicle release from intestinal organoids is modulated by Apc mutation and other colorectal cancer progression factors. *Cell Mol Life Sci.* **2019**, *76*, 2463-2476.
 56. Abdollahi, S. Extracellular vesicles from organoids and 3D culture systems. *Biotechnol Bioeng.* **2021**, *118*, 1029-1049.
 57. Wu, W.; Zhou, W.; Jiang, J.; Wang, M.; Zhang, J.; Yang, J.; Tang, Q.; Liu, H.; Liu, D.; Xu, W.; Zhong, J. L.; Yang, L.; Lei, M. Mechanical stimuli-induced CCL2 restores adult mouse cells to regenerate hair follicles. *Mol Ther Nucleic Acids.* **2023**, *32*, 94-110.
 58. Rocha, S.; Carvalho, J.; Oliveira, P.; Voglstaetter, M.; Schwartz, D.; Thomsen, A. R.; Walter, N.; Khanduri, R.; Sanchez, J. C.; Keller, A.; Oliveira, C.; Nazarenko, I. 3D cellular architecture affects microRNA and protein cargo of extracellular vesicles. *Adv Sci (Weinh).* **2019**, *6*, 1800948.
 59. Yuan, X.; Sun, L.; Jeske, R.; Nkosi, D.; York, S. B.; Liu, Y.; Grant, S. C.; Meckes, D. G., Jr.; Li, Y. Engineering extracellular vesicles by three-dimensional dynamic culture of human mesenchymal stem cells. *J Extracell Vesicles.* **2022**, *11*, e12235.
 60. Liu, C.; Chen, X.; Liu, Y.; Sun, L.; Yu, Z.; Ren, Y.; Zeng, C.; Li, Y. Engineering extracellular matrix-bound nanovesicles secreted by three-dimensional human mesenchymal stem cells. *Adv Healthc Mater.* **2023**, *12*, e2301112.
 61. Zhang, Y.; Chopp, M.; Zhang, Z. G.; Katakowski, M.; Xin, H.; Qu, C.; Ali, M.; Mahmood, A.; Xiong, Y. Systemic administration of cell-free exosomes generated by human bone marrow derived mesenchymal stem cells cultured under 2D and 3D conditions improves functional recovery in rats after traumatic brain injury. *Neurochem Int.* **2017**, *111*, 69-81.
 62. Jalilian, E.; Massoumi, H.; Bigit, B.; Amin, S.; Katz, E. A.; Guaiquil, V. H.; Anwar, K. N.; Hematti, P.; Rosenblatt, M. I.; Djalilian, A. R. Bone marrow mesenchymal stromal cells in a 3D system produce higher concentration of extracellular vesicles (EVs) with increased complexity and enhanced neuronal growth properties. *Stem Cell Res Ther.* **2022**, *13*, 425.
 63. Ural, E. E.; Toomajian, V.; Hoque Apu, E.; Veleic, M.; Balasingham, I.; Ashammakhi, N.; Kanada, M.; Contag, C. H. Visualizing extracellular vesicles and their function in 3D tumor microenvironment models. *Int J Mol Sci.* **2021**, *22*, 4784.
 64. He, C.; Zheng, S.; Luo, Y.; Wang, B. Exosome theranostics: biology and translational medicine. *Theranostics.* **2018**, *8*, 237-255.
 65. Yang, B.; Chen, Y.; Shi, J. Exosome biochemistry and advanced nanotechnology for next-generation theranostic platforms. *Adv Mater.* **2019**, *31*, e1802896.
 66. Cully, M. Exosome-based candidates move into the clinic. *Nat Rev Drug Discov.* **2021**, *20*, 6-7.
 67. Zinger, A.; Cvetkovic, C.; Sushnitha, M.; Naoi, T.; Baudo, G.; Anderson, M.; Shetty, A.; Basu, N.; Covelto, J.; Tasciotti, E.; Amit, M.; Xie, T.; Taraballi, F.; Krencik, R. Humanized biomimetic nanovesicles for neuron targeting. *Adv Sci (Weinh).* **2021**, *8*, e2101437.
 68. Tauro, B. J.; Greening, D. W.; Mathias, R. A.; Mathivanan, S.; Ji, H.; Simpson, R. J. Two distinct populations of exosomes are released from LIM1863 colon carcinoma cell-derived organoids. *Mol Cell Proteomics.* **2013**, *12*, 587-598.
 69. Jurj, A.; Pasca, S.; Braicu, C.; Rusu, I.; Korban, S. S.; Berindan-Neagoe, I. Focus on organoids: cooperation and interconnection with

Organoid extracellular vesicles

- extracellular vesicles - Is this the future of in vitro modeling? *Semin Cancer Biol.* **2022**, *32*, 367-381.
70. Valadi, H.; Ekström, K.; Bossios, A.; Sjöstrand, M.; Lee, J. J.; Lötvall, J. O. Exosome-mediated transfer of mRNAs and microRNAs is a novel mechanism of genetic exchange between cells. *Nat Cell Biol.* **2007**, *9*, 654-659.
 71. Théry, C.; Duban, L.; Segura, E.; Véron, P.; Lantz, O.; Amigorena, S. Indirect activation of naïve CD4+ T cells by dendritic cell-derived exosomes. *Nat Immunol.* **2002**, *3*, 1156-1162.
 72. Zhang, Y.; Yan, Y.; Meng, J.; Girotra, M.; Ramakrishnan, S.; Roy, S. Immune modulation mediated by extracellular vesicles of intestinal organoids is disrupted by opioids. *Mucosal Immunol.* **2021**, *14*, 887-898.
 73. Roush, S.; Slack, F. J. The let-7 family of microRNAs. *Trends Cell Biol.* **2008**, *18*, 505-516.
 74. Lee, H.; Han, S.; Kwon, C. S.; Lee, D. Biogenesis and regulation of the let-7 miRNAs and their functional implications. *Protein Cell.* **2016**, *7*, 100-113.
 75. Watanabe, S.; Kobayashi, S.; Ogasawara, N.; Okamoto, R.; Nakamura, T.; Watanabe, M.; Jensen, K. B.; Yui, S. Transplantation of intestinal organoids into a mouse model of colitis. *Nat Protoc.* **2022**, *17*, 649-671.
 76. Vissink, A.; Mitchell, J. B.; Baum, B. J.; Limesand, K. H.; Jensen, S. B.; Fox, P. C.; Elting, L. S.; Langendijk, J. A.; Coppes, R. P.; Reyland, M. E. Clinical management of salivary gland hypofunction and xerostomia in head-and-neck cancer patients: successes and barriers. *Int J Radiat Oncol Biol Phys.* **2010**, *78*, 983-991.
 77. Sun, B. K.; Siprashvili, Z.; Khavari, P. A. Advances in skin grafting and treatment of cutaneous wounds. *Science.* **2014**, *346*, 941-945.
 78. Adine, C.; Ng, K. K.; Rungarunlert, S.; Souza, G. R.; Ferreira, J. N. Engineering innervated secretory epithelial organoids by magnetic three-dimensional bioprinting for stimulating epithelial growth in salivary glands. *Biomaterials.* **2018**, *180*, 52-66.
 79. Chansaenroj, A.; Adine, C.; Charoenlapanit, S.; Roytrakul, S.; Sariya, L.; Osathanon, T.; Rungarunlert, S.; Urkasemsin, G.; Chaisuparat, R.; Yodmuang, S.; Souza, G. R.; Ferreira, J. N. Magnetic bioassembly platforms towards the generation of extracellular vesicles from human salivary gland functional organoids for epithelial repair. *Bioact Mater.* **2022**, *18*, 151-163.
 80. Liang, Y.; Duan, L.; Lu, J.; Xia, J. Engineering exosomes for targeted drug delivery. *Theranostics.* **2021**, *11*, 3183-3195.
 81. Liang, Y.; Xu, X.; Li, X.; Xiong, J.; Li, B.; Duan, L.; Wang, D.; Xia, J. Chondrocyte-targeted microRNA delivery by engineered exosomes toward a cell-free osteoarthritis therapy. *ACS Appl Mater Interfaces.* **2020**, *12*, 36938-36947.
 82. Zou, J.; Shi, M.; Liu, X.; Jin, C.; Xing, X.; Qiu, L.; Tan, W. Aptamer-functionalized exosomes: elucidating the cellular uptake mechanism and the potential for cancer-targeted chemotherapy. *Anal Chem.* **2019**, *91*, 2425-2430.
 83. Wen, M.; Wang, J.; Ou, Z.; Nie, G.; Chen, Y.; Li, M.; Wu, Z.; Xiong, S.; Zhou, H.; Yang, Z.; Long, G.; Su, J.; Liu, H.; Jing, Y.; Wen, Z.; Fu, Y.; Zhou, T.; Xie, H.; Guan, W.; Sun, X.; Wang, Z.; Wang, J.; Chen, X.; Jiang, L.; Qin, X.; Xue, Y.; Huang, M.; Huang, X.; Pan, R.; Zhen, H.; Du, Y.; Li, Q.; Huang, X.; Wu, Y.; Wang, P.; Zhao, K.; Situ, B.; Hu, X.; Zheng, L. Bacterial extracellular vesicles: A position paper by the microbial vesicles task force of the Chinese society for extracellular vesicles. *Interdiscip Med.* **2023**, *1*, e20230017.
 84. Lin, L.; Guo, Z.; He, E.; Long, X.; Wang, D.; Zhang, Y.; Guo, W.; Wei, Q.; He, W.; Wu, W.; Li, J.; Wo, L.; Hong, D.; Zheng, J.; He, M.; Zhao, Q. SIRT2 regulates extracellular vesicle-mediated liver-bone communication. *Nat Metab.* **2023**, *5*, 821-841.
 85. Wang, L.; Wang, D.; Ye, Z.; Xu, J. Engineering extracellular vesicles as delivery systems in therapeutic applications. *Adv Sci (Weinh).* **2023**, *10*, e2300552.
 86. Ji, N.; Wang, F.; Wang, M.; Zhang, W.; Liu, H.; Su, J. Engineered bacterial extracellular vesicles for central nervous system diseases. *J Control Release.* **2023**, *364*, 46-60.
 87. Lin, Y.; Wu, J.; Gu, W.; Huang, Y.; Tong, Z.; Huang, L.; Tan, J. Exosome-liposome hybrid nanoparticles deliver CRISPR/Cas9 system in MSCs. *Adv Sci (Weinh).* **2018**, *5*, 1700611.
 88. Cui, Y.; Guo, Y.; Kong, L.; Shi, J.; Liu, P.; Li, R.; Geng, Y.; Gao, W.; Zhang, Z.; Fu, D. A bone-targeted engineered exosome platform delivering siRNA to treat osteoporosis. *Bioact Mater.* **2022**, *10*, 207-221.
 89. Smyth, T.; Petrova, K.; Payton, N. M.; Persaud, I.; Redzic, J. S.; Graner, M. W.; Smith-Jones, P.; Anchordoquy, T. J. Surface functionalization of exosomes using click chemistry. *Bioconjug Chem.* **2014**, *25*, 1777-1784.
 90. Shi, Y.; Guo, S.; Liang, Y.; Liu, L.; Wang, A.; Sun, K.; Li, Y. Construction and evaluation of liraglutide delivery system based on milk exosomes: a new idea for oral peptide delivery. *Curr Pharm Biotechnol.* **2022**, *23*, 1072-1079.
 91. Cheng, K.; Zhao, R.; Li, Y.; Qi, Y.; Wang, Y.; Zhang, Y.; Qin, H.; Qin, Y.; Chen, L.; Li, C.; Liang, J.; Li, Y.; Xu, J.; Han, X.; Anderson, G. J.; Shi, J.; Ren, L.; Zhao, X.; Nie, G. Bioengineered bacteria-derived outer membrane vesicles as a versatile antigen display platform for tumor vaccination via plug-and-display technology. *Nat Commun.* **2021**, *12*, 2041.
 92. Li, Y.; Zhao, R.; Cheng, K.; Zhang, K.; Wang, Y.; Zhang, Y.; Li, Y.; Liu, G.; Xu, J.; Xu, J.; Anderson, G. J.; Shi, J.; Ren, L.; Zhao, X.; Nie, G. Bacterial outer membrane vesicles presenting programmed death 1 for improved cancer immunotherapy via immune activation and checkpoint inhibition. *ACS Nano.* **2020**, *14*, 16698-16711.
 93. Yang, Y.; Hong, Y.; Nam, G. H.; Chung, J. H.; Koh, E.; Kim, I. S. Virus-mimetic fusogenic exosomes for direct delivery of integral membrane proteins to target cell membranes. *Adv Mater.* **2017**, *29*, 1605604.
 94. Chatterjee, M.; Özdemir, S.; Kunadt, M.; Koel-Simmelink, M.; Boiten, W.; Piepkorn, L.; Pham, T. V.; Chiasserini, D.; Piersma, S. R.; Knol, J. C.; Möbius, W.; Mollenhauer, B.; van der Flier, W. M.; Jimenez, C. R.; Teunissen, C. E.; Jahn, O.; Schneider, A. C1q is increased in cerebrospinal fluid-derived extracellular vesicles in Alzheimer's disease: A multi-cohort proteomics and immuno-assay validation study. *Alzheimers Dement.* **2023**, *19*, 4828-4840.
 95. Piffoux, M.; Silva, A. K. A.; Wilhelm, C.; Gazeau, F.; Taresté, D. Modification of extracellular vesicles by fusion with liposomes for the design of personalized biogenic drug delivery systems. *ACS Nano.* **2018**, *12*, 6830-6842.
 96. Chen, Q.; Huang, G.; Wu, W.; Wang, J.; Hu, J.; Mao, J.; Chu, P. K.; Bai, H.; Tang, G. A hybrid eukaryotic-prokaryotic nanoplatform with photothermal modality for enhanced antitumor vaccination. *Adv Mater.* **2020**, *32*, e1908185.
 97. Yi, K.; Rong, Y.; Huang, L.; Tang, X.; Zhang, Q.; Wang, W.; Wu, J.; Wang, F. Aptamer-exosomes for tumor theranostics. *ACS Sens.* **2021**, *6*, 1418-1429.
 98. Sun, S.; Liu, H.; Hu, Y.; Wang, Y.; Zhao, M.; Yuan, Y.; Han, Y.; Jing, Y.; Cui, J.; Ren, X.; Chen, X.; Su, J. Selection and identification of a novel ssDNA aptamer targeting human skeletal muscle. *Bioact Mater.* **2023**, *20*, 166-178.
 99. Haney, M. J.; Klyachko, N. L.; Zhao, Y.; Gupta, R.; Plotnikova, E. G.; He, Z.; Patel, T.; Piroyan, A.; Sokolsky, M.; Kabanov, A. V.; Batrakov, A.

- E. V. Exosomes as drug delivery vehicles for Parkinson's disease therapy. *J Control Release*. **2015**, *207*, 18-30.
100. Hajipour, H.; Farzadi, L.; Roshangar, L.; Latifi, Z.; Kahroba, H.; Shahnazi, V.; Hamdi, K.; Ghasemzadeh, A.; Fattahi, A.; Nouri, M. A human chorionic gonadotropin (hCG) delivery platform using engineered uterine exosomes to improve endometrial receptivity. *Life Sci*. **2021**, *275*, 119351.
 101. Zha, Y.; Li, Y.; Lin, T.; Chen, J.; Zhang, S.; Wang, J. Progenitor cell-derived exosomes endowed with VEGF plasmids enhance osteogenic induction and vascular remodeling in large segmental bone defects. *Theranostics*. **2021**, *11*, 397-409.
 102. Alvarez-Erviti, L.; Seow, Y.; Yin, H.; Betts, C.; Lakkhal, S.; Wood, M. J. Delivery of siRNA to the mouse brain by systemic injection of targeted exosomes. *Nat Biotechnol*. **2011**, *29*, 341-345.
 103. Chen, C. Y.; Rao, S. S.; Yue, T.; Tan, Y. J.; Yin, H.; Chen, L. J.; Luo, M. J.; Wang, Z.; Wang, Y. Y.; Hong, C. G.; Qian, Y. X.; He, Z. H.; Liu, J. H.; Yang, F.; Huang, F. Y.; Tang, S. Y.; Xie, H. Glucocorticoid-induced loss of beneficial gut bacterial extracellular vesicles is associated with the pathogenesis of osteonecrosis. *Sci Adv*. **2022**, *8*, eabg8335.
 104. Liu, J. H.; Chen, C. Y.; Liu, Z. Z.; Luo, Z. W.; Rao, S. S.; Jin, L.; Wan, T. F.; Yue, T.; Tan, Y. J.; Yin, H.; Yang, F.; Huang, F. Y.; Guo, J.; Wang, Y. Y.; Xia, K.; Cao, J.; Wang, Z. X.; Hong, C. G.; Luo, M. J.; Hu, X. K.; Liu, Y. W.; Du, W.; Luo, J.; Hu, Y.; Zhang, Y.; Huang, J.; Li, H. M.; Wu, B.; Liu, H. M.; Chen, T. H.; Qian, Y. X.; Li, Y. Y.; Feng, S. K.; Chen, Y.; Qi, L. Y.; Xu, R.; Tang, S. Y.; Xie, H. Extracellular vesicles from child gut microbiota enter into bone to preserve bone mass and strength. *Adv Sci (Weinh)*. **2021**, *8*, 2004831.
 105. Liu, H.; Wu, Y.; Wang, F.; Wang, S.; Ji, N.; Wang, M.; Zhou, G.; Han, R.; Liu, X.; Weng, W.; Tan, H.; Jing, Y.; Zhang, W.; Zhang, H.; Shi, Z.; Su, J. Bone-targeted engineered bacterial extracellular vesicles delivering miRNA to treat osteoporosis. *Compos B Eng*. **2023**, *267*, 111047.
 106. Kalluri, R.; McAndrews, K. M. The role of extracellular vesicles in cancer. *Cell*. **2023**, *186*, 1610-1626.
 107. Eastlake, K.; Wang, W.; Jayaram, H.; Murray-Dunning, C.; Carr, A. J. F.; Ramsden, C. M.; Vugler, A.; Gore, K.; Clemo, N.; Stewart, M.; Coffey, P.; Khaw, P. T.; Limb, G. A. Phenotypic and functional characterization of Müller glia isolated from induced pluripotent stem cell-derived retinal organoids: improvement of retinal ganglion cell function upon transplantation. *Stem Cells Transl Med*. **2019**, *8*, 775-784.
 108. Eastlake, K.; Lamb, W. D. B.; Luis, J.; Khaw, P. T.; Jayaram, H.; Limb, G. A. Prospects for the application of Müller glia and their derivatives in retinal regenerative therapies. *Prog Retin Eye Res*. **2021**, *85*, 100970.
 109. Xu, X.; Song, J. Segmental long bone regeneration guided by degradable synthetic polymeric scaffolds. *Biomater Transl*. **2020**, *1*, 33-45.
 110. Yuan, G.; Li, Z.; Lin, X.; Li, N.; Xu, R. New perspective of skeletal stem cells. *Biomater Transl*. **2022**, *3*, 280-294.
 111. Arthur, P.; Kandoi, S.; Sun, L.; Kalvala, A.; Kutlehria, S.; Bhattacharya, S.; Kulkarni, T.; Nimma, R.; Li, Y.; Lamba, D. A.; Singh, M. Biophysical, molecular and proteomic profiling of human retinal organoid-derived exosomes. *Pharm Res*. **2023**, *40*, 801-816.
 112. Liu, C.; Helsen, S.; Marzano, M.; Chen, X.; Muok, L.; Esmonde, C.; Zeng, C.; Sun, L.; Grant, S. C.; Li, Y. Human forebrain organoid-derived extracellular vesicle labeling with iron oxides for in vitro magnetic resonance imaging. *Biomedicines*. **2022**, *10*, 3060.
 113. Wang, Y.; Chu, X.; Wang, B. Recombinant adeno-associated virus-based gene therapy combined with tissue engineering for musculoskeletal regenerative medicine. *Biomater Transl*. **2021**, *2*, 19-29.

Received: September 30, 2023

Revised: November 24, 2023

Accepted: December 5, 2023

Available online: December 28, 2023

Advances in electrode interface materials and modification technologies for brain-computer interfaces

Yunke Jiao¹, Miao Lei¹, Jianwei Zhu¹, Ronghang Chang¹, Xue Qu^{1,2,3,*}

Key Words:

biomaterials; brain-computer interface; conductive polymer; interface materials; microstructure; neuroelectrode

From the Contents

Introduction	213
Challenges of Implantable Neuroelectrodes in Brain Tissue	214
Literature Search	215
Interface Determines Electrode Function	215
Neuroelectrode Materials	215
Neuroelectrode Interface Materials	219
Coating Fabrication Techniques	223
Structure Design of Coatings with Cellular Modulation Capabilities	225
Conclusion and Prospect	226

ABSTRACT

Recent advances in neuroelectrode interface materials and modification technologies are reviewed. Brain-computer interface is the new method of human-computer interaction, which not only can realise the exchange of information between the human brain and external devices, but also provides a brand-new means for the diagnosis and treatment of brain-related diseases. The neural electrode interface part of brain-computer interface is an important area for electrical, optical and chemical signal transmission between brain tissue system and external electronic devices, which determines the performance of brain-computer interface. In order to solve the problems of insufficient flexibility, insufficient signal recognition ability and insufficient biocompatibility of traditional rigid electrodes, researchers have carried out extensive studies on the neuroelectrode interface in terms of materials and modification techniques. This paper introduces the biological reactions that occur in neuroelectrodes after implantation into brain tissue and the decisive role of the electrode interface for electrode function. Following this, the latest research progress on neuroelectrode materials and interface materials is reviewed from the aspects of neuroelectrode materials and modification technologies, firstly taking materials as a clue, and then focusing on the preparation process of neuroelectrode coatings and the design scheme of functionalised structures.

*Corresponding author:

Xue Qu,
quxue@ecust.edu.cn.

<http://doi.org/10.12336/biomatertransl.2023.04.003>

How to cite this article:

Jiao, Y.; Lei, M.; Zhu, J.; Chang, R.; Qu, X.
Advances in electrode interface materials and modification technologies for brain-computer interfaces. *Biomater Transl.* 2023, 4(4), 213-233.



Introduction

Since the discovery of electrical signals in the brain in the 1920s, people have been constantly searching for ways to decipher its thinking process and explore new methods of interaction between the human brain and the outside world. Brain-computer interface (BCI) recognises multiple electrical signals generated by the human brain during thought processes through neural electrodes, and converts them into meaningful information. This innovative approach does not rely on conventional extracerebral peripheral nerve-to-muscle output pathways but instead establishes a novel non-muscular channel between the human brain and computers or other electronic devices, enabling barrier-free interaction and control of information. The new non-muscular channel established between the

human brain and computers or other electronic devices achieves barrier-free interaction and control of information. Implantable electrodes used to detect local neural signals have probes that can be embedded in designated areas of the cerebral cortex, providing a very high degree of accuracy in electroencephalogram signal transmission, while implantable BCIs can not only output and interpret human brain signals from the inside out, but also input and transform electrical signals from the outside in to reverse stimulate neurons and restore specific neural activity. BCI has provided a brand-new window for the study of brain activities and diagnosis of brain-related diseases,^{1,2} as well as serving as a novel treatment tool for neurological damage caused by diseases or injuries. For example, technological and theoretical advances in

neuroscience and implantable BCIs have introduced potential solutions for a wide range of common neurological-related disorders, including deafness, blindness, epilepsy, and depression.³ Neuroelectrodes play a crucial role in signalling within BCIs as they determine the quality and efficiency of communication. This is essential to ensure the stable and effective operation of the BCI system. The electrode interface serves as the area where electrical, optical, and chemical signals are transmitted between the brain tissue system and external electronic devices. As the “bridge” of the BCI, it is also where the electrode material directly contacts biological tissues. The signal interaction ability, biocompatibility, and long-term stability of this interface directly impact the working efficiency and lifespan of BCI electrodes.

Currently, the mainstream neuroelectrodes on the market are still dominated by conventional electronic materials, such as metals and inorganic semiconductor materials; however, the high modulus of elasticity of the conventional electrode materials obviously leads to their inability to match the brain tissue. To solve this problem, electrode interface materials have been extensively investigated. One approach is to modify the structure of conventional metal and semiconductor electrode materials to enhance their flexibility. For example, a promising direction is to fabricate electrodes with smaller dimensions, such as thin films or filament structures.⁴⁻⁶ Meanwhile, modifying the electrode surface with nanostructures,⁷⁻⁹ such as modifying metal nanopatterns, or rough surface electrodes with nanoparticles, not only increases the surface area of the electrode interface and improves the contact with the neural tissue, but the surfaces with some specific structures also make the electrode interface have more biocompatible, which is more conducive to the neuron cell growth in the contact. After metals and semiconductors, another category that has received attention is the carbon nanomaterials for electrodes, which range from carbon quantum dots, carbon nanowires, and carbon nanotubes (CNTs), to graphene, and have variable structural features and therefore a wide range of tunable properties.¹⁰⁻¹² In addition, carbon nanomaterials have better biocompatibility than metals and semiconductor materials, as well as good electrical properties.¹²⁻¹⁵ With the rise of conductive polymers (CPs),¹⁶⁻¹⁸ more flexible organic materials have successfully expanded the choice of interface materials for neuroelectrodes. Polymer hydrogels as well as bio-based materials,^{19, 20} as implants, possess better biocompatibility and even bioactivity, and have been widely used in the field of tissue repair and other areas since early days, and after improving the electrical properties through specific structures or doping with conductive components,²¹⁻²³ these organic materials have also demonstrated promising prospects in the field of neuroelectrodes.

In this review, we first introduce the biological responses of neuroelectrodes after implantation into brain tissues and the decisive role of the interfaces for electrode function.

Afterwards, we review the latest research progress of neuroelectrode materials and interface materials from the aspects of neuroelectrode materials and modification technologies. Specifically, we discuss the materials used for neuroelectrodes as a starting point and subsequently delve into the preparation process of neuroelectrode coatings and the design of functional structures.

Challenges of Implantable Neuroelectrodes in Brain Tissue

Specificity of brain tissue

Brain tissue is one of the softest and most fragile tissues compared to other tissues in the human body.²⁴ Neural axons in brain tissue break at about 18% strain,²⁵ so rigid implants will inevitably cause damage to neural tissue when entering the brain. The brain and other central nervous tissues are mechanically protected throughout the body by other sturdy tissues, such as the dura mater and skull. Therefore, compared to other tissues, brain tissue is hardly exposed to mechanical stress from the outside nor does it generate as much internal mechanical stress as tissues such as muscles or blood vessels.²⁶ So once exposed to external mechanical stress, brain tissue is more susceptible to mechanical injury. Moreover, although brain tissue has a regenerative mechanism, self-repair of neural tissue after damage is difficult. One point is due to the unfavourable microenvironment formed by post-injury inflammation, and the second is the lack of healthy extracellular matrix, and the presence of neuroglial scarring affects neuronal survival, regeneration and axonal growth.²⁷

Foreign body reaction after electrode implantation

Foreign body reaction inevitably occurs when implanting any material into the tissues of a living organism,²⁸ and similarly, foreign body reaction occurs during the implantation of neuroelectrodes into brain tissues. The first and most critical event that occurs during the implantation of electrodes is the disruption of the blood-brain barrier,^{29, 30} where the infiltration of blood cells and plasma proteins triggers a series of dynamic biochemical alterations and an inflammatory cascade with multicellular involvement at the tissue-electrode material interface. Within minutes after blood-brain barrier injury, resting microglia are activated as primary effectors, transforming into a “pro-inflammatory” phenotype³¹ and initiating an acute immune response. In the following hours, oligodendrocytes are activated and begin to participate in neuronal repair.³² And in the subsequent days, astrocytes are activated by interleukin-1 β , tumour necrosis factor- α , and complement component 1q from microglia,³³ and gradually accumulate near the electrode and form a glial scar.³⁴ Further, activated astrocytes no longer provide an appropriate nerve regeneration matrix while synthesising and secreting inhibitory and damaging factors leading to neuronal loss and reduced fibre density.³⁵ In summary, the stress response initiated by

1 Key Laboratory for Ultrafine Materials of Ministry of Education, School of Material Science and Engineering, Frontiers Science Center for Materiobiology and Dynamic Chemistry, East China University of Science and Technology, Shanghai, China; 2 Wenzhou Institute of Shanghai University, Wenzhou, Zhejiang Province, China; 3 Shanghai Frontier Science Center of Optogenetic Techniques for Cell Metabolism, Shanghai, China

microglia undergoes several days of indirect cellular forces that ultimately prevents the intimate contact and communication between neurons and electrodes, both in terms of physical space and biochemical cues. And when the electrodes are implanted in brain tissue, a highly dynamic and complex inflammatory microenvironment consisting of multiple cells and factors forms on their surface, thereby impeding direct dialogue between neurons and the electrode surface.

Literature Search

Articles on neuroelectrode materials for BCIs and neuroelectrode coating technology were searched using the search terms: “brain-computer interfaces” or “neuroelectrodes” combined with “coating materials”, “coating technology”, and “microstructure”, respectively. These searches were conducted on the Web of Science in July 2023, and articles published after 2018 have been collected in order of publication. After careful screening, 145 articles were included in this review.

Interface Determines Electrode Function

Electrical properties

The most basic function of implantable microelectrodes is to acquire electrophysiological signals from neurons, and the signal quality is reflected in several metrics, including signal-to-noise ratio, single-unit recording capability, and long-term recording capability.^{36,37} In BCI systems, ions are the carriers of signals transmitted along the nerve, and electrons are the medium in the electrode. Therefore, the neuroelectrode interface is where the ionic signals are converted into electronic signals, and the electrical properties of the neuroelectrode, such as the interface impedance between the electrode and the brain tissue, and the amount of charge storage, determine the quality of the signals recorded by the electrode.^{38,39} The interfacial impedance, in turn, is affected by the roughness of the neuroelectrode interface, its area, and the electrical/ion exchange capacity of the interfacial material.⁴⁰

Biocompatibility

Biocompatibility is reflected in several aspects. Firstly, the electrode material itself should be non-biotoxic. Secondly, it should cause as little mechanical damage to the brain tissue as possible during and after implantation, and lastly, it should induce as little immune response as possible during long-term use. Mechanical damage caused during the implantation of neuroelectrodes is the beginning of the immune response, which triggers a series of inflammatory cascade reactions that will firstly disturb the local tissue microenvironment around the neuroelectrode, thus affecting the collection of electrophysiological signals from the electrode to the surrounding area.⁴¹⁻⁴³ In contrast, reducing the size of the implant⁴⁴⁻⁴⁶ and increasing its flexibility⁴⁷⁻⁴⁹ are methods to minimise mechanical damage to the implant. The long-term biocompatibility of the electrodes after implantation, on the other hand, is challenged by the ability to adapt the elastic modulus of the neuroelectrode to the brain tissue,⁵⁰⁻⁵² the ability of the electrode interface to inhibit immune responses,⁵³⁻⁵⁵ and the stability of the electrodes during long-term use.⁵⁶⁻⁵⁸

Bioactivity

Bioactivity is a higher requirement for current neuroelectrode interfaces. Biocompatibility aims to make the implant “invisible” to biological tissues, thus escaping immune tracking and minimising the impact of immune responses. However, due to the unavoidable damage caused by implantation and the difficulty of repairing neuronal cells that are damaged, biocompatibility alone cannot meet the requirement for high quality signal transmission. To achieve the goal of non-destructive implantation, the neuroelectrode needs to be bioactive. In other words, through specific morphology of the electrode interface^{59,60} and modification of the bioactive components,⁶¹⁻⁶³ the neuronal cell repair can be actively regulated, and the neural axon growth can be promoted, so that the neural tissues around the electrodes can restore the pre-implantation state, and even establish a tighter connection.

Neuroelectrode Materials

Inorganic materials

Metal and inorganic semiconductor materials are traditional neuroelectrode materials with good chemical inertness and electrical properties, but it is often difficult for metal and semiconductor materials to adapt to the needs of brain tissues for elastic modulus and biocompatibility. In recent years, researchers have made progress in improving the performance of neuroelectrodes made of inorganic materials by designing the composition and structure of neuroelectrodes made of metals and semiconductors. Meanwhile, the rise of new carbon nanomaterials, such as nanodiamond, CNTs, and graphene, has also provided new directions for inorganic neuroelectrodes. Carbon nanomaterials have great potential in the field of neuroelectrodes due to their extremely low toxicity, high biocompatibility and unique optical, electrical, magnetic and chemical properties.

Metal electrodes

Traditional metal electrodes often use precious metals such as aurum (Au), platinum (Pt), etc. Precious metals have good electrical conductivity and chemical stability, but their excessive elastic modulus makes them difficult to be compatible with brain tissue. One way to reduce the elastic modulus of metal electrodes is to make the metal partially ultrathin.⁶⁴⁻⁶⁶ For example, cylindrical three dimensional (3D) Au thin-film microelectrodes fabricated using the microelectrode array (MEA) technique, with the sidewalls insulated with poly(parylene C) and the tip modified by wet etching and/or the application of a titanium nitride coating, exhibit low impedance and low intrinsic noise levels.⁴ Hong et al.⁶⁷ developed nucleation-inducing seed layers using biocompatible polyelectrolyte multilayer metal films using flexible and transparent ultrathin (< 10 nm) Au MEAs (**Figure 1A**) with low sheet resistance (< 5 Ω^{-1}), high light transmission (> 77%), and excellent mechanical bending performance (600 mm bending radius for one cycle) (**Figure 1B**). Miniaturising metal electrodes is an effective way to increase their flexibility, but the size of bioelectrode materials is limited by the electron mean free range, and materials with sizes smaller than the electron average free range inhibit electron mobility. Lim et

al.⁶⁸ prepared a nanocomposite of whiskered Au nanosheets (Figure 1C). While possessing high tensile properties, the permeation threshold (1.56 vol%) was maintained below that of Au nanoparticles (5.02 vol%) and Au nanosheets (2.74 vol%). Another category of metallic materials suitable for neuroelectrodes is room-temperature liquid metals (LMs) such as gallium-based alloys that are liquid at room temperature. LMs show potential for neuroelectrodes due to their fluidity, high electrical conductivity, and high biocompatibility.^{69–71} LM-based fluidic cuff electrodes, which are highly flexible and maintain excellent electrical conductivity even when stretched to 200% of their original length, are capable of transducing peripheral nerve signals and delivering neural stimuli for up to 2 weeks under exercise.⁷² Zhang et al.⁷¹ developed a 20-channel neuroelectrode array based on the eutectic Ga–In alloy (75.5%

gallium and 24.5% indium) in a 20-channel neural electrode array. Electrochemical impedance spectroscopy tests showed that the studied LM electrode has a similar interfacial impedance to the Pt electrode; the maximum and minimum impedances of the LM-type electrode are 0.75 M Ω /4.1 k Ω (2.77 M Ω /5.2 k Ω for the Pt electrode), in the same range, over the test frequency range of 1×10^{-1} – 1×10^5 Hz (Figure 1D). Dong et al.⁶⁹ prepared highly stretchable neural electrode arrays by screen-printing an LM conductor onto a poly(dimethylsiloxane) substrate (Figure 1E), which exhibited stable electrical properties at 100% strain. However, the chemical properties of LMs under physiological conditions limit their *in vivo* application, e.g., in environments above 1 ppm oxygen content, an oxidised layer rapidly forms on the surface of Ga, leading to a decrease in conductivity at the interface.^{73,74}

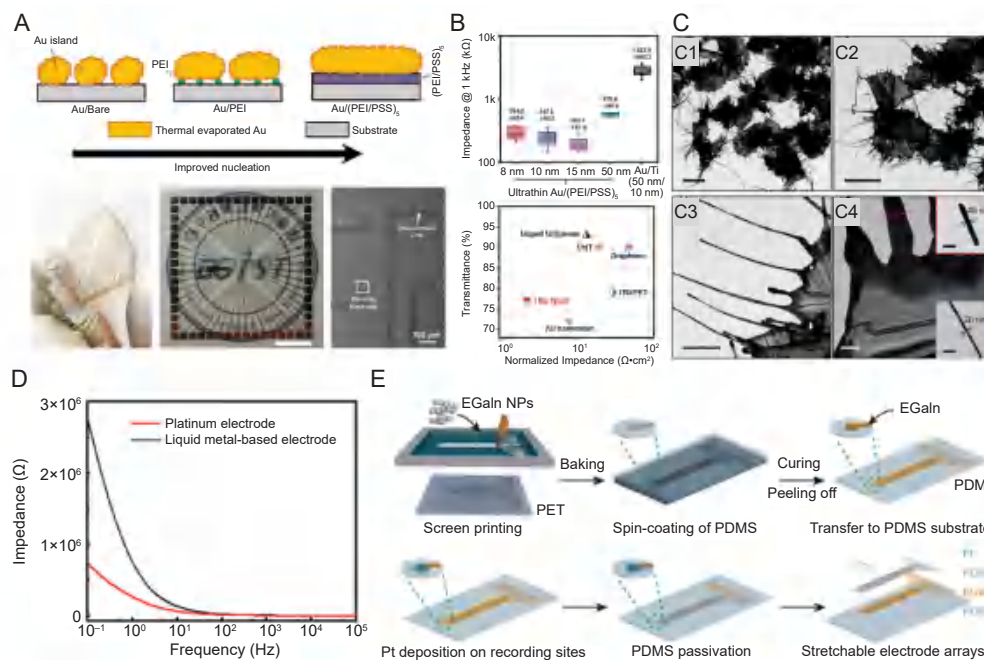


Figure 1. New metal material electrode. (A) Schematic of the formation process of ultrathin Au electrodes on polyelectrolyte coatings and photographic and microscopic images of Au/(PEI/PSS)₅ MEA on plastic. (B) The magnitude of the impedance at 1 kHz (top) and a comparison of the area-normalised electrochemical impedance and light transmittance in a recently developed neuro-microelectrode (bottom). A and B were reprinted from Hong et al.⁶⁷ Copyright 2022 Wiley-VCH GmbH. Reproduced with permission. (C) TEM images of whiskered Au nanosheets showing the overall morphology and magnified views of the edge portion of the whiskers. Scale bars: 5 μ m (C1, C2), 1 μ m (C3), 200 nm (C4). Reprinted with permission from Lim et al.⁶⁸ Copyright 2022 American Chemical Society. (D) The EIS curves of the LM-based and Pt electrodes under 1×10^{-1} up to 1×10^5 Hz at a scan rate of 0.1 V/s (in normal saline, 10 mV sine wave).⁷¹ (E) Fabrication of stretchable metal electrodes based on liquid metal-polymer conductors using screen printing, which reprinted from Dong et al.⁶⁹ Copyright 2021 Wiley-VCH GmbH. Reproduced with permission. Au: aurum; EGaIn: eutectic gallium–indium alloy; EIS: electrochemical impedance spectroscopy; LM: liquid metal; MEA: microelectrode array; NP: nanoparticle; PDMS: poly(dimethylsiloxane); PEI: polyethylenimine; PET: polyethylene terephthalate; PSS: poly(styrene sulfonate); Pt: platinum; TEM: transmission electron microscopy.

Semiconductor materials

Semiconductor materials are rich in composition and structure, and can be tuned and processed to exhibit a variety of properties and produce a multitude of functions to suit applications in different scenarios.

Traditional silicon-based electrodes can conform to brain movements when processed into microneedle arrays on flexible stretchable substrates. Lee et al.⁷⁵ demonstrated a 1024-channel penetrating silicon microneedle array using a double-sided lithographic microfabrication process (Figure

2A–C) to successfully record single-cell activity in mice under both optogenetic and whisker-air blowing stimuli for up to 196 days. Suzuki et al.⁷⁶ used a complementary metal oxide semiconductor MEA with 236,880 electrodes each measuring $11.22 \mu\text{m}^2$ and covering an area of $5.5 \times 5.9 \text{ mm}^2$ to provide a detailed single-cell level neural activity analysis platform for brain slices, human induced pluripotent stem cell-derived cortical networks, peripheral neurons, and organ tissues of the human brain. Two-dimensional transition metal carbides (MXene) have excellent metal conductivity, electrochemical stability, and higher volumetric capacitance than conventional carbon-based electrode materials.^{77–79} Rafieerad et al.⁷⁸ prepared a novel Ta₄C₃T_x MXene-tantalum oxide hybrid-structure electrode based on MXenes, innovatively using

a fluorine-free etching technique to achieve superior bulk capacitance while maintaining biocompatibility. As shown in **Figure 2D**, the titanium dioxide (TiO₂)-based electrode arrays of reconfigurable anatase-brookite polycrystalline mesoporous layers exhibited excellent selectivity and fast photoconductive response to ultraviolet radiation, high stability in aqueous solution while maintaining a high switching ratio of 10 for 5 more than 30 days, and excellent biocompatibility for cell transfer and growth.⁸⁰ Zhang et al.⁸¹ developed an active fully transparent electrocorticography array based on zinc oxide thin-film transistors (**Figure 2E**, and **F**) with a transparency of up to 85% and a higher signal-to-noise ratio than Au grid electrodes (zinc oxide thin-film transistors 13.2 dB, Au grids 19.9 dB).

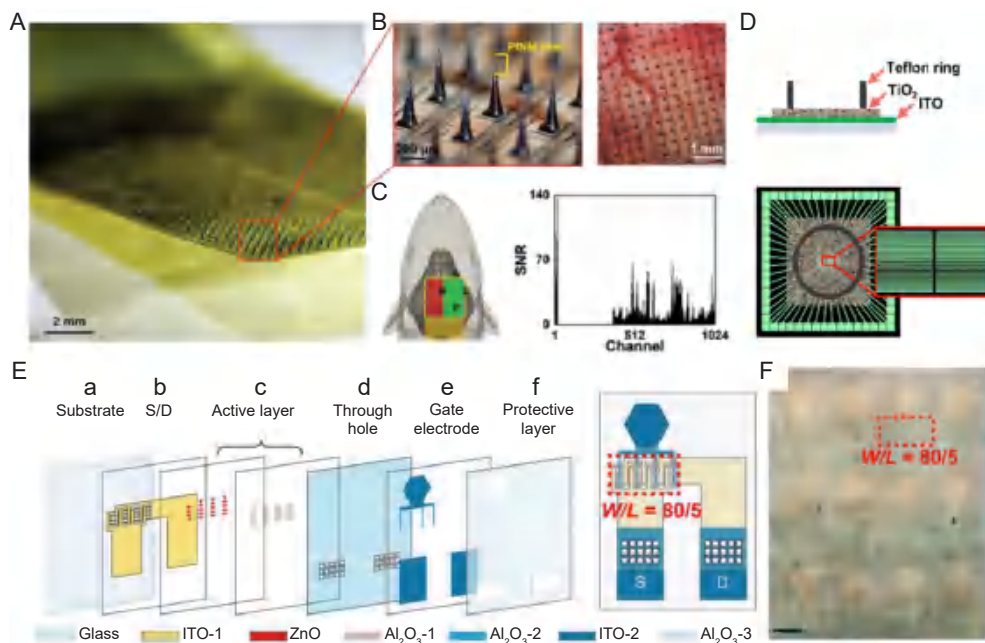


Figure 2. Semiconductor materials neuroelectrodes. (A) Photograph of a 1024-channel SiMNA and a magnified view of an array with a tapered SiMN with a height of approximately $300 \mu\text{m}$ and a tip coated with PtNM. Scale bar: 2 mm . (B) Magnified view of a 1024-channel SiMNA implanted in the right hemisphere of the rat brain. Scale bar: $200 \mu\text{m}$ (left), 1 mm (right). (C) Schematic diagram of SiMNA implantation in the right hemisphere with electrical connections pointing toward the back of the rat (green highlighted area indicates successful implantation of cortical SiMNs, while the SiMN in the red highlighted area is located at the top of the rat skull) and a signal-to-noise histogram of whisker blowing stimulation evoked LFP response. A–C were reprinted from Lee et al.⁷⁵ Copyright 2022 Wiley-VCH GmbH. Reproduced with permission. (D) Side and top views of patterned TiO₂ electrodes. The green parallel lines in the top view represent ITO patterns attached to 60 external contact pads.⁷⁸ (E) Left: (a, b) The first ITO layer of 100-nm thickness for source and drain, (c) 20-nm thick ZnO active layer and the first Al₂O₃ layer of 10-nm thickness for the ZnO layer protection, (d) the second Al₂O₃ layer of 20-nm thickness as the gate dielectric layer and through-holes punched in the layer, (e) the second ITO layer of 100-nm thickness for the gate electrodes, and (f) the third Al₂O₃ layer of 20-nm thickness to protect the whole device. Right: Structure of a ZnO-TFT electrode. The red dashed square labels a transistor with $W/L = 80/5$, which consist of 16 transistors with $W/L = 5/5$ in parallel. (F) Microscopic image of a 3×4 ZnO-TFT array. The red dashed frame labels an active region consisting of 16 paralleled ZnO-TFT, corresponding to that in the red dashed frame in E (right). Scale bar: $200 \mu\text{m}$. E and F were reprinted from Zhang et al.⁸¹ Al₂O₃: aluminum oxide; D: drain; ITO: indium-tin-oxide; LFP: local field potential; PtNM: platinum nanomesh; S: source; SiMNA: silicon microneedle array; SNR: signal-to-noise ratio; TFT: thin-film transistor; TiO₂: titanium dioxide; W/L : width-to-length ratio; ZnO: zinc oxide.

Carbon nanomaterials

Carbon nanomaterials, ranging from carbon quantum dots, CNTs to graphene, have versatile structural features, which also contribute to the special functionality of carbon nanomaterials,

which are widely used as neuroelectrode materials on the basis of possessing high chemical stability and biocompatibility.^{82–84} Flexible CNT fibre were able to continuously record signals from the spinal cord of freely moving rats for 3–4 months

without electrode repositioning and successfully recorded individual neurons and local field potential activities in response to mechanical stimulation of somatic cells.⁸⁵ Yang et al.⁸⁶ developed a flexible multifunctional electrode based on CNT arrays, which, compared with conventional Au electrodes, has a larger electrochemically active area (3.54 times), higher specific capacitance (13.75 times) and charge storage capacity (2.66 times). As shown in **Figure 3A**, Xiong et al.^{87,88} prepared a multilayer graphene hydrogel membrane by flow self-assembly of chemically transformed graphene nanosheets. Although Young's modulus of this multilayer graphene hydrogel membrane was not sufficient to match the nerve tissue,

there was almost no inflammatory response after 8 weeks of implantation in the sciatic nerve of rats. It can be concluded that due to the sliding between the graphene layers, the multilayer graphene hydrogel membrane showed significant viscoelasticity, which enhanced contact while reducing compression (**Figure 3B**), thus reducing inflammation due to the stiffness mismatch. Xiong et al.⁸⁹ developed a graphene-based fibre optical electrode, which dramatically enhanced the charge storage capacity of the graphene fibre electrode while maintaining the excellent electrical properties of the graphene fibre electrode, which was able to safely deliver stimulation currents up to 504.04 mC/cm².

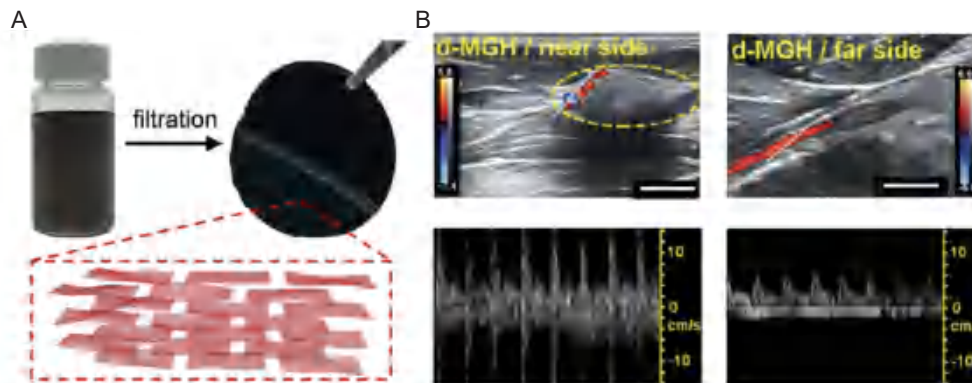


Figure 3. Neuroelectrodes are made of carbon nanomaterials. (A) Photograph of graphene dispersion and MGH membrane (top). The inset (bottom) outlines the multilayer structure of the MGH membrane made of CCG nanosheets (red).⁸⁷ (B) Proximal and distal d-MGH at 8 weeks after implantation. The color bars represent the blood flow velocity. Scale bars: 5.0 mm (left), 2.0 mm (right).⁸⁷ CCG: chemically converted graphene; d-MGH: CCG nanosheets densely packed MGH; MGH: multilayer graphene hydrogel.

Conductive polymers

CP materials provide a softer interface and excellent biocompatibility while being able to guarantee the required electrical properties of nerve electrodes.⁹⁰⁻⁹² Hydrogels have a tunable 3D structure, are water-rich and have a low modulus of elasticity, as can imitate the chemical-mechanical properties of neural tissues, and CP hydrogels are therefore widely used as neuroelectrode materials. Liang et al.⁹³ used polypyrrole (PPy)-modified microgel as a cross-linking agent to generate electrically conductive transparent hydrogels. By restricting the conductive components to the surface of the microgel, the interaction between the particles and light waves was reduced, thus improving the transparency of the hydrogel while maintaining good electrical conductivity. Xia et al.⁹⁴ developed a set of polymer network hydrogels interpenetrated with poly(N-isopropylacrylamide) and poly(Cu-arylacetyl) (HCuM). Poly(Cu-arylacetates) has intrinsic electronic conductivity and unique fluorescent properties for optoelectronic, photocatalytic, and bioimaging applications. The presence of the poly(Cu-arylacetyl) component allows it to exhibit extreme adhesion, resistance to swelling (**Figure 4A**, and **B**), excellent antimicrobial properties, and high biocompatibility. Hydrogels have a wide range of advantages as neuroelectrode materials, but the inherent electrical conductivity is generally poor and other methods are needed to enhance their electrical properties. Among these,

doping of nanometallic materials (nanowires, nanosheets or nanoparticles) and carbon materials (nanotubes or graphene) are common ways to improve the conductivity of hydrogels. Rinoldi et al.⁹⁵ developed a flexible neuroelectrode interface material consisting of a polyacrylamide hydrogel loaded with plasmonic Ag nanocubes. The incorporation of Ag nanocubes enabled the hydrogel to obtain excellent conductive properties, with a 2.4-fold enhancement in conductivity at 10 Hz compared to pure polyacrylamide hydrogel (**Figure 4C**, and **D**). Won et al.⁹⁶ prepared conductive fibres doped with Au nanoparticles in the outer layer by using osmotic pressure to control the distribution of Au ions in the polymer network, and the uptake and reduction of the Au precursor in polyurethane fibres. High electrical conductivity ($\sigma = 7.68 \times 10^4$ S/m) and low impedance ($|Z| = 2.88 \times 10^3 \Omega$) were obtained while maintaining the original modulus of elasticity of the polyurethane fibres.

Poly(3,4-ethylenedioxythiophene):poly(styrene sulfonate) (PEDOT:PSS) hydrogels⁹⁷⁻⁹⁹ have attracted much attention among CP hydrogels due to their higher electrical conductivity induced by well-connected CP networks.¹⁰⁰⁻¹⁰² Li et al.¹⁰³ designed a stretchable network electrode by combining the CP PEDOT:PSS hydrogel as a top layer with a resilient polystyrene-ethylene-butylene-styrene substrate bond. It is characterised by the use of a network design with a large strain range, which maintains a remarkably high level of electrical properties under huge strains compared to conventional electrodes.

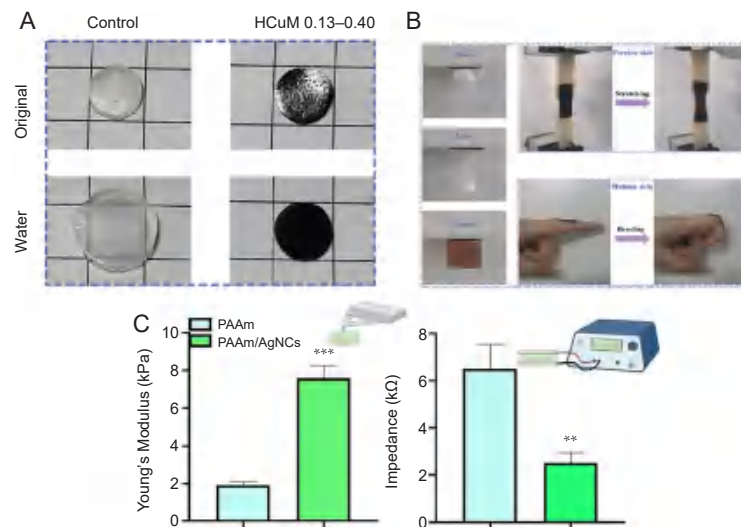


Figure 4. Neuroelectrodes are made of conductive polymer materials. (A) Swelling study of pNIPAm hydrogel and HCuM 0.13–0.40 in water for 5 days. (B) Demonstration of adhesion of HCuM 0.13–0.40. A and B were reprinted from Hong et al.⁹⁴ Copyright 2022 Wiley-VCH GmbH. Reproduced with permission. (C) Histogram of Young's modulus, showing the mechanical properties of PAAm/AgNCs compared to PAAm hydrogels, measured by nanoindentation method (left) and histogram of the electrical impedance values, measured at a physiologically significant frequency (10 Hz), showing the superior electrical properties of the PAAm/AgNCs hydrogel (right). Data are expressed as mean \pm SD. $^{***}P \leq 0.01$, $^{**}P \leq 0.001$. Reprinted with permission from Rinoldi et al.⁹⁵ Copyright 2023 American Chemical Society. AgNC: silver nanocube; HCuM: a set of polymer network hydrogels interpenetrated with poly(*N*-isopropylacrylamide) and poly(*Cu*-arylacetyl); PAAm: polyacrylamide.

Bio-based materials

Biobased materials are characterised by high biocompatibility, biodegradability, and sustainability, whereas biopolymers such as hyaluronic acid,¹⁰⁴ alginate,^{105, 106} chitosan,^{107, 108} filipin,^{109–111} and collagen^{112–114} not only possess the general characteristics of biobased materials, but also low immunogenicity, anti-inflammatory, and even bioactivity.¹¹⁵ These biological properties, which are difficult to be possessed by inorganic and polymer materials, have led to the widespread interest in bio-based materials in the field of neuroelectrodes. Zhou et al.¹¹⁶ designed a hybrid probe consisting of multiple flexible MEAs wrapped in silk proteins. Zhou's team took advantage of the properties of silk proteins, which have a high stiffness when dry and a significant decrease in stiffness after absorbing water, to design a neuroelectrode that actively adapts to its environment. The filipin-coated probes remain hard before implantation to facilitate surgical implantation, and after implantation, the filipin softens when it comes into contact with body fluids and absorbs water, which reduces its mechanical strength and allows it to remain mechanically compliant with the surrounding tissue. This variable mechanical property ensured high-fidelity implantation of the electrodes, and the electrode worked appropriately and elicited a small immune response when observed 2 months after implantation. Yang et al.¹¹⁷ used bacterial cellulose, a flexible substrate synthesised by microorganisms with low mechanical strength, as the electrode substrate material to fabricate a bacterial cellulose-based neuroelectrode system, and eight weeks after implantation, the bacterial cellulose electrodes remained conformally adhered to the surface of the surrounding tissues and maintained the curvilinear shape with minimal immunoreactivity.

Neuroelectrode Interface Materials

In addition to designing the structure and performance of the electrode body material, decorating the basic electrode with functional coating materials is another feasible solution to the functional limitations of the electrode body. The electrode interface is the area where the electrode body is in direct contact with the brain tissue, and it is also an important area for the transmission of electrical signals and cellular activities. Therefore, it can be considered that the performance of this interface determines overall electrode functionality. As an interface material, coatings can exist temporarily or permanently alongside the body electrode, providing a functional surface that extends or compensates for its capabilities.

In terms of modulating the bioactivity of the implanted materials, some studies have doped anti-inflammatory agents,¹¹⁸ cell attachment molecules,^{119, 120} and neurotrophic factors^{121, 122} into the coating materials to improve the microenvironment around the neuroelectrodes and coordinate the biological responses of different cell types through passive diffusion or controlled delivery. In addition, well-designed coatings can provide micro-woven surfaces, such as microconical structures or random nano-textures that match the cellular characteristics of neurons. These textured surfaces or 3D structures located at cellular and subcellular scales can modulate the immune response of glial cells, promote direct neuronal attachment and growth, as well as synaptic growth and extension, and strengthen neuronal survival.

Metal coating

Although traditional precious metal materials possess extremely high electrical conductivity, it is often difficult to avoid the problem of mismatch between elastic modulus and brain tissue when used for the electrode body, but using nano-metallic materials for the coating material of flexible electrode substrate is another approach to solve the problem.

Through adjusting the immersion and exudation time, a network of Au nanoparticles was formed on the polymer fibre shell, which showed excellent electrical properties (conductivity 7.68×10^4 S/m impedance $2.88 \times 10^3 \Omega$ at 1 kHz) with an elastic modulus approximating the brain tissue and achieved stable recording of electrical signals for up to 4 months.⁹⁶ In addition to being used to improve organic flexible electrode material substrates, metal coatings are often used to modify metal electrodes because the added coating does not affect the biocompatibility of the original electrode when the electrode substrate is identical to the coating material. Ramesh et al.¹²³⁻¹²⁵ performed pulsed direct-current electrophoretic deposition of laser-generated platinum nanoparticles on platinum-based 3D neuroelectrodes and found that this coating of platinum nanoparticles was sufficiently stable (Figure 5A) and the total mass of platinum around the electrodes was below the systemic toxicity-related concentrations after 4 weeks of experiments in the rat brain. By functionalising the metal coating with a structural design, the liquid can improve the performance of the electrode without changing the coating material. The internal structure and surface morphology of metal

electrodes also affect the flexibility, electrical conductivity, and biocompatibility of neuroelectrodes. As shown in Figure 5B, Yang et al.¹²⁶ proposed a dual-microcrack coupling strategy to enhance the stretchability of metal electrodes by utilising the complementarity between two layers of Au microcracked films. The double-microcrack-coupled electrode fabricated using this method has a much lower resistance change ($R/R_0 = 5.6$) and exhibits a high stretchability of $\sim 200\%$ at 100% strain (Figure 5C, and D).

Inorganic coatings

The combination of inorganic semiconductor materials and metal electrode substrates can achieve controllable tuning of the electrical properties of neuroelectrodes. The impedance and intrinsic noise level of microelectrodes were successfully reduced by modifying titanium nitride coatings by wet etching on micro-Au cylindrical MEAs.⁴ Nguyen et al.¹²⁷ designed a wide bandgap material system consisting of silicon carbide (SiC) nanomembranes as the Faraday interface and silicon dioxide (SiO₂) as the encapsulation layer, which, while maintaining the bio-interface and biosensing functions, showing remarkable electrical stability (Figure 5E). The hybrid structure of SiC/SiO₂ is extremely resistant to degradation and can guarantee the proper functioning of the underlying electronic components for at least a decade, with the potential for long-term sustained use over the lifetime of the patient. Cyclic bending test surfaces that the hybrid structure has excellent mechanical flexibility and electrical stability, and is able to form conformal contacts with biological tissues.

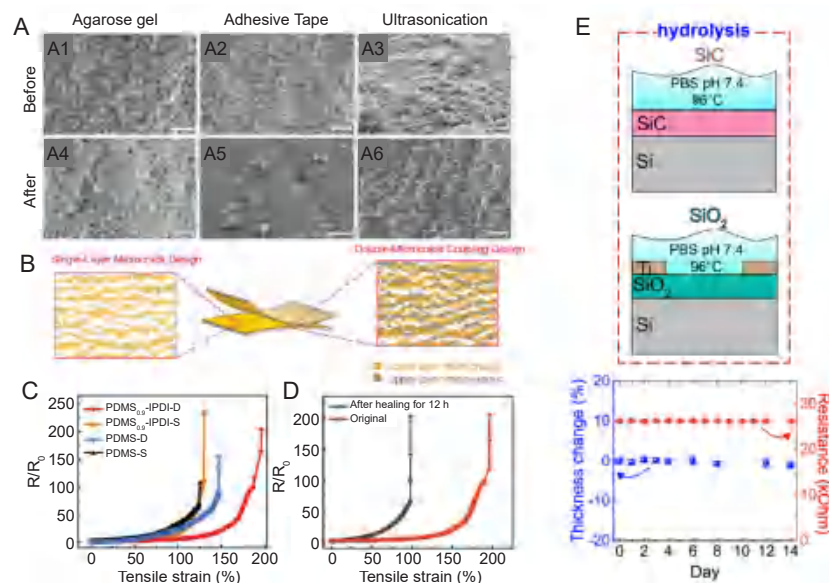


Figure 5. Coating of metallic materials for neural electrodes. (A) SEM images of the side of the PDC-coated neural electrode before (A1–3) and after (A4–6) mechanical stability tests. Scale bars: 500 nm.¹²³ (B) Schematic diagrams of stretchable electrodes based on a single-layer microcrack design and a dual microcrack-coupled design. (C) R/R_0 versus tensile strain for Au electrodes based on PDMS 0.9-IPDI and PDMS substrates, respectively (-D for a double-layer microcrack, -S for a single-layer microcrack). (D) Dual microcrack-coupled PDMS 0.9-IPDI electrodes Change in tensile resistance after 12 hours of healing at 25°C. B–D were reprinted from Yang et al.¹²⁶ Copyright 2023 Wiley-VCH GmbH. Reproduced with permission. (E) Soaking test of hydrolysis in SiC and as-grown SiO₂ in 1× PBS at different temperatures up to 96°C (top) and SiC thickness and electrical resistance variations after the accelerated hydrolysis test in PBS at 96°C after up to 14 days (bottom).¹²⁷ Au: aurum; IPDI: isophorone diisocyanate; PBS: phosphate buffer solution; PDC: pulsed direct current; PDMS: poly(dimethylsiloxane); R/R_0 : resistance change; SEM: scanning electron microscope; SiC: silicon carbide; SiO₂: silicon dioxide; Ti: titanium.

Carbon materials are also frequently used as coating materials for neuroelectrodes due to their excellent electrical conductivity and good biocompatibility. Pt/iridium (Ir) neuroelectrodes coated with graphene oxide, fabricated using electrochemical reduction techniques, resulted in a 15.2-fold increase in charge storage capacity and a 90% reduction in impedance with only a 3.8% increase in electrode diameter.¹²⁸ A hybrid coating of reduced graphene oxide and Pt was able to reduce impedance by a factor of 60 by electrodeposition on planar Pt microelectrodes, allowing long-term detection of neural spike potentials in epileptic mice.¹²⁹ Liu et al.⁸² modified conventional metallic silver electrodes with graphene to form a van der Waals heterostructure at the interface. The graphene/silver electrode interface impedance was reduced to $161.4 \pm 13.4 \text{ M}\Omega/\mu\text{m}^2$, and the cathode charge storage capacity reached $24.2 \pm 1.9 \text{ mC}/\text{cm}^2$, which was 6.3 and 48.4 times higher than that of commercial silver electrodes, respectively.

Conductive polymer coatings

CPs can be used both as a substrate material for neuroelectrodes and as a modified coating material for neuroelectrodes. The construction of hydrogel networks using CPs can confer other important characteristics required for their neuroelectrode materials, such as bioadhesion, flexibility, and antifouling ability. One study prepared a PEDOT/polydopamine melanin coating (**Figure 6A**) by doping polydopamine melanin with PEDOT, which enabled it to exhibit better electrochemical and mechanical stability than PEDOT/PSS and was able to maintain cell proliferation and even promote cell differentiation into neuronal networks (**Figure 6B**, and **C**).¹³⁰ Saunier et al.¹³¹ electrochemically method by depositing carbon nanofibres with PEDOT on Au MEAs to prepare PEDOT:carbon nanofibre thin film coatings. The synergistic effect of carbon nanofibres and PEDOT resulted in coatings with remarkable electrochemical properties combining low impedance, high charge injection capability, and reliable neurotransmitter monitoring. The properties of CPs are affected by doping compositions and synthesis modes, and in addition to varying the CPs'. In addition to changing the doping composition of CPs, the use of different polymerisation techniques can also lead to tunable properties of CPs. Some studies have used chemical polymerisation to directly polymerise PEDOT on the electrode sites, obtaining similar impedance and good stability to that of electro-polymerisation, which greatly improves the modification efficiency of multichannel electrodes compared to electro-polymerisation.¹³² Lim et al.¹³³ encapsulated Ga-based LM electrodes with PEDOT:PSS by electrochemical deposition to prevent LM from oxidising and degrading under physiological conditions. The study showed that the PEDOT-encapsulated LM electrodes, in a 6-week invertebrate model, recorded statistically higher signal-to-noise ratios compared to those of bare LM ($P = 0.017$) versus conventional platinum electrodes ($P = 0.061$; **Figure 6D**).

However, weak adhesion between PEDOT and metal electrodes is common, and unstable connections can easily lead to coating detachment thus leading to interface failure and loss of PEDOT functionality. There have been several previous attempts to improve the adhesion of PEDOT

coatings, such as roughening the substrate material¹³⁴ and introducing functional groups into the PEDOT monomer for modification.^{135,136} All of these approaches have made progress in enhancing the adhesion of PEDOT coatings, but there are still problems such as affecting the interfacial conductivity. Tian et al.¹³⁷ pre-polymerised thin layers of polydopamine (PDA) as an adhesive and then electropolymerised it with hydroxymethylated 3,4-ethylenedioxythiophene with PSS to form a stable interpenetrating PEDOT-MeOH:PSS/PDA network. The interfacial adhesion of the PEDOT-MeOH:PSS/PDA interface to the metal electrode substrate was significantly improved, retaining 93% of the area after 20 minutes of vigorous sonication, and the interfacial impedance was reduced by two orders of magnitude compared with that of the uncoated platinum-iron wire microelectrode.

Active substance grafting

A significant reason for the reduced signal reception efficiency of nerve electrodes during service is the contamination of nerve electrode materials with biomolecules from biological fluids, such as nonspecific adsorption of proteins such as bovine serum albumin, lysozyme and fibrinogen. Modification of antifouling molecules on the surface of neuroelectrodes can effectively reduce biomolecule adsorption, attenuate inflammatory responses and prolong the service life of neuroelectrodes. Lubricin is a biological anti-adhesion glycoprotein that rapidly self-assembles and firmly adheres to most interfaces including PPy (**Figure 7A**), resulting in an easy-to-apply and efficient coating.¹³⁸ Amphiphilic ion coatings are another common class of antifouling coatings, such as carboxybetaine, sulfobetaine, and phosphatidylcholine, which are active substances that enhance the hydrophilic properties of neuroelectrode surfaces. An ultrathin sulfobetaine coating consisting of PDA, polyethyleneimine, and poly(sulfobetaine methacrylate-co-methacrylic acid), was able to completely inhibit fibroblast adhesion *in vitro*, preventing cell adhesion for at least 31 days and maintaining stable electrode impedance.¹³⁹ Another study used a methacryloyloxyethyl phosphorylcholine coating polymerised *in situ* by gamma radiation to introduce antifouling properties to the surface of PPy, which showed excellent resistance to biofouling without affecting the conductivity of the electrode body and reduced scar tissue formation *in vivo*.¹⁴⁰ Lee et al.¹⁴¹ designed a virtually frictionless lubrication layer modification with a silicon-based neural probe, where the surface of the probe was functionalised with hydroxyl (-OH) groups by oxygen (O_2) plasma treatment, and then a self-assembled monolayer was formed with trichloro(1H,1H,2H,2H-perfluorooctyl)-silane using gas-phase deposition. As shown in **Figure 7B**, the lubricant layer-modified probe implantation friction was reduced by 86-fold, and the expression levels of ionised calcium-binding adapter molecule 1 and glial fibrillary acidic protein were significantly reduced in microglia and astrocytes in the vicinity of the probe.

Composite coating

As the "bridge" between brain tissue and external equipment, the interface of neuroelectrode needs to coordinate the dual needs of biological tissue and mechanical equipment, although

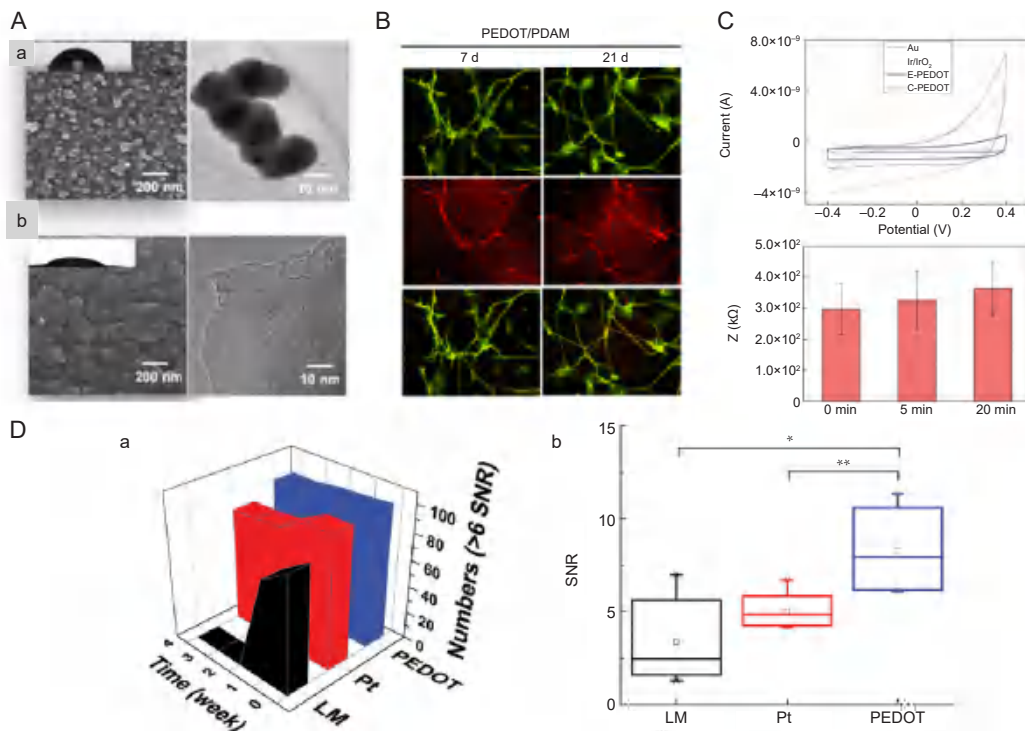


Figure 6. Conductive polymer material coatings for nerve electrodes. (A) SEM and TEM images of (a) PEDOT and (b) PEDOT/PDAM films. Scale bars: 200 nm (left), 10 nm (right). (B) Fluorescence images showing immunofluorescence staining of β -tubulin III (green), MAP2 (red), and nuclei (blue) after culturing neuronal progenitor cells in PEDOT/PDAM films for 21 days. (C) Cyclic voltammetry curves of chemically polymerised PEDOT and other interfaces ($n = 3$), impedance of electrodes at 20 kHz frequency after sonication. A–C were reprinted with permission from Huang et al.¹³⁰ Copyright 2022 American Chemical Society. (D) (a) The numbers of high-quality recording spikes (SNR > 6) of LM wire, Pt wire, and PEDOT LMEs for 4 weeks, and (b) analysis of variance test revealed the significant difference among the electrodes. * $P < 0.05$, ** $P < 0.01$. D was reprinted from Lim et al.¹³³ Copyright 2022 Wiley-VCH GmbH. Reproduced with permission. Au: aurum; C-PEDOT: chemical polymerization PEDOT; E-PEDOT: electropolymerization PEDOT; Ir: iridium; IrO₃: iridium trioxide; LM: liquid metal; LME: liquid metal based electrode; MAP2: microtubule-associated protein 2; PDAM: 1-pyrenyldiazomethane; PEDOT: poly(3,4-ethylenedioxythiophene); Pt: platinum; SEM: scanning electron microscope; SNR: signal-to-noise ratio; TEM: transmission electron microscope.

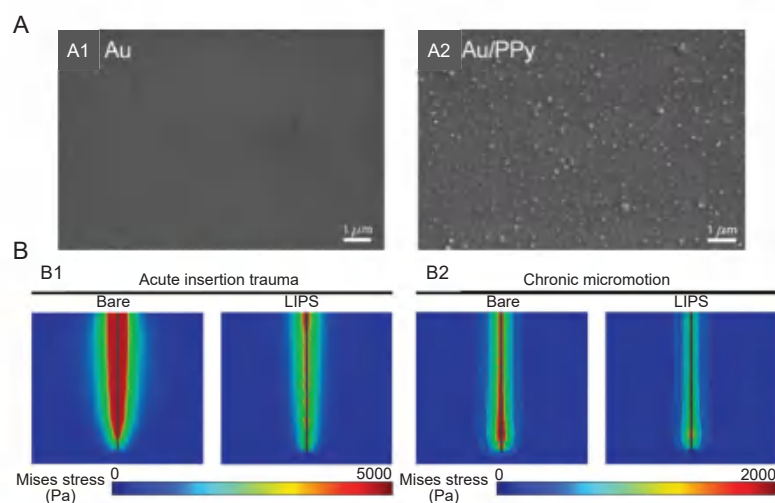


Figure 7. Coating with active substance grafts. (A) SEM images of (Aa) Au polyester film electrode and (A2) Au/PPy electrode surface. Reprinted with permission from Desroches et al.¹³⁸ Copyright 2020 American Chemical Society. (B) von Mises stress profiles of bare and LIPS-coated probes within brain tissue during insertion (B1) and under lateral micromotion of 100 μ m (B2).¹⁴¹ Au: aurum; LIPS: lubricated immune-stealthy probe surface; PPy: polypyrrole.

a variety of materials have been developed, a single material is often difficult to simultaneously meet the biological needs and electrical performance requirements. Combining different materials to prepare composite coatings is a common way to enhance the functionality of coatings.

Coatings made from metal and polymer materials are the most common composite coatings, and the excellent electrical conductivity of metals and the mechanical flexibility and biocompatibility of polymers can easily reach a mutual complementarity. Jain et al.¹⁴² designed a Au wire electrode with a nanoparticle Au shell and a hydrogel layer, which achieved an effective electrical/ionic coupling between the hydrogel and the Au wire through the nanostructured Au shells on the surface of the Au wire (**Figure 8A**). Chen et al.¹⁴³ proposed a tissue-like metal-doped hydrogel, which could achieve excellent electrical biosensing by introducing disulfide-modified silver nanowires into a bifunctional hyaluronic acid/carboxymethyl chitosan composite. Plasma silver nanocubes were also introduced into polyacrylamide hydrogels in a similar manner to enhance the electrical properties of the system.⁹⁵ Carbon materials, as discussed previously, are also common neuroelectrode coating materials as both excellent electrical properties and biocompatible materials. However, carbon materials such as CNT, although generally considered to be non-cytotoxic to neuronal cells, their direct exposure in human tissues has also been suggested to lead to abnormal activation of immune cells,¹⁴⁴ and increased neuronal excitability induced by CNT can promote neuronal regeneration, but overexcitability may also lead to neurological damage.¹⁴⁵ For neuroelectrode materials applied to brain tissues, in order to pursue higher biocompatibility, the risk of carbon material application can be reduced by compositing with polymer hydrogels. Ye et al.¹⁴⁶ mixed CNT with ionic liquids to obtain reticulated CNTs and transferred them into hydrogel matrices by *in-situ* polymerisation of suitable monomers in ionic liquids, which were then converted into CNT-poly(ethylene glycol) hydrogel composites by solvent substitution. poly(ethylene glycol) hydrogel composite (**Figure 8B**). PC-12 cells cultured on this composite showed enhanced differentiation and increased neuronal to astrocyte ratio in neural stem cells. Another study prepared a multifunctional coating presenting both the anti-inflammatory drug dexamethasone and neuroprotective factor on top of multiwalled CNTs (MWCNTs) and PPy composite coatings (**Figure 8C**),¹⁴⁷ which was capable of releasing dexamethasone mediated by exogenous stimuli and effectively inhibiting inflammatory factor secretion and astrocyte proliferation. The charge storage capacitances of PPy/PSS and MWCNTs/dexamethasone-PPy/ γ -poly(L-glutamic acid)/PSS-poly-L-lysine-nerve growth factor-modified electrodes were much larger than those of bare Au electrodes (**Figure 8D**). Among them, the capacitance change of MWCNTs/dexamethasone-PPy/ γ -poly(L-glutamic acid)/PSS-poly-L-lysine-nerve growth factor-modified electrode was small, suggesting that drug loading in the CP may lead to weakening of the long-term stability of conductive coatings, whereas MWCNTs sandwiched between smooth electrodes and CPs enhance the stability of the coating materials, and thus the electrochemical performance.

Natural biomaterials have excellent biocompatibility and even bioactivity, but they are also often used in combination with conductive materials because they generally do not possess conductive properties. Wei et al.¹⁴⁸ prepared a novel multimodal transparent electrophysiological hydrogel, by freeze-thawing method using polyvinyl alcohol, quaternary ammonium chitosan, and hyaluronic acid (PVA@HACC@HA) as a polymer network. multimodal transparent electrophysiological hydrogel has a low modulus of elasticity (0.15 MPa) and can be conformably and tightly adhered to brain tissues (**Figure 8C**, and **D**) causing minimal immune response due to mechanical damage; conducts electricity through ions and has a low interfacial impedance with brain tissues (150 Ω at 1 kHz); and has a transmittance of 93% in the wavelength range of 300–1100 nm. Ding et al.¹¹¹ constructed a conductive hydrogel electrode material of filipin protein by chemically grafting tyramine monomers onto CNTs and simultaneously constructing a 3D covalent network between silk fibroin and CNTs, which enabled faster gelation of silk fibroin. The 3D covalent network has good electro-permeability properties, which enhances the conductivity of the hydrogel by promoting the movement of electrons at the interface of the neuroelectrode, and enables more effective recording of weak neuroelectric signals.

Coating Fabrication Techniques

A variety of coating preparation techniques have been applied to the fabrication of neural electrode coatings, while neural electrodes are often characterised by low mechanical strength and miniaturized dimensions, and need to be in long-term service in the human body, which also puts forward higher requirements for coating technology. In addition to ensuring the long-term stability of the connection between the coating material and the electrode, advanced coating technology should also support the internal structure of the coating as well as the controllable preparation of the surface morphology. Currently, technologies for the controlled fabrication of coatings with specific structures and patterns can be roughly categorised into subtractive manufacturing (photolithography, etching)^{149–152} and additive manufacturing (chemical vapour deposition (CVD),^{153–155} electrochemical deposition,^{156–158} electrospinning,^{159–161} and microcontact printing).^{162–164} Using these techniques, it is possible to customise microscopic morphologies with specific geometric patterns, 3D structures, and roughness on electrode surfaces with different compositional structures and physicochemical properties at the micro (nano) metre scale.

Subtractive manufacturing

Photo-lithography, etching and laser ablation are common micro-fabrication processes that are now widely used for the preparation of micro-electrode arrays or other 3D electrode materials. Seo et al.¹⁶⁵ used photo-lithography to fabricate a high-density filamentary neuroelectrode array. 256 electrodes were integrated in a small area of $2300 \times 300 \mu\text{m}^2$, with each electrode site being only $34 \times 7 \mu\text{m}^2$. Using photomasks designed by complex patterns, Roh et al.¹⁶⁶ used photo-lithography and ion etching in conjunction to simplify the fabrication of MEAs with different heights and cross-sectional shapes.

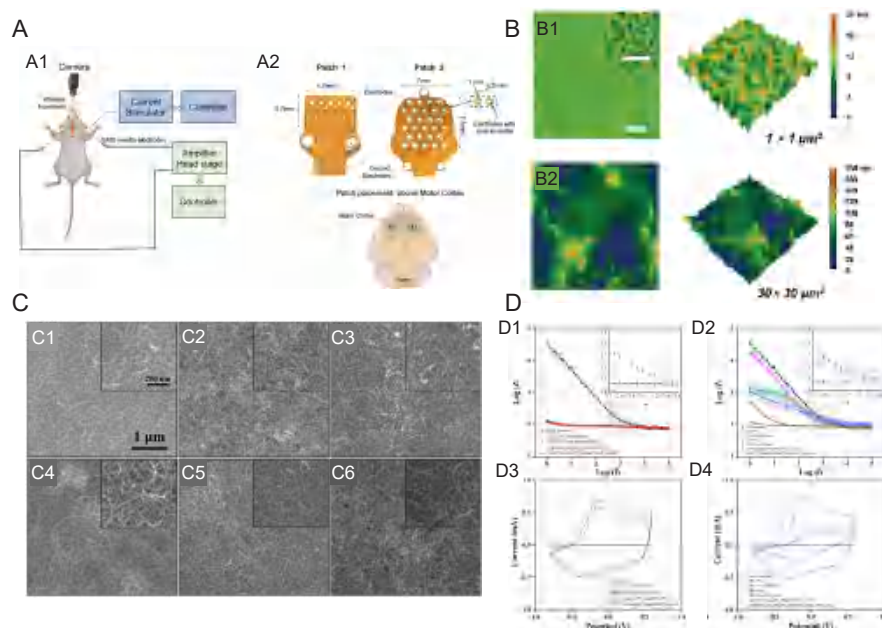


Figure 8. Neuroelectrodes with composite coatings. (A) (A1) Schematic representation of stimulation paradigm showing connection of the stimulation patch and EMG electrodes placement along with camera for whisker movement recording. (A2) Two different flexible patches were used for HD-ECS. Patch 1 contained 24 disk electrodes arranged in a 6×4 array in a cartesian grid, and Patch 2 had 27 ring-shaped electrodes arranged in a hexagonal grid. The patch was placed above the skull with its centre aligned to bregma, covering the motor cortex of both hemispheres.¹⁴² (B) Surface morphology (2D and 3D height images) of c-PEG-0 (B1) and c-PEG-20 (B2) samples in water taken by AFM. Scale bars: $5 \mu\text{m}$ (inset: 500 nm).¹⁴⁶ (C) SEM images of different functional coatings. (C1) MWCNTs, (C2) MWCNTs/Dex-PPy/PSS, (C3) MWCNTs/Dex-PPy/PGLu/PSS, (C4) MWCNTs/Dex-PPy/PGLu/PSS-PLys, (C5) MWCNTs/Dex-PPy/PGLu/PSS-PLys-NGF (before CV stimulation), and (C6) MWCNTs/Dex-PPy/PGLu/PSS-PLys-NGF coatings (after 500 cycles of CV stimulation). Insets are corresponding images with higher magnification. (D) (D1, D3) EIS (D1) and CV (D3) of bare Au electrodes, MWCNTs/Dex-PPy/PSS, MWCNTs/Dex-PPy/PGLu/PSS, MWCNTs/Dex-PPy/PGLu/PSS-PLys, and MWCNTs/Dex-PPy/PGLu/PSS-PLys-NGF functional coatings. Comparison of EIS (D2) and CV (D4) of bare Au electrodes, PPy/PSS films, PPy/Dex films, and MWCNTs/Dex-PPy/PGLu/PSS-PLys-NGF functional coatings. Data are represented by mean \pm standard deviation ($n \geq 3$). Reprinted with permission from Tian et al.¹⁴⁷ Copyright 2022 American Chemical Society. 2D: two dimensional; 3D: three dimensional; AFM: atomic force microscope; Au: aurum; c-PEG: carbon nanotube-poly(ethylene glycol); CV: cyclic voltammetry; Dex: dexamethasone; MWCNT: multiwalled carbon nanotube; NGF: nerve growth factor; PGLu: poly(glutamic acid); PLys: poly(lysine); PPy: polypyrrole; PSS: poly(styrene sulfonate); SEM: scanning electron microscope.

Compared to lithography, the fabrication of polymer masks (e.g. polyimide films) by laser ablation allows for simpler preparation of patterned macro molecular biomaterials or polymer coatings.¹⁶⁷ There have been numerous applications of laser technology for patterning neuroelectrode materials, including the use of lasers to cut and pattern metal electrodes,^{168, 169} the use of laser melting to increase the electrode surface area,¹⁷⁰ and the improvement of the electrode surface electrochemical activity,¹⁷¹ etc. Yang et al.¹⁷² developed a patterning technique based on ultrafast pulsed laser ablation for the large-volume sequential fabrication of various groups of organic and inorganic degradable materials, with high resolution of coating patterns and the ability to prepare multilayer structures with precise superposition. Amini et al.¹⁷³ developed a new method of hierarchical surface restructuring of electrode surfaces using femtosecond laser technology, which significantly improved the electrical properties of Pt-Ir electrode surfaces. Won et al.¹⁷⁴ developed an ultrafast digital patterning process using a 3D-printing-like approach by laser-induced PEDOT:PSS phase separation, and the processed

PEDOT:PSS has good water stability and can retain only the laser-patterned portion after water washing.

Additive manufacturing

CVD is widely used for the growth of carbon material coatings. Through the application of different catalyst lithography patterns, CVD-synthesised CNTs can be grown into highly porous mats or highly ordered and vertically aligned column bundles.¹⁷⁵ Highly porous CNTs with fluffy mat-like structures have a larger charge transfer surface area and preferential adhesion of nerve cells to CNTs via dendritic entanglement can significantly improve signal recording at nerve electrodes.¹⁷⁶ In addition to CVD-fabricated flexible graphene electrode arrays with low impedance and high signal-to-noise ratio,¹⁷⁷ multilayer graphene electrodes fabricated by CVD using a wafer-level no-transfer process exhibited very low impedance ($4.1 \text{ k}\Omega$) comparable to precious metal electrodes.¹⁷⁸

Electrostatic spinning is another simple and highly versatile technique which is widely applicable in a variety of polymers

and composites and allows large-scale fabrication of continuous ultrafine fibres. Fibres manufactured by electrostatic spinning are known for high uniformity, high porosity, high surface area and high mechanical strength. Lee et al.¹⁷⁹ fabricated nanofibrous conductive scaffolds by deposition of nano-thick PPy on poly(lactic-co-glycolic acid) nanofibres using electrostatic spinning technique. Electrical stimulation of PC-12 cells on conductive PPy/poly(lactic-co-glycolic acid) nanofibre scaffolds was found to improve neurite growth compared to unstimulated cells.

Electrodeposition is a versatile coating technique that can be widely used for the preparation of coatings on metals, polymers, and natural biomaterials. By adjusting the electrochemical parameters of the deposition process, the structure and morphology of the coatings can be controllably altered during the deposition process. Mousavi et al.¹⁸⁰ investigated the relationship between the mechanical stability of the electro-polymerisation of PEDOT:PSS on substrate materials and the thickness of the coatings, the adhesive surface properties, and the parameters of the electrodeposition operation (applied voltage/current, duration, and number of repetitions). The results show that the morphology of the PEDOT:PSS coatings and their adhesion to the electrode surfaces mainly depend on the properties of the electrode surfaces themselves. PEDOT:PSS forms a cauliflower-like shape on carbon microfilament electrodes, but is smoother on flat half-in and Au microfilament electrodes. One of the major problems faced by electrodeposited PEDOT coatings is the mechanical stability between the coating and the electrode, problems such as cracking and peeling of the coating can greatly affect the service life of the electrode, in order to enhance the stability of PEDOT coatings, there have been a number of studies to improve on the electrodeposition technology. Zhang et al.⁵⁶ combined a functional long-chain polymer poly(styrenesulfonate-co-4-vinylpyridine) chemically grafted onto a metal substrate, followed by electrochemical deposition of PEDOT and chemical cross-linking to form a PEDOT:poly(styrenesulfonate-co-4-vinylpyridine) interpenetrating network. This integrated polymer chain anchoring and chemical cross-linking method enabled the conductive hydrogel coating and metal electrode substrate to exhibit excellent interfacial robustness under long-term charge/discharge cycling and strong mechanical ultrasonic treatments. Yang et al.¹⁸¹ prepared poly(5-nitroindole) thin films by an electro-polymerisation and electro-grafting method as an Au/poly(5-nitroindole)/PEDOT conductive and adhesive interface layer for neural electrodes, which significantly enhanced the adhesion between PEDOT and Au electrode substrates (peel strength over 1.72 N/mm).

Structure Design of Coatings with Cellular Modulation Capabilities

Micromorphology regulates neuronal activity

Extracellular matrix not only provides nutrients for cells and regulates cell behaviours such as adhesion, growth, and differentiation through soluble biochemical signals, but also constitutes a growth environment for cells with complex physical parameters. It has been shown that a large number

of cells, including neural cells, are affected by the physical parameters of the growth environment (e.g., microstructure, surface morphology, and mechanical strength) during their growth and development.¹⁸²⁻¹⁸⁴

From a previous study, the influence of microforms on cell growth comes from two main pathways:¹⁸⁵ i) direct influence on the cytoskeleton through mechanical signalling; ii) indirect influence on the cell through extracellular chemical signalling.

Adhesion molecules are a functional cellular mechanism by which cells recognise external physical environment, and topographical cues. This has been widely demonstrated in cells other than neuronal cells. Adhesion molecules are primarily based on integrin formation.¹⁸⁶ When integrins are activated by external mechanical features, they induce the assembly of focal adhesion and cause integrins to attach to actin filaments of the cytoskeleton, leading to a change in cell shape.¹⁸⁷ In neuronal cells, integrins are also widely present, and the presence of integrins in neurons primarily affects neuronal migration and axonal growth. Another view is that surface morphology indirectly influences cellular activity by adsorbing proteins in the extracellular matrix.¹⁸⁸ In the usual culture process, cells often do not come into direct contact with the material, as the material tends to be encapsulated in a monolayer of adsorbed proteins in the supernatant first, and then comes into contact with the cells later. Thus, the host cell is not actually directly affected by the material, but by the surface proteins. Nanoscale surface morphology has different effects on the morphology and conformation of surface-bound proteins.

Micro-morphology design of nerve electrode coatings

There have been studies summarised the effects of different morphological cues on neuronal cell growth and development,^{185, 189-191} such as groove structures with staggered cell/subcell widths can enhance the directional growth of neuronal cells along the direction of the grooves; discontinuous dots, columns, and cones bumps of cell/subcell dimensions can be oriented to neuronal and glial cells; and nanoscale random topographies can also affect the specific behaviour of nerve cells. The effects of microtopography on neuronal cells can be categorised mainly into cell adhesion, orientation guidance, and neurite growth.

Neurons, like other anchorage-dependent cells, require proper adhesion to substrates for growth and development, so enhancing the adhesion of neuronal cells on the surface of nerve electrodes by microtopography can promote neuronal cell growth. As shown in **Figure 9A**, an irregularly distributed structured Au surface mimicking natural collagen fibres,¹⁹² with 1% decrease in impedance amplitude and 35% increase in critical free surface energy at frequencies lower than 50 kHz, improved the adhesion and growth of mouse enteric neuronal cells on its surface. Yang et al.⁵⁸ designed an electrode surface consisting of a conductive PEDOT:PSS network and a multifunctional polyazo-polyether-poly((sulfonyl) betaine) network to form a multifunctional hydrogel with semi-interpenetrating network. Since the polyazo-polyether-poly((sulfonyl) betaine) network can be covalently crosslinked by ultraviolet light triggering and constructed by photolithography with a high-resolution

pattern of 50 μm in both line and gap widths (**Figure 9B**), it possesses bio adhesive and antifouling properties.

The intimate contact and communication between neurons and electrodes determine the working efficiency of neural electrodes, and neurons, as special cells, have unique neural protrusion structures as carriers of electrical signals. The development and growth direction of the neurites on the electrode surface greatly affect the signal communication ability between the neuron and the electrode. Grooves or ridges of cellular/subcellular dimensions can guide the directional growth of neuronal synapses, biomimetic porous scaffold structures can guide neurons to form a network within the scaffolds, and such patterning of the electrode coatings can promote the tight connection between neurons and electrodes. Tringides et al.¹⁹³ prepared scaffolds that mimic the environment of neural tissue by doping carbon nanomaterials

in alginate hydrogel matrix and freeze-drying them. The neural progenitor cells in the scaffolds were able to form neuronal networks that spanned the material in three dimensions and differentiated into astrocytes and myelinated oligodendrocytes, as shown in **Figure 9C**. Wang et al.¹⁹⁴ fabricated 3D conductive scaffolds based on printed microfibrillar structures using near-field electrostatic printing and graphene oxide coating. Various ultrafine fibre patterns were obtained from poly(L-lactic-co-caprolactone) by near-field electrostatic printing, and the coverage angle of poly(L-lactic-co-caprolactone) fibres and fibre diameters were adjusted to construct spiderweb-like and tubular fibrous spatial tissues with complex spatial structures (**Figure 9D**, and **E**). This conductive scaffold showed excellent electrical conductivity ($\sim 0.95\text{ S/cm}$) and was able to induce the formation of neuron-like networks in the scaffold under exogenous electrical stimulation.

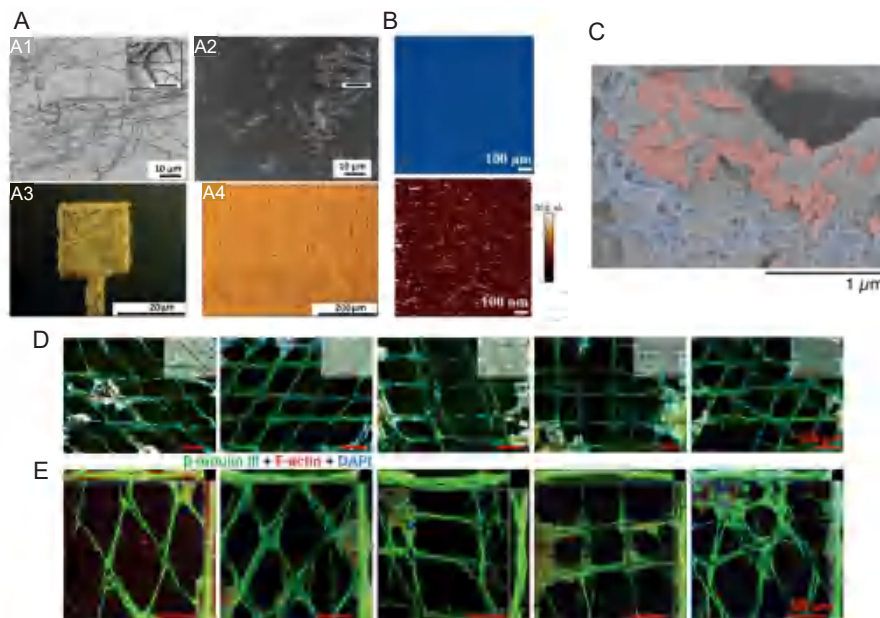


Figure 9. Neuroelectrode coatings for regulating cellular activity through microforms. (A) SEM images of (A1) collagen fibres coated on silicon wafer and (A2) collagen-like Au nanostructures developed from the nanoimprint process; Application of CLGNS nanostructuring process on (A3) microelectrode array surface and (A4) meander pattern, as proof of concept.¹⁹² Scale bars: 10 μm (A1, A2), 20 μm (A3, A4) (inset scale bar 1 μm). (B) Photograph of photopatterned MH (15 wt% SBMA) and AFM current image of PEDOT:PSS treated with SBMA (15 wt%). Reprinted with permission from Yang et al.⁵⁸ Copyright 2023 American Chemical Society. (C) SEM micrographs of the scaffolds with alginate left gray, GF pseudo-colored red, and CNTs pseudo-colored blue. Scale bar: 1 μm . C was reprinted from Tringides et al.¹⁹³ Copyright 2023 Wiley-VCH GmbH. (D) Representative immunofluorescence images and (E) confocal microscopy images of PC-12 cells cultured on microfibrils with different cladding angles for 14 days under ES conditions. Cultures were immunofluorescently stained with β -tubulin III (green), F-actin (red) and DAPI (blue). Inset: merged bright field images. D was reprinted from Wang et al.¹⁹⁴ Copyright 2020 Wiley-VCH GmbH. Scale bars: 150 μm . AFM: atomic force microscope; CLGNS: collagen-like gold nanostructure; DAPI: 4,6-diamidino-2-phenylindole; ES: electrical stimulation; MH: multifunctional hydrogel; PEDOT:PSS: poly(3,4-ethylenedioxythiophene):poly(styrene sulfonate); SBMA: 3-[dimethyl-2-(2-methylprop-2-enoyloxy)ethyl] azaniumyl] propane-1-sulfonate; SEM: scanning electron microscope.

Conclusion and Prospect

The function of BCI in the acquisition and identification of neuroelectric signals and the application of reverse electrical stimulation is of great significance for the diagnosis of clinical diseases, the treatment of neurological related diseases, and the recovery of body functions. And the neuroelectrode,

as the key part of physiological electrical signal acquisition in BCI, is of great significance for the development of BCI technology. This paper introduces the challenges faced by neuroelectrodes in applications and the key issues that need to be solved. Improvements in electrode substrate materials for neuroelectrode interfaces are highlighted from a

material design perspective, while recent advances in coating preparation techniques and structured design are discussed. Due to the huge difference between the fragile physiological structure of brain tissue and the external mechanical structure, the neuroelectrodes, as a “bridge” connecting the biological tissue and the external mechanical structure, need to satisfy the completely different functional requirements of the two ends at the same time, which has made the fabrication of neuroelectrodes always facing a great challenge.

Great progress has been made in the fabrication of neuroelectrodes, but there are still unresolved challenges that still require further attention. For implantable neuroelectrodes, biocompatibility is still the main issue. In addition to improvements in electrode structure, mechanical properties, and material selection, more attention should be paid to the role of the neuroimmune response during electrode implantation. This is because neuronal growth and glial scar formation not only affect the biosafety, but also directly affect the signal reception ability of the neuroelectrode. Secondly the long-term stability of the neuroelectrode needs to be further evaluated, e.g., it is necessary to assess the use of the electrode several years or more after implantation. In addition, the signal-to-noise ratio of the recorded electrophysiological signals needs to be further improved.

Although the ideal neuroelectrode is still a long way off, novel electrode materials and processing technologies have been introduced, such as nanometallic materials, semiconductor materials, carbon nanomaterials, CPs, and bio-based materials, which continue to open up the possibilities of neuroelectrode materials. A single material is difficult to meet the multiple needs of neuroelectrodes, and composite neuroelectrodes with multiple materials, or coating modification of the base electrode using a combination of different materials, can provide more comprehensive advantages than single-material electrodes, such as (i) higher electrical and optical properties, such as low impedance, low signal-to-noise ratio, and stimulation ability of exogenous signals; (ii) lower modulus of elasticity, better adhesion properties, and brain tissue tight fitting to avoid mechanical damage and slippage; (iii) better physicochemical stability, biocompatibility, and bioactivity. On this basis, the use of more advanced micromachining molding technology to fabricate electrodes with lower volume and more complex structure; higher resolution patterning or structured design of coatings, and the modulation of nerve cells through morphological cues provide another direction for the functionalization of nerve electrodes. The combination of multiple materials and the expansion of new synthetic processing processes are all expected to realize truly ideal neuroelectrodes that will achieve the goal of seamless BCIs and make significant contributions to the fields of clinical medicine, brain function analysis, and human-computer interaction.

This review provides a comprehensive overview of the research in neuroelectrode substrate materials and coating modification technologies in the last 5 years, but mainly focuses on representative advances and does not provide overall statistics and analyses. The field of neuroelectrodes involves a large number of materials, a wide range of classifications, and

a long history of development, so the content of this review is limited and does not cover the long-term development trend.

Author contributions

YJ, ML, JZ conceptualised and designed the review; YJ drafted the manuscript; YJ, RC, XQ checked and revised the manuscript. All authors reviewed and approved the final version of the manuscript.

Financial support

The work was supported by the National Key Research and Development Program, No. 2021YFB3800800, the National Natural Science Foundation of China, Nos. 31922041, 32171341, 32301113, the 111 Project, No. B14018, the Science and Technology Innovation Project and Excellent Academic Leader Project of Shanghai Science and Technology Committee, Nos. 21S31901500, 21XD1421100, the National Postdoctoral Program for Innovative Talents, No. BX20230122, the Shanghai Sailing Program, No. 23YF1409700, and the China Postdoctoral Science Foundation, No. D100-5R-22114.

Acknowledgement

None.

Conflicts of interest statement

The authors declare no conflict of interest.

Open access statement

This is an open access journal, and articles are distributed under the terms of the Creative Commons Attribution-NonCommercial-ShareAlike 4.0 License, which allows others to remix, tweak, and build upon the work non-commercially, as long as appropriate credit is given and the new creations are licensed under the identical terms.

- Serino, A.; Bockbrader, M.; Bertoni, T.; Colachis Iv, S.; Solcà, M.; Dunlap, C.; Eipel, K.; Ganzer, P.; Annetta, N.; Sharma, G.; Orepic, P.; Friedenber, D.; Sederberg, P.; Faivre, N.; Rezai, A.; Blanke, O. Sense of agency for intracortical brain-machine interfaces. *Nat Hum Behav.* **2022**, *6*, 565-578.
- Shanechi, M. M. Brain-machine interfaces from motor to mood. *Nat Neurosci.* **2019**, *22*, 1554-1564.
- Young, M. J.; Lin, D. J.; Hochberg, L. R. Brain-Computer Interfaces in Neurorecovery and Neurorehabilitation. *Semin Neurol.* **2021**, *41*, 206-216.
- Steins, H.; Mierzejewski, M.; Brauns, L.; Stumpf, A.; Kohler, A.; Heusel, G.; Corna, A.; Herrmann, T.; Jones, P. D.; Zeck, G.; von Metzner, R.; Stieglitz, T. A flexible protruding microelectrode array for neural interfacing in bioelectronic medicine. *Microsyst Nanoeng.* **2022**, *8*, 131.
- Choi, J. S.; Lee, H. J.; Rajaraman, S.; Kim, D. H. Recent advances in three-dimensional microelectrode array technologies for in vitro and in vivo cardiac and neuronal interfaces. *Biosens Bioelectron.* **2021**, *171*, 112687.
- Fattahi, P.; Yang, G.; Kim, G.; Abidian, M. R. A review of organic and inorganic biomaterials for neural interfaces. *Adv Mater.* **2014**, *26*, 1846-1885.
- Cruz, A. M.; Casañ-Pastor, N. Graded conducting titanium-iridium oxide coatings for bioelectrodes in neural systems. *Thin Solid Films.* **2013**, *534*, 316-324.
- Chapman, C. A.; Chen, H.; Stamou, M.; Biener, J.; Biener, M. M.; Lein, P. J.; Seker, E. Nanoporous gold as a neural interface coating: effects of topography, surface chemistry, and feature size. *ACS Appl Mater Interfaces.* **2015**, *7*, 7093-7100.
- Boehler, C.; Stieglitz, T.; Asplund, M. Nanostructured platinum grass enables superior impedance reduction for neural microelectrodes. *Biomaterials.* **2015**, *67*, 346-353.
- Li, J.; Cheng, Y.; Gu, M.; Yang, Z.; Zhan, L.; Du, Z. Sensing and stimulation applications of carbon nanomaterials in implantable brain-

- computer interface. *Int J Mol Sci.* **2023**, *24*, 5182.
11. Kim, T.; Park, J.; Sohn, J.; Cho, D.; Jeon, S. Bioinspired, highly stretchable, and conductive dry adhesives based on 1D-2D hybrid carbon nanocomposites for all-in-one ECG electrodes. *ACS Nano.* **2016**, *10*, 4770-4778.
 12. Kuzum, D.; Takano, H.; Shim, E.; Reed, J. C.; Juul, H.; Richardson, A. G.; de Vries, J.; Bink, H.; Dichter, M. A.; Lucas, T. H.; Coulter, D. A.; Cubukcu, E.; Litt, B. Transparent and flexible low noise graphene electrodes for simultaneous electrophysiology and neuroimaging. *Nat Commun.* **2014**, *5*, 5259.
 13. Golparvar, A. J.; Yapici, M. K. Electrooculography by wearable graphene textiles. *IEEE Sens J.* **2018**, *18*, 8971-8978.
 14. Apollo, N. V.; Maturana, M. I.; Tong, W.; Nayagam, D. A. X.; Shivdasani, M. N.; Foroughi, J.; Wallace, G. G.; Prawer, S.; Ibbotson, M. R.; Garrett, D. J. Soft, Flexible freestanding neural stimulation and recording electrodes fabricated from reduced graphene oxide. *Adv Funct Mater.* **2015**, *25*, 3551-3559.
 15. Du, X.; Jiang, W.; Zhang, Y.; Qiu, J.; Zhao, Y.; Tan, Q.; Qi, S.; Ye, G.; Zhang, W.; Liu, N. Transparent and stretchable graphene electrode by intercalation doping for epidermal electrophysiology. *ACS Appl Mater Interfaces.* **2020**, *12*, 56361-56371.
 16. Green, R.; Abidian, M. R. Conducting polymers for neural prosthetic and neural interface applications. *Adv Mater.* **2015**, *27*, 7620-7637.
 17. Green, R. A.; Lovell, N. H.; Wallace, G. G.; Poole-Warren, L. A. Conducting polymers for neural interfaces: challenges in developing an effective long-term implant. *Biomaterials.* **2008**, *29*, 3393-3399.
 18. Guo, L.; Ma, M.; Zhang, N.; Langer, R.; Anderson, D. G. Stretchable polymeric multielectrode array for conformal neural interfacing. *Adv Mater.* **2014**, *26*, 1427-1433.
 19. Han, L.; Lu, X.; Wang, M.; Gan, D.; Deng, W.; Wang, K.; Fang, L.; Liu, K.; Chan, C. W.; Tang, Y.; Weng, L. T.; Yuan, H. A mussel-inspired conductive, self-adhesive, and self-healable tough hydrogel as cell stimulators and implantable bioelectronics. *Small.* **2017**, *13*, 1601916.
 20. Kim, D. H.; Viventi, J.; Amsden, J. J.; Xiao, J.; Vigeland, L.; Kim, Y. S.; Blanco, J. A.; Panilaitis, B.; Frechette, E. S.; Contreras, D.; Kaplan, D. L.; Omenetto, F. G.; Huang, Y.; Hwang, K. C.; Zakin, M. R.; Litt, B.; Rogers, J. A. Dissolvable films of silk fibroin for ultrathin conformal bio-integrated electronics. *Nat Mater.* **2010**, *9*, 511-517.
 21. Adewole, D. O.; Serruya, M. D.; Wolf, J. A.; Cullen, D. K. Bioactive neuroelectronic interfaces. *Front Neurosci.* **2019**, *13*, 269.
 22. Chalmers, E.; Lee, H.; Zhu, C.; Liu, X. Increasing the conductivity and adhesion of polypyrrole hydrogels with electropolymerized polydopamine. *Chem Mater.* **2020**, *32*, 234-244.
 23. Gajendiran, M.; Choi, J.; Kim, S. J.; Kim, K.; Shin, H.; Koo, H. J.; Kim, K. Conductive biomaterials for tissue engineering applications. *J Ind Eng Chem.* **2017**, *51*, 12-26.
 24. Franze, K.; Janmey, P. A.; Guck, J. Mechanics in neuronal development and repair. *Annu Rev Biomed Eng.* **2013**, *15*, 227-251.
 25. Budday, S.; Ovaert, T. C.; Holzapfel, G. A.; Steinmann, P.; Kuhl, E. Fifty shades of brain: a review on the mechanical testing and modeling of brain tissue. *Arch Comput Methods Eng.* **2020**, *27*, 1187-1230.
 26. Betz, T.; Koch, D.; Lu, Y. B.; Franze, K.; Käs, J. A. Growth cones as soft and weak force generators. *Proc Natl Acad Sci U S A.* **2011**, *108*, 13420-13425.
 27. Zamproni, L. N.; Mundim, M.; Porcionatto, M. A. Neurorepair and regeneration of the brain: a decade of bioscaffolds and engineered microtissue. *Front Cell Dev Biol.* **2021**, *9*, 649891.
 28. Carnicer-Lombarte, A.; Chen, S. T.; Malliaras, G. G.; Barone, D. G. Foreign body reaction to implanted biomaterials and its impact in nerve neuroprosthetics. *Front Bioeng Biotechnol.* **2021**, *9*, 622524.
 29. Michelson, N. J.; Vazquez, A. L.; Eles, J. R.; Salatino, J. W.; Purcell, E. K.; Williams, J. J.; Cui, X. T.; Kozai, T. D. Y. Multi-scale, multi-modal analysis uncovers complex relationship at the brain tissue-implant neural interface: new emphasis on the biological interface. *J Neural Eng.* **2018**, *15*, 033001.
 30. Bennett, C.; Mohammed, F.; Álvarez-Ciara, A.; Nguyen, M. A.; Dietrich, W. D.; Rajguru, S. M.; Streit, W. J.; Prasad, A. Neuroinflammation, oxidative stress, and blood-brain barrier (BBB) disruption in acute Utah electrode array implants and the effect of deferoxamine as an iron chelator on acute foreign body response. *Biomaterials.* **2019**, *188*, 144-159.
 31. Kozai, T. D.; Vazquez, A. L.; Weaver, C. L.; Kim, S. G.; Cui, X. T. In vivo two-photon microscopy reveals immediate microglial reaction to implantation of microelectrode through extension of processes. *J Neural Eng.* **2012**, *9*, 066001.
 32. Wellman, S. M.; Cambi, F.; Kozai, T. D. The role of oligodendrocytes and their progenitors on neural interface technology: A novel perspective on tissue regeneration and repair. *Biomaterials.* **2018**, *183*, 200-217.
 33. Biran, R.; Martin, D. C.; Tresco, P. A. Neuronal cell loss accompanies the brain tissue response to chronically implanted silicon microelectrode arrays. *Exp Neurol.* **2005**, *195*, 115-126.
 34. Chen, K.; Wellman, S. M.; Yaxiaer, Y.; Eles, J. R.; Kozai, T. D. In vivo spatiotemporal patterns of oligodendrocyte and myelin damage at the neural electrode interface. *Biomaterials.* **2021**, *268*, 120526.
 35. Savva, S. P.; Li, F.; Lam, S.; Wellman, S. M.; Stieger, K. C.; Chen, K.; Eles, J. R.; Kozai, T. D. Y. In vivo spatiotemporal dynamics of astrocyte reactivity following neural electrode implantation. *Biomaterials.* **2022**, *289*, 121784.
 36. Kim, G. H.; Kim, K.; Nam, H.; Shin, K.; Choi, W.; Shin, J. H.; Lim, G. CNT-Au nanocomposite deposition on gold microelectrodes for improved neural recordings. *Sens Actuators B Chem.* **2017**, *252*, 152-158.
 37. Yuan, X.; Hierlemann, A.; Frey, U. Extracellular recording of entire neural networks using a dual-mode microelectrode array with 19584 electrodes and high SNR. *IEEE J Solid-State Circuits.* **2021**, *56*, 2466-2475.
 38. Lin, C. M.; Lee, Y. T.; Yeh, S. R.; Fang, W. Flexible carbon nanotubes electrode for neural recording. *Biosens Bioelectron.* **2009**, *24*, 2791-2797.
 39. Sabetian, P.; Popovic, M. R.; Yoo, P. B. Optimizing the design of bipolar nerve cuff electrodes for improved recording of peripheral nerve activity. *J Neural Eng.* **2017**, *14*, 036015.
 40. Díaz, D. R.; Carmona, F. J.; Palacio, L.; Ochoa, N. A.; Hernández, A.; Prádanos, P. Impedance spectroscopy and membrane potential analysis of microfiltration membranes. The influence of surface fractality. *Chem Eng Sci.* **2018**, *178*, 27-38.
 41. Wellman, S. M.; Li, L.; Yaxiaer, Y.; McNamara, I.; Kozai, T. D. Y. Revealing spatial and temporal patterns of cell death, glial proliferation, and blood-brain barrier dysfunction around implanted intracortical neural interfaces. *Front Neurosci.* **2019**, *13*, 493.
 42. Wellman, S. M.; Kozai, T. D. Y. In vivo spatiotemporal dynamics of NG2 glia activity caused by neural electrode implantation. *Biomaterials.* **2018**, *164*, 121-133.
 43. Camuñas-Mesa, L. A.; Quiroga, R. Q. A detailed and fast model of extracellular recordings. *Neural Comput.* **2013**, *25*, 1191-1212.
 44. Kozai, T. D.; Langhals, N. B.; Patel, P. R.; Deng, X.; Zhang, H.; Smith, K. L.; Lahann, J.; Kotov, N. A.; Kipke, D. R. Ultrasmall implantable composite microelectrodes with bioactive surfaces for chronic neural

- interfaces. *Nat Mater.* **2012**, *11*, 1065-1073.
45. Lee, H. C.; Ejsnerholm, F.; Gaire, J.; Currllin, S.; Schouenborg, J.; Wallman, L.; Bengtsson, M.; Park, K.; Otto, K. J. Histological evaluation of flexible neural implants; flexibility limit for reducing the tissue response? *J Neural Eng.* **2017**, *14*, 036026.
 46. Seymour, J. P.; Kipke, D. R. Neural probe design for reduced tissue encapsulation in CNS. *Biomaterials.* **2007**, *28*, 3594-3607.
 47. Kuo, J. T.; Kim, B. J.; Hara, S. A.; Lee, C. D.; Gutierrez, C. A.; Hoang, T. Q.; Meng, E. Novel flexible parylene neural probe with 3D sheath structure for enhancing tissue integration. *Lab Chip.* **2013**, *13*, 554-561.
 48. Gao, K.; Li, G.; Liao, L.; Cheng, J.; Zhao, J.; Xu, Y. Fabrication of flexible microelectrode arrays integrated with microfluidic channels for stable neural interfaces. *Sens Actuators A Phys.* **2013**, *197*, 9-14.
 49. Du, Z. J.; Kolarcik, C. L.; Kozai, T. D. Y.; Luebben, S. D.; Sapp, S. A.; Zheng, X. S.; Nabity, J. A.; Cui, X. T. Ultrasoft microwire neural electrodes improve chronic tissue integration. *Acta Biomater.* **2017**, *53*, 46-58.
 50. Hong, G.; Lieber, C. M. Novel electrode technologies for neural recordings. *Nat Rev Neurosci.* **2019**, *20*, 330-345.
 51. Zhu, M.; Wang, H.; Li, S.; Liang, X.; Zhang, M.; Dai, X.; Zhang, Y. Flexible electrodes for in vivo and in vitro electrophysiological signal recording. *Adv Healthc Mater.* **2021**, *10*, e2100646.
 52. Hu, Z.; Niu, Q.; Hsiao, B. S.; Yao, X.; Zhang, Y. Bioactive polymer-enabled conformal neural interface and its application strategies. *Mater Horiz.* **2023**, *10*, 808-828.
 53. Potter-Baker, K. A.; Nguyen, J. K.; Kovach, K. M.; Gitomer, M. M.; Srail, T. W.; Stewart, W. G.; Skousen, J. L.; Capadona, J. R. Development of superoxide dismutase mimetic surfaces to reduce accumulation of reactive oxygen species for neural interfacing applications. *J Mater Chem B.* **2014**, *2*, 2248-2258.
 54. Zheng, X. S.; Snyder, N. R.; Woeppl, K.; Barengo, J. H.; Li, X.; Eles, J.; Kolarcik, C. L.; Cui, X. T. A superoxide scavenging coating for improving tissue response to neural implants. *Acta Biomater.* **2019**, *99*, 72-83.
 55. Golabchi, A.; Wu, B.; Li, X.; Carlisle, D. L.; Kozai, T. D. Y.; Friedlander, R. M.; Cui, X. T. Melatonin improves quality and longevity of chronic neural recording. *Biomaterials.* **2018**, *180*, 225-239.
 56. Zhang, J.; Wang, L.; Xue, Y.; Lei, I. M.; Chen, X.; Zhang, P.; Cai, C.; Liang, X.; Lu, Y.; Liu, J. Engineering electrodes with robust conducting hydrogel coating for neural recording and modulation. *Adv Mater.* **2023**, *35*, e2209324.
 57. Yuk, H.; Lu, B.; Zhao, X. Hydrogel bioelectronics. *Chem Soc Rev.* **2019**, *48*, 1642-1667.
 58. Yang, M.; Chen, P.; Qu, X.; Zhang, F.; Ning, S.; Ma, L.; Yang, K.; Su, Y.; Zang, J.; Jiang, W.; Yu, T.; Dong, X.; Luo, Z. Robust neural interfaces with photopatternable, bioadhesive, and highly conductive hydrogels for stable chronic neuromodulation. *ACS Nano.* **2023**. doi: 10.1021/acsnano.2c04606.
 59. Wu, Z. Z.; Zhao, Y.; Kisaalita, W. S. Interfacing SH-SY5Y human neuroblastoma cells with SU-8 microstructures. *Colloids Surf B Biointerfaces.* **2006**, *52*, 14-21.
 60. Fan, Y. W.; Cui, F. Z.; Hou, S. P.; Xu, Q. Y.; Chen, L. N.; Lee, I. S. Culture of neural cells on silicon wafers with nano-scale surface topograph. *J Neurosci Methods.* **2002**, *120*, 17-23.
 61. Kushwah, N.; Woeppl, K.; Dhawan, V.; Shi, D.; Cui, X. T. Effects of neuronal cell adhesion molecule L1 and nanoparticle surface modification on microglia. *Acta Biomater.* **2022**, *149*, 273-286.
 62. Woeppl, K. M.; Cui, X. T. Nanoparticle and biomolecule surface modification synergistically increases neural electrode recording yield and minimizes inflammatory host response. *Adv Healthc Mater.* **2021**, *10*, e2002150.
 63. Sikder, M. K. U.; Tong, W.; Pingle, H.; Kingshott, P.; Needham, K.; Shivdasani, M. N.; Fallon, J. B.; Seligman, P.; Ibbotson, M. R.; Prawer, S.; Garrett, D. J. Laminin coated diamond electrodes for neural stimulation. *Mater Sci Eng C Mater Biol Appl.* **2021**, *118*, 111454.
 64. Chou, N.; Byun, D.; Kim, S. MEMS-based microelectrode technologies capable of penetrating neural tissues. *Biomed Eng Lett.* **2014**, *4*, 109-119.
 65. Trevathan, J. K.; Baumgart, I. W.; Nicolai, E. N.; Gosink, B. A.; Asp, A. J.; Settell, M. L.; Polaconda, S. R.; Malerick, K. D.; Brodnick, S. K.; Zeng, W.; Knudsen, B. E.; McConico, A. L.; Sanger, Z.; Lee, J. H.; Aho, J. M.; Suminski, A. J.; Ross, E. K.; Lujan, J. L.; Weber, D. J.; Williams, J. C.; Franke, M.; Ludwig, K. A.; Shoffstall, A. J. An injectable neural stimulation electrode made from an in-body curing polymer/metal composite. *Adv Healthc Mater.* **2019**, *8*, e1900892.
 66. Patel, P. R.; Zhang, H.; Robbins, M. T.; Nofar, J. B.; Marshall, S. P.; Kobylarek, M. J.; Kozai, T. D.; Kotov, N. A.; Chestek, C. A. Chronic in vivo stability assessment of carbon fiber microelectrode arrays. *J Neural Eng.* **2016**, *13*, 066002.
 67. Hong, W.; Lee, J. W.; Kim, D.; Hwang, Y.; Lee, J.; Kim, J.; Hong, N.; Kwon, H. J.; Jang, J. E.; Punga, A. R.; Kang, H. Ultrathin gold microelectrode array using polyelectrolyte multilayers for flexible and transparent electro-optical neural interfaces. *Adv Funct Mater.* **2022**, *32*, 2106493.
 68. Lim, C.; Park, C.; Sunwoo, S. H.; Kim, Y. G.; Lee, S.; Han, S. I.; Kim, D.; Kim, J. H.; Kim, D. H.; Hyeon, T. Facile and scalable synthesis of whiskered gold nanosheets for stretchable, conductive, and biocompatible nanocomposites. *ACS Nano.* **2022**, *16*, 10431-10442.
 69. Dong, R.; Wang, L.; Hang, C.; Chen, Z.; Liu, X.; Zhong, L.; Qi, J.; Huang, Y.; Liu, S.; Wang, L.; Lu, Y.; Jiang, X. Printed stretchable liquid metal electrode arrays for in vivo neural recording. *Small.* **2021**, *17*, e2006612.
 70. Guo, R.; Liu, J. Implantable liquid metal-based flexible neural microelectrode array and its application in recovering animal locomotion functions. *J Micromech Microeng.* **2017**, *27*, 104002.
 71. Zhang, X.; Liu, B.; Gao, J.; Lang, Y.; Lv, X.; Deng, Z.; Gui, L.; Liu, J.; Tang, R.; Li, L. Liquid metal-based electrode array for neural signal recording. *Bioengineering (Basel).* **2023**, *10*, 578.
 72. Tang, R.; Zhang, C.; Liu, B.; Jiang, C.; Wang, L.; Zhang, X.; Huang, Q.; Liu, J.; Li, L. Towards an artificial peripheral nerve: Liquid metal-based fluidic cuff electrodes for long-term nerve stimulation and recording. *Biosens Bioelectron.* **2022**, *216*, 114600.
 73. Kim, D.; Thissen, P.; Viner, G.; Lee, D. W.; Choi, W.; Chabal, Y. J.; Lee, J. B. Recovery of nonwetting characteristics by surface modification of gallium-based liquid metal droplets using hydrochloric acid vapor. *ACS Appl Mater Interfaces.* **2013**, *5*, 179-185.
 74. So, J. H.; Koo, H. J.; Dickey, M. D.; Velev, O. D. Ionic current rectification in soft-matter diodes with liquid-metal electrodes. *Adv Funct Mater.* **2012**, *22*, 625-631.
 75. Lee, S. H.; Thunemann, M.; Lee, K.; Cleary, D. R.; Tonsfeldt, K. J.; Oh, H.; Azzazy, F.; Tchoe, Y.; Bourhis, A. M.; Hossain, L.; Ro, Y. G.; Tanaka, A.; Kılıç, K.; Devor, A.; Dayeh, S. A. Scalable thousand channel penetrating microneedle arrays on flex for multimodal and large area coverage brain-machine interfaces. *Adv Funct Mater.* **2022**, *32*, 2112045.
 76. Suzuki, I.; Matsuda, N.; Han, X.; Noji, S.; Shibata, M.; Nagafuku, N.; Ishibashi, Y. Large-area field potential imaging having single neuron resolution using 236 880 electrodes CMOS-MEA technology. *Adv Sci*

- (Weinh). **2023**, *10*, e2207732.
77. Li, S.; Shi, Q.; Li, Y.; Yang, J.; Chang, T. H.; Jiang, J.; Chen, P. Y. Intercalation of metal ions into Ti₃C₂T_x MXene electrodes for high-areal-capacitance microsupercapacitors with neutral multivalent electrolytes. *Adv Funct Mater.* **2020**, *30*, 2003721.
 78. Rafieerad, A.; Amiri, A.; Sequiera, G. L.; Yan, W.; Chen, Y.; Polycarpou, A. A.; Dhingra, S. Development of fluorine-free tantalum carbide MXene hybrid structure as a biocompatible material for supercapacitor electrodes. *Adv Funct Mater.* **2021**, *31*, 2100015.
 79. Zhang, Y.; Zhang, L.; Li, C.; Han, J.; Huang, W.; Zhou, J.; Yang, Y. Hydrophilic antifouling 3D porous MXene/holey graphene nanocomposites for electrochemical determination of dopamine. *Microchem J.* **2022**, *181*, 107713.
 80. Xu, J.; Shirinkami, H.; Hwang, S.; Jeong, H. S.; Kim, G.; Jun, S. B.; Chun, H. Fast reconfigurable electrode array based on titanium oxide for localized stimulation of cultured neural network. *ACS Appl Mater Interfaces.* **2023**, *15*, 19092-19101.
 81. Zhang, F.; Zhang, L.; Xia, J.; Zhao, W.; Dong, S.; Ye, Z.; Pan, G.; Luo, J.; Zhang, S. Multimodal electrocorticogram active electrode array based on zinc oxide-thin film transistors. *Adv Sci (Weinh).* **2023**, *10*, e2204467.
 82. Liu, S.; Liu, L.; Zhao, Y.; Wang, Y.; Wu, Y.; Zhang, X. D.; Ming, D. A high-performance electrode based on van der waals heterostructure for neural recording. *Nano Lett.* **2022**, *22*, 4400-4409.
 83. Park, D. W.; Brodnick, S. K.; Ness, J. P.; Atry, F.; Krugner-Higby, L.; Sandberg, A.; Mikael, S.; Richner, T. J.; Novello, J.; Kim, H.; Baek, D. H.; Bong, J.; Frye, S. T.; Thongpang, S.; Swanson, K. I.; Lake, W.; Pashaie, R.; Williams, J. C.; Ma, Z. Fabrication and utility of a transparent graphene neural electrode array for electrophysiology, in vivo imaging, and optogenetics. *Nat Protoc.* **2016**, *11*, 2201-2222.
 84. Park, S. Y.; Park, J.; Sim, S. H.; Sung, M. G.; Kim, K. S.; Hong, B. H.; Hong, S. Enhanced differentiation of human neural stem cells into neurons on graphene. *Adv Mater.* **2011**, *23*, H263-267.
 85. Liu, X.; Xu, Z.; Fu, X.; Liu, Y.; Jia, H.; Yang, Z.; Zhang, J.; Wei, S.; Duan, X. Stable, long-term single-neuronal recording from the rat spinal cord with flexible carbon nanotube fiber electrodes. *J Neural Eng.* **2022**, *19*, 056024.
 86. Yang, H.; Qian, Z.; Wang, J.; Feng, J.; Tang, C.; Wang, L.; Guo, Y.; Liu, Z.; Yang, Y.; Zhang, K.; Chen, P.; Sun, X.; Peng, H. Carbon nanotube array-based flexible multifunctional electrodes to record electrophysiology and ions on the cerebral cortex in real time. *Adv Funct Mater.* **2022**, *32*, 2204794.
 87. Xiong, Z.; Huang, W.; Liang, Q.; Cao, Y.; Liu, S.; He, Z.; Zhang, R.; Zhang, B.; Green, R.; Zhang, S.; Li, D. Harnessing the 2D structure-enabled viscoelasticity of graphene-based hydrogel membranes for chronic neural interfacing. *Small Methods.* **2022**, *6*, e2200022.
 88. Yang, X.; Zhu, J.; Qiu, L.; Li, D. Bioinspired effective prevention of restacking in multilayered graphene films: towards the next generation of high-performance supercapacitors. *Adv Mater.* **2011**, *23*, 2833-2838.
 89. Xiong, J.; Zhang, B.; Balilonda, A.; Yang, S.; Li, K.; Zhang, Q.; Li, Y.; Wang, H.; Hou, C. Graphene-based implantable neural electrodes for insect flight control. *J Mater Chem B.* **2022**, *10*, 4632-4639.
 90. Goding, J.; Gilmour, A.; Martens, P.; Poole-Warren, L.; Green, R. Interpenetrating conducting hydrogel materials for neural interfacing electrodes. *Adv Healthc Mater.* **2017**, *6*, 1601177.
 91. Tomaskovic-Crook, E.; Zhang, P.; Ahtinen, A.; Kaisvuo, H.; Lee, C. Y.; Beirne, S.; Aqrave, Z.; Svirskis, D.; Hyttinen, J.; Wallace, G. G.; Travas-Sejdic, J.; Crook, J. M. Human neural tissues from neural stem cells using conductive biogel and printed polymer microelectrode arrays for 3D electrical stimulation. *Adv Healthc Mater.* **2019**, *8*, e1900425.
 92. Widge, A. S.; Jeffries-El, M.; Cui, X.; Lagenaur, C. F.; Matsuoka, Y. Self-assembled monolayers of polythiophene conductive polymers improve biocompatibility and electrical impedance of neural electrodes. *Biosens Bioelectron.* **2007**, *22*, 1723-1732.
 93. Liang, Q.; Shen, Z.; Sun, X.; Yu, D.; Liu, K.; Mugo, S. M.; Chen, W.; Wang, D.; Zhang, Q. Electron conductive and transparent hydrogels for recording brain neural signals and neuromodulation. *Adv Mater.* **2023**, *35*, e2211159.
 94. Xia, X.; Liang, Q.; Sun, X.; Yu, D.; Huang, X.; Mugo, S. M.; Chen, W.; Wang, D.; Zhang, Q. Intrinsically electron conductive, antibacterial, and anti-swelling hydrogels as implantable sensors for bioelectronics. *Adv Funct Mater.* **2022**, *32*, 2208024.
 95. Rinoldi, C.; Ziai, Y.; Zargarian, S. S.; Nakielski, P.; Zembrzycki, K.; Haghighat Bayan, M. A.; Zakrzewska, A. B.; Fiorelli, R.; Lanzi, M.; Kostrzewska-Księżyk, A.; Czajkowski, R.; Kublik, E.; Kaczmarek, L.; Pierini, F. In vivo chronic brain cortex signal recording based on a soft conductive hydrogel biointerface. *ACS Appl Mater Interfaces.* **2023**, *15*, 6283-6296.
 96. Won, C.; Jeong, U. J.; Lee, S.; Lee, M.; Kwon, C.; Cho, S.; Yoon, K.; Lee, S.; Chun, D.; Cho, I. J.; Lee, T. Mechanically tissue-like and highly conductive Au nanoparticles embedded elastomeric fiber electrodes of brain-machine interfaces for chronic in vivo brain neural recording. *Adv Funct Mater.* **2022**, *32*, 2205145.
 97. Carli, S.; Bianchi, M.; Zucchini, E.; Di Lauro, M.; Prato, M.; Murgia, M.; Fadiga, L.; Biscarini, F. Electrodeposited PEDOT:nafion composite for neural recording and stimulation. *Adv Healthc Mater.* **2019**, *8*, e1900765.
 98. Mandal, H. S.; Knaack, G. L.; Charkhkar, H.; McHail, D. G.; Kastee, J. S.; Dumas, T. C.; Peixoto, N.; Rubinson, J. F.; Pancrazio, J. J. Improving the performance of poly(3,4-ethylenedioxythiophene) for brain-machine interface applications. *Acta Biomater.* **2014**, *10*, 2446-2454.
 99. Pranti, A. S.; Schander, A.; Bödecker, A.; Lang, W. PEDOT: PSS coating on gold microelectrodes with excellent stability and high charge injection capacity for chronic neural interfaces. *Sens Actuators B Chem.* **2018**, *275*, 382-393.
 100. Liu, Y.; Liu, J.; Chen, S.; Lei, T.; Kim, Y.; Niu, S.; Wang, H.; Wang, X.; Foudeh, A. M.; Tok, J. B.; Bao, Z. Soft and elastic hydrogel-based microelectronics for localized low-voltage neuromodulation. *Nat Biomed Eng.* **2019**, *3*, 58-68.
 101. Lu, B.; Yuk, H.; Lin, S.; Jian, N.; Qu, K.; Xu, J.; Zhao, X. Pure PEDOT:PSS hydrogels. *Nat Commun.* **2019**, *10*, 1043.
 102. Feig, V. R.; Tran, H.; Lee, M.; Bao, Z. Mechanically tunable conductive interpenetrating network hydrogels that mimic the elastic moduli of biological tissue. *Nat Commun.* **2018**, *9*, 2740.
 103. Li, T. L.; Liu, Y.; Forro, C.; Yang, X.; Beker, L.; Bao, Z.; Cui, B.; Paşca, S. P. Stretchable mesh microelectronics for the biointegration and stimulation of human neural organoids. *Biomaterials.* **2022**, *290*, 121825.
 104. Wang, S.; Guan, S.; Wang, J.; Liu, H.; Liu, T.; Ma, X.; Cui, Z. Fabrication and characterization of conductive poly(3,4-ethylenedioxythiophene) doped with hyaluronic acid/poly(l-lactic acid) composite film for biomedical application. *J Biosci Bioeng.* **2017**, *123*, 116-125.
 105. Ohm, Y.; Pan, C.; Ford, M. J.; Huang, X.; Liao, J.; Majidi, C. An electrically conductive silver-polyacrylamide-alginate hydrogel composite for soft electronics. *Nat Electron.* **2021**, *4*, 185-192.
 106. Alizadeh, R.; Zarrintaj, P.; Kamrava, S. K.; Bagher, Z.; Farhadi, M.; Heidari, F.; Komeili, A.; Gutiérrez, T. J.; Saeb, M. R. Conductive

- hydrogels based on agarose/alginate/chitosan for neural disorder therapy. *Carbohydr Polym.* **2019**, *224*, 115161.
107. Mili, B.; Das, K.; Kumar, A.; Saxena, A. C.; Singh, P.; Ghosh, S.; Bag, S. Preparation of NGF encapsulated chitosan nanoparticles and its evaluation on neuronal differentiation potentiality of canine mesenchymal stem cells. *J Mater Sci Mater Med.* **2017**, *29*, 4.
 108. Qasim, S. B.; Zafar, M. S.; Najeeb, S.; Khurshid, Z.; Shah, A. H.; Husain, S.; Rehman, I. U. Electrospinning of chitosan-based solutions for tissue engineering and regenerative medicine. *Int J Mol Sci.* **2018**, *19*, 407.
 109. Aznar-Cervantes, S.; Pagán, A.; Martínez, J. G.; Bernabeu-Escapaz, A.; Otero, T. F.; Meseguer-Olmo, L.; Paredes, J. I.; Cenis, J. L. Electrospun silk fibroin scaffolds coated with reduced graphene promote neurite outgrowth of PC-12 cells under electrical stimulation. *Mater Sci Eng C Mater Biol Appl.* **2017**, *79*, 315-325.
 110. Cui, Y.; Zhang, F.; Chen, G.; Yao, L.; Zhang, N.; Liu, Z.; Li, Q.; Zhang, F.; Cui, Z.; Zhang, K.; Li, P.; Cheng, Y.; Zhang, S.; Chen, X. A stretchable and transparent electrode based on PEGylated silk fibroin for in vivo dual-modal neural-vascular activity probing. *Adv Mater.* **2021**, *33*, e2100221.
 111. Ding, J.; Chen, Z.; Liu, X.; Tian, Y.; Jiang, J.; Qiao, Z.; Zhang, Y.; Xiao, Z.; Wei, D.; Sun, J.; Luo, F.; Zhou, L.; Fan, H. A mechanically adaptive hydrogel neural interface based on silk fibroin for high-efficiency neural activity recording. *Mater Horiz.* **2022**, *9*, 2215-2225.
 112. Cho, Y.; Borgens, R. B. The effect of an electrically conductive carbon nanotube/collagen composite on neurite outgrowth of PC12 cells. *J Biomed Mater Res A.* **2010**, *95*, 510-517.
 113. Liu, X.; Yue, Z.; Higgins, M. J.; Wallace, G. G. Conducting polymers with immobilised fibrillar collagen for enhanced neural interfacing. *Biomaterials.* **2011**, *32*, 7309-7317.
 114. Yue, Z.; Liu, X.; Molino, P. J.; Wallace, G. G. Bio-functionalisation of polydimethylsiloxane with hyaluronic acid and hyaluronic acid-collagen conjugate for neural interfacing. *Biomaterials.* **2011**, *32*, 4714-4724.
 115. Dhawan, V.; Cui, X. T. Carbohydrate based biomaterials for neural interface applications. *J Mater Chem B.* **2022**, *10*, 4714-4740.
 116. Zhou, Y.; Gu, C.; Liang, J.; Zhang, B.; Yang, H.; Zhou, Z.; Li, M.; Sun, L.; Tao, T. H.; Wei, X. A silk-based self-adaptive flexible opto-electro neural probe. *Microsyst Nanoeng.* **2022**, *8*, 118.
 117. Yang, J.; Du, M.; Wang, L.; Li, S.; Wang, G.; Yang, X.; Zhang, L.; Fang, Y.; Zheng, W.; Yang, G.; Jiang, X. Bacterial cellulose as a supersoft neural interfacing substrate. *ACS Appl Mater Interfaces.* **2018**, *10*, 33049-33059.
 118. Potter-Baker, K. A.; Stewart, W. G.; Tomaszewski, W. H.; Wong, C. T.; Meador, W. D.; Ziats, N. P.; Capadona, J. R. Implications of chronic daily anti-oxidant administration on the inflammatory response to intracortical microelectrodes. *J Neural Eng.* **2015**, *12*, 046002.
 119. Golabchi, A.; Woepfel, K. M.; Li, X.; Lagenaur, C. F.; Cui, X. T. Neuroadhesive protein coating improves the chronic performance of neuroelectronics in mouse brain. *Biosens Bioelectron.* **2020**, *155*, 112096.
 120. Azemi, E.; Lagenaur, C. F.; Cui, X. T. The surface immobilization of the neural adhesion molecule L1 on neural probes and its effect on neuronal density and gliosis at the probe/tissue interface. *Biomaterials.* **2011**, *32*, 681-692.
 121. Oakes, R. S.; Polei, M. D.; Skousen, J. L.; Tresco, P. A. An astrocyte derived extracellular matrix coating reduces astrogliosis surrounding chronically implanted microelectrode arrays in rat cortex. *Biomaterials.* **2018**, *154*, 1-11.
 122. Vitale, F.; Shen, W.; Driscoll, N.; Burrell, J. C.; Richardson, A. G.; Adewole, O.; Murphy, B.; Ananthkrishnan, A.; Oh, H.; Wang, T.; Lucas, T. H.; Cullen, D. K.; Allen, M. G.; Litt, B. Biomimetic extracellular matrix coatings improve the chronic biocompatibility of microfabricated subdural microelectrode arrays. *PLoS One.* **2018**, *13*, e0206137.
 123. Ramesh, V.; Stratmann, N.; Schaufler, V.; Angelov, S. D.; Nordhorn, I. D.; Heissler, H. E.; Martínez-Hincapié, R.; Čolić, V.; Rehbock, C.; Schwabe, K.; Karst, U.; Krauss, J. K.; Barcikowski, S. Mechanical stability of nano-coatings on clinically applicable electrodes, generated by electrophoretic deposition. *Adv Healthc Mater.* **2022**, *11*, e2102637.
 124. Ramesh, V.; Rehbock, C.; Giera, B.; Karnes, J. J.; Forien, J. B.; Angelov, S. D.; Schwabe, K.; Krauss, J. K.; Barcikowski, S. Comparing direct and pulsed-direct current electrophoretic deposition on neural electrodes: deposition mechanism and functional influence. *Langmuir.* **2021**. doi: 10.1021/acs.langmuir.1c01081.
 125. Angelov, S. D.; Koenen, S.; Jakobi, J.; Heissler, H. E.; Alam, M.; Schwabe, K.; Barcikowski, S.; Krauss, J. K. Electrophoretic deposition of ligand-free platinum nanoparticles on neural electrodes affects their impedance in vitro and in vivo with no negative effect on reactive gliosis. *J Nanobiotechnology.* **2016**, *14*, 3.
 126. Yang, D.; Tian, G.; Liang, C.; Yang, Z.; Zhao, Q.; Chen, J.; Ma, C.; Jiang, Y.; An, N.; Liu, Y.; Qi, D. Double-microcrack coupling stretchable neural electrode for electrophysiological communication. *Adv Funct Mater.* **2023**, *33*, 2300412.
 127. Nguyen, T. K.; Barton, M.; Ashok, A.; Truong, T. A.; Yadav, S.; Leitch, M.; Nguyen, T. V.; Kashaninejad, N.; Dinh, T.; Hold, L.; Yamauchi, Y.; Nguyen, N. T.; Phan, H. P. Wide bandgap semiconductor nanomembranes as a long-term biointerface for flexible, implanted neuromodulator. *Proc Natl Acad Sci U S A.* **2022**, *119*, e2203287119.
 128. Dong, M.; Coleman, H. A.; Tonta, M. A.; Xiong, Z.; Li, D.; Thomas, S.; Liu, M.; Fallon, J. B.; Parkington, H. C.; Forsythe, J. S. Rapid electrophoretic deposition of biocompatible graphene coatings for high-performance recording neural electrodes. *Nanoscale.* **2022**, *14*, 15845-15858.
 129. Xiao, G.; Song, Y.; Zhang, Y.; Xing, Y.; Xu, S.; Lu, Z.; Wang, M.; Cai, X. Cellular-scale microelectrode arrays to monitor movement-related neuron activities in the epileptic hippocampus of awake mice. *IEEE Trans Biomed Eng.* **2021**, *68*, 19-25.
 130. Huang, W. C.; Hung, C. H.; Lin, Y. W.; Zheng, Y. C.; Lei, W. L.; Lu, H. E. Electrically copolymerized polydopamine melanin/poly(3,4-ethylenedioxythiophene) applied for bioactive multimodal neural interfaces with induced pluripotent stem cell-derived neurons. *ACS Biomater Sci Eng.* **2022**, *8*, 4807-4818.
 131. Saunier, V.; Flahaut, E.; Blatché, M. C.; Bergaud, C.; Maziz, A. Carbon nanofiber-PEDOT composite films as novel microelectrode for neural interfaces and biosensing. *Biosens Bioelectron.* **2020**, *165*, 112413.
 132. Yang, X.; Pei, W.; Wei, C.; Yang, X.; Zhang, H.; Wang, Y.; Yuan, M.; Gui, Q.; Liu, Y.; Wang, Y.; Chen, H. Chemical polymerization of conducting polymer poly(3,4-ethylenedioxythiophene) onto neural microelectrodes. *Sens Actuators A Phys.* **2023**, *349*, 114022.
 133. Lim, T.; Kim, M.; Akbarian, A.; Kim, J.; Tresco, P. A.; Zhang, H. Conductive polymer enabled biostable liquid metal electrodes for bioelectronic applications. *Adv Healthc Mater.* **2022**, *11*, e2102382.
 134. Ganji, M.; Hossain, L.; Tanaka, A.; Thunemann, M.; Halgren, E.; Gilja, V.; Devor, A.; Dayeh, S. A. Monolithic and scalable Au nanorod substrates improve PEDOT-metal adhesion and stability in neural electrodes. *Adv Healthc Mater.* **2018**, *7*, e1800923.
 135. Wei, B.; Liu, J.; Ouyang, L.; Kuo, C. C.; Martin, D. C. Significant

- enhancement of PEDOT thin film adhesion to inorganic solid substrates with EDOT-acid. *ACS Appl Mater Interfaces*. **2015**, *7*, 15388-15394.
136. Istif, E.; Mantione, D.; Vallan, L.; Hadziioannou, G.; Brochon, C.; Cloutet, E.; Pavlopoulou, E. Thiophene-based aldehyde derivatives for functionalizable and adhesive semiconducting polymers. *ACS Appl Mater Interfaces*. **2020**, *12*, 8695-8703.
 137. Tian, F.; Yu, J.; Wang, W.; Zhao, D.; Cao, J.; Zhao, Q.; Wang, F.; Yang, H.; Wu, Z.; Xu, J.; Lu, B. Design of adhesive conducting PEDOT-MeOH:PSS/PDA neural interface via electropolymerization for ultrasmall implantable neural microelectrodes. *J Colloid Interface Sci*. **2023**, *638*, 339-348.
 138. Desroches, P. E.; Silva, S. M.; Gietman, S. W.; Quigley, A. F.; Kapsa, R. M. I.; Moulton, S. E.; Greene, G. W. Lubricin (PRG4) antiadhesive coatings mitigate electrochemical impedance instabilities in polypyrrole bionic electrodes exposed to fouling fluids. *ACS Appl Bio Mater*. **2020**, *3*, 8032-8039.
 139. Wellens, J.; Deschaume, O.; Putzeys, T.; Eyley, S.; Thielemans, W.; Verhaert, N.; Bartic, C. Sulfobetaine-based ultrathin coatings as effective antifouling layers for implantable neuroprosthetic devices. *Biosens Bioelectron*. **2023**, *226*, 115121.
 140. Jeong, J. O.; Kim, S.; Park, J.; Lee, S.; Park, J. S.; Lim, Y. M.; Lee, J. Y. Biomimetic nonbiofouling polypyrrole electrodes grafted with zwitterionic polymer using gamma rays. *J Mater Chem B*. **2020**, *8*, 7225-7232.
 141. Lee, Y.; Shin, H.; Lee, D.; Choi, S.; Cho, I. J.; Seo, J. A lubricated nonimmunogenic neural probe for acute insertion trauma minimization and long-term signal recording. *Adv Sci (Weinh)*. **2021**, *8*, e2100231.
 142. Jain, V.; Forssell, M.; Tansel, D. Z.; Goswami, C.; Fedder, G. K.; Grover, P.; Chamanzar, M. Focused epicranial brain stimulation by spatial sculpting of pulsed electric fields using high density electrode arrays. *Adv Sci (Weinh)*. **2023**, *10*, e2207251.
 143. Chen, Z.; Liu, X.; Ding, J.; Tian, Y.; Zhang, Y.; Wei, D.; Sun, J.; Luo, F.; Zhou, L.; Fan, H. Tissue-like electrophysiological electrode interface construction by multiple crosslinked polysaccharide-based hydrogel. *Carbohydr Polym*. **2022**, *296*, 119923.
 144. Fabbro, A.; Prato, M.; Ballerini, L. Carbon nanotubes in neuroregeneration and repair. *Adv Drug Deliv Rev*. **2013**, *65*, 2034-2044.
 145. Ramer, L. M.; Ramer, M. S.; Bradbury, E. J. Restoring function after spinal cord injury: towards clinical translation of experimental strategies. *Lancet Neurol*. **2014**, *13*, 1241-1256.
 146. Ye, L.; Ji, H.; Liu, J.; Tu, C. H.; Kappl, M.; Koynov, K.; Vogt, J.; Butt, H. J. Carbon nanotube-hydrogel composites facilitate neuronal differentiation while maintaining homeostasis of network activity. *Adv Mater*. **2021**, *33*, e2102981.
 147. Tian, G.; Yang, D.; Chen, C.; Duan, X.; Kim, D. H.; Chen, H. Simultaneous presentation of dexamethasone and nerve growth factor via layered carbon nanotubes and polypyrrole to interface neural cells. *ACS Biomater Sci Eng*. **2023**, *9*, 5015-5027.
 148. Wei, W.; Hao, M.; Zhou, K.; Wang, Y.; Lu, Q.; Zhang, H.; Wu, Y.; Zhang, T.; Liu, Y. In situ multimodal transparent electrophysiological hydrogel for in vivo miniature two-photon neuroimaging and electrocorticogram analysis. *Acta Biomater*. **2022**, *152*, 86-99.
 149. Lee, J.; Jeong, H.; Kim, J.; Seo, J. M. Investigation of neural electrode fabrication process on Polycarbonate substrate. *Annu Int Conf IEEE Eng Med Biol Soc*. **2022**, *2022*, 3089-3092.
 150. Baek, C.; Kim, J.; Lee, Y.; Seo, J. M. Fabrication and evaluation of cyclic olefin copolymer based implantable neural electrode. *IEEE Trans Biomed Eng*. **2020**, *67*, 2542-2551.
 151. Altuna, A.; Menendez de la Prida, L.; Bellistri, E.; Gabriel, G.; Guimerá, A.; Berganzo, J.; Villa, R.; Fernández, L. J. SU-8 based microprobes with integrated planar electrodes for enhanced neural depth recording. *Biosens Bioelectron*. **2012**, *37*, 1-5.
 152. Ware, T.; Simon, D.; Arreaga-Salas, D. E.; Reeder, J.; Rennaker, R.; Keefer, E. W.; Voit, W. Fabrication of responsive, softening neural interfaces. *Adv Funct Mater*. **2012**, *22*, 3470-3479.
 153. Castagnola, E.; Ansaldo, A.; Fadiga, L.; Ricci, D. Chemical vapour deposited carbon nanotube coated microelectrodes for intracortical neural recording. *Phys Status Solidi B*. **2010**, *247*, 2703-2707.
 154. Choi, D. S.; Fung, A. O.; Moon, H.; Villareal, G.; Chen, Y.; Ho, D.; Presser, N.; Stupian, G.; Leung, M. Detection of neural signals with vertically grown single platinum nanowire-nanobud. *J Nanosci Nanotechnol*. **2009**, *9*, 6483-6486.
 155. Paik, S. J.; Cho, D. D. Development of recording microelectrodes with low surface impedance for neural chip applications. *J Korean Phys Soc*. **2002**, *41*, 1046-1049.
 156. Niederhoffer, T.; Vanhoostenberghe, A.; Lancashire, H. T. Methods of poly(3,4)-ethylenedioxythiophene (PEDOT) electrodeposition on metal electrodes for neural stimulation and recording. *J Neural Eng*. **2023**, *20*, 011002.
 157. Wang, Y.; Graham, E. S.; Unsworth, C. P. Superior galvanostatic electrochemical deposition of platinum nanograss provides high performance planar microelectrodes for intraneural recording. *J Neural Eng*. **2021**, *18*, 0460d0468.
 158. Zhang, C.; Driver, N.; Tian, Q.; Jiang, W.; Liu, H. Electrochemical deposition of conductive polymers onto magnesium microwires for neural electrode applications. *J Biomed Mater Res A*. **2018**, *106*, 1887-1895.
 159. Abidian, M. R.; Martin, D. C. Multifunctional nanobiomaterials for neural interfaces. *Adv Funct Mater*. **2009**, *19*, 573-585.
 160. Heo, D. N.; Kim, H. J.; Lee, Y. J.; Heo, M.; Lee, S. J.; Lee, D.; Do, S. H.; Lee, S. H.; Kwon, I. K. Flexible and highly biocompatible nanofiber-based electrodes for neural surface interfacing. *ACS Nano*. **2017**, *11*, 2961-2971.
 161. Jenkins, P. M.; Laughter, M. R.; Lee, D. J.; Lee, Y. M.; Freed, C. R.; Park, D. A nerve guidance conduit with topographical and biochemical cues: potential application using human neural stem cells. *Nanoscale Res Lett*. **2015**, *10*, 972.
 162. James, C. D.; Davis, R.; Meyer, M.; Turner, A.; Turner, S.; Withers, G.; Kam, L.; Banker, G.; Craighead, H.; Isaacson, M.; Turner, J.; Shain, W. Aligned microcontact printing of micrometer-scale poly-L-lysine structures for controlled growth of cultured neurons on planar microelectrode arrays. *IEEE Trans Biomed Eng*. **2000**, *47*, 17-21.
 163. Beom Jun, S.; Hynd, M.; Dowell-Mesfin, N.; Smith, K.; Turner, J.; Shain, W.; June Kim, S. Synaptic connectivity of a low density patterned neuronal network produced on the poly-L-lysine stamped microelectrode array. *Conf Proc IEEE Eng Med Biol Soc*. **2005**, *2005*, 7604-7607.
 164. Mehenti, N. Z.; Tsien, G. S.; Leng, T.; Fishman, H. A.; Bent, S. F. A model retinal interface based on directed neuronal growth for single cell stimulation. *Biomed Microdevices*. **2006**, *8*, 141-150.
 165. Seo, K. J.; Hill, M.; Ryu, J.; Chiang, C. H.; Rachinskiy, I.; Qiang, Y.; Jang, D.; Trumpis, M.; Wang, C.; Viventi, J.; Fang, H. A soft, high-density neuroelectronic array. *Npj Flex Electron*. **2023**, *7*, 40.
 166. Roh, H.; Yoon, Y. J.; Park, J. S.; Kang, D. H.; Kwak, S. M.; Lee, B. C.;

- Im, M. Fabrication of high-density out-of-plane microneedle arrays with various heights and diverse cross-sectional shapes. *Nanomicro Lett.* **2021**, *14*, 24.
167. Ando, D.; Teshima, T. F.; Zurita, F.; Peng, H.; Ogura, K.; Kondo, K.; Weiß, L.; Hirano-Iwata, A.; Becherer, M.; Alexander, J.; Wolfrum, B. Filtration-processed biomass nanofiber electrodes for flexible bioelectronics. *J Nanobiotechnology.* **2022**, *20*, 491.
168. Mailley, S. C.; Hyland, M.; Mailley, P.; McLaughlin, J. M.; McAdams, E. T. Electrochemical and structural characterizations of electrodeposited iridium oxide thin-film electrodes applied to neurostimulating electrical signal. *Mater Sci Eng C.* **2002**, *21*, 167-175.
169. Stöver, T.; Paasche, G.; Lenarz, T.; Ripken, T.; Breitenfeld, P.; Lubatschowski, H.; Fabian, T. Development of a drug delivery device: using the femtosecond laser to modify cochlear implant electrodes. *Cochlear Implants Int.* **2007**, *8*, 38-52.
170. Henle, C.; Raab, M.; Cordeiro, J. G.; Doostkam, S.; Schulze-Bonhage, A.; Stieglitz, T.; Rickert, J. First long term in vivo study on subdurally implanted micro-ECoG electrodes, manufactured with a novel laser technology. *Biomed Microdevices.* **2011**, *13*, 59-68.
171. Li, L.; Jiang, C.; Li, L. Hierarchical platinum-iridium neural electrodes structured by femtosecond laser for superwicking interface and superior charge storage capacity. *Bio-des Manuf.* **2022**, *5*, 163-173.
172. Yang, Q.; Hu, Z.; Seo, M. H.; Xu, Y.; Yan, Y.; Hsu, Y. H.; Berkovich, J.; Lee, K.; Liu, T. L.; McDonald, S.; Nie, H.; Oh, H.; Wu, M.; Kim, J. T.; Miller, S. A.; Jia, Y.; Butun, S.; Bai, W.; Guo, H.; Choi, J.; Banks, A.; Ray, W. Z.; Kozorovitskiy, Y.; Becker, M. L.; Pet, M. A.; MacEwan, M. R.; Chang, J. K.; Wang, H.; Huang, Y.; Rogers, J. A. High-speed, scanned laser structuring of multi-layered eco/bioresorbable materials for advanced electronic systems. *Nat Commun.* **2022**, *13*, 6518.
173. Amini, S.; Seche, W.; May, N.; Choi, H.; Tavousi, P.; Shahbazmohamadi, S. Femtosecond laser hierarchical surface restructuring for next generation neural interfacing electrodes and microelectrode arrays. *Sci Rep.* **2022**, *12*, 13966.
174. Won, D.; Kim, J.; Choi, J.; Kim, H.; Han, S.; Ha, I.; Bang, J.; Kim, K. K.; Lee, Y.; Kim, T. S.; Park, J. H.; Kim, C. Y.; Ko, S. H. Digital selective transformation and patterning of highly conductive hydrogel bioelectronics by laser-induced phase separation. *Sci Adv.* **2022**, *8*, eabo3209.
175. Pant, M.; Singh, R.; Negi, P.; Tiwari, K.; Singh, Y. A comprehensive review on carbon nano-tube synthesis using chemical vapor deposition. *Mater Today Proc.* **2021**, *46*, 11250-11253.
176. Ansaldo, A.; Castagnola, E.; Maggolini, E.; Fadiga, L.; Ricci, D. Superior electrochemical performance of carbon nanotubes directly grown on sharp microelectrodes. *ACS Nano.* **2011**, *5*, 2206-2214.
177. Lee, M.; Lee, S.; Kim, J.; Lim, J.; Lee, J.; Masri, S.; Bao, S.; Yang, S.; Ahn, J. H.; Yang, S. Graphene-electrode array for brain map remodeling of the cortical surface. *NPG Asia Mater.* **2021**, *13*, 65.
178. Bakhshae Babaroud, N.; Palmar, M.; Velea, A. I.; Coletti, C.; Weingärtner, S.; Vos, F.; Serdijn, W. A.; Vollebregt, S.; Giagka, V. Multilayer CVD graphene electrodes using a transfer-free process for the next generation of optically transparent and MRI-compatible neural interfaces. *Microsyst Nanoeng.* **2022**, *8*, 107.
179. Lee, J. Y.; Bashur, C. A.; Goldstein, A. S.; Schmidt, C. E. Polypyrrole-coated electrospun PLGA nanofibers for neural tissue applications. *Biomaterials.* **2009**, *30*, 4325-4335.
180. Mousavi, H.; Ferrari, L. M.; Whiteley, A.; Ismailova, E. Kinetics and physicochemical characteristics of electrodeposited PEDOT:PSS thin film growth. *Adv Electron Mater.* **2023**, *9*, 2201282.
181. Yang, M.; Yang, T.; Deng, H.; Wang, J.; Ning, S.; Li, X.; Ren, X.; Su, Y.; Zang, J.; Li, X.; Luo, Z. Poly(5-nitroindole) thin film as conductive and adhesive interfacial layer for robust neural interface. *Adv Funct Mater.* **2021**, *31*, 2105857.
182. Skoog, S. A.; Kumar, G.; Narayan, R. J.; Goering, P. L. Biological responses to immobilized microscale and nanoscale surface topographies. *Pharmacol Ther.* **2018**, *182*, 33-55.
183. Newman, P.; Galenano Niño, J. L.; Graney, P.; Raza, J. M.; Minett, A. I.; Ribas, J.; Ovalle-Robles, R.; Biro, M.; Zreiqat, H. Relationship between nanotopographical alignment and stem cell fate with live imaging and shape analysis. *Sci Rep.* **2016**, *6*, 37909.
184. Zijl, S.; Vasilevich, A. S.; Viswanathan, P.; Helling, A. L.; Beijer, N. R. M.; Walko, G.; Chiappini, C.; de Boer, J.; Watt, F. M. Micro-scaled topographies direct differentiation of human epidermal stem cells. *Acta Biomater.* **2019**, *84*, 133-145.
185. Simitzi, C.; Ranella, A.; Stratakis, E. Controlling the morphology and outgrowth of nerve and neuroglial cells: The effect of surface topography. *Acta Biomater.* **2017**, *51*, 21-52.
186. Luo, J.; Walker, M.; Xiao, Y.; Donnelly, H.; Dalby, M. J.; Salmeron-Sanchez, M. The influence of nanotopography on cell behaviour through interactions with the extracellular matrix - a review. *Bioact Mater.* **2022**, *15*, 145-159.
187. Geiger, B.; Spatz, J. P.; Bershadsky, A. D. Environmental sensing through focal adhesions. *Nat Rev Mol Cell Biol.* **2009**, *10*, 21-33.
188. Lord, M. S.; Foss, M.; Besenbacher, F. Influence of nanoscale surface topography on protein adsorption and cellular response. *Nano Today.* **2010**, *5*, 66-78.
189. Kim, M. H.; Park, M.; Kang, K.; Choi, I. S. Neurons on nanometric topographies: insights into neuronal behaviors in vitro. *Biomater Sci.* **2014**, *2*, 148-155.
190. Arora, S.; Lin, S.; Cheung, C.; Yim, E. K. F.; Toh, Y. C. Topography elicits distinct phenotypes and functions in human primary and stem cell derived endothelial cells. *Biomaterials.* **2020**, *234*, 119747.
191. Curtis, A.; Wilkinson, C. Topographical control of cells. *Biomaterials.* **1997**, *18*, 1573-1583.
192. Nowduri, B.; Schulte, S.; Decker, D.; Schäfer, K. H.; Saumer, M. Biomimetic nanostructures fabricated by nanoimprint lithography for improved cell-coupling. *Adv Funct Mater.* **2020**, *30*, 2004227.
193. Tringides, C. M.; Boulingre, M.; Khalil, A.; Lungjangwa, T.; Jaenisch, R.; Mooney, D. J. Tunable conductive hydrogel scaffolds for neural cell differentiation. *Adv Healthc Mater.* **2023**, *12*, e2202221.
194. Wang, J.; Wang, H.; Mo, X.; Wang, H. Reduced graphene oxide-encapsulated microfiber patterns enable controllable formation of neuronal-like networks. *Adv Mater.* **2020**, *32*, e2004555.

Received: September 30, 2023

Revised: November 13, 2023

Accepted: November 24, 2023

Available online: December 28, 2023

Recent advances of medical polyhydroxyalkanoates in musculoskeletal system

Chen-Hui Mi^{1, #}, Xin-Ya Qi^{1, #}, Yan-Wen Ding^{1, #}, Jing Zhou¹, Jin-Wei Dao^{1, 3}, Dai-Xu Wei^{1, 2, 4, *}

Key Words:

drug delivery; musculoskeletal system; polyhydroxyalkanoate; tissue engineering

From the Contents

Introduction	234
The Advantages of Polyhydroxyalkanoate for the Musculoskeletal System	236
Applications of Tissue-Engineered Polyhydroxyalkanoate Scaffolds in the Musculoskeletal System	236
Applications of Polyhydroxyalkanoate Carriers in Drug Delivery in the Musculoskeletal System	240
Application of Polyhydroxyalkanoate Degradation Products and Derivatives in the Musculoskeletal System	241
Conclusions and Future Perspectives	242

ABSTRACT

Infection and rejection in musculoskeletal trauma often pose challenges for natural healing, prompting the exploration of biomimetic organ and tissue transplantation as a common alternative solution. Polyhydroxyalkanoates (PHAs) are a large family of biopolyesters synthesised in microorganism, demonstrating excellent biocompatibility and controllable biodegradability for tissue remodelling and drug delivery. With different monomer-combination and polymer-types, multi-mechanical properties of PHAs making them have great application prospects in medical devices with stretching, compression, twist in long time, especially in musculoskeletal tissue engineering. This review systematically summarises the applications of PHAs in multiple tissues repair and drug release, encompassing areas such as bone, cartilage, joint, skin, tendons, ligament, cardiovascular tissue, and nervous tissue. It also discusses challenges encountered in their application, including high production costs, potential cytotoxicity, and uncontrollable particle size distribution. In conclusion, PHAs offer a compelling avenue for musculoskeletal system applications, striking a balance between biocompatibility and mechanical performance. However, addressing challenges in their production and application requires further research to unleash their full potential in tackling the complexities of musculoskeletal regeneration.

*Corresponding author:

Dai-Xu Wei,
daviddxwei@163.com, or
weidaixu@nwu.edu.cn.

#Author equally.

<http://doi.org/10.12336/biomatertransl.2023.04.004>

How to cite this article:

Mi, C. H.; Qi, X. Y.;
Ding, Y. W.; Zhou, J.;
Dao, J. W.; Wei, D. X.
Recent advances of medical
polyhydroxyalkanoates in
musculoskeletal system.
Biomater Transl. 2023, 4(4),
234-247.



Introduction

The musculoskeletal system is the largest human organ system, including the supporting bone, cartilage and joint, skin, tendon and ligament, cardiovascular tissue and nervous tissue, which are the basis of human life activities.¹ As one of the systems most commonly affected by trauma, the ability of the musculoskeletal system to spontaneously repair itself after injury varies greatly. In many cases, healing is incomplete.²⁻⁵ Transplantation is the only possible option for functional recovery, but problems such as infections, complications and even immune rejection occur in both autologous and allogeneic transplantation.⁶⁻⁸ To solve these transplantation problems, biodegradable biomaterials have been developed. Polyhydroxyalkanoate (PHA) scaffolds

are characterised by good biodegradability, biocompatibility and variable mechanical properties, providing a new idea for the repair and regeneration of the musculoskeletal system.⁹⁻¹¹

PHAs were discovered by Lemogine in 1926 and is kinds of bacteria-synthesised polymers,¹² which can replace non-biodegradable fossil plastics, thereby reducing health hazards and negative environmental impacts.¹³ Compared with other biomaterials, PHAs have excellent biodegradability and biocompatibility, which has led to increasing research in the fields of biomedicine, food, cosmetics, and healthcare.¹⁴⁻¹⁷ From a chemical perspective, PHAs are aliphatic polyesters. The nanofibres range in diameter from 50 nm to 500 nm, and can perfectly simulate the collagen fibres required for the

PHA and its composites in musculoskeletal system

repair process of the musculoskeletal system.^{18, 19} The PHAs' family includes short-chain length PHA (scl-PHA; three to five carbon atoms), medium-chain length PHA (mcl-PHA; six to fourteen carbon atoms), and long-chain length PHA (fifteen or more carbon atoms).²⁰ Scl-PHA consists of 3-hydroxybutyrate (3HB), 4-hydroxybutyrate (4HB), or 3-hydroxyvalerate. Mcl-PHA is the largest category in the PHA family, including monomeric units of 3-hydroxyhexanoate (HHx), 3-hydroxyoctanoate, 3-hydroxydecanoate, 3-hydroxydodecanoate, 3-hydroxytetradecanoate, or even longer-chain comonomer units.²¹ Scl-PHA and its copolymers are semi-crystalline polymers with high melting temperature, which are hard, brittle and highly crystalline in nature.^{22, 23} Mcl-PHA, on the other hand, is a crystalline polymer that melts at a lower temperature than scl-PHA (in the range of 39–65°C), is inherently elastomer, more flexible, and has a lower crystallinity (25%), and is called true elastomer because of its

lower melting point, when the temperature reaches melting temperature, they become viscous and amorphous. Can be better used in health care.^{24–27} Currently, six main types of PHA have been widely applied (**Figure 1**). PHAs have different mechanical properties with different molecular weights, alkyl side group lengths, and comonomer unit ratios, making them suitable for tissue engineering with different hardness levels.^{20, 28} Currently, multiple methods have been used to prepare PHA scaffolds. The commonly used technologies include solvent casting particle leaching, fibre spinning technology, melt forming, special leaching injection moulding, freeze drying, phase separation, electrospinning, and gas foaming. This article reviews the properties of PHA scaffolds as biomaterials for musculoskeletal repair and regeneration and also summarises the applications of PHAs in bone, cartilage and joint, skin, tendon and ligament, cardiovascular tissue and nervous tissue (**Figure 2**).

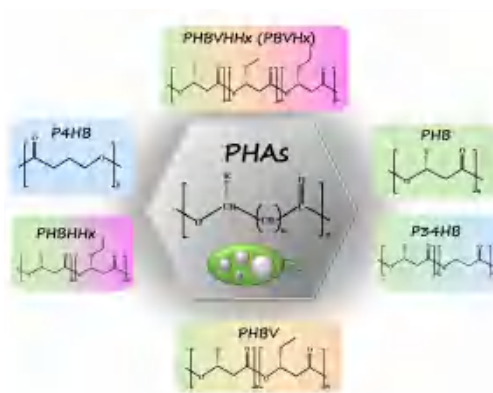


Figure 1. The general structure of PHAs and six commercial PHAs. Created with ChemDraw 2022 and Microsoft PowerPoint 2019. P34HB: poly(3-hydroxybutyrate-co-4-hydroxybutyrate); P4HB: poly(4-hydroxybutyric acid); PHA: polyhydroxyalkanoate; PHB: poly(3-hydroxybutyric acid); PHBHHx: poly(3-hydroxybutyrate-co-3-hydroxyhexanoate); PHBV: poly(3-hydroxybutyrate-co-3-hydroxyvalerate); PHBVHHx (PBVHx): poly(3-hydroxybutyric acid-co-3-hydroxyvaleric acid-co-3-hydroxyhexanoic acid trimer).

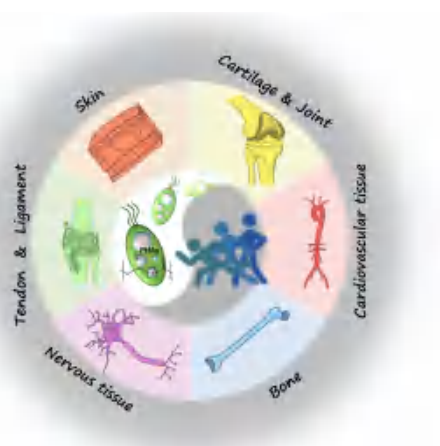


Figure 2. Applications of PHA in the musculoskeletal system. Created with Microsoft PowerPoint 2019. PHA: polyhydroxyalkanoate.

1 Key Laboratory of Resource Biology and Biotechnology in Western China, Ministry of Education, School of Medicine, Department of Life Sciences and Medicine, Northwest University, Xi'an, Shaanxi Province, China; 2 Zigong Affiliated Hospital of Southwest Medical University, Zigong Psychiatric Research Center, Zigong Institute of Brain Science, Zigong, Sichuan Province, China; 3 Dehong Biomedical Engineering Research Center, Dehong Teachers' College, Dehong, Yunnan Province, China; 4 Shaanxi Key Laboratory for Carbon Neutral Technology, Xi'an, Shaanxi Province, China

The Advantages of Polyhydroxyalkanoate for the Musculoskeletal System

Materials used for musculoskeletal tissue engineering must not only have good biocompatibility, support cell growth, guide and organise cells, enable tissue ingrowth, and ultimately degrade into non-toxic products, but also have mechanical and chemical properties of the scaffold.^{29, 30} Recent studies have found that some types of PHA have good biocompatibility and can support cell growth and proliferation.³¹⁻³⁴ Furthermore, the tunable mechanical properties of PHA enable it to be widely used as a scaffold in bone tissue engineering.³⁵ For example, by changing the percentage of HHx, the elastic properties of poly(3-hydroxybutyrate-co-3-hydroxyhexanoate) (PHBHHx) can be adjusted and can be applied to engineered tissues with different hardness requirements: bone, cartilage, nerves and blood vessels.³¹

Biocompatibility

The biocompatibility of the material reflects whether the material will be toxic to the body after implantation; therefore, good biocompatibility is a necessary prerequisite for the successful transplantation of materials for the musculoskeletal system into the human body or animals.³⁶ In recent years, the biocompatibility of different types of PHA materials has been tested through a variety of studies. Poly(3-hydroxybutyric acid) (PHB), or polyhydroxybutyrate-co-valerate (PHBV) as a commonly used PHA material, can be used to prepare *in vitro* proliferation cell matrix. Chen et al.³¹ found that PHB and PHBV promote cell adhesion from various sources, such as fibroblasts, endothelial cells, and isolated hepatocytes. PHBV films proved to have the same properties.³⁷ In addition, another PHA called poly(3-hydroxybutyric acid-co-3-hydroxyvaleric acid-co-3-hydroxyhexanoic acid trimer) (PHBVHHx) can significantly promote the proliferation and adhesion of human umbilical cord mesenchymal stem cells³⁸ and bone marrow mesenchymal stem cells.³³

However, different types of PHA have different biocompatibilities. A study found that although both PHB and PHBV can promote cell proliferation and adhesion, PHBV has better biocompatibility.³⁹ Another study with inoculating rabbit bone marrow cells on the PHBHHx triad scaffold found that its cell adhesion proliferation ability was significantly better than that of PHB, proving that PHBHHx also has better biocompatibility than PHB.⁴⁰ In addition, some studies have shown that the biocompatibility of PHB and PHBV can be improved by surface modification. Tesema et al.⁴¹ used collagen to physically and chemically fix the surface of PHBV membrane and found that PHBV could better promote cell proliferation. Chen et al.⁴² improved the cytocompatibility by ion implantation into the posterior membrane. Wu et al.⁴³ modified the surface of the PHB using gelatin and implanted adrenal cortical cells into the modified PHB. The study has shown that the modified PHB is prone to cell proliferation.⁴³ Yu et al.⁴⁴ used hyaluronic acid (HA) to modify the surface properties of PHA films. They found that HA coated on PHA membranes can improve the metabolic activity of mesenchymal stem cells.⁴⁴ All of the above studies indicate that PHA has good biocompatibility and can be used in the musculoskeletal system.

Biodegradability

PHAs are a type of biopolymer made of polyesters with many different hydroxycarboxylic acid molecules,⁴⁵ which can be degraded into monomers or oligomers. Whether the degradation products are toxic is closely related to whether PHA can be used in tissue engineering.³⁶ Fortunately, among the degradation products of PHA, 3HB and 4HB are natural metabolites in the human body. 3HB is a component of the blood, and 4HB is widely distributed in all major organs of the body.³⁰ In addition, another study has found that PHA must be degraded at an appropriate rate to prevent inflammation and rejection of the implant material.⁴⁰ The biodegradability of five different types of PHA was found the biodegradability of HA is related to its chemical composition.⁴⁶ Qu et al.⁴⁷ found the degradation rate of PHB < PHBHHx < polylactic acid (PLA) by studying the *in vivo* tissue reaction and biodegradation of PHBHHx, PLA, PHB, PHBHHx (X), and poly(ethylene glycol) (PEG) (E) blends.

Multiple mechanical properties

The biomaterials used for musculoskeletal system recovery require a certain tensile strength, elongation at break and toughness.^{48, 49} The reconstruction of bones, cartilage and joints in the musculoskeletal system requires a certain degree of hardness, while the recovery of muscles, tendons and ligaments requires a certain degree of toughness. Since the mechanical strength of PHA scaffolds is determined by the monomer composition of PHA, the chain length, and the distance between the ester bond and the R base, they can be widely used in the musculoskeletal system.^{50, 51} As an important member of scl-PHA, PHB has superior thermoplastic properties, but its mechanical properties are poor and can be used to induce osteogenic processes.⁵² On the contrary, another type of scl-PHA, poly(4-hydroxybutyric acid), has strong ductility, tensile strength, and elasticity. In summary, scl-PHA is relatively hard and brittle, lacks toughness, and can be used for bone tissue reconstruction.³⁰ Mcl-PHA is different from scl-PHA in that it has good flexibility and elasticity and can be used as a semi-crystalline biomaterial. As the side chain length further increases, they become stickier.⁵³ Scl-PHA-mcl-PHA copolymer like PHBHHx can combine the benefits of both to better support the musculoskeletal system recovery. In order to obtain copolymers with more suitable mechanical properties of PHA, researchers have made many efforts to make PHA can be applied to a greater extent.^{54, 55}

Applications of Tissue-Engineered Polyhydroxyalkanoate Scaffolds in the Musculoskeletal System

As a biomaterial with good performance, various PHA types and manufacturing technologies can be used for a variety of biomedical applications, including the musculoskeletal system.⁵⁶ When applied to the musculoskeletal system, PHA should not only have biocompatibility, biological activity, and good mechanical properties but also have bone conductivity and even bone sensitivity to promote the growth of new tissue.⁵⁷ Due to its biological characteristics, it helps to maintain the mechanical integrity, strength, and toughness

PHA and its composites in musculoskeletal system

of the musculoskeletal system. In addition, it actively participates in various important biological processes such as cell adhesion, migration, proliferation, differentiation, and neuroangiogenesis and plays an important role in regulating inflammation, wound healing, and tissue repair, such as promoting the differentiation and growth of osteoblasts and chondrocytes and inhibiting the proliferation of bacteria such as *Escherichia coli*.^{58–62} The specific applications are listed in **Table 1**.^{36, 45, 63–97}

Bone

Although significant progress has been made in the field of regenerative medicine, bone tissue engineering repair and regeneration still faces major challenges given the peculiarities of bone tissue engineering.⁶⁶ Many studies have shown that PHA, as a biomaterial with good properties, can promote the adhesion, proliferation, and differentiation of mesenchymal stem cells and bone cells, can inhibit bacteria to some extent, and has excellent mechanical properties compared with other biological materials. Its complexes are often used in bone tissues. In addition, scaffolds for bone tissue repair also have appropriate porous structures and microenvironments that promote cell adhesion and growth, mimicking the microstructure and function of natural bone.^{98,99} For example, the highly porous microspheres prepared by Wei et al.¹⁰⁰ using PHA not only improved differentiation of human bone marrow mesenchymal stem cells, but also support stronger osteoblast regeneration. Codreanu et al.⁶³ investigated the restorative ability of bacterial cellulose (BC)-modified polyhydroxychain alkanoate (PHB/BC) stents obtained using salt roomision technology in skull fractures of mice and showed that PHB/BC stents can promote osteoblast differentiation in mice. Nishizuka et al.⁶⁷ developed a technology for intramedullary fixation of long bone fractures made of biodegradable materials. In animal experiments, there was no fracture displacement in the intramedullary-fixation with biodegradable materials group (poly(L-lactide) + calcium phosphate cement + PHA), even when the rabbits were fully loaded. It is shown that this type of biological scaffold can be used to strengthen and stabilise fractures of long bones.⁶⁷ On the other hand, PHA scaffolds can promote cell proliferation and differentiation. Research shows that PHBHHx scaffold has adequate osteoblast attachment and proliferation roughness compared with PHB and PLA, which is suitable for myelocyte attachment, proliferation and differentiation.³² Pecorini et al.⁶⁴ found that the PHBV-poly (D, L-lacrolide-co-glycol ester) hybrid scaffold prepared by the scaffold can promote the colonisation and differentiation of rat osteoblasts into osteoblastic phenotypes. Two studies also confirmed that when PHA (polyhydroxyoctanoate and poly(3-hydrobutyric acid)) is mixed with tricalcium phosphate, it can promote cell proliferation, maintain high cell activity, and nourish surrounding tissues.^{68,71} In addition, the materials implanted during bone regeneration should also have certain antibacterial properties. Marcello et al.³⁶ found that the composite sample prepared from PHA and a new antibacterial HA containing strontium selenide could inhibit the bacterial cell activity of *Staphylococcus aureus* 6538P and *Escherichia coli* 8739 with

good antibacterial performance through *in vitro* antibacterial tests. Experiments show that P(3HO-co-3HD-co-3HDD) composite membrane loaded with different contents of Se-Sr-HA, the bactericidal effect on *Staphylococcus aureus* 6538P is not the same: Composite membranes containing 10 wt% Se-Sr-HA resulted in an average 90% reduction in cell numbers, but bacterial cells were reduced by an average of 96% when the Se-Sr-HA content was 30 wt%.³⁶ Chotchindakun et al.⁶⁹ used the emission solvent extraction/evaporation method to incorporate mesoporous bioactive glass nanoparticles into PHBV, while cinnamaldehyde was loaded in mesoporous bioactive glass nanoparticles. The microspheres loaded with cinnamaldehyde showed that the activity of *Staphylococcus aureus* and *Escherichia coli* could be significantly inhibited in the first 3 hours, and cinnamaldehyde release behaviour lasted for 7 days. The research results suggest that the system represents an alternative model for antibacterial biomaterials and can be used for potential applications in bone tissue engineering.⁶⁹ In addition, Zhao et al.¹⁰¹ simulated the preparation of an intracellular growth factor release system based on PLA and PHA nanoparticles under microgravity conditions, and the results proved that the mixed nanoparticles can be used as a reliable and stable medium and long term osteogenic differentiation in future space medicine.¹⁰¹

Cartilage and joint

At the heart of the musculoskeletal system, articular cartilage plays a role in connecting bones, absorbing mechanical loads and providing lubrication. Articular cartilage is usually understood to be an elastic connective tissue without blood vessels, nerves, or lymphatic vessels. Its damage can be caused by various causes, and the internal repair capacity of the tissue is very limited.^{102,103} When defects in articular cartilage cannot be repaired, it often leads to degenerative joint diseases, such as arthritis. Unfortunately, current clinical interventions have shown little effectiveness in treating such diseases, while cartilage tissue engineering offers new strategies and directions.¹⁰⁴ Considering that PHAs have excellent properties in cartilage tissue engineering, they can be widely used as biomaterials in cartilage tissue engineering. Ching et al.⁷⁰ found that nanofibre PHB/poly(3-hydroxycaprylic acid) scaffolds matched the collagen fibres and stiffness of natural cartilage and could be a good material for cartilage repair. Research has shown that the addition of halloysite nanotubes to scaffolds (such as PHB-chitosan and PHB-starch) can improve the performance of the scaffold: the tensile strength is improved, the hydrophilicity of the material is also improved, and the scaffold with halloysite nanotubes supports cell growth and attachment, and cell activity is also increased. It is expected to find application in cartilage tissue engineering.^{73,105} Studies have shown that polyhydroxyalkanoate granule-binding protein (PhaP) or phasin is a heat-stable amphiphilic protein located on the surface of microbial stored polyhydroxyalkanoate particles, which can be used as a natural environmentally friendly surfactant for food, cosmetics and pharmaceuticals.¹⁰⁶ By coating the PHBHHx membrane onto the surface of Arg-Gly-Asp (RGD) peptide-fused PhaP, Li et al.⁷⁴ found that PHAP-RGD coating can promote the proliferation and cartilage differentiation of

Table 1. Applications of PHAs in the musculoskeletal system

Application	Material type	Fabrication method	Function	Reference
Bone	PHB/BC	Salt leaching technique	Promote bone formation in critical size calvarial defects in mice	63
	PHAs/Se-Sr-HA	Solvent casting	A high reduction of the number of <i>Staphylococcus aureus</i> 6538P and <i>Escherichia coli</i> 8739 bacterial cells	36
	PHBV/PLGA	Computer-aided wet-spinning	Support murine preosteoblast cell colonisation and differentiation towards an osteoblastic phenotype	64
	TCP/PHO	Soaking and drying	Enhance the wettability towards more cell-friendly material, enhance the durability of the composites (stress-strain characteristics)	65
	P(3HO-co-3HHX)/HA	Solvent casting-particulate leaching	Allow migration and proliferation of osteoblasts and mesenchymal cells as well as vascularisation	66
	IM-BM(PLLA+CPC+PHA)	Electrospinning	Reinforce and stabilise incomplete fractures with both mechanical testing and an animal experiment	67
	β TCP/P(3HB)	Polyurethane sponge replica method followed by polymer infiltration	Provide cell-friendly environment, ensure high cell viability, and reduce surface hydrophobicity	68
	PHBV/MBGN/CIN	Emulsion solvent extraction/evaporation	High biological activity and antibacterial performance applied simultaneously in bone tissue engineering	69
Cartilage and joint	Poly(3-hydroxybutyrate)/poly(3-hydroxyoctanoate)	Electrospinning	Allow to produce a cartilage repair kit for clinical use to reduce the risk of developing secondary osteoarthritis	70
	PLCL/PHBV	Emulsion solvent evaporation	Enhance the compressive modulus of PLCL scaffolds, but could also serve as scaffolding structures for cartilaginous tissue formation	71
	PHB-CS/HNT	Electrospinning	Demonstrate a significant increase in cell viability of chondrocytes	72
	PHB-starch/HNTs	Electrospinning	Improve the tensile strength, support cell growth and attachment without any toxicity for biomedical applications	73
	PhaP-RGD/PHBHHx	Solvent evaporation	The biomaterial films of PHBHHx modified with PhaP-RGD fusion protein can promote its biocompatibility with chondrocytes	72
			Promote the proliferation and chondrogenic differentiation of human umbilical-cord-derived mesenchymal stem cells seeded on PHBHHx films	74
			Lead to more homogeneous cell spreading, better cell adhesion, proliferation and chondrogenic differentiation in the scaffolds	75
Skin	PHB/PHB-HV	Electrospinning	Improve vascularisation of engineered bone tissue	76
	PHB/CA	Electrospinning	Improve cell proliferation	77
	PHB/HEAA	Grafting	Promote the proliferation of human fibroblasts	78
	P(3HB-co-4HB)	Freeze-drying	Promote the adhesion of mouse fibroblasts	79
	PHB	Electrospinning	Support the growth of normal human dermal fibroblasts and keratinocytes	80
			Promote the healing of diabetic wounds	81, 82
Tendon and ligament	PHBA/CA	Electrospinning	Improve fibroblast adhesion and growth	83
	PHB/PHBV/PHUE/PHOUE	Electrospinning	Promote cell adhesion and proliferation	84
	PHBHHX	Electrospinning	Promote tendon repair <i>in vivo</i> , which is conducive to restoring weight-bearing and motor function	45

Table 1. Continued

Application	Material type	Fabrication method	Function	Reference
Cardiovascular	PHA	Make thin films	Promote adhesion and migration of mesenchymal stem cells and tendon cells	85
		Mesh-augmented single-row RCRs and nonaugmented RCRs	Improve the initial biomechanical repair strength of tears at risk of rupture	86
	PHA	Electrospinning	Promote the fusion of scaffolds with cells	87
	PHB	Electrospinning	Promote the adhesion and growth of cardiomyocytes and cardiac fibroblasts	88
	PHBHHx/SF P(3HO)	Make thin films Cardiac patches	Promote cell adhesion and proliferation Promote the adhesion and proliferation of neonatal ventricular rat muscle cells	89 90
Nervous	PHB	Electrospinning	Have high biocompatibility with human mesenchymal stem cells	91
			Promotes the adhesion and differentiation of embryonic cells into nerve cells	92
			Support the survival and regeneration of neurons after spinal cord injury	93
	PHB/PHBV	Electrospinning	Promote the interaction between Schwann cells and scaffolds	93
	PCL-PHB	Electrospinning	Triggers the activity of Schwann cells	94
			Pluripotent stem cells were induced to differentiate into neurons	95
PHBHHx	Porous nerve conduit	Electrospinning	Have good nerve regeneration ability, which can promote the rapid functional recovery of damaged nerves	96
		Electrospinning	Promote the differentiation of neural stem cells into neurons	97

Note: CA: cellulose; CIN: cinnamaldehyde; CPC: calcium phosphate cement; HA: hyaluronic acid; HEAA: N-hydroxyethyl acrylamide; HNTs: halloysite nanotubes; HV: 3-hydroxyvalerate; IM-BM: intramedullary-fixation with biodegradable materials; MBGN: mesoporous bioactive glass nanoparticles; P(3HB): poly(3-hydroxybutyric acid); P(3HB-co-4HB): poly(3-hydroxybutyric acid co-4-hydroxybutyric acid); P(3HO): poly(3-hydroxyoctanoate); P(3HO-co-3HHX): poly(3-hydroxyoctanoate-co-3-hydroxyhexanoate); PCL: poly(ϵ -caprolactone); PhaP: polyhydroxyalkanoate granule-binding protein; PHA: polyhydroxyalkanoate; PHB: polyhydroxybutyrate; PHB/BC: polyhydroxychain alkanoate; PHB-CS: PHB-chitosan; PHBHHx: poly(D, L-lactide co glycol ester); PHBV: polyhydroxy-butyrate-co-valerate; PHO: polyhydroxyoctanoate; PHOUE: poly([R]-3-hydroxy-omega-undecenoate-co-3-hydroxy-omega-nonenoate-co-3-hydroxyoctanoate-co-3-hydroxy-omega-heptenoate-co-3-hydroxyhexanoate); PLCL: poly L-lactide co- ϵ -caprolactone; PLGA: poly(3-hydroxybutyric acid); PLLA: poly(L-lactide); RGD: Arg-Gly-Asp; SF: silk fibroin; TCP: tricalcium phosphate.

human umbilical cord blood-derived mesenchymal stem cells inoculated on the PHBHHx membrane. Despite their similar surface topography, it is worth noting that the coated film can reduce the water contact Angle from 98.69° to 10.63°.74 In addition, You et al.75 found that PHBHHx scaffolds coated with PhaP-RGD can promote the proliferation and cartilage differentiation of human bone marrow mesenchymal stem cells. Additionally, RGD also had a positive influence on the extracellular matrix: increased expression of chondrocyte-specific genes and increased content of cartilage-specific extracellular substances.75 Meanwhile, PHBHHx biomaterial membrane modified with PhaP-RGD fusion protein can also promote its biocompatibility with chondrocytes.72 Not only are porous scaffolds widely used as biodegradable biomaterials, but microspheres can also serve as potential candidates for cartilage tissue engineering. Li et al.71 found that mixing PHBV microspheres with poly L-lactide co- ϵ -caprolactone porous scaffolds can not only improve the compression modulus of

poly L-lactide-co-caprolactone scaffolds but also serve as scaffolds formed by cartilage tissue.

Skin

Because skin wound healing is an extremely complex process, high standards apply to biomaterials used for skin tissue engineering.107, 108 PHAs not only have good biocompatibility, but can also support cell growth and are often used in skin tissue engineering. PHB is the most common one in PHAs. Zonari et al.76 found that electrospun PHB/PHB-3-hydroxyvalerate fibre sheets can be used in combination with endothelial differentiated cells to promote vascularisation of bone tissue. Zhijiang et al.77 found that PHB/cellulose hybrid nanofibre scaffolds have biological activity, can promote cell proliferation, and can be used as wound dressings or tissue engineering scaffolds. Ochoa-Segundo et al.78 found that the prepared N-hydroxyethyl acrylamide monomer and PHB graft copolymer had adequate degradation and porosity, improved

mechanical properties, and could promote human fibroblast culture, which could be widely used in skin tissue engineering. The biocomposite scaffold prepared by Kanimozhi et al.⁷⁹ with poly (3-hydroxybutyric acid co-4-hydroxybutyric acid) and BC as raw materials can promote the adhesion of mouse fibroblasts and can be used for wound repair or tissue engineering scaffolds. The PHB-core-coated coaxial electrospun fibre prepared by Nagiah et al.⁸⁰ has good stretch properties in skin regeneration and can support the growth of normal human dermal fibroblasts and keratinocytes, indicating its potential as a scaffold for skin regeneration. In addition, studies have shown that PHB can promote the healing of diabetic wounds, so PHAs may play a role in the regeneration of diabetic wound tissue.^{81,82} PHBV is another polymer of PHA, and studies have shown that PHBV/chitosan (4:1) scaffolds have an excellent ability to improve the adhesion and growth of fibroblasts and can better adapt to the wound healing process *in vivo*.^{83,109}

Tendon and ligament

In tendon and ligament tissue engineering, it is required that the biomaterials used not only have good mechanical properties but also that the degradation rate of polymers cannot be too fast, and the members of PHA just meet the above conditions. Rathbone et al.⁸⁴ used L929 mouse fibroblasts to study the biocompatibility of PHAs. They found that the membranes prepared by PHB and PHBV not only had good biocompatibility but could effectively promote cell adhesion and proliferation and could also degrade slowly due to surface erosion. Therefore, PHA can be widely used in tendon and ligament tissue engineering.⁸⁴

Since tendon injury is not easy to repair and all repair methods may have potential problems (such as foreign body reactions) and fracture again, it is required that materials used for tendon tissue engineering can simulate the structure and mechanical properties of natural tendon tissue.^{45,110-116} Webb et al.⁴⁵ found that the PHBHHx stent can promote the repair of the Achilles tendon in rats, which is conducive to the recovery of weight-bearing and motor function. Lomas et al.⁸⁵ found that PHBHHx may be a suitable polymer for cell/polymer replacement strategies in future tendon repair. Tashjian et al.⁸⁶ suggested that PHA could be used to improve the initial biomechanical repair strength of tears at risk of rupture.

Cardiovascular tissue

Because the musculoskeletal system is rich in blood vessels, these blood vessels can effectively maintain the homeostasis of the musculoskeletal system and effectively promote bone formation to a certain extent.¹¹⁷ Therefore, the vascular repair is particularly important of the musculoskeletal system. Considering that PHA has good angiogenesis, biocompatibility and biodegradability and can prevent adverse remodelling of defective tissues, PHA has been successfully used in vascular tissue engineering.^{88,109} The regenerative filament protein silk fibroin and PHBHHx porous scaffold prepared by Sun et al.⁸⁹ can promote cell adhesion and proliferation. Therefore, the silk fibroin-modified PHBHHx material could be a potential material for vascular tissue engineering.⁸⁹ Bagdadi et al.⁹⁰ used a novel functional material, poly (3-hydroxyoctane ester),

a *mcl*-PHA, to create engineered structures with improved mechanical properties, and they found that the polymer enhances the adhesion and proliferation of neonatal ventricular rat myocytes. The mechanical properties of the final patch were similar to those of the myocardium.⁹⁰ The above studies show that PHA can be widely used in musculoskeletal vascular repair.

Nervous tissue

Nerve damage can block the connection between the neuroregulatory brain and muscles, ultimately affecting motor function and even leading to permanent disability.^{93,109} Therefore, the fabrication of effective biomaterial scaffolds is a more successful treatment to promote nerve tissue regeneration in nerve injuries.¹¹⁸ Some studies have shown that PHA can promote nerve repair and is widely used in nerve tissue engineering. Köse et al.⁹¹ combined random or arranged electrospun nanofibre PHB membranes with human mesenchymal stem cells to form axon scaffolds for bone and spinal cord, and they found that the PHB membrane has high biocompatibility with human mesenchymal stem cells and provides good biomaterials for bone or nerve tissue engineering. Because Schwann cells physiologically promote the growth of regenerated axons, the interaction between Schwann cells and scaffolds is particularly important in neural tissue engineering. The data presented by Masaeli et al.⁹⁴ manufactured PHB/PHBV/collagen fibres can effectively promote the proliferation of Schwann cells and facilitate the regeneration of the myelin membrane. Therefore, PHB/PHBV electrostatic spinning nanofibres can be used in nerve tissue engineering.^{93,94} The PHB scaffold prepared by Khorasani et al.⁹² can promote the attachment and differentiation of mouse embryonic cells into nerve cells. The results show that PHB can be used as a material for neural tissue engineering. Kuo et al.⁹⁵ found that poly(ϵ -caprolactone)-PHB scaffolds transplanted with neuron growth factor can induce pluripotent stem cells to differentiate into neurons, and this scaffold is promising in neural tissue engineering. Novikova et al.¹¹⁹ found that PHBs support the survival and regeneration of neurons after spinal cord injury.

In addition to PHB, other PHA materials can also effectively promote the repair of nerve injuries. Bian et al.⁹⁶ found that the porous nerve conduit prepared by PHBHHx not only has good mechanical properties but also can promote nerve regeneration and rapid functional recovery of damaged nerves. In addition, it has been found that PLA, PHB, the copolymer of 3HB and 4HB, and PHBHHx can promote the growth and differentiation of neural stem cells. PHBHHx has the strongest potential to promote the differentiation of neural stem cells into neurons. Therefore, these materials are conducive to the repair of the central nervous system.^{97,120}

Applications of Polyhydroxyalkanoate Carriers in Drug Delivery in the Musculoskeletal System

Drug delivery technology, as an important part of healthcare, aims to deliver pharmacologically active drugs to specific sites of action using appropriate drug carriers at the most appropriate

PHA and its composites in musculoskeletal system

drug delivery rate and dose, while minimising the impact on the body and the occurrence of adverse reactions. Silicone, as an organic compound, is widely used to encapsulate hydrophobic drugs, but recent studies have shown that silicone has the potential to cause cancer.^{121, 122} In recent decades, researchers have shown great interest in developing biodegradable polymeric materials from natural sources as drug delivery materials and have achieved positive results. Due to their good biocompatibility and biodegradability, PHAs have attracted great attention in drug delivery systems.^{123, 124} The reason why PHAs can serve as good drug carriers is not only because of their unique physicochemical properties but also because they can be processed into films, scaffolds, microspheres, and nanoparticles as needed, which facilitates drug encapsulation. Some studies have shown that drug delivery systems such as hydrogels, microspheres, microcapsules, polymer vesicles, microns and nanoparticles are widely used to deliver a variety of therapeutic drugs, such as proteins, narcotics, antibiotics, anti-inflammatory drugs, anticancer drugs, hormones, etc. PHA can be used as a drug delivery carrier to participate in these processes.¹²⁴⁻¹²⁹

Considering the properties of tetracycline, Sendil et al.¹³⁰ prepared PHBV microspheres and microcapsules that can be successfully used to load tetracycline, an antibiotic for periodontitis. The author investigated their encapsulation efficiency, loading, release kinetics, and morphological properties. At the same time, it was found that the antibiotics were fully released before degradation of PHBV was observed.¹³⁰ Kassab et al.¹³¹ performed experiments using PHB microspheres, with a drug loading of up to 407.6 mg of rifampicin/g PHB. The release rate of the drug is very high. Xiong et al.¹³² compared the controlled intracellular drug release behaviour encapsulated in PHB, PHBHHx, and PLA nanoparticles. The results showed that PHB and PHBHHx nanoparticles could load over 75% of rhodamine B isothiocyanate, while PHB and PHBHHx nanoparticles continued to release drugs for at least 20 days, while PLA nanoparticles only for 15 days release. This study is the first to demonstrate that PHB and PHBHHx can effectively control intracellular drug release.¹³² Because the PHA delivery system can deliver and maintain sufficient antibiotic concentrations at the infection site, PHB can be widely used for local administration to treat osteomyelitis. However, since systemic administration may be ineffective due to damage to the vascular system, in diseases such as osteomyelitis it is best to ensure local administration through the implantation of pharmaceutical preparations. A study found that PHBV rods containing 7%, 14% and 22% (mol) 14-hydroxyvalvonic acid exhibit late antibiotic release behaviour lasting approximately 2 months in physiological phosphate buffers under *in vitro* conditions, whereas appropriate antibiotic treatment produces a minimum effective concentration of at least 6 weeks.¹³³ It was found that, in addition to PHBV, PHB and P(3HB-4HB) can also be processed into implantable rods for local administration of antibiotics for the treatment of osteomyelitis.¹³³⁻¹³⁵ Scheithauer et al.¹³⁶ prepared PHBV microspheres loaded with phytoestrogens; daidzein did not cause any shear or temperature stress on the drugs. The encapsulated daidzein was initially released at a low level (6.1% for 7 hours) and then

continuously for 3 days. Therefore, PHBV microspheres with daidzein delivery functions can also be used in the treatment of osteoporosis and bone tissue engineering.¹³⁶ Peng et al.¹³⁷ explored a novel PHB nanoparticle loaded with hydrophilic recombinant human bone morphogenetic protein 2 and amphiphilic phosphatide (BPC-PHB NP). The osteogenic differentiation gene markers of BPC-PHB NPs samples were significantly upregulated, suggesting that BPC-PHB NPs could serve as a fast-acting and long-acting bone morphogenetic protein 2 delivery system for osteogenic differentiation.¹³⁷ Chen et al.¹³⁸ designed a novel long-acting bone morphogenetic protein 7 release system based on poly(4-hydroxybutyric acid) nanoparticles to achieve osteogenic differentiation of human adipose mesenchymal stem cells. The results indicate that bone morphogenetic protein 7-soybean lecithin-poly(3-hydroxybutyrate-co-4-hydroxybutyrate) nanoparticles can be used as a fast and long-acting bone morphogenetic protein 7 delivery system for osteogenic differentiation.¹³⁸ PHA drug delivery systems have great potential due to their non-immunogenic, sustained and controlled drug release, targeted delivery, and high drug loading capabilities.¹³⁹ Nevertheless, certain properties of PHAs may hinder their use in drug delivery systems. Some of these include high hydrophobicity, low thermal stability, and slow degradation rates.¹⁴⁰

Application of Polyhydroxyalkanoate Degradation Products and Derivatives in the Musculoskeletal System

PHA is a biodegradable biopolymer, and as one of the degradation products of PHA, 3HB is a component of the blood and is widely used in the musculoskeletal system.^{30, 141-143} Zhao et al.¹⁴⁴ found that 3HB can promote osteoblast growth *in vitro* and anti-osteoporosis *in vivo*. Therefore, 3HB monomers containing PHA can be used as an effective bone implant material.¹⁴⁴ Skibiński et al.⁶⁸ found that novel composite materials based on β -tricalcium phosphate and poly (3-hydroxybutyric acid) bacteria-derived biopolymer can promote the adhesion and proliferation of mesenchymal stem cells and consider this material as a potential candidate for bone tissue regeneration. Czechowska et al.¹⁴⁵ found that the β -tricalcium phosphate-based polyporous scaffold modified with silver and coated with the biopolymer poly (3-hydroxybutyrate)-poly (3-hydroxybutyric acid) bacteria-derived biopolymer can promote the regeneration of bone tissue, and this scaffold is considered more promising bone substitute. A study has found that 3HB can also significantly inhibit the loss of muscle weight, muscle fibre size, and muscle fibre diameter, so it can effectively treat muscle atrophy.¹⁴⁶

4HB and 3HHx are also degradation products of PHA, and when they coexist with 3HB, they can also be used in the musculoskeletal system. Wang et al.¹⁴⁷ found that the electrospun poly (3-hydroxybutyric acid co-4-hydroxybutyric acid)/octacalcium phosphate nanofibre membrane had good mechanical properties and bone induction ability. Ang et al.¹⁴⁸ found that the mixture of P(3HB-co-3HHx) and fibroin protein could promote the proliferation and osteogenic differentiation of human umbilical cord mesenchymal stem cells. Studies have shown that poly(3-hydroxybutyrate-co-4-hydroxybutyrate-co-3-

hydroxyhexanoate) (P(3HB-4HB-3HHx)) can significantly promote cell proliferation, so P(3HB-4HB-3HHx) can be used in the musculoskeletal system.³⁴

Conclusions and Future Perspectives

The musculoskeletal system, as the heart of human movement, has certain peculiarities in its regeneration and recovery: repairing bone tissue requires a certain level of hardness, while tendons and ligaments pay more attention to toughness. Many treatment methods have their advantages and disadvantages, and biomaterials have provided new ideas for the treatment of musculoskeletal disorders in recent years. The selection of biomaterials has also attracted considerable attention from researchers. In addition to its special mechanical properties, a suitable biomaterial must also have good biocompatibility, a suitable degradation time and certain antibacterial properties in order to avoid local infections. As a biomaterial in regenerative medicine, PHA has great potential for use in the musculoskeletal system. With the addition of many manufacturing technologies and other materials, the various properties of PHA have been significantly improved. Furthermore, PHA scaffolds have shown great potential for drug delivery.

The production process and material properties of PHA are constantly improving, but there are still many challenges.¹⁴⁹ Unlike other biopolymers (such as marine-derived collagen, which has a wide range of sources and simple extraction methods), one of the most significant disadvantages of PHA is its high production cost, and its high price is the result of the need for large quantities of high-purity substrates as well as labour-intensive production and downstream processing.¹⁵⁰ At the same time, there may be some cases during PHA processing where organic solvents are not completely removed, which may lead to PHA being cytotoxic and not conducive to musculoskeletal tissue repair.^{151, 152} We can control the physical and chemical properties of PHA through certain technical means, but it is undeniable that there are reports that PHA can cause acute and chronic inflammation, and at the same time, the particle size and distribution of PHA are still very uncontrollable.^{65, 147} According to the current trend of PHA application, it has inestimable potential in the musculoskeletal system, but the great challenges it faces are also a fact that cannot be ignored. On the one hand, the large-scale high-quality production of PHA requires researchers to devote more energy to research, on the other hand, the specific problems encountered in the specific application of PHA, for example, How the hydrophobicity is applied in human tissues, the degradation rate under specific conditions, whether there is a suitable drug release rate, how to make the elasticity and hardness meet the tissue requirements, and maintain the integrity of the scaffold structure need further research and exploration.

Author contributions

Conceptualization: DXW, JWD; data collection and literature reviewing: CHM, XYQ and JZ; manuscript draft: CHM; manuscript revision: CHM, DXW, YWD. All authors read and approved the final version of the manuscript.

Financial support

This work was supported by the National Natural Science Foundation of China, Nos. 31900950 and 32000944 and Key Science and Technology Plan Projects in Zigong, No. 2022ZCNKY07.

Acknowledgement

None.

Conflicts of interest statement

The authors declare that they have no competing interests.

Open access statement

This is an open access journal, and articles are distributed under the terms of the Creative Commons Attribution-NonCommercial-ShareAlike 4.0 License, which allows others to remix, tweak, and build upon the work non-commercially, as long as appropriate credit is given and the new creations are licensed under the identical terms.

1. Barone, R.; Szychlinska, M. A. Highlights in pathophysiology of the musculoskeletal system. *Int J Mol Sci.* **2023**, *24*, 6412.
2. Christensen, L. V. Physiology and pathophysiology of skeletal muscle contractions. Part I. Dynamic activity. *J Oral Rehabil.* **1986**, *13*, 451-461.
3. Christensen, L. V. Physiology and pathophysiology of skeletal muscle contractions. Part II. Static activity. *J Oral Rehabil.* **1986**, *13*, 463-477.
4. Evans, C. H. Advances in regenerative orthopedics. *Mayo Clin Proc.* **2013**, *88*, 1323-1339.
5. Evans, C. H.; Huard, J. Gene therapy approaches to regenerating the musculoskeletal system. *Nat Rev Rheumatol.* **2015**, *11*, 234-242.
6. Gobbi, A.; Francisco, R. A.; Lubowitz, J. H.; Allegra, F.; Canata, G. Osteochondral lesions of the talus: randomized controlled trial comparing chondroplasty, microfracture, and osteochondral autograft transplantation. *Arthroscopy.* **2006**, *22*, 1085-1092.
7. Jackson, D. W.; Grood, E. S.; Goldstein, J. D.; Rosen, M. A.; Kurzweil, P. R.; Cummings, J. F.; Simon, T. M. A comparison of patellar tendon autograft and allograft used for anterior cruciate ligament reconstruction in the goat model. *Am J Sports Med.* **1993**, *21*, 176-185.
8. Kolesky, D. B.; Truby, R. L.; Gladman, A. S.; Busbee, T. A.; Homan, K. A.; Lewis, J. A. 3D bioprinting of vascularized, heterogeneous cell-laden tissue constructs. *Adv Mater.* **2014**, *26*, 3124-3130.
9. Ren, Z. W.; Wang, Z. Y.; Ding, Y. W.; Dao, J. W.; Li, H. R.; Ma, X.; Yang, X. Y.; Zhou, Z. Q.; Liu, J. X.; Mi, C. H.; Gao, Z. C.; Pei, H.; Wei, D. X. Polyhydroxyalkanoates: the natural biopolyester for future medical innovations. *Biomater Sci.* **2023**, *11*, 6013-6034.
10. Zhao, X. H.; Niu, Y. N.; Mi, C. H.; Gong, H. L.; Yang, X. Y.; Cheng, J. S. Y.; Zhou, Z. Q.; Liu, J. X.; Peng, X. L.; Wei, D. X. Electrospinning nanofibers of microbial polyhydroxyalkanoates for applications in medical tissue engineering. *J Polym Sci.* **2021**, *59*, 1994-2013.
11. Wang, Z. Y.; Zhang, X. W.; Ding, Y. W.; Ren, Z. W.; Wei, D. X. Natural biopolyester microspheres with diverse structures and surface topologies as micro-devices for biomedical applications. *Smart Mater Med.* **2023**, *4*, 15-36.
12. Anderson, A. J.; Dawes, E. A. Occurrence, metabolism, metabolic role, and industrial uses of bacterial polyhydroxyalkanoates. *Microbiol Rev.* **1990**, *54*, 450-472.
13. Palencia, M.; Lerma, T. A.; Garcés, V.; Mora, M. A.; Martínez, J. M.; Palencia, S. L. Chapter 19 - Functional and eco-friendly polymers in textile applications. In *Eco-friendly functional polymers*, Palencia, M.; Lerma, T. A.; Garcés, V.; Mora, M. A.; Martínez, J. M.; Palencia, S. L., eds. Elsevier: 2021; pp 285-293.
14. Mastrogiacomo, M.; Muraglia, A.; Komlev, V.; Peyrin, F.; Rustichelli, F.; Crovace, A.; Cancedda, R. Tissue engineering of bone: search for a better scaffold. *Orthod Craniofac Res.* **2005**, *8*, 277-284.
15. Troschl, C.; Meixner, K.; Drosog, B. Cyanobacterial PHA production-

- review of recent advances and a summary of three years' working experience running a pilot plant. *Bioengineering (Basel)*. **2017**, *4*, 26.
16. Peng, X. L.; Cheng, J. S.; Gong, H. L.; Yuan, M. D.; Zhao, X. H.; Li, Z.; Wei, D. X. Advances in the design and development of SARS-CoV-2 vaccines. *Mil Med Res*. **2021**, *8*, 67.
 17. Liu, J.; Zhou, Z.; Li, H.; Yang, X.; Wang, Z.; Xiao, J.; Wei, D. X. Current status and challenges in the application of microbial PHA particles. *Particuology*. **2024**, *87*, 286-302.
 18. Li, X. T.; Zhang, Y.; Chen, G. Q. Nanofibrous polyhydroxyalkanoate matrices as cell growth supporting materials. *Biomaterials*. **2008**, *29*, 3720-3728.
 19. Bassas-Galià, M.; Gonzalez, A.; Micaux, F.; Gaillard, V.; Piantini, U.; Schintke, S.; Zinn, M.; Mathieu, M. Chemical modification of polyhydroxyalkanoates (PHAs) for the preparation of hybrid biomaterials. *Chimia*. **2015**, *69*, 627-630.
 20. Ai, M.; Zhu, Y.; Jia, X. Recent advances in constructing artificial microbial consortia for the production of medium-chain-length polyhydroxyalkanoates. *World J Microbiol Biotechnol*. **2021**, *37*, 2.
 21. Chen, S.; Liu, Q.; Wang, H.; Zhu, B.; Yu, F.; Chen, G. Q.; Inoue, Y. Polymorphic crystallization of fractionated microbial medium-chain-length polyhydroxyalkanoates. *Polymer*. **2009**, *50*, 4378-4388.
 22. Grigore, M. E.; Grigorescu, R. M.; Iancu, L.; Ion, R. M.; Zaharia, C.; Andrei, E. R. Methods of synthesis, properties and biomedical applications of polyhydroxyalkanoates: a review. *J Biomater Sci Polym Ed*. **2019**, *30*, 695-712.
 23. Witholt, B.; Kessler, B. Perspectives of medium chain length poly(hydroxyalkanoates), a versatile set of bacterial bioplastics. *Curr Opin Biotechnol*. **1999**, *10*, 279-285.
 24. Ishak, K. A.; Velayutham, T. S.; Annuar, M. S. M.; Sirajudeen, A. A. O. Structure-property interpretation of biological polyhydroxyalkanoates with different monomeric composition: dielectric spectroscopy investigation. *Int J Biol Macromol*. **2021**, *169*, 311-320.
 25. Savenkova, L.; Gercberga, Z.; Nikolaeva, V.; Dzene, A.; Bibers, I.; Kalnin, M. Mechanical properties and biodegradation characteristics of PHB-based films. *Process Biochem*. **2000**, *35*, 573-579.
 26. Ciesielski, S.; Pokoj, T.; Mozejko, J.; Klimiuk, E. Molecular identification of polyhydroxyalkanoates-producing bacteria isolated from enriched microbial community. *Pol J Microbiol*. **2013**, *62*, 45-50.
 27. Wecker, P.; Moppert, X.; Simon-Colin, C.; Costa, B.; Berteaux-Lecellier, V. Discovery of a mcl-PHA with unexpected biotechnical properties: the marine environment of French Polynesia as a source for PHA-producing bacteria. *AMB Express*. **2015**, *5*, 74.
 28. Koller, M. Biodegradable and biocompatible polyhydroxy-alkanoates (PHA): auspicious microbial macromolecules for pharmaceutical and therapeutic applications. *Molecules*. **2018**, *23*, 362.
 29. Williams, S. F.; Martin, D. P.; Horowitz, D. M.; Peoples, O. P. PHA applications: addressing the price performance issue: I. Tissue engineering. *Int J Biol Macromol*. **1999**, *25*, 111-121.
 30. Lim, J.; You, M.; Li, J.; Li, Z. Emerging bone tissue engineering via polyhydroxyalkanoate (PHA)-based scaffolds. *Mater Sci Eng C Mater Biol Appl*. **2017**, *79*, 917-929.
 31. Chen, G. Q.; Wu, Q. The application of polyhydroxyalkanoates as tissue engineering materials. *Biomaterials*. **2005**, *26*, 6565-6578.
 32. Wang, Y. W.; Wu, Q.; Chen, G. Q. Attachment, proliferation and differentiation of osteoblasts on random biopolyester poly(3-hydroxybutyrate-co-3-hydroxyhexanoate) scaffolds. *Biomaterials*. **2004**, *25*, 669-675.
 33. Hu, Y. J.; Wei, X.; Zhao, W.; Liu, Y. S.; Chen, G. Q. Biocompatibility of poly(3-hydroxybutyrate-co-3-hydroxyvalerate-co-3-hydroxyhexanoate) with bone marrow mesenchymal stem cells. *Acta Biomater*. **2009**, *5*, 1115-1125.
 34. Wei, X.; Hu, Y. J.; Xie, W. P.; Lin, R. L.; Chen, G. Q. Influence of poly(3-hydroxybutyrate-co-4-hydroxybutyrate-co-3-hydroxyhexanoate) on growth and osteogenic differentiation of human bone marrow-derived mesenchymal stem cells. *J Biomed Mater Res A*. **2009**, *90*, 894-905.
 35. Wu, Y. L.; Wang, H.; Qiu, Y. K.; Liow, S. S.; Li, Z.; Loh, X. J. PHB-based gels as delivery agents of chemotherapeutics for the effective shrinkage of tumors. *Adv Healthc Mater*. **2016**, *5*, 2679-2685.
 36. Marcello, E.; Maqbool, M.; Nigmatullin, R.; Cresswell, M.; Jackson, P. R.; Basnett, P.; Knowles, J. C.; Boccaccini, A. R.; Roy, I. Antibacterial composite materials based on the combination of polyhydroxyalkanoates with selenium and strontium co-substituted hydroxyapatite for bone regeneration. *Front Bioeng Biotechnol*. **2021**, *9*, 647007.
 37. Shishatskaya, E. I.; Volova, T. G. A comparative investigation of biodegradable polyhydroxyalkanoate films as matrices for in vitro cell cultures. *J Mater Sci Mater Med*. **2004**, *15*, 915-923.
 38. Ji, G. Z.; Wei, X.; Chen, G. Q. Growth of human umbilical cord Wharton's Jelly-derived mesenchymal stem cells on the terpolyester poly(3-hydroxybutyrate-co-3-hydroxyvalerate-co-3-hydroxyhexanoate). *J Biomater Sci Polym Ed*. **2009**, *20*, 325-339.
 39. Ahmed, T.; Marçal, H.; Lawless, M.; Wanandy, N. S.; Chiu, A.; Foster, L. J. Polyhydroxybutyrate and its copolymer with polyhydroxyvalerate as biomaterials: influence on progression of stem cell cycle. *Biomacromolecules*. **2010**, *11*, 2707-2715.
 40. Yang, M.; Zhu, S.; Chen, Y.; Chang, Z.; Chen, G.; Gong, Y.; Zhao, N.; Zhang, X. Studies on bone marrow stromal cells affinity of poly(3-hydroxybutyrate-co-3-hydroxyhexanoate). *Biomaterials*. **2004**, *25*, 1365-1373.
 41. Tesema, Y.; Raghavan, D.; Stubbs Iii, J. Bone cell viability on collagen immobilized poly(3-hydroxybutyrate-co-3-hydroxyvalerate) membrane: Effect of surface chemistry. *J Appl Polym Sci*. **2004**, *93*, 2445-2453.
 42. Chen, X.; Zhang, X.; Zhu, Y.; Zhang, J.; Hu, P. Surface modification of polyhydroxyalkanoates by ion implantation. Characterization and cytocompatibility improvement. *Polym J*. **2003**, *35*, 148-154.
 43. Wu, T. P.; Hu, R.; Zhang, X. B.; Li, W.; Chen, F. Biocompatibility of modified poly-β-hydroxybutyric acid to adrenocortical cells. *J Wuhan Univ Technol Mater Sci Ed*. **2004**, *19*, 38-40.
 44. Yu, B. Y.; Chen, P. Y.; Sun, Y. M.; Lee, Y. T.; Young, T. H. Effects of the surface characteristics of polyhydroxyalkanoates on the metabolic activities and morphology of human mesenchymal stem cells. *J Biomater Sci Polym Ed*. **2010**, *21*, 17-36.
 45. Webb, W. R.; Dale, T. P.; Lomas, A. J.; Zeng, G.; Wimpenny, I.; El Haj, A. J.; Forsyth, N. R.; Chen, G. Q. The application of poly(3-hydroxybutyrate-co-3-hydroxyhexanoate) scaffolds for tendon repair in the rat model. *Biomaterials*. **2013**, *34*, 6683-6694.
 46. Volova, T. G.; Shishatskaya, E. I.; Nikolaeva, E. D.; Sinskey, A. J. In vivo study of 2D PHA matrices of different chemical compositions: tissue reactions and biodegradations. *Mater Sci Technol*. **2014**, *30*, 549-557.
 47. Qu, X. H.; Wu, Q.; Zhang, K. Y.; Chen, G. Q. In vivo studies of poly(3-hydroxybutyrate-co-3-hydroxyhexanoate) based polymers: biodegradation and tissue reactions. *Biomaterials*. **2006**, *27*, 3540-3548.
 48. Fan, L.; Hu, L.; Xie, J.; He, Z.; Zheng, Y.; Wei, D.; Yao, D.; Su, F. Biosafe, self-adhesive, recyclable, tough, and conductive hydrogels for

- multifunctional sensors. *Biomater Sci.* **2021**, *9*, 5884-5896.
49. Li, Y.; Xiao, L.; Wei, D.; Liu, S.; Zhang, Z.; Lian, R.; Wang, L.; Chen, Y.; Jiang, J.; Xiao, Y.; Liu, C.; Li, Y.; Zhao, J. Injectable biomimetic hydrogel guided functional bone regeneration by adapting material degradation to tissue healing. *Adv Funct Mater.* **2023**, *33*, 2213047.
 50. Dwivedi, R.; Pandey, R.; Kumar, S.; Mehrotra, D. Poly hydroxyalkanoates (PHA): role in bone scaffolds. *J Oral Biol Craniofac Res.* **2020**, *10*, 389-392.
 51. Anjum, A.; Zuber, M.; Zia, K. M.; Noreen, A.; Anjum, M. N.; Tabasum, S. Microbial production of polyhydroxyalkanoates (PHAs) and its copolymers: A review of recent advancements. *Int J Biol Macromol.* **2016**, *89*, 161-174.
 52. Arrington, E. D.; Smith, W. J.; Chambers, H. G.; Bucknell, A. L.; Davino, N. A. Complications of iliac crest bone graft harvesting. *Clin Orthop Relat Res.* **1996**, 300-309.
 53. Hazer, B.; Steinbüchel, A. Increased diversification of polyhydroxyalkanoates by modification reactions for industrial and medical applications. *Appl Microbiol Biotechnol.* **2007**, *74*, 1-12.
 54. Sharma, V.; Sehgal, R.; Gupta, R. Polyhydroxyalkanoate (PHA): properties and modifications. *Polymer.* **2021**, *212*, 123161.
 55. Sudesh, K.; Abe, H.; Doi, Y. Synthesis, structure and properties of polyhydroxyalkanoates: biological polyesters. *Prog Polym Sci.* **2000**, *25*, 1503-1555.
 56. Pryadko, A.; Surmeneva, M. A.; Surmenev, R. A. Review of hybrid materials based on polyhydroxyalkanoates for tissue engineering applications. *Polymers (Basel).* **2021**, *13*, 1738.
 57. Velasco, M. A.; Narváez-Tovar, C. A.; Garzón-Alvarado, D. A. Design, materials, and mechanobiology of biodegradable scaffolds for bone tissue engineering. *Biomed Res Int.* **2015**, *2015*, 729076.
 58. Mota, C.; Wang, S. Y.; Puppi, D.; Gazzarri, M.; Migone, C.; Chiellini, F.; Chen, G. Q.; Chiellini, E. Additive manufacturing of poly[(R)-3-hydroxybutyrate-co-(R)-3-hydroxyhexanoate] scaffolds for engineered bone development. *J Tissue Eng Regen Med.* **2017**, *11*, 175-186.
 59. Doyle, C.; Tanner, E. T.; Bonfield, W. In vitro and in vivo evaluation of polyhydroxybutyrate and of polyhydroxybutyrate reinforced with hydroxyapatite. *Biomaterials.* **1991**, *12*, 841-847.
 60. Wang, Y.; Jiang, X. L.; Yang, S. C.; Lin, X.; He, Y.; Yan, C.; Wu, L.; Chen, G. Q.; Wang, Z. Y.; Wu, Q. MicroRNAs in the regulation of interfacial behaviors of MSCs cultured on microgrooved surface pattern. *Biomaterials.* **2011**, *32*, 9207-9217.
 61. Ellis, G.; Cano, P.; Jadraque, M.; Martín, M.; López, L.; Núñez, T.; de la Peña, E.; Marco, C.; Garrido, L. Laser microperforated biodegradable microbial polyhydroxyalkanoate substrates for tissue repair strategies: an infrared microspectroscopy study. *Anal Bioanal Chem.* **2011**, *399*, 2379-2388.
 62. Wei, D.; Zhang, X. Biosynthesis, bioactivity, biotoxicity and applications of antimicrobial peptides for human health. *Biosaf Health.* **2022**, *4*, 118-134.
 63. Codreanu, A.; Balta, C.; Herman, H.; Cotoraci, C.; Mihali, C. V.; Zurbau, N.; Zaharia, C.; Rapa, M.; Stanescu, P.; Radu, I. C.; Vasile, E.; Lupu, G.; Galateanu, B.; Hermenean, A. Bacterial cellulose-modified polyhydroxyalkanoates scaffolds promotes bone formation in critical size calvarial defects in mice. *Materials (Basel).* **2020**, *13*, 1433.
 64. Pecorini, G.; Braccini, S.; Parrini, G.; Chiellini, F.; Puppi, D. Additive manufacturing of poly(3-hydroxybutyrate-co-3-hydroxyvalerate)/poly(D,L-lactide-co-glycolide) biphasic scaffolds for bone tissue regeneration. *Int J Mol Sci.* **2022**, *23*, 3895.
 65. Lezcano, M. F.; Álvarez, G.; Chuhuaicura, P.; Godoy, K.; Alarcón, J.; Acevedo, F.; Gareis, I.; Dias, F. J. Polyhydroxybutyrate (PHB) scaffolds for peripheral nerve regeneration: a systematic review of animal models. *Biology (Basel).* **2022**, *11*, 706.
 66. Ansari, N. F.; Annuar, M. S. M.; Murphy, B. P. A porous medium-chain-length poly(3-hydroxyalkanoates)/hydroxyapatite composite as scaffold for bone tissue engineering. *Eng Life Sci.* **2017**, *17*, 420-429.
 67. Nishizuka, T.; Kurahashi, T.; Hara, T.; Hirata, H.; Kasuga, T. Novel intramedullary-fixation technique for long bone fragility fractures using bioresorbable materials. *PLoS One.* **2014**, *9*, e104603.
 68. Skibiński, S.; Czechowska, J. P.; Cichoń, E.; Seta, M.; Gondek, A.; Cudnoch-Jędrzejewska, A.; Ślósarczyk, A.; Guzik, M.; Zima, A. Study on β TCP/P(3HB) scaffolds-physicochemical properties and biological performance in low oxygen concentration. *Int J Mol Sci.* **2022**, *23*, 11587.
 69. Chotchindakun, K.; Pekkoh, J.; Ruangsuriya, J.; Zheng, K.; Unalan, I.; Boccaccini, A. R. Fabrication and characterization of cinnamaldehyde-loaded mesoporous bioactive glass nanoparticles/PHBV-based microspheres for preventing bacterial infection and promoting bone tissue regeneration. *Polymers (Basel).* **2021**, *13*, 1794.
 70. Ching, K. Y.; Andriotis, O. G.; Li, S.; Basnett, P.; Su, B.; Roy, I.; Tare, R. S.; Sengers, B. G.; Stolz, M. Nanofibrous poly(3-hydroxybutyrate)/poly(3-hydroxyoctanoate) scaffolds provide a functional microenvironment for cartilage repair. *J Biomater Appl.* **2016**, *31*, 77-91.
 71. Li, C.; Zhang, J.; Li, Y.; Moran, S.; Khang, G.; Ge, Z. Poly (1-lactide-co-caprolactone) scaffolds enhanced with poly (β -hydroxybutyrate-co- β -hydroxyvalerate) microspheres for cartilage regeneration. *Biomed Mater.* **2013**, *8*, 025005.
 72. Gao, T.; Chang, H.; Fan, M.; Lu, X.; Wang, Z.; Zhang, X.; Jing, X.; Shi, Y.; Li, Z. Bio-modification of polyhydroxyalkanoates and its biocompatibility with chondrocytes. *Zhongguo Xiu Fu Chong Jian Wai Ke Za Zhi.* **2014**, *28*, 1023-1029.
 73. Movahedi, M.; Karbasi, S. Electrospun halloysite nanotube loaded polyhydroxybutyrate-starch fibers for cartilage tissue engineering. *Int J Biol Macromol.* **2022**, *214*, 301-311.
 74. Li, X.; Chang, H.; Luo, H.; Wang, Z.; Zheng, G.; Lu, X.; He, X.; Chen, F.; Wang, T.; Liang, J.; Xu, M. Poly (3-hydroxybutyrate-co-3-hydroxyhexanoate) scaffolds coated with PhaP-RGD fusion protein promotes the proliferation and chondrogenic differentiation of human umbilical cord mesenchymal stem cells in vitro. *J Biomed Mater Res A.* **2015**, *103*, 1169-1175.
 75. You, M.; Peng, G.; Li, J.; Ma, P.; Wang, Z.; Shu, W.; Peng, S.; Chen, G. Q. Chondrogenic differentiation of human bone marrow mesenchymal stem cells on polyhydroxyalkanoate (PHA) scaffolds coated with PHA granule binding protein PhaP fused with RGD peptide. *Biomaterials.* **2011**, *32*, 2305-2313.
 76. Zonari, A.; Novikoff, S.; Electro, N. R.; Breyner, N. M.; Gomes, D. A.; Martins, A.; Neves, N. M.; Reis, R. L.; Goes, A. M. Endothelial differentiation of human stem cells seeded onto electrospun polyhydroxybutyrate/polyhydroxybutyrate-co-hydroxyvalerate fiber mesh. *PLoS One.* **2012**, *7*, e35422.
 77. Zhijiang, C.; Yi, X.; Haizheng, Y.; Jia, J.; Liu, Y. Poly(hydroxybutyrate)/cellulose acetate blend nanofiber scaffolds: preparation, characterization and cytocompatibility. *Mater Sci Eng C Mater Biol Appl.* **2016**, *58*, 757-767.
 78. Ochoa-Segundo, E. I.; González-Torres, M.; Cabrera-Wrooman, A.; Sánchez-Sánchez, R.; Huerta-Martínez, B. M.; Melgarejo-Ramírez, Y.; Leyva-Gómez, G.; Rivera-Muñoz, E. M.; Cortés, H.; Velasquillo, C.; Vargas-Muñoz, S.; Rodríguez-Talavera, R. Gamma radiation-induced grafting of n-hydroxyethyl acrylamide onto poly(3-hydroxybutyrate): A companion study on its polyurethane scaffolds meant for potential skin

- tissue engineering applications. *Mater Sci Eng C Mater Biol Appl.* **2020**, *116*, 111176.
79. Kanimozhi, K.; Basha, S. K.; Kaviyarasu, K.; SuganthaKumari, V. Salt leaching synthesis, characterization and in vitro cytocompatibility of chitosan/poly(vinyl alcohol)/methylcellulose - ZnO nanocomposites scaffolds using L929 fibroblast cells. *J Nanosci Nanotechnol.* **2019**, *19*, 4447-4457.
 80. Nagiah, N.; Madhavi, L.; Anitha, R.; Anandan, C.; Srinivasan, N. T.; Sivagnanam, U. T. Development and characterization of coaxially electrospun gelatin coated poly (3-hydroxybutyric acid) thin films as potential scaffolds for skin regeneration. *Mater Sci Eng C Mater Biol Appl.* **2013**, *33*, 4444-4452.
 81. Sanhueza, C.; Hermosilla, J.; Bugallo-Casal, A.; Da Silva-Candal, A.; Taboada, C.; Millán, R.; Concheiro, A.; Alvarez-Lorenzo, C.; Acevedo, F. One-step electrospun scaffold of dual-sized gelatin/poly-3-hydroxybutyrate nano/microfibers for skin regeneration in diabetic wound. *Mater Sci Eng C Mater Biol Appl.* **2021**, *119*, 111602.
 82. Feng, J.; Niu, Y.; Zhang, Y.; Zuo, H.; Wang, S.; Liu, X. Ficus carica extract impregnated amphiphilic polymer scaffold for diabetic wound tissue regenerations. *Artif Cells Nanomed Biotechnol.* **2021**, *49*, 219-229.
 83. Veleirinho, B.; Coelho, D. S.; Dias, P. F.; Maraschin, M.; Ribeiro-do-Valle, R. M.; Lopes-da-Silva, J. A. Nanofibrous poly(3-hydroxybutyrate-co-3-hydroxyvalerate)/chitosan scaffolds for skin regeneration. *Int J Biol Macromol.* **2012**, *51*, 343-350.
 84. Rathbone, S.; Furrer, P.; Lübben, J.; Zinn, M.; Cartmell, S. Biocompatibility of polyhydroxyalkanoate as a potential material for ligament and tendon scaffold material. *J Biomed Mater Res A.* **2010**, *93*, 1391-1403.
 85. Lomas, A. J.; Chen, G. G.; El Haj, A. J.; Forsyth, N. R. Poly(3-hydroxybutyrate-co-3-hydroxyhexanoate) supports adhesion and migration of mesenchymal stem cells and tenocytes. *World J Stem Cells.* **2012**, *4*, 94-100.
 86. Tashjian, R. Z.; Kolz, C. W.; Suter, T.; Henninger, H. B. Biomechanics of polyhydroxyalkanoate mesh-augmented single-row rotator cuff repairs. *Am J Orthop (Belle Mead NJ).* **2016**, *45*, E527-E533.
 87. Sodian, R.; Sperling, J. S.; Martin, D. P.; Egozy, A.; Stock, U.; Mayer, J. E., Jr.; Vacanti, J. P. Fabrication of a trileaflet heart valve scaffold from a polyhydroxyalkanoate biopolyester for use in tissue engineering. *Tissue Eng.* **2000**, *6*, 183-188.
 88. Leor, J.; Amsalem, Y.; Cohen, S. Cells, scaffolds, and molecules for myocardial tissue engineering. *Pharmacol Ther.* **2005**, *105*, 151-163.
 89. Sun, M.; Zhou, P.; Pan, L. F.; Liu, S.; Yang, H. X. Enhanced cell affinity of the silk fibroin- modified PHBHHx material. *J Mater Sci Mater Med.* **2009**, *20*, 1743-1751.
 90. Bagdadi, A. V.; Safari, M.; Dubey, P.; Basnett, P.; Sofokleous, P.; Humphrey, E.; Locke, I.; Edirisinghe, M.; Terracciano, C.; Boccaccini, A. R.; Knowles, J. C.; Harding, S. E.; Roy, I. Poly(3-hydroxyoctanoate), a promising new material for cardiac tissue engineering. *J Tissue Eng Regen Med.* **2018**, *12*, e495-e512.
 91. Köse, S.; Kaya, F. A.; Denkbaş, E. B.; Korkusuz, P.; Çetinkaya, F. D. Evaluation of biocompatibility of random or aligned electrospun polyhydroxybutyrate scaffolds combined with human mesenchymal stem cells. *Turk J Biol.* **2016**, *40*, 410-419.
 92. Khorasani, M. T.; Mirmohammadi, S. A.; Irani, S. Polyhydroxybutyrate (PHB) scaffolds as a model for nerve tissue engineering application: fabrication and in vitro assay. *Int J Polym Mater Polym Biomater.* **2011**, *60*, 562-575.
 93. Masaeli, E.; Morshed, M.; Nasr-Esfahani, M. H.; Sadri, S.; Hilderink, J.; van Apeldoorn, A.; van Blitterswijk, C. A.; Moroni, L. Fabrication, characterization and cellular compatibility of poly(hydroxy alkanooate) composite nanofibrous scaffolds for nerve tissue engineering. *PLoS One.* **2013**, *8*, e57157.
 94. Masaeli, E.; Wieringa, P. A.; Morshed, M.; Nasr-Esfahani, M. H.; Sadri, S.; van Blitterswijk, C. A.; Moroni, L. Peptide functionalized polyhydroxyalkanoate nanofibrous scaffolds enhance Schwann cells activity. *Nanomedicine.* **2014**, *10*, 1559-1569.
 95. Kuo, Y. C.; Huang, M. J. Material-driven differentiation of induced pluripotent stem cells in neuron growth factor-grafted poly(ϵ -caprolactone)-poly(β -hydroxybutyrate) scaffolds. *Biomaterials.* **2012**, *33*, 5672-5682.
 96. Bian, Y. Z.; Wang, Y.; Aibaidoula, G.; Chen, G. Q.; Wu, Q. Evaluation of poly(3-hydroxybutyrate-co-3-hydroxyhexanoate) conduits for peripheral nerve regeneration. *Biomaterials.* **2009**, *30*, 217-225.
 97. Xu, X. Y.; Li, X. T.; Peng, S. W.; Xiao, J. F.; Liu, C.; Fang, G.; Chen, K. C.; Chen, G. Q. The behaviour of neural stem cells on polyhydroxyalkanoate nanofiber scaffolds. *Biomaterials.* **2010**, *31*, 3967-3975.
 98. Rahman, M.; Peng, X. L.; Zhao, X. H.; Gong, H. L.; Sun, X. D.; Wu, Q.; Wei, D. X. 3D bioactive cell-free-scaffolds for in-vitro/in-vivo capture and directed osteoinduction of stem cells for bone tissue regeneration. *Bioact Mater.* **2021**, *6*, 4083-4095.
 99. Wei, D. X.; Dao, J. W.; Liu, H. W.; Chen, G. Q. Suspended polyhydroxyalkanoate microspheres as 3D carriers for mammalian cell growth. *Artif Cells Nanomed Biotechnol.* **2018**, *46*, 473-483.
 100. Wei, D. X.; Dao, J. W.; Chen, G. Q. A micro-ark for cells: highly open porous polyhydroxyalkanoate microspheres as injectable scaffolds for tissue regeneration. *Adv Mater.* **2018**, *30*, e1802273.
 101. Zhao, X. H.; Peng, X. L.; Gong, H. L.; Wei, D. X. Osteogenic differentiation system based on biopolymer nanoparticles for stem cells in simulated microgravity. *Biomed Mater.* **2021**, *16*, 044102.
 102. Armiento, A. R.; Stoddart, M. J.; Alini, M.; Eglin, D. Biomaterials for articular cartilage tissue engineering: Learning from biology. *Acta Biomater.* **2018**, *65*, 1-20.
 103. Decker, R. S. Articular cartilage and joint development from embryogenesis to adulthood. *Semin Cell Dev Biol.* **2017**, *62*, 50-56.
 104. Swieszkowski, W.; Tuan, B. H.; Kurzydowski, K. J.; Huttmacher, D. W. Repair and regeneration of osteochondral defects in the articular joints. *Biomol Eng.* **2007**, *24*, 489-495.
 105. Asl, M. A.; Karbasi, S.; Beigi-Boroujeni, S.; Zamanlui Benisi, S.; Saeed, M. Evaluation of the effects of starch on polyhydroxybutyrate electrospun scaffolds for bone tissue engineering applications. *Int J Biol Macromol.* **2021**, *191*, 500-513.
 106. Wei, D. X.; Chen, C. B.; Fang, G.; Li, S. Y.; Chen, G. Q. Application of polyhydroxyalkanoate binding protein PhaP as a bio-surfactant. *Appl Microbiol Biotechnol.* **2011**, *91*, 1037-1047.
 107. Fan, L.; He, Z.; Peng, X.; Xie, J.; Su, F.; Wei, D. X.; Zheng, Y.; Yao, D. Injectable, intrinsically antibacterial conductive hydrogels with self-healing and pH stimulus responsiveness for epidermal sensors and wound healing. *ACS Appl Mater Interfaces.* **2021**, *13*, 53541-53552.
 108. Fan, L.; Xie, J.; Zheng, Y.; Wei, D.; Yao, D.; Zhang, J.; Zhang, T. Antibacterial, self-adhesive, recyclable, and tough conductive composite hydrogels for ultrasensitive strain sensing. *ACS Appl Mater Interfaces.* **2020**, *12*, 22225-22236.
 109. Dhanias, S.; Bernela, M.; Rani, R.; Parsad, M.; Grewal, S.; Kumari, S.; Thakur, R. Scaffolds the backbone of tissue engineering: Advancements in use of polyhydroxyalkanoates (PHA). *Int J Biol Macromol.* **2022**, *208*,

- 243-259.
110. Doral, M. N.; Alam, M.; Bozkurt, M.; Turhan, E.; Atay, O. A.; Dönmez, G.; Maffulli, N. Functional anatomy of the Achilles tendon. *Knee Surg Sports Traumatol Arthrosc.* **2010**, *18*, 638-643.
 111. Ahmed, I. M.; Lagopoulos, M.; McConnell, P.; Soames, R. W.; Sefton, G. K. Blood supply of the Achilles tendon. *J Orthop Res.* **1998**, *16*, 591-596.
 112. Theobald, P.; Benjamin, M.; Nokes, L.; Pugh, N. Review of the vascularisation of the human Achilles tendon. *Injury.* **2005**, *36*, 1267-1272.
 113. Longo, U. G.; Lamberti, A.; Maffulli, N.; Denaro, V. Tendon augmentation grafts: a systematic review. *Br Med Bull.* **2010**, *94*, 165-188.
 114. Wilkins, R.; Bisson, L. J. Operative versus nonoperative management of acute Achilles tendon ruptures: a quantitative systematic review of randomized controlled trials. *Am J Sports Med.* **2012**, *40*, 2154-2160.
 115. Cetti, R.; Christensen, S. E.; Ejsted, R.; Jensen, N. M.; Jorgensen, U. Operative versus nonoperative treatment of Achilles tendon rupture. A prospective randomized study and review of the literature. *Am J Sports Med.* **1993**, *21*, 791-799.
 116. García-Germán, D.; Rubio-Quevedo, R.; Lopez-Goenaga, J.; Martin-Guinea, J. Achilles tendon recurrent rupture following surgical repair: report on two cases. *Foot Ankle Surg.* **2009**, *15*, 152-154.
 117. Kusumbe, A. P.; Ramasamy, S. K.; Adams, R. H. Coupling of angiogenesis and osteogenesis by a specific vessel subtype in bone. *Nature.* **2014**, *507*, 323-328.
 118. Straley, K. S.; Foo, C. W.; Heilshorn, S. C. Biomaterial design strategies for the treatment of spinal cord injuries. *J Neurotrauma.* **2010**, *27*, 1-19.
 119. Novikov, L. N.; Novikova, L. N.; Mosahebi, A.; Wiberg, M.; Terenghi, G.; Kellerth, J. O. A novel biodegradable implant for neuronal rescue and regeneration after spinal cord injury. *Biomaterials.* **2002**, *23*, 3369-3376.
 120. Wang, L.; Wang, Z. H.; Shen, C. Y.; You, M. L.; Xiao, J. F.; Chen, G. Q. Differentiation of human bone marrow mesenchymal stem cells grown in terpolyesters of 3-hydroxyalkanoates scaffolds into nerve cells. *Biomaterials.* **2010**, *31*, 1691-1698.
 121. Zhang, C.; Zhao, L.; Dong, Y.; Zhang, X.; Lin, J.; Chen, Z. Folate-mediated poly(3-hydroxybutyrate-co-3-hydroxyoctanoate) nanoparticles for targeting drug delivery. *Eur J Pharm Biopharm.* **2010**, *76*, 10-16.
 122. Pramual, S.; Assavanig, A.; Bergkvist, M.; Batt, C. A.; Sunintaboon, P.; Lirdpramongkol, K.; Svasti, J.; Niamsiri, N. Development and characterization of bio-derived polyhydroxyalkanoate nanoparticles as a delivery system for hydrophobic photodynamic therapy agents. *J Mater Sci Mater Med.* **2016**, *27*, 40.
 123. Li, Z.; Loh, X. J. Recent advances of using polyhydroxyalkanoate-based nanovehicles as therapeutic delivery carriers. *Wiley Interdiscip Rev Nanomed Nanobiotechnol.* **2017**, *9*, e1429.
 124. Shah, M.; Ullah, N.; Choi, M. H.; Yoon, S. C. Nanoscale poly(4-hydroxybutyrate)-mPEG carriers for anticancer drugs delivery. *J Nanosci Nanotechnol.* **2014**, *14*, 8416-8421.
 125. Nobes, G. A.; Marchessault, R. H.; Maysinger, D. Polyhydroxyalkanoates: materials for delivery systems. *Drug Deliv.* **1998**, *5*, 167-177.
 126. Elmowafy, E.; Abdal-Hay, A.; Skouras, A.; Tiboni, M.; Casettari, L.; Guarino, V. Polyhydroxyalkanoate (PHA): applications in drug delivery and tissue engineering. *Expert Rev Med Devices.* **2019**, *16*, 467-482.
 127. Hu, J.; Wang, M.; Xiao, X.; Zhang, B.; Xie, Q.; Xu, X.; Li, S.; Zheng, Z.; Wei, D.; Zhang, X. A novel long-acting azathioprine polyhydroxyalkanoate nanoparticle enhances treatment efficacy for systemic lupus erythematosus with reduced side effects. *Nanoscale.* **2020**, *12*, 10799-10808.
 128. Yan, Y.; Wei, D.; Li, J.; Zheng, J.; Shi, G.; Luo, W.; Pan, Y.; Wang, J.; Zhang, L.; He, X.; Liu, D. A poly(L-lysine)-based hydrophilic star block co-polymer as a protein nanocarrier with facile encapsulation and pH-responsive release. *Acta Biomater.* **2012**, *8*, 2113-2120.
 129. Wei, D.; Qiao, R.; Dao, J.; Su, J.; Jiang, C.; Wang, X.; Gao, M.; Zhong, J. Soybean lecithin-mediated nanoporous PLGA microspheres with highly entrapped and controlled released BMP-2 as a stem cell platform. *Small.* **2018**, *14*, e1800063.
 130. Sendil, D.; Gürsel, I.; Wise, D. L.; Hasirci, V. Antibiotic release from biodegradable PHBV microparticles. *J Control Release.* **1999**, *59*, 207-217.
 131. Kassab, A. C.; Xu, K.; Denkbas, E. B.; Dou, Y.; Zhao, S.; Pişkin, E. Rifampicin carrying polyhydroxybutyrate microspheres as a potential chemoembolization agent. *J Biomater Sci Polym Ed.* **1997**, *8*, 947-961.
 132. Xiong, Y. C.; Yao, Y. C.; Zhan, X. Y.; Chen, G. Q. Application of polyhydroxyalkanoates nanoparticles as intracellular sustained drug-release vectors. *J Biomater Sci Polym Ed.* **2010**, *21*, 127-140.
 133. Türesin, F.; Gürsel, I.; Hasirci, V. Biodegradable polyhydroxyalkanoate implants for osteomyelitis therapy: in vitro antibiotic release. *J Biomater Sci Polym Ed.* **2001**, *12*, 195-207.
 134. Yagmurlu, M. F.; Korkusuz, F.; Gürsel, I.; Korkusuz, P.; Ors, U.; Hasirci, V. Sulbactam-cefoperazone polyhydroxybutyrate-co-hydroxyvalerate (PHBV) local antibiotic delivery system: in vivo effectiveness and biocompatibility in the treatment of implant-related experimental osteomyelitis. *J Biomed Mater Res.* **1999**, *46*, 494-503.
 135. Gürsel, I.; Korkusuz, F.; Türesin, F.; Alaeddinoglu, N. G.; Hasirci, V. In vivo application of biodegradable controlled antibiotic release systems for the treatment of implant-related osteomyelitis. *Biomaterials.* **2001**, *22*, 73-80.
 136. Scheithauer, E. C.; Li, W.; Ding, Y.; Harhaus, L.; Roether, J. A.; Boccaccini, A. R. Preparation and characterization of electrosprayed daidzein-loaded PHBV microspheres. *Mater Lett.* **2015**, *158*, 66-69.
 137. Peng, X.; Chen, Y.; Li, Y.; Wang, Y.; Zhang, X. A long-acting BMP-2 release system based on poly(3-hydroxybutyrate) nanoparticles modified by amphiphilic phospholipid for osteogenic differentiation. *Biomed Res Int.* **2016**, *2016*, 5878645.
 138. Chen, R.; Yu, J.; Gong, H. L.; Jiang, Y.; Xue, M.; Xu, N.; Wei, D. X.; Shi, C. An easy long-acting BMP7 release system based on biopolymer nanoparticles for inducing osteogenic differentiation of adipose mesenchymal stem cells. *J Tissue Eng Regen Med.* **2020**, *14*, 964-972.
 139. Shrivastav, A.; Kim, H. Y.; Kim, Y. R. Advances in the applications of polyhydroxyalkanoate nanoparticles for novel drug delivery system. *Biomed Res Int.* **2013**, *2013*, 581684.
 140. Li, Z.; Yang, J.; Loh, X. J. Polyhydroxyalkanoates: opening doors for a sustainable future. *NPG Asia Mater.* **2016**, *8*, e265-e265.
 141. Nelson, T.; Kaufman, E.; Kline, J.; Sokoloff, L. The extraneural distribution of gamma-hydroxybutyrate. *J Neurochem.* **1981**, *37*, 1345-1348.
 142. Wang, B. L.; Wu, J. F.; Xiao, D.; Wu, B.; Wei, D. X. 3-hydroxybutyrate in the brain: biosynthesis, function, and disease therapy. *Brain-X.* **2023**, *1*, e6.
 143. Xiang, Y.; Wang, Q. Q.; Lan, X. Q.; Zhang, H. J.; Wei, D. X. Function and treatment strategies of β -hydroxybutyrate in aging. *Smart Mater Med.* **2023**, *4*, 160-172.
 144. Zhao, Y.; Zou, B.; Shi, Z.; Wu, Q.; Chen, G. Q. The effect of 3-hydroxybutyrate on the in vitro differentiation of murine osteoblast

PHA and its composites in musculoskeletal system

- MC3T3-E1 and in vivo bone formation in ovariectomized rats. *Biomaterials*. **2007**, *28*, 3063-3073.
145. Czechowska, J.; Skibiński, S.; Guzik, M.; Zima, A. Silver decorated β TCP-poly(3hydroxybutyrate) scaffolds for bone tissue engineering. *Materials (Basel)*. **2021**, *14*, 4227.
146. Chen, J.; Li, Z.; Zhang, Y.; Zhang, X.; Zhang, S.; Liu, Z.; Yuan, H.; Pang, X.; Liu, Y.; Tao, W.; Chen, X.; Zhang, P.; Chen, G. Q. Mechanism of reduced muscle atrophy via ketone body (D)-3-hydroxybutyrate. *Cell Biosci*. **2022**, *12*, 94.
147. Wang, Z.; Ma, K.; Jiang, X.; Xie, J.; Cai, P.; Li, F.; Liang, R.; Zhao, J.; Zheng, L. Electrospun poly(3-hydroxybutyrate-co-4-hydroxybutyrate)/Octacalcium phosphate Nanofibrous membranes for effective guided bone regeneration. *Mater Sci Eng C Mater Biol Appl*. **2020**, *112*, 110763.
148. Ang, S. L.; Shaharuddin, B.; Chuah, J. A.; Sudesh, K. Electrospun poly(3-hydroxybutyrate-co-3-hydroxyhexanoate)/silk fibroin film is a promising scaffold for bone tissue engineering. *Int J Biol Macromol*. **2020**, *145*, 173-188.
149. Kourmentza, C.; Plácido, J.; Venetsaneas, N.; Burniol-Figols, A.; Varrone, C.; Gavala, H. N.; Reis, M. A. M. Recent advances and challenges towards sustainable polyhydroxyalkanoate (PHA) production. *Bioengineering (Basel)*. **2017**, *4*, 55.
150. Xu, N.; Peng, X. L.; Li, H. R.; Liu, J. X.; Cheng, J. S.; Qi, X. Y.; Ye, S. J.; Gong, H. L.; Zhao, X. H.; Yu, J.; Xu, G.; Wei, D. X. Marine-derived collagen as biomaterials for human health. *Front Nutr*. **2021**, *8*, 702108.
151. Volova, T.; Shishatskaya, E.; Sevastianov, V.; Efremov, S.; Mogilnaya, O. Results of biomedical investigations of PHB and PHB/PHV fibers. *Biochem Eng J*. **2003**, *16*, 125-133.
152. Turkyilmaz, S.; Chen, W. H.; Mitomo, H.; Regen, S. L. Loosening and reorganization of fluid phospholipid bilayers by chloroform. *J Am Chem Soc*. **2009**, *131*, 5068-5069.

Received: October 14, 2023

Revised: November 3, 2023

Accepted: November 29, 2023

Available online: December 28, 2023

Bioactive elements manipulate bone regeneration

Long Bai^{1,2,3,#}, Peiran Song^{1,3,#}, Jiacan Su^{1,2,3,*}

Key Words:

bioactive elements; biomaterials; bone organoid; bone regeneration; controllable release

From the Contents

Introduction	248
The Process of Bone Regeneration	249
The Role of Bioactive Elements in Bone Regeneration	251
Challenges and Perspectives	262

ABSTRACT

While bone tissue is known for its inherent regenerative abilities, various pathological conditions and trauma can disrupt its meticulously regulated processes of bone formation and resorption. Bone tissue engineering aims to replicate the extracellular matrix of bone tissue as well as the sophisticated biochemical mechanisms crucial for effective regeneration. Traditionally, the field has relied on external agents like growth factors and pharmaceuticals to modulate these processes. Although efficacious in certain scenarios, this strategy is compromised by limitations such as safety issues and the transient nature of the compound release and half-life. Conversely, bioactive elements such as zinc (Zn), magnesium (Mg) and silicon (Si), have garnered increasing interest for their therapeutic benefits, superior stability, and reduced biotic risks. Moreover, these elements are often incorporated into biomaterials that function as multifaceted bioactive components, facilitating bone regeneration via release on-demand. By elucidating the mechanistic roles and therapeutic efficacy of the bioactive elements, this review aims to establish bioactive elements as a robust and clinically viable strategy for advanced bone regeneration.

*Corresponding author:

Jiacan Su,
drsujacan@163.com.

#Author equally.

<http://doi.org/10.12336/biomatertransl.2023.04.005>

How to cite this article:

Bai, L.; Song, P.; Su, J. Bioactive elements manipulate bone regeneration. *Biomater Transl.* 2023, 4(4), 248-269.

Introduction

Bone is a complex and hierarchical organ, the remodelling of which depends on specific macro- and micro-environments. The primary function of bone tissue is to provide mechanical stability to the body and protect major organs. Additionally, bone tissue exhibits high metabolic turnover, aiding in maintaining ionic balance within the body.¹⁻³ Diseases or traumatic injuries can impair bone function, making it crucial to restore lost functionality swiftly and efficiently. Autografts and allografts remain the benchmark in tissue engineering, yet their clinical utility is curtailed by supply constraints and the risk of disease transmission.⁴⁻⁶ In light of this, there is an urgent need to develop alternative bone substitutes through bone tissue engineering, which could offer functionalities similar to natural grafts while avoiding associated issues.

For successful bone regeneration, it is vital that bone substitutes mimic the highly ordered steps of bone regeneration to a maximum extent. Bone

repair is a dynamic biological process evolving over time, mainly involving post-operative bleeding, clot formation, inflammatory response, angiogenesis, and new bone formation.⁷ The regulation at each stage impacts subsequent biological events and ultimately determines the pace and quality of bone regeneration. The primary focus has been on integrating growth factors into bone tissue scaffolds or implants.⁸⁻¹⁰ Growth factors like insulin-like growth factors can activate cellular signalling cascades in stem cells surrounding bone lesions, thereby inducing proactive repair, including the angiogenesis process crucial for tissue regeneration.^{11, 12} However, the use of these growth factors presents significant drawbacks, including instability, immunogenicity, and high costs.¹³⁻¹⁵ Recently, many small molecules such as peptides have attracted researchers' attention. Yet, controlling their proper release in the defect area and their low half-life once implanted in the defect area are major barriers to their clinical translation.¹⁶⁻¹⁸



Biomaterials contain bioactive elements for bone repair

In contrast, employing bioactive elements is an appealing option, given their known therapeutic effects, higher stability, and lower risks compared to using biomolecules. The therapeutic elements released from biomaterials can regulate tissue regeneration steps in a manner akin to bioactive molecules. In recent years, researchers have been exploring the role of multiple bioactive elements in bone regeneration. Evidence suggests that elements, such as calcium (Ca),¹⁹ cobalt (Co),²⁰ copper (Cu),²¹ fluoride (F),²² lithium (Li),²³ magnesium (Mg),²⁴ silicon (Si),²⁵ silver (Ag),²⁶ strontium (Sr),²⁷ zinc (Zn),²⁸ can induce osteoprogenitor cell differentiation through growth factor signalling pathways or stimulate other processes supporting bone tissue growth.

Overall, this review meticulously delineates the impact of bioactive elements during various stages of bone regeneration, elucidating their mechanisms in osteoimmunomodulation, orchestrating neuroregulation, stimulating angiogenesis, and promoting osteogenesis (**Figure 1**). The comprehensive analysis of these bioactive ions not only furnishes a robust theoretical scaffold for ensuing basic research but also unveils novel therapeutic vistas and design principles for clinicians and materials scientists. Especially in the milieu of confronting the limitations inherent to natural grafts and growth factors, the exploration of bioactive elements emerges as a cost-effective, low-risk, and viable avenue for bone regeneration.

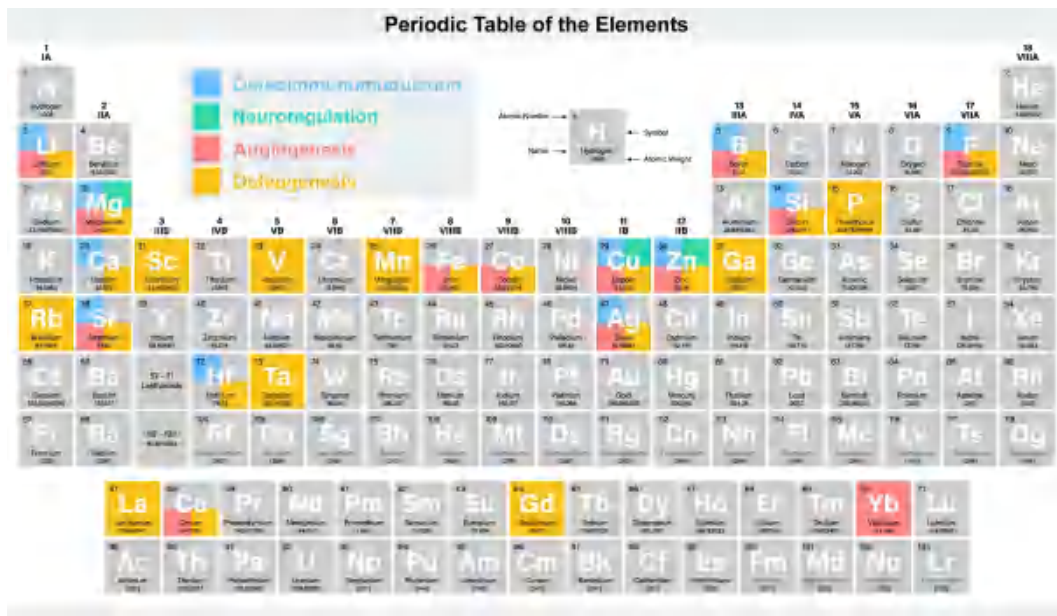


Figure 1. The role of bioactive elements in bone regeneration. Created with BioRender.com.

The Process of Bone Regeneration

Bone regeneration unfolds through a meticulously orchestrated cascade of biological processes: osteoimmunomodulation, neuroregulation, angiogenesis, and bone formation (**Figure 2**). Initially, osteoimmunomodulation, mediated by macrophage polarisation, establishes a favourable inflammatory landscape.²⁹ Concurrently, neuroregulation or skeletal interoception, steers physiological responses essential for bone healing.²⁸ Advancing, angiogenesis, directed by endothelial progenitor and mature cells, forms new vasculature, delivering crucial resources to the regenerative callus.³⁰ Lastly, osteogenesis, led by cellular entities like osteoblasts and mesenchymal stem cells (MSCs), governs the synthesis and remodelling of bone tissue.³¹

Osteoimmunomodulation

Osteoimmunomodulation represents a pivotal nexus where the realms of immunology and bone biology converge, under the auspices of bone biomaterials, to orchestrate a harmonious response between bone formation and resorption, thereby augmenting the bone repair capacity.^{19, 32-34} The crucible of this interplay lies in the role of immune cells, notably macrophages, whose interactions with bone cells and biomaterials significantly shape the trajectory and efficacy of bone repair endeavors.³⁵⁻³⁷ Macrophages, serving as the quintessential effector cells in immune responses to implants, are indispensable for promoting osteogenic functionality. The tapestry of immune-bone interplay is further enriched by the polarisation dynamics of macrophages into M1 and M2 subtypes, mediating pro-inflammatory and anti-

1 Organoid Research Center, Institute of Translational Medicine, Shanghai University, Shanghai, China; 2 Department of Orthopedics, Xinhua Hospital Affiliated to Shanghai Jiao Tong University School of Medicine, Shanghai, China; 3 National Center for Translational Medicine (Shanghai) SHU Branch, Shanghai University, Shanghai, China

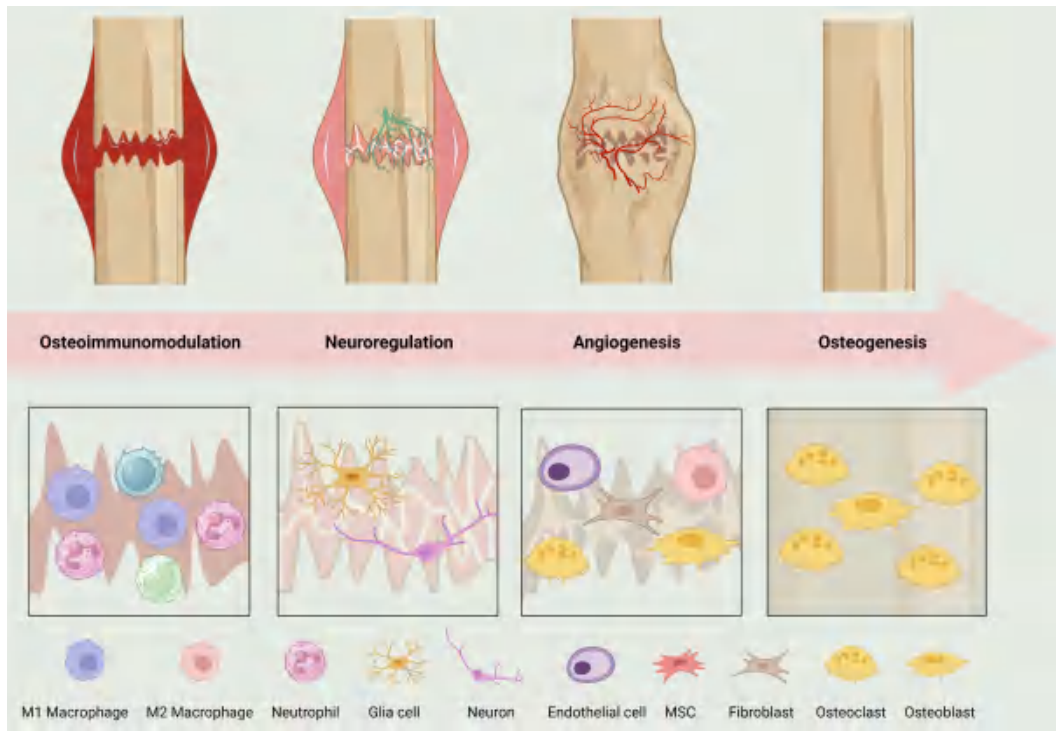


Figure 2. The process of bone regeneration. Created with BioRender.com. MSC: mesenchymal stem cell.

inflammatory responses respectively, which are integral for bone repair across diverse stages.³⁸ While M2 macrophages are emblematic for promoting bone tissue regeneration, the spotlight is gradually shifting towards unraveling the critical role of M1 macrophages in osteoimmunomodulation, particularly during the early inflammatory stages where they enhance the recruitment and commitment of angiogenic and osteogenic precursors.³⁹ Recent scholarly endeavors have also unveiled the central role of exosomes, secreted by macrophages, in mediating osteoimmunomodulation. These exosomes, upon internalisation by pivotal cells engaged in *de novo* bone formation such as endothelial cells and osteoblasts, significantly intervene in osseointegration, thereby opening new frontiers in understanding and leveraging macrophage-mediated immune modulation for enhanced bone repair.⁴⁰ In summation, osteoimmunomodulation, through the lens of macrophage-mediated interactions, unveils a complex yet rich array of mechanisms and interactions that not only deepen the comprehension of bone repair processes but also propel the development of novel therapeutic strategies and bone biomaterials.

Neuroregulation

Neuroregulation, a crucial mechanism orchestrated by the nervous system, governs the physiological and biochemical responses across various systems, organs, and cells in the body.⁴¹ This regulation is facilitated through the release of chemical substances, impacting an array of biological processes. In the realm of bone repair, neuroregulation, either known as skeletal interoception, emerges as a pivotal player in fostering the regeneration of bone tissues. It holds a significant

sway in maintaining the equilibrium of bone mass. Moreover, an assortment of neural factors, including neurotrophic growth factors, neuropeptides, and prostaglandin E2 (PGE2), are known to exercise a substantial influence over the growth, regeneration, and repair processes of bone tissues.⁴² Neuroregulation manoeuvres the balance of bone remodelling through diverse mechanisms, such as the activation of TrkA signalling pathway in osteoblastic cells, modulation of Wnt signalling pathway, and regulation of PGE2 production and secretion, thereby propelling the process of bone rebuilding. The promising horizon of skeletal interoception in bone repair is further bolstered by the supplementary use of PGE2, which, by modulating the proliferation and differentiation of stem cells, and promoting bone regeneration, augments the processes of bone repair and regeneration.⁴³⁻⁴⁶ Hence, the domain of neuroregulation not only unveils a profound understanding of the intricate interplay between neural and bone tissues but also heralds a promising avenue for advancements in bone repair methodologies, thereby contributing significantly to the broader spectrum of regenerative medicine.

Angiogenesis

Angiogenesis, the formation of new blood vessels from pre-existing vessels, is a cornerstone of bone repair, serving as the conduit for essential resources to the regenerative callus, a temporary tissue formed during bone healing. This process is orchestrated by endothelial progenitor cells and mature endothelial cells through recruitment, proliferation, differentiation, and reconstruction, facilitating the sprouting of microvessels from existing blood vessels.^{47, 48} The newly formed vasculature is indispensable for delivering oxygen

Biomaterials contain bioactive elements for bone repair

and nutrients to the metabolically active regenerating callus and facilitating the migration of inflammatory cells, as well as cartilage and bone precursor cells to the injury site, thereby providing a conducive environment for bone regeneration. The vitality of angiogenesis is underscored during fracture healing where the creation of new blood vessels is pivotal for supplying the requisite oxygen and nutrients to the evolving bone tissue. A sluggish or partial vascularisation process could hamper the supply of these essential resources to the bone defect area, which may lead to cell death, thus, emphasizing the need for prompt and robust angiogenesis during the bone regeneration. Notably, the angiogenic process is driven by various growth factors such as fibroblast growth factor, platelet-derived growth factor, and transforming growth factor- β (TGF- β), which invoke the proliferation, migration, differentiation, and vascularisation of endothelial cells and/or endothelial progenitor cells.^{49,50} The intricate biochemical and physical interplay between angiogenesis and bone repair processes elucidates a complex yet harmonious orchestration of events that are crucial for effective bone regeneration.

Osteogenesis

Osteogenesis is the pivotal process of bone tissue formation and remodelling, orchestrated chiefly by several cellular entities including osteoblasts, bone marrow-derived mesenchymal stem cells (BMSCs), osteoclasts, and osteocytes.⁵¹ Osteoblasts are the primary architects of bone formation. They migrate to the site of bone repair, especially at the implant-bone tissue interface during implant osseointegration, and govern the synthesis, secretion, and mineralisation of the extracellular matrix (ECM). Their activity is markedly enhanced by the expression of growth factors such as bone morphogenetic protein-2 (BMP-2) and TGF- β , which facilitate the formation and mineralisation of bone tissue.^{52,53} BMSCs, residing within the bone structure, BMSCs hold the potential to differentiate into osteoblasts, a transformation triggered by signals such as the release of TGF- β 1 from neighboring osteoclasts. This differentiation is a critical step towards the formation of new bone tissue, setting the stage for further maturation and mineralisation processes.^{54,55} Osteoclasts are principally involved in bone resorption, a process vital for the subsequent bone formation by osteoblasts. The resorption pits created by osteoclasts serve as the sites for new bone formation, where osteoblasts deposit the new bone material. Moreover, the resorption process also releases factors that, in turn, activate osteoblast proliferation, maturation, and differentiation, establishing a coordinated homeostatic mechanism integral for bone remodelling.⁵⁶ Osteocytes, originating from osteoblasts that become entrapped within the mineralized matrix, osteocytes play a crucial role in bone maintenance and remodelling. They are instrumental in attracting osteoclasts to implant sites, thereby facilitating the process of bone remodelling. In the process of bone regeneration, the orchestrated interplay of these cellular entities is indispensable.^{57,58} Through a deeper understanding of the cellular and molecular mechanisms underlying osteogenesis, novel therapeutic strategies and biomaterials can be developed, potentially advancing orthopedic and dental applications.

The Role of Bioactive Elements in Bone Regeneration

The role of bioactive elements in osteoimmunomodulation

Ag

Chen et al.⁵⁹ developed a titanium dioxide (TiO₂) nanotube loaded with Ag nanoparticles (Ag@TiO₂-NTs) that releases ultra-low amounts of Ag ions to improve immunoregulation and enhance bone repair. The study demonstrated that Ag@TiO₂-NTs, releasing ultra-low-dose Ag ions, effectively induced M2 macrophage polarisation and promoted a favourable osteoimmune environment by modulating phosphatidylinositol 3-kinase (PI3K)/protein kinase B (Akt), glucose transporter 1, and autophagy *in vitro*. *In vivo*, Ag@TiO₂-NTs enhanced bone formation, reduced inflammation, and promoted osteoimmune microenvironment compared to TiO₂-NTs and polished Ti surfaces.

Boron

Boron (B) has been demonstrated to amplify pro-inflammatory conditions by facilitating lymphocyte proliferation and enhancing nitric oxide and pro-inflammatory cytokine secretion in lipopolysaccharide-activated macrophages from B-exposed mice.⁶⁰ The precise molecular pathways involved are yet to be elucidated. Contrarily, B ions emanating from a calcium silicate layer on titanium surfaces have been found to downregulate pro-inflammatory cytokines and upregulate anti-inflammatory ones, potentially via attenuating the activation of the myeloid differentiation primary response 88-nuclear factor- κ B (NF- κ B) pathway.⁶¹

Ca

Ca, an essential mineral, plays a pivotal role in various physiological processes, including bone mineralisation, muscle contraction, and signal transduction in human body. Bioceramic degradation generated Ca ions, which triggered the Wnt/ β -catenin signalling pathway through calcium-sensing receptor (CaSR).⁶² Blocking CaSR activity decreased the inflow of macrophage-promoting Ca ions, hindered Wnt/ β -catenin signalling and the production of M2-like macrophages, and attenuated the MSC mineralisation promoted by the supernatants when they were treated with a CaSR antagonist. It implies that the Ca ions in bioceramics are dependent on CaSR-mediated Wnt/ β -catenin activation for macrophage M2 polarisation and novo bone production. The Wnt/ β -catenin pathway has been shown to be an important mediator of M2 polarisation in macrophages. During phage M2 polarisation, β -catenin is activated and transported to the nucleus, where it binds to the transcription factor T-cell factor/lymphoid enhancer factor family, triggering transcription of downstream target genes. As a major inhibitor of the Wnt/ β -catenin signal axis, glycogen synthase kinase (GSK)3 β can enhance the ubiquitination and degradation of β -catenin, diminish its protein stability, and limit its nuclear entrance in this pathway. By increasing the phosphorylation of downstream GSK3, phosphorylated AKT suppresses its function. It's worth mentioning that Ca can play a role in Wnt/ β -catenin signalling by boosting the phosphorylation of GSK3.¹⁹ Extracellular Ca

influx may positively control the Wnt/ β -catenin signalling pathway by increasing GSK3 phosphorylation, because GSK3 is a negative regulator of Wnt/ β -catenin. As a result, increased intracellular Ca stimulated the PI3K/AKT signalling pathway and caused AKT phosphorylation, which was followed by decreased downstream activity GSK3 due to its higher phosphorylation, resulting in increased β -catenin translocation.⁶³

Cu

Cu, a crucial micronutrient, functions as a cofactor in enzymes related to respiration, oxygen transport, and antioxidant defence. Cu ions can trigger oxidative damage, potentially leading to DNA damage and low-density lipoprotein peroxidation.^{64, 65} For instance, some research demonstrates the ability of Cu ions to catalyse the production of hydroxyl radicals via the Haber-Weiss reaction.⁶⁶ Therefore, Cu ion levels in the intra and extracellular are tightly regulated to minimise these effects. Wilson's disease, characterised by Cu accumulation, highlights the oxidative potential of Cu, which can cause organ damage and chronic inflammation.⁶⁷ Recent studies have produced varied results regarding the influence of Cu ions on macrophages. Some studies indicate that lower Cu concentrations promote anti-inflammatory markers, while higher concentrations induce pro-inflammatory markers. Huang et al.⁶⁸ showed that when macrophages were cultured on titanium plates containing 0.2 and 2 mM Cu ions, the pro-inflammatory markers of the cells increased in a concentration-dependent manner, and the anti-inflammatory factors (arginine, interleukin (IL)-4, IL-6) decreased in a concentration-dependent manner. Additionally, the incorporation of Cu into biomaterials has yielded conflicting findings. Wang et al.⁶⁹ investigated the inflammatory response of stainless-steel biomaterials containing nano-Cu. When it was implanted in mice, the secretion of inflammatory factors was significantly increased at the early stage, but was significantly reduced after 2 weeks.⁶⁹ Further research is essential to understand the factors governing Cu's impact on macrophage polarisation.

F

F is an essential trace element, which can be an effective osteoimmunomodulatory agent. Wu et al.⁷⁰ have shown that macrophages can be greatly influenced by F-mediated osteoimmunomodulation. F can stimulate macrophages to produce a bone immune environment conducive to osteogenesis and angiogenesis. In their research, 2.4 and 24 μ M sodium F can promote osteogenesis by increasing polyamine production in macrophages.^{70, 71} And macrophages stimulated by F showed an inhibited inflammatory response. Fluorine can promote the expression of inhibitor of κ B- α to inhibit the expression of pro-inflammatory genes such as tumour necrosis factor- α and IL-6. *In vivo*, fluorine also can influence other immune cells such as T cells and mast cells to create an immune environment suitable for bone regeneration.⁷²

Gadolinium

Gadolinium (Gd) is a rare earth element. Zhao et al.⁷³ developed

multifunctional scaffolds composed of gadolinium phosphate (GdPO_4), chitosan, and ferroferric oxide (Fe_3O_4) with a precise 100 nm pore size, and three-dimensional network of macropores. These scaffolds, embellished with hydrated GdPO_4 nanorods in a c-axis orientation on macropore walls, were crafted for addressing breast cancer bone metastases.⁷³ The structured architecture and macropores facilitated cell adhesion and new bone tissue formation. Gd ions released from the GdPO_4 /chitosan/ Fe_3O_4 scaffolds initiated M2 macrophage polarisation, and led to a significant upsurge in anti-inflammatory cytokines as indicated by CD206 expression. Moreover, the GdPO_4 /chitosan/ Fe_3O_4 and GdPO_4 /chitosan scaffolds markedly stimulated new blood vessel development, and supported osteogenesis through enhanced vascularisation.

Hafnium

Severyn et al.⁷⁴ investigated the immunomodulatory effects of hafnium (Hf) oxide (HfO_2) by analysing macrophage M1/M2 polarisation utilizing reverse transcription quantitative polymerase chain reaction. Following 4 hours of lipopolysaccharide stimulation, an increase in anti-inflammatory IL-10 expression was observed in lipopolysaccharide-treated macrophages cultured on HfO_2 . The data underline the potential immunomodulatory capacity of HfO_2 , and herald promising application in bone regeneration.

Li

Bartnikowski et al.⁷⁵ investigated the effect on bone by mixing Li carbonate with the biomaterial polymer polycaprolactone to achieve sustained release of Li. Experimental results showed that the released Li significantly polarised macrophages towards an immunomodulatory M2 phenotype, reduced pro-inflammatory M1 phase, and inhibited osteoclast activity, demonstrating an effective targeted tissue engineering system with the potential for further innovative ion release.

Mg

Mg is crucial for cellular metabolism, activating over 300 enzymes involved in the metabolism of carbohydrates, nucleic acids, and proteins.⁷⁶ It is also vital for the structural and functional integrity of cellular organelles.⁷⁷ In immunology, Mg modulates white blood cell functions, such as phagocytosis and lymphocyte production, and exhibits anti-inflammatory properties.⁷⁸ Mg deficiency has been linked to heightened inflammatory responses, including the activation of white blood cells and macrophages, increased cytokine release, and excess free radical production.⁷⁹ Qiao et al.⁸⁰ found that Mg ions induce a distinct cytokine profile, characterised by elevated levels of C-C motif chemokine ligand-5, IL-8, and IL-1ra, and a decrease in IL-1. This profile suggests that Mg ions facilitate monocyte recruitment and maturation into macrophages, while concurrently inhibiting pro-inflammatory cytokines like IL-1 through the up-regulation of IL-1ra, thus contributing to bone formation.

Si

Si ions, emanating from silica-based materials, have been shown to suppress pro-inflammatory cytokines and M1

Biomaterials contain bioactive elements for bone repair

markers through the Wnt5a/Ca²⁺ signalling pathway, thereby promoting osteogenesis by enhancing mineralisation and alkaline phosphatase (ALP) activity in BMSCs.^{81,82} Similarly, Si ions from titanium nanotube arrays also modulate the immune response by decreasing M1 markers and elevating anti-inflammatory markers like IL-10 and CD206.⁸³ Moreover, Si ions derived from various titanium-based materials have demonstrated an ability to inhibit pro-inflammatory cytokine secretion, such as tumour necrosis factor- α , IL-1 β , and IL-6, *in vitro*, likely via the attenuation of NF- κ B activation.^{84,85}

Sr

Sr exhibits a notable potential in modulating macrophage polarisation, crucial for immune response in bone regeneration. Zhao et al.⁸⁶ demonstrated that a Sr-Zn-phosphorus (P) coating on Ti substrates could preferentially steer macrophages toward the M2 phenotype by activating hypoxia-inducible factor-1 (HIF-1) signalling through the release of Sr ions and Zn ions, thereby bolstering bone integration in rat femur with titanium implants. Concurrently, Yu et al.⁸⁷ delineated that Sr ions doped nanorods array expedited the phenotypic transition of macrophages to M2, consequently amplifying osteogenic cytokine and growth factors (TGF- β 1 and BMP-2) expressions. Furthermore, the study elucidated that STSr₇ (Sr-doped Ti coated with sodium titanate, prepared via ion exchange at 100°C for 24 hours in 1000 mM 10 mL Sr(CH₃COO)₂ solution) outperformed *in vivo* in terms of osseointegration, releasing a higher concentration of Sr ions compared to STSr₄ (prepared under similar conditions but with 10 mM 10 mL Sr(CH₃COO)₂ solution). This enhanced Sr ions ion release from STSr₇ demonstrated a more consistent and effective stimulation of macrophage transition to M2, establishing a conducive environment for bone regeneration.

Zn

Zn, a pivotal element in human physiology, partakes in diverse cellular responses, profoundly influencing immune function,

cell division, and skeletal morphogenesis. As an essential trace element, it is indispensable for specific key enzymes and transcription factors, which is integral to immune responsiveness. Optimal Zn levels mitigate inflammatory cytokine secretion by macrophages, enhance anti-inflammatory cytokine expression, and maintain an anti-inflammatory milieu. Zhao et al.⁸⁸ demonstrated that Zn ions, derived from Zn-coated materials, modulate macrophage polarisation, inducing anti-inflammatory and osteoblastic cytokine secretion, thereby augmenting osteogenic differentiation potential of BMSCs. According to another study, Zn ions proficiently modulate activated macrophage polarisation towards the M2 phenotype, exerting an anti-inflammatory effect.⁸⁹ The release of Zn ions from Zn-doped tricalcium phosphate (TCP) has been noted to amplify tartrate-resistant acid phosphatase and ALP activity in human BMSCs, and regulate the formation of multi-nucleated giant cells and RAW264.7 macrophage activity.⁹⁰

In summary, bioactive elements such as Zn, F, Mg, Ca, Gd, Hf, and Sr play critical roles in osteoimmunomodulation, contributing to bone regeneration (**Figure 3**). Zn ions aid in anti-inflammatory cytokine expression and osteogenic differentiation of bone marrow stem cells. F ions influence macrophages to create an osteogenic and angiogenic bone immune environment. Mg ions modulate monocyte recruitment and activation, impacting cytokine profiles favourable for bone healing. Ca ions, primarily through CaSR-mediated Wnt/ β -catenin signalling, promote macrophage M2 polarisation and subsequent bone formation. Gd ions in scaffolds initiate M2 macrophage polarisation and enhance vascularisation. HfO₂ shows promise in immunomodulation, particularly in increasing anti-inflammatory IL-10 expression. Sr ions in coatings and nanorods induce M2 macrophage polarisation, consequently amplifying osteogenic cytokines and growth factors, fostering bone integration and regeneration. These elements not only modulate immune responses but also activate signalling pathways crucial for bone tissue engineering and regeneration.

Periodic Table of the Elements

Bioactive Elements in Osteoimmunomodulation

1	2											10	11	12	13	14	15	16	17	18	19	20																																																																																																																																																																																																																																																																																																																																																																																																																																																																																																																																																																																																																																																																																																																																																																																																																																																																																																													
1	2											10	11	12	13	14	15	16	17	18	19	20																																																																																																																																																																																																																																																																																																																																																																																																																																																																																																																																																																																																																																																																																																																																																																																																																																																																																																													
3	4											10	11	12	13	14	15	16	17	18	19	20																																																																																																																																																																																																																																																																																																																																																																																																																																																																																																																																																																																																																																																																																																																																																																																																																																																																																																													
5	6	7	8	9	10	11	12	13	14	15	16	17	18	19	20	21	22	23	24	25	26	27	28	29	30	31	32	33	34	35	36	37	38	39	40																																																																																																																																																																																																																																																																																																																																																																																																																																																																																																																																																																																																																																																																																																																																																																																																																																																																																																
39	40	41	42	43	44	45	46	47	48	49	50	51	52	53	54	55	56	57	58	59	60	61	62	63	64	65	66	67	68	69	70	71	72	73	74	75	76	77	78	79	80	81	82	83	84	85	86	87	88	89	90	91	92	93	94	95	96	97	98	99	100	101	102	103	104	105	106	107	108	109	110	111	112	113	114	115	116	117	118	119	120																																																																																																																																																																																																																																																																																																																																																																																																																																																																																																																																																																																																																																																																																																																																																																																																																																																		
101	102	103	104	105	106	107	108	109	110	111	112	113	114	115	116	117	118	119	120	121	122	123	124	125	126	127	128	129	130	131	132	133	134	135	136	137	138	139	140	141	142	143	144	145	146	147	148	149	150	151	152	153	154	155	156	157	158	159	160	161	162	163	164	165	166	167	168	169	170	171	172	173	174	175	176	177	178	179	180	181	182	183	184	185	186	187	188	189	190	191	192	193	194	195	196	197	198	199	200	201	202	203	204	205	206	207	208	209	210	211	212	213	214	215	216	217	218	219	220	221	222	223	224	225	226	227	228	229	230	231	232	233	234	235	236	237	238	239	240	241	242	243	244	245	246	247	248	249	250	251	252	253	254	255	256	257	258	259	260	261	262	263	264	265	266	267	268	269	270	271	272	273	274	275	276	277	278	279	280	281	282	283	284	285	286	287	288	289	290	291	292	293	294	295	296	297	298	299	300	301	302	303	304	305	306	307	308	309	310	311	312	313	314	315	316	317	318	319	320	321	322	323	324	325	326	327	328	329	330	331	332	333	334	335	336	337	338	339	340	341	342	343	344	345	346	347	348	349	350	351	352	353	354	355	356	357	358	359	360	361	362	363	364	365	366	367	368	369	370	371	372	373	374	375	376	377	378	379	380	381	382	383	384	385	386	387	388	389	390	391	392	393	394	395	396	397	398	399	400	401	402	403	404	405	406	407	408	409	410	411	412	413	414	415	416	417	418	419	420	421	422	423	424	425	426	427	428	429	430	431	432	433	434	435	436	437	438	439	440	441	442	443	444	445	446	447	448	449	450	451	452	453	454	455	456	457	458	459	460	461	462	463	464	465	466	467	468	469	470	471	472	473	474	475	476	477	478	479	480	481	482	483	484	485	486	487	488	489	490	491	492	493	494	495	496	497	498	499	500	501	502	503	504	505	506	507	508	509	510	511	512	513	514	515	516	517	518	519	520	521	522	523	524	525	526	527	528	529	530	531	532	533	534	535	536	537	538	539	540	541	542	543	544	545	546	547	548	549	550	551	552	553	554	555	556	557	558	559	560	561	562	563	564	565	566	567	568	569	570	571	572	573	574	575	576	577	578	579	580	581	582	583	584	585	586	587	588	589	590	591	592	593	594	595	596	597	598	599	600	601	602	603	604	605	606	607	608	609	610	611	612	613	614	615	616	617	618	619	620	621	622	623	624	625	626	627	628	629	630	631	632	633	634	635	636	637	638	639	640	641	642	643	644	645	646	647	648	649	650	651	652	653	654	655	656	657	658	659	660	661	662	663	664	665	666	667	668	669	670	671	672	673	674	675	676	677	678	679	680	681	682	683	684	685	686	687	688	689	690	691	692	693	694	695	696	697	698	699	700	701	702	703	704	705	706	707	708	709	710	711	712	713	714	715	716	717	718	719	720	721	722	723	724	725	726	727	728	729	730	731	732	733	734	735	736	737	738	739	740	741	742	743	744	745	746	747	748	749	750	751	752	753	754	755	756	757	758	759	760	761	762	763	764	765	766	767	768	769	770	771	772	773	774	775	776	777	778	779	780	781	782	783	784	785	786	787	788	789	790	791	792	793	794	795	796	797	798	799	800	801	802	803	804	805	806	807	808	809	810	811	812	813	814	815	816	817	818	819	820	821	822	823	824	825	826	827	828	829	830	831	832	833	834	835	836	837	838	839	840	841	842	843	844	845	846	847	848	849	850	851	852	853	854	855	856	857	858	859	860	861	862	863	864	865	866	867	868	869	870	871	872	873	874	875	876	877	878	879	880	881	882	883	884	885	886	887	888	889	890	891	892	893	894	895	896	897	898	899	900	901	902	903	904	905	906	907	908	909	910	911	912	913	914	915	916	917	918	919	920	921	922	923	924	925	926	927	928	929	930	931	932	933	934	935	936	937	938	939	940	941	942	943	944	945	946	947	948	949	950	951	952	953	954	955	956	957	958	959	960	961	962	963	964	965	966	967	968	969	970	971	972	973	974	975	976	977	978	979	980	981	982	983	984	985	986	987	988	989	990	991	992	993	994	995	996	997	998	999	1000

Figure 3. The role of bioactive elements in osteoimmunomodulation. Created with BioRender.com.

The role of bioactive elements in neuroregulation

Cu

In the neuroregulation of bone regeneration, Cu can act as an intracellular signalling molecule, binding with neurons to promote new bone formation, and affecting the process of bone repair. Cu can also regulate the excitability of neurons, having a significant neural regulation role in bone regeneration. Moreover, as one of the components of biodegradable metal implant, Cu can promote bone regeneration. The specific mechanisms and modes of action require further research to elucidate.²⁸

A novel biohybrid biodegradable hydrogel (gelatin methacrylate, GelMA) that incorporates copper ion-modified germanium-phosphorus (GeP) nanosheets. These nanosheets exhibit properties that promote neuro-vascular regeneration and possess antibacterial activity. The modification of GeP nanosheets with copper ions improves their stability and enables sustained release of bioactive ions. The integrated hydrogel demonstrates a significant enhancement in the osteogenic differentiation of BMSCs, facilitates angiogenesis in human umbilical vein endothelial cells (HUVECs), and upregulates neural differentiation-related proteins in neural stem cells. *In vitro* studies with injectable electroactive GelMA/GeP@Cu biohybrid hydrogel scaffolds show enhanced nerve differentiation and axon regeneration. These findings suggest that GelMA/GeP@Cu has great potential as a valuable biomaterial for neuro-vascularised bone regeneration and infection prevention in the field of bone tissue engineering.⁹¹

Mg

Mg ions can promote bone regeneration by stimulating the release of PGE2 through the activation of bone marrow macrophages. In the early stage of fracture healing (1st week), Mg ions can significantly increase the concentration of PGE2 in bone and serum, simultaneously activating sensory nerves, thereby stimulating PGE2 receptor-4 receptors. This induces the phosphorylation of cAMP-response element binding protein and upregulation of 5-hydroxytryptamine receptor 2C in the hypothalamus, ultimately downregulating sympathetic nerve activity related to bone repair. Under the influence of the medullary macrophage-sympathetic neuron-osteoblast neural circuit, this process promotes bone formation.²⁸

A photosensitive conductive hydrogel by incorporating Mg-modified black phosphorus (BP@Mg) into GelMA. The combined effect of conductive nanosheets and bioactive ions released from BP@Mg enhances the migration and secretion of Schwann cells, which directly promote innervated bone regeneration through the secretion of nerve growth factor and brain-derived neurotrophic factor. In an infected skull defect model, the GelMA-BP@Mg hydrogel demonstrates effective antibacterial activity and enhances the regeneration of bone and calcitonin gene-related polypeptide- α (CGRP) nerve fibres. This phototherapy conductive hydrogel offers a novel approach to repairing infected bone defects, utilizing skeletal-associated innervation as a therapeutic strategy.⁹² Zhang et al.⁹³ implanted a pure Mg pin into the intact distal femur of rats. This led to a notable increase in neuronal CGRP levels in the

peripheral cortex of the femur and the ipsilateral dorsal root ganglia. CGRP promotes the activation of adenosine 3,5-cyclic monophosphate-responsive element binding protein 1 and SP7 (osterix) through calcitonin receptor-like receptor and receptor activity modifying protein 1. Consequently, this enhances the osteogenic differentiation of stem cells.⁹³

Zn

Zn ions can promote the neural regulation of bone repair through modulating anti-inflammatory pathways. Specifically, under the influence of Zn, sensory nerve endings secrete PGE2, which can activate the PGE2 receptor-4 signalling in CGRP⁺ sensory nerve endings, becoming an intraneural sensory signal, and thereby activating sensory nerves. This activation, through the mutual regulation with the central nervous system, realizes the positive regulation function in bone repair. Additionally, research has indicated that under the influence of Zn ions, sensory nerve endings can also release CGRP, which can promote the proliferation and differentiation of osteoblasts, thereby better facilitating the process of bone repair.²⁸

Briefly, bioactive elements such as Cu, Mg, and Zn play critical roles in neuroregulation and contribute to bone regeneration (Figure 4). Mg ions stimulate bone repair by increasing PGE2 levels through bone marrow macrophage activation, influencing the neural circuit encompassing medullary macrophages, sympathetic neurons, and osteoblasts, thereby enhancing bone formation. Zn ions enhance neuroregulation via anti-inflammatory pathways, facilitating sensory nerve activation and osteoblast function. Cu ions, an intracellular signalling agent in bone neuroregulation, binds with neurons to bolster new bone formation and modulate neuronal excitability. Its role in biodegradable metal implants suggests potential in bone regeneration, though detailed mechanisms warrant further investigation.

The role of bioactive elements in angiogenesis

Ag

Ag has a long history for the use of antibiotics, which is a classic implant material. In recent years, scientists have discovered that Ag is a functional promoter of bone regeneration. According to Jeanmonod et al.'s study,⁹⁴ Ag acetate can promote angiogenesis. They implanted Ag acetate-coated Dacron vascular grafts into the dorsal skinfold chamber in mice, and discovered that functional capillaries were more dense than uncoated grafts. Meanwhile, Ag acetate coating could stimulate the ingrowth of new microvessels into Dacron vascular grafts. Most importantly, due to the dacron Ag graft controlling the release of Ag ions, the concentration of Ag ions wouldn't be too high to damage the normal cells. Therefore, Ag acetate-coated Dacron vascular grafts do not induce a severe inflammatory response.^{94,95} Ag nanoparticles (AgNPs) also have the function of promoting angiogenesis. Kang et al.⁹⁶ found that AgNPs induced tube formation on growth factor-reduced matrix glue, produced reactive oxygen species and released angiogenic factors vascular endothelial growth factor and nitric oxide via SVEC4-10 endothelial cells. Therefore, both Ag ions and nanoparticles can promote angiogenesis.⁹⁶

The image shows a standard periodic table of elements. A green rectangular box is placed over the middle section of the table, containing the elements Magnesium (Mg), Copper (Cu), and Zinc (Zn). Above this box, the text 'Bioactive Elements in Neuroregulation' is written in a light blue font. The periodic table includes element symbols, atomic numbers, and names, with the highlighted elements being Mg (atomic number 12), Cu (atomic number 29), and Zn (atomic number 30).

Figure 4. The role of bioactive elements in neuroregulation. Created with BioRender.com.

B

B, like the previously discussed ions, also exhibits a beneficial effect on angiogenesis, although the specific mechanisms remain less explored. B is often integrated into ceramic biomaterials, such as B-doped bioactive glass scaffolds. Different concentrations of B in these scaffolds have been tested, with lower doses (up to 925 μM) demonstrating enhanced angiogenic effects compared to higher doses (around 3700 μM).⁹⁷ A similar study showed that lower B concentrations enhanced endothelial cell proliferation and tubule formation.⁹⁸ A *in vivo* study with B-containing bioactive glass demonstrated increased angiogenic gene expression patterns and vascular density.⁹⁹ B has also been incorporated into composites of polymers and ceramics, Xia et al.⁹⁷ studied the effects of polycaprolactone containing B-bioactive glass at different levels (0, 10, 20, 30 and 40 wt%) on angiogenesis, showing that optimal angiogenic effects were achieved at specific concentrations (30 wt%), while higher concentrations (40 wt%) proved cytotoxic to cells. Additionally, when combined with other ions, B has shown synergistic effects on vascular endothelial growth factor (VEGF) secretion. Chen et al.¹⁰⁰ studied the effects of B-based glass and Cu-Zn doped B-based glass on human fibroblast cell lines. The results showed that VEGF secretion was increased in both cells, but the latter was more obvious.¹⁰⁰

Cu

Cu is one of the most important elements in humans, which is the third most prevalent mineral present in the body. Copper is mainly found in the body as Cu^{2+} and Cu^+ , and they are involved in a number of important biological reactions. Cu has an effect of promoting angiogenesis. Kong et al.²¹ found that Cu^{2+} can positively affect the expression of angiogenic growth factors in HUVECs and human dermal fibroblasts. VEGF is one of the most important mediators of angiogenesis during the proliferation phase. Angiogenin (ANG) is a ribonuclease which is a strong stimulator of angiogenesis and

interacts with endothelial cells. Cu^{2+} can not only promote the expression of VEGF, but also regulate the transcription of angiopoietin and influence the localization of ANG to enhance its function. Meanwhile, copper has a big effect on matrix metalloproteinases (MMPs), which can regulate the activity of VEGF and other growth factors and promote cell proliferation in angiogenesis.¹⁰¹ Researches have shown that low concentrations of Cu can stimulate the activity of MMPs, while high concentrations of copper can increase the expression of MMPs in fibroblasts. Therefore, Cu ions are important to angiogenesis in bone formation.¹⁰²

Cerium

Xiang et al.¹⁰³ modified a tissue engineering bone scaffold with cerium (Ce) oxide nanoparticles and evaluated the impact of Ce oxide nanoparticles on the growth and paracrine activity of MSCs on the scaffold surface. Ce oxide nanoparticles have the potential to increase MSC proliferation while also inhibiting apoptosis. Finally, large levels of the angiogenic factor VEGF were found. As a result of the improved paracrine of VEGF, endothelial progenitor cell proliferation, differentiation, and tube forming ability may be enhanced.

Co

Because of its ability to stabilise HIF-1 and hence activate VEGF, Co ions have been utilised to accelerate vascularisation.¹⁰⁴ The addition of Co ions to silk fibroin/F/calcium phosphide (CaP) may aid adipose-derived stem cells in the formation of tube-like structures.¹⁰⁵ However, because collagen type 1 matrix deposition was reduced, cell proliferation and endothelial network formation were inhibited. Chai et al.²⁰ found that preconditioning human periosteum-derived mesenchymal stem cell-seeded tissue engineered constructs with a fine-tuned solution containing Co increased VEGF secretion and improved human periosteum-derived mesenchymal stem cell development and endothelial network formation.

F

F has been shown to augment angiogenesis in a dose-dependent manner, demonstrating synergistic regulation of osteogenesis and angiogenesis by modulating the expression of key factors such as BMP-2, oncostatin M (OSM), spermine/spermidine synthase, insulin-like growth factor-1, and VEGF. Wu et al.²² observed that active angiogenesis was consistently present in F-treated groups, and attributed this to VEGF expression under varying F treatments. Further, F was found to stimulate insulin-like growth factor-1 production, a critical factor in endothelial cell migration and tubular formation.¹⁰⁶ Given the dose-dependent variations in its impact, F exerts multifaceted effects on osteogenesis, osteoclastogenesis, and angiogenesis.⁷¹

Iron

Shi et al.¹⁰⁷ studied the effect of Fe³⁺ release on the angiogenic response of bone grafts. As a controlled ferric agent, iron (Fe)-doped octacalcium phosphate was produced. The affinity, survival, proliferation, and angiogenic differentiation of HUVECs were all greatly improved by Fe-doped octacalcium phosphate. The scaffold promoted endothelial cell adhesion and spreading, as well as angiogenesis, as evidenced by the development of additional blood vessels and increased expression of particular markers. Fe³⁺ can boost HIF-1 α and VEGF levels, as well as nitric oxide secretion and endothelial nitric oxide synthase synthesis, all of which influence endothelial cell activity and angiogenesis.

Li

Li-incorporated bioactive glass ceramic has been shown to enhance the pro-angiogenic capabilities of HUVECs both *in vitro* and *in vivo*.²³ This enhancement is mediated through the induction of miR-130a in BMSC-derived exosomes, leading to phosphatase and tensin homolog deleted on chromosome ten (PTEN) downregulation and AKT pathway activation. The resultant cellular activities include increased endothelial cell proliferation, migration, tube formation, and increased expression of pro-angiogenic genes.

Mg

Mg ions improved the proliferation, migration, and osteogenic differentiation of BMSCs, as well as having evident impacts on angiogenesis, by selectively activating the mitogen-activated protein kinase/extracellular signal-regulated kinase pathway. Directly promoting the migration of ECs and up-regulating the production of VEGF in BMSCs increase angiogenesis.¹⁰⁸ The sensory nerve-endothelial cell interaction mediated by Mg through the CGRP-focal adhesion kinase-VEGF signalling pathway enhanced the repair of critical size bone defects.¹⁰⁹ Lai et al.⁴⁵ have developed a new bioactive porous scaffold using low temperature rapid prototyping technology, comprising of poly (lactide-co-glycolide), TCP, and Mg. By incorporating Mg into the scaffold, they observed that it not only provided a favourable template for vessel infiltration but also stimulated neo-angiogenesis. This ultimately led to new bone formation and remodelling in challenging bone defects, specifically those associated with steroid-induced osteonecrosis.⁴⁵

Sr

Sr can play a great effect on bone regeneration, including immune response, angiogenesis and new bone formation. Previous studies have shown that Sr-containing materials have the ability to promote angiogenesis. Yan et al.²⁷ have found that appropriate doses of Sr ions (0.2–1 mM) can enhance the secretion of VEGFA and ANG-1 in HUVECs and BMSCs co-culture systems, which has the potential to create an angiogenic microenvironment at an early stage. Sr not only promotes angiogenesis by stimulating osteoblasts to secrete angiogenic cytokines,¹¹⁰ but also significantly promotes early angiogenesis by regulating macrophage phenotype. Zhao et al.¹¹¹ have found that the monodispersed Sr-containing bioactive glasses microspheres could stimulate macrophages to exhibit a tendency towards the M2 phenotype and express high levels of platelet-derived growth factor-BB *in vitro*. What is the most important is that this access can play a big role in the early vascularisation, which is different from the way of osteoblasts.¹¹¹

Si

Si is one of the essential trace elements in human body, which is necessary in the development and growth of bone and connective tissue.¹¹² Studies have shown that Si ions can stimulate angiogenesis. Li and Chang¹¹³ found that the 0.7–1.8 $\mu\text{g}/\text{mL}$ Si ions provided by 1/64 and 1/256 diluted Ca silicate extracts stimulated the proliferation of HUVECs and upregulate the expression of pro-angiogenic factors (VEGF and basic fibroblast growth factor). Their receptors activate the expression of endothelial nitric oxide synthase and increase the expression of nitric oxide in HUVECs.¹¹³ Zhai et al.¹¹⁴ have shown that akermanite ceramics, which is a suitable source of Si ions, can promote angiogenesis. It can release and keep the suitable Si ions to induce angiogenesis by increasing gene expression of pro-angiogenic cytokine receptors and upregulating downstream signalling, such as nitric oxide synthase and nitric oxide.¹¹⁴ Their experiment successfully demonstrated that akermanite ceramics were the first silicone-containing ceramics capable of inducing angiogenesis during bone regeneration. Mao et al.¹¹⁵ have found that Sr and Si ions had synergistic effects on osteogenesis, osteoclast formation and angiogenesis. They use the SMS bioceramics, which has Sr and Si ionic compositions, to study the influence of angiogenesis. And they had made the conclusion that SMS bioceramics can enhance osteogenic differentiation and expression of preferred angiogenic factors in BMSC from ovariectomized rats, rebalance the osteoprotegerin/receptor activator of nuclear factor- κB ligand (RANKL) ratio in BMSC from ovariectomized rats at early stage, and inhibit RANKL-induced osteoclast formation at late stage. The effect of Si ions on promoting osteogenesis and Sr ions on enhancing angiogenesis and inhibiting osteoclast formation can be well combined by SMC.¹¹⁵

Ytterbium

Tang et al.¹¹⁶ used lyophilization and mineralisation techniques to successfully create magnetic Y-doped hydroxyapatite/chitosan nanohybrid scaffolds with ytterbium (Yb) dopants as

Biomaterials contain bioactive elements for bone repair

well as magnetic SrFe₁₂O₁₉ nanoplates. Yb ions from magnetic Y-doped hydroxyapatite/chitosan nanohybrid scaffolds only reached a maximum concentration of 0.30 μM, according to *in vitro* tests. The osteogenic and angiogenic properties of the magnetic Y-doped hydroxyapatite/chitosan nanohybrid scaffolds were remarkably improved by the Yb dopants and magnetic SrFe₁₂O₁₉ nanoplates. For one thing, the bioactive components promoted the migration of endothelial cells, the up-regulation of angiogenic protein VEGFA expression, and macrophage polarisation toward M2 phenotype, leading to the rapid development of blood vessels in bone defects. *In vivo* bone mineralisation was made possible by the sufficient nutrients and oxygen that the newly created blood vessels provided. For another, by activating the BMP-2/Smad pathway in the scaffolds, both the Yb dopants and magnetic SrFe₁₂O₁₉ nanoplates enhanced osteogenic differentiation of rat BMSCs and *in vivo* bone tissue regeneration, suggesting a beneficial influence in the entire osteogenic process. The majority of bone abnormalities were filled with newly created bone tissues 12 weeks after surgery. In order to speed up the repair of bone defects, Yb dopants and magnetic SrFe₁₂O₁₉ nanoplates would be expected.

Zn

The influence of Zn on angiogenesis is primarily regulated via the Zn-sensing receptor/G protein-coupled receptor 39.¹¹⁷ Within a concentration range of 20–60 μM, Zn enhances human coronary artery endothelial cell viability, proliferation, and angiogenic marker expression.¹¹⁸ Biomaterials such as 5% Zn-Bioglass®-incorporated calcium phosphate cement have been shown to upregulate VEGF and induce tubule formation in endothelial cells.¹¹⁹ Likewise, polycaprolactone matrices with zinc oxide (ZnO) nanoparticles promote cell proliferation and elevate VEGF and fibroblast growth factor expression, with the nanoparticles also catalysing reactive oxygen species generation via hydrogen peroxide (H₂O₂), a ZnO byproduct.¹²⁰ Elevated ZnO concentrations, however,

inhibit angiogenesis due to excessive reactive oxygen species production. The angiogenic potential of Zn varies with the biomaterial's morphological properties, such as nanoparticle configuration.¹²¹ Anti-angiogenic aspects of Zn are also being explored for cancer therapeutics by inhibiting tumour vasculature.¹²² When combined with Si, Zn can activate the p38 pathway, contributing to bone regeneration and angiogenesis via cytokine expression.¹²³ Further investigations are warranted to comprehensively understand angiogenic roles and underlying mechanisms of Zn.

In summary, various bioactive elements such as Mg, Sr, Si, and Ag play pivotal roles in promoting angiogenesis, which is instrumental for bone regeneration (Figure 5). Ag, historically recognised for its antibiosis, now stands out as a bone regeneration stimulant, with Ag acetate-coated grafts showing enhanced microvessel ingrowth without inducing inflammation. B, integrated into ceramic biomaterials, demonstrates angiogenic effects at specific concentrations. Cu, vital for angiogenesis, influences angiogenic growth factor expression in key cellular components. Co ions, by stabilising HIF-1, expedite new vessel formation. Ce oxide nanoparticles on scaffolds enhance MSC proliferation, subsequently promoting VEGF secretion. Fe³⁺ boosts angiogenesis by modulating endothelial cell activity. F, in a dose-dependent manner, orchestrates angiogenesis through osteogenesis and angiogenic factor regulation. Li-incorporated bioactive glass ceramic shows enhanced angiogenic potential both *in vivo* and *in vitro*. Mg ions, channelling through the mitogen-activated protein kinase/extracellular signal-regulated kinase pathway, have a positive impact on angiogenesis. Sr, through VEGF and ANG-1 modulation, plays a significant role in early vascularisation. Si ions stimulate angiogenesis via BMP-2/Smad pathway activation. Yb dopants in scaffolds combined with magnetic particles promote angiogenesis and bone tissue regeneration. Lastly, Zn mediates its angiogenic effects through specific cellular interactions, with its potential varying based on the morphology of the biomaterial.

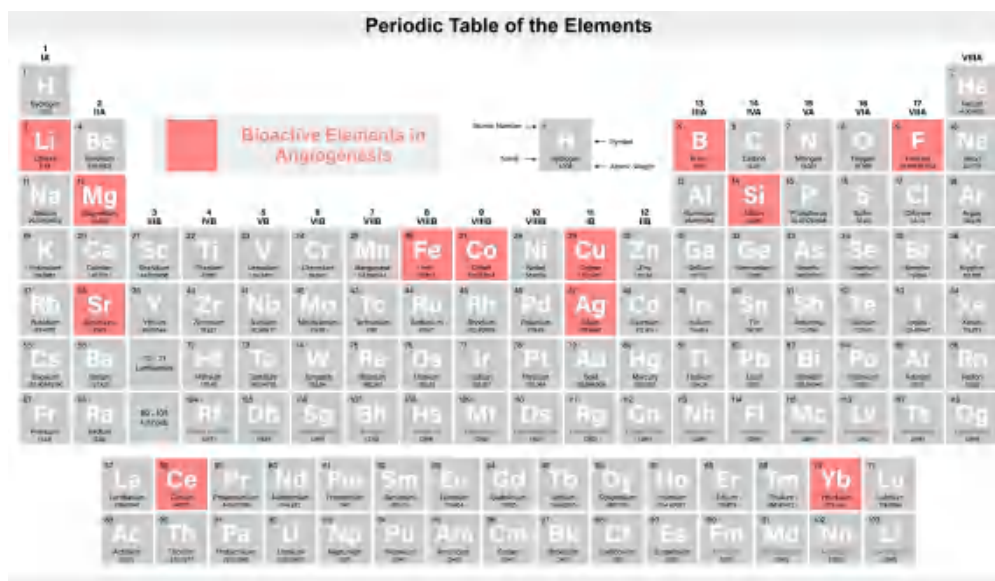


Figure 5. The role of bioactive elements in angiogenesis. Created with BioRender.com.

The role of bioactive elements in osteogenesis

Ag

Ag could not only promote angiogenesis, but also promote new bone formation. It has been reported that AgNPs can promote osteogenic lineage induction and actin aggregation in new bone formation. These promotions can only be found in AgNPs, not silver nitrate (AgNO_3). These promotions about AgNPs are achieved by stimulating the physiological activity of new bone-forming cells. AgNPs have been shown to promote mineralisation in MC3T3-E1 osteoblasts through microRNA-mediated upregulation of bone morphogenetic genes. Two studies revealed that, aside from the elevated expression of osteogenesis-critical bone morphogenetic proteins, the most significant transcriptional change was a decrease in osteoclast markers.^{124, 125} AgNPs also foster keratinocyte proliferation, fibroblast differentiation, and MSC osteogenic differentiation *in vitro*.¹²⁶ While the underlying mechanisms remain unidentified, these activities collectively contribute to new bone cell proliferation and differentiation, thereby facilitating new bone formation.

B

B, an essential trace element, plays a pivotal role in various biological processes, notably bone growth and maintenance.¹²⁷ Its supplementation has been linked to enhanced bone strength and microstructure.¹²⁸ Mechanistically, B fosters osteogenesis via the activation of the Wnt/ β -catenin pathway, particularly through the up-regulation of the transcription factor transcription factor 7-like 2.¹²⁹ This suggests its potential in bone regeneration therapies. Experimentally, B ions, when released from B nitride nanotubes, have been observed to induce osteogenesis, evidenced by enhanced protein adsorption, MSC attachment, and upregulation of osteogenic markers.¹³⁰ Furthermore, B-doped bioactive-glass scaffolds, have displayed promising osteogenic outcomes,¹³¹ amplifying cell adhesion, differentiation markers, and mineralisation. Specifically, B-enriched bioactive glass scaffolds activated the Wnt/ β -catenin pathway, influencing osteoblastic differentiation.¹³² However, while the role of Setd7 in B-mediated osteoblast differentiation has been identified, additional studies are required to uncover other potential contributing factors.

Ca

Doping Ca ions can notably accelerate adhesion, proliferation, and mineralisation of osteoblasts.¹³³ Ca, one of the ions that form the bone matrix, affect cells and living systems in several ways. The calcium phosphates in bone tissues cause bone formation and maturation through calcification.¹³⁴ Ca ions also influence bone repair via cellular communication. Ca causes bone tissue regeneration by accelerating mature bone cells and inducing bone growth precursor cells through the creation of nitric oxide.^{135, 136} Ca ions also activate the extracellular signal-regulated kinase1/2 pathway,¹³⁷ which stimulates osteoblastic bone production, and the PI3K/Akt pathways,¹³⁸ which prolongs the lifespan of osteoblasts. Ca ions also control the production and resorption activities of osteoclasts. Integrin β 1 and vinculin proteins are important factors of focal adhesion complexes that prove effective on the adhesion, proliferation,

and differentiation of BMSCs. Ca ions show helpful to the high expression of integrin β 1 and vinculin proteins. Hence Ca ions increase the protein expression and support cell adherence. The incorporation of Ca accelerates the proliferation of stem cells and the early differentiation of osteoblasts in the cell. The expression of the related proteins like osteopontin (OPN),¹³⁹ Runx2 and ALP would verify the conclusion. As a secretory phosphorylated glycoprotein, OPN adheres to HA via its distinct binding domain during osteogenesis and holds the formation of osteoid nodules *in vivo*, which directly influence the construction of the three-dimensional structure of newly formed bone.¹⁴⁰ The introduction of Ca ions suggests the abundant expression of OPN protein and supports the osteogenic differentiation of BMSCs.

Ce

Ce-doped mesoporous bioactive glass nanoparticles used as vectors for local administration of Ce have shown to stimulate the expression of pro-osteogenic genes in Saos-2 cells, as well as the development and calcification of a primitive osseous ECM. Westhauser et al.¹⁴¹ studied the impact of the ionic dissolution products of mesoporous bioactive glass nanoparticle on cellular osteogenic differentiation and their ability to form and mature a primitive osseous ECM. In the presence of Ce-doped mesoporous bioactive glass nanoparticles, the development and calcification of a primitive osseous ECM was greatly enhanced in a positive concentration-dependent manner, as evidenced by an increased presence of collagen and increased ECM calcification.

Co

Co-TCP increased the vitality of BMSCs.¹⁰⁴ *In vitro*, 2% Co-TCP increased ALP activity, matrix mineralisation, and osteogenic gene expression in BMSCs. Excessive Co doping, on the other hand, reduced TCP-induced osteogenesis. Additionally, Co^{2+} can inhibit the osteogenic differentiation of MSCs by mimicking hypoxia. Hsu et al.¹⁴² have shown that hypoxia caused by Co^{2+} activation of HIF impairing osteogenic differentiation, as evidenced by reduced ALP activity and expression of osteogenic markers core-binding factor alpha(1) (*Cbfa1*) and osteopontin. There are also some studies have shown that hypoxia caused by release of Co^{2+} can enhance the osteogenic potential of MSC after having a certain pretreatment.¹⁴³ The specific influence mechanism of Co needs to be studied in the future.

Cu

Cu can play a big role in bone metabolism, and severe Cu deficiency can lead to bone abnormalities, such as decreased bone strength. Cu can enhance the osteogenic differentiation of MSCs. The early studies on the effect of Cu on MSCs in postmenopausal women showed that Cu ions reduced osteoblast proliferation, increased differentiation by 2 folds, and, particularly, increased calcium deposition. Cu ions can enhance cell activity and proliferation and enhance the expression of bone specific protein.⁹⁵ Burghardt et al.¹⁴⁴ produced a composite material that deposited copper on a titanium alloy. The proliferation of MSC was stimulated by 0.1

Biomaterials contain bioactive elements for bone repair

mM Cu ions, ALP activity was increased, and mineralisation was increased 144. And other studies found an increase in the osteogenic gene expression of collagen type 1, ALP, OPN and Runx2 from rat BMSCs cultured with Cu-containing calcium phosphate cement.^{145,146}

F

F-containing biomaterials have been shown to have osteogenic properties, which are usually used as implant coating. F-containing biomaterials also can stimulate the proliferation and differentiation of osteoblasts *in vitro* and even promote bone formation of osteoblasts *in vivo*.¹⁴⁷ Chen et al.¹⁴⁸ have shown that the coating consisting of F can improve the activity of adhesion, proliferation and differentiation of osteoblasts, and has a good biocompatibility. Meanwhile, F can enhance bone-associated glycoprotein synthesis in BMSCs, leading to increased mineral deposition. But excessive F intake over a long period of time can eventually lead to damage to bone structure. Optimal osteogenic differentiation is achieved with F ion concentrations of 50 and 500 μM ⁷² and osteoblast mineralisation to be between 0.01 to 10 μM .¹⁴⁹ Thus, the physiological impact of F on skeletal tissue is dose-dependent in the local environment.

Fe

The addition of Fe ions ($\text{Fe}^{3+}/\text{Fe}^{2+}$) to calcium phosphate cement can speed up osteoblast proliferation. Doping Fe into bone cement boosted MC3T3-E1 cell proliferation and migration while also increasing their ALP activity and expression of osteogenic-related genes. The expression of HIF- α increased after cells were grown with Fe-dicalcium phosphate dihydrate scaffold extract, enhancing cell chemokine receptor activation and promoting cell migration.¹⁵⁰

Gallium

Gallium (Ga) is used in medicine mainly in antibacterial and cancer treatments. Ga nitrate is a drug that speeds up bone absorption. Short-term Ga therapy can effectively reduce bone turnover *in vivo* and increase bone calcium in patients with bone calcification to treat cancer-related hypercalcaemia.⁹⁵ According to Strazic Geljic et al.¹⁵¹, bone cement containing Ga can significantly inhibit the expression of osteoclast- and osteoblast-associated genes. And they found that TCP/phosphate-based scaffolds with single Ga promoted cell proliferation and significantly inhibited osteogenic differentiation and osteoclast activity *in vitro*. For the current literature, Ga has a range of promising qualities for future applications in tissue engineering.

Gd

The Gd dopants in the scaffolds triggered the signalling pathway (Wnt/ β -catenin,¹⁵² Smad/Runx2,¹⁵³ Akt/GSK3 β ¹⁵⁴), enabling BMSCs to proliferate and differentiate into osteoblasts.

Hf

HfO₂ was found to encourage pre-osteoblasts while impairing the viability of pre-osteoclasts.⁷⁴ HfO₂ stimulates the expression of OPN, Runx2, and TGF- β in osteoblasts

on the mRNA and protein levels. Meanwhile, the major regulators of osteoclast differentiation: c-Fos, MMP-9, PU.1, receptor activator of nuclear factor- κ B, and tartrate-resistant acid phosphatase, are expressed less when HfO₂ is present. HfO₂ stimulates pre-osteoclast death while simultaneously protecting pre-osteoblast from apoptosis by increasing the expression of the Bcl-2 transcript. Thus, a technique to stop the overactivity of osteoclasts during bone repair was raised. Moreover, HfO₂ protects pre-osteoblasts from apoptosis not only by activating specific genes relevant to osteogenesis but also by inducing the production of miR-17-5p and miR-7a-5p, two essential regulators of osteoblast proliferative activity and apoptosis. While miR-16 inhibits MSC production of important osteogenic markers and calcium mineral deposition during osteogenic differentiation, miR-21-5p is a well-known osteogenesis activator. Hopefully, HfO₂ may be used as a bioactive agent to modify and activate osteogenesis when administered to implantable metallic materials.

Lanthanum

Lanthanum (La)-substituted MgAl layered double hydroxide scaffolds activate the Wnt/ β -catenin pathway, thereby promoting BMSC proliferation and osteogenic differentiation due to the release of La ions. This activation leads to the upregulation of ALP, Runx2, collagen type 1, and OCN gene expressions. Additionally, the scaffolds act to obstruct the NF- κ B signalling pathway, significantly diminishing RANKL-induced osteoclastogenesis.¹⁵⁵

Li

Li increases bone regeneration via blocking GSK3 and thereby activating the β -catenin signalling pathway.¹⁵⁶ The release of Li ions stimulated the adhesion and proliferation of BMSCs more effectively. Furthermore, Li doped mesoporous silica nanospheres may improve BMSC ALP activity as well as the expression of osteogenesis-related genes (OPN, ALP, Runx2, and OCN).¹⁵⁷ Mo et al.¹⁵⁸ investigated how low concentration Li stimulation caused BMSCs to proliferate and differentiate into osteoblasts. They also discovered that adding 500 μM of Li to the canonical Wnt signalling pathway and osteogenesis differentiation in BMSCs reversed the inhibitory effect of 10 μM of XAV-939.¹⁵⁹ Huang et al.¹⁶⁰ found the RANKL/osteoprotegerin signalling axis was also involved in these effects.

Mg

Mg ions, via the PI3K/Akt signalling pathway, can influence the expression of bone-related genes such as Runx2, ALP, OCN, and OPN.¹⁶¹ *In vitro*, an appropriate concentration of Mg ions can greatly enhance pre-osteoblast proliferation and differentiation, as well as the up-regulation of osteogenic genes, and *in vivo*, significant new bone formation.²⁴

Manganese

Manganese ion (Mn^{2+}) has been shown to enhance the expression of osteogenic genes described in osteoblasts by increasing ALP activity, collagen type 1, OCN, BMP, and soluble intercellular adhesion molecule-1. Mn-doped implants have

been shown to stimulate cell proliferation, cell differentiation and biological activity, they are promising materials for bone tissue regeneration.¹⁶² Additionally, the release of Mn^{2+} from bioactive glass caused hMSCs differentiation through a bone route and subsequent mineralisation, according to the findings.¹⁶³ Mn^{2+} had a concentration-dependent effect on cell activities, and a lower Mn^{2+} concentration could encourage BMSCs to differentiate into osteoblasts. Wu et al.¹⁶⁴ discovered that Mn^{2+} concentrations below 7.17 g/L stimulated the proliferation of BMSCs and increased the expression of osteogenesis-related genes.

Rubidium

Rb, recognised as a crucial trace element in the human body, is known for its low toxicity.¹⁶⁵ Research indicates that biomaterials infused with rubidium significantly advance osteoblastic differentiation, particularly in the middle and late stages, and also enhance osteogenic capacities. A pivotal attribute of rubidium is its remarkable antibacterial properties, establishing it as an effective agent for enhancing biomaterials.^{166, 167} Tan et al.¹⁶⁸ have developed glass-ceramics infused with varying levels of Rb. Within the glass matrix, hydroxyapatite crystals are formed. The incorporation of rubidium enhances the formation and growth of these crystals. These rubidium-enriched glass-ceramics demonstrate superior bending strength compared to their rubidium-free counterparts. Crucially, the presence of rubidium fosters the proliferation and adhesion of human hBMSCs and increases ALP activity. Exhibiting robust mechanical properties, exceptional bioactivity, and biocompatibility, these rubidium-modified glass-ceramics hold promise for applications in bone regeneration.¹⁶⁸

Scandium (Sc)

$ScCl_3$ promotes osteogenesis and inhibits adipogenesis in the Wnt/ β -catenin signalling pathway when used at the optimal concentration.¹⁶⁹ Moreover, $ScCl_3$ can enhance bone remodelling by improving osteogenic differentiation in lineage commitment of rBMSCs.

Si

Si is an essential element for the development and growth of bone and connective tissue. *In vivo*, water-soluble forms of Si, chiefly as orthosilicic acid [OSA, $Si(OH)_4$]. It can accelerate bone mineralisation by affecting collagen and inhibits bone resorption in postmenopausal women.¹⁷⁰ And it can also play an important effect on stimulation of osteoblasts and bone formation and inhibition of osteoclast formation and bone resorption. A study has shown that OSA stimulated osteoblast differentiation at a physiological concentration of 20 μ M.¹⁷¹ Dong et al.¹⁷² have found that OSA could promote the osteogenic differentiation of rat BMSCs through the BMP-2/ $Smad1/5/Runx2$ signalling pathway to participate in the induction of collagen type 1 and osteocalcin synthesis. Zhou et al.¹⁷³ have found that OSA could accelerate bone formation in human osteoblast-like cells through the PI3K-Akt-mammalian target of rapamycin pathway. Zhou et al.¹⁷⁴ have shown that OSA and $Si(OH)_4$ could stimulate osteoblast differentiation *in vitro* through upregulating miR-146a to antagonize NF- κ B

activation. OSA can also play an effect on osteoclast. A study has shown that OSA inhibits RANKL-induced osteoclastogenesis by promoting the expression of miR-130b, which can counteract the negative effect of oophorectomy on miR-130b expression in rats.¹⁷⁵ miR-130b plays a role in cell proliferation, differentiation, apoptosis, tumour progression and metastasis, and serves as a biomarker for recurrence and prognosis. You et al.¹⁷⁶ have shown that the expression of miR-130b increased with the application of OSA. *In vitro*, the overexpression or inhibition of miR-130b significantly promoted or inhibited the osteogenic differentiation of osteoblasts under the application of OSA.¹⁷⁶ And as the scaffold material, dicalcium silicate is a good choice used as containing bioactive coating materials for prosthetic bone implant. It can induce the deposition of carbonised hydroxyapatite at the material-tissue interface, form a strong binding with bone tissue, inhibit the formation of osteoclast, promote the proliferation and differentiation of human osteoblasts and the expression of bone-related genes.¹⁷⁷

Sr

The addition of Sr in biomaterials reduced the capacity to generate apatite, but it also encouraged cell division, proliferation, differentiation into osteoblasts, and mineralisation of the ECM.¹⁷⁸ Li et al.¹⁷⁹ verified the influence of Sr^{2+} on MSC osteogenic differentiation. Sr^{2+} stimulated noncanonical Wnt signalling to regulate the production and distribution of the PAR complex, hence regulating cell division, and the increased cell population contributed to enhanced osteogenic differentiation. Meanwhile, Sr^{2+} release increased the expression of genes involved in hMSC osteogenic development; early indicators (Runx2, collagen type 1) were proportionate to the amount of Sr^{2+} released, and late markers (ALP, OCN) were higher.¹⁸⁰ To some extent, Sr^{2+} could prevent osteoclastogenesis on its own. Sr^{2+} decreased osteoclast activity more than recombinant human BMP-2.¹⁸¹ By inhibiting the RANKL-activated p38 signalling and NF- κ B signalling pathways, Sr-substituted sub-micron bioactive glass with the combined action of substituted sub-micron bioactive glass extract and Sr^{2+} demonstrated the most inhibitory effect on osteoclast differentiation.¹⁸²

Vanadium

Vanadium (V), a ubiquitous trace element in both plants and animals, has intriguing biological effects.¹⁸³ Found in a variety of oxidation states, from -1 to +5, certain forms like V III, IV, and V are noted for their insulin and growth factor mimicking properties at therapeutic levels. Notably, V compounds influence bone metabolism due to their primary storage in bone tissue.¹⁸³ Recent studies have unveiled that a complex of V (IV) with ascorbic acid can promote osteoblast differentiation and mineralisation in a lab setting, underscoring its potential in bone formation.¹⁸⁴ The amount of collagen type 1 produced in osteoblasts was found to be directly correlated with the dose of the V compound.

Zn

Zn is integral to bone development and is found in calcification sites such as osteons and calcified cartilage. Its levels in bone tissue rise with increasing mineralisation. Zn promotes

Biomaterials contain bioactive elements for bone repair

osteoblast proliferation and elevates ALP activity within a narrow dose range (1–50 μM).¹⁸⁵ Beyond this range, osteogenic activity diminishes. Kwun et al.¹⁸⁶ reported that Zn-deficient media reduced ALP activity, matrix-related gene expression, and mineralised matrix deposition in MC3T3-E1 cells. Zn also safeguards osteoblasts from apoptosis and enhances their spreading, attachment, and chemotaxis. Furthermore, Zn is crucial for osteoclastogenesis. Reduced numbers of osteoclasts were observed in the distal femur growth plates of Zn-deficient rats.^{186, 187} Zn exhibits a dose-response effect on osteoclast formation and activity, and at certain concentrations, can induce osteoclast apoptosis.^{188, 189} A study by O'Connor et al.¹⁹⁰ showed that Zn deficiency in Turkey poults and Sprague-Dawley rats led to reduced growth, bone shortening, and diminished ALP activity. The rats developed osteopenia, characterised by significant reductions in cancellous bone, osteoblast surface area, and osteoclast numbers.¹⁹⁰ Thus, the multifaceted roles of Zn in bone metabolism warrant further investigation.

Tantalum

Due to its exceptional osteogenic activity, corrosion resistance, and antibacterial adhesion, biomedical tantalum (Ta) has attracted considerable attention as a promising implantable material for bone repair. Hu et al.¹⁹¹ developed Ta/polyetheretherketone composites by blending Ta nanoparticles with polyetheretherketone for load-bearing bone repair applications. The incorporation of Ta nanoparticles in Ta/polyetheretherketone composites resulted in favourable surface roughness, hydrophilicity, and surface energy, thereby enhancing the osteoconductivity of fibrous electrospun polylactic acid (PLA) membranes used in guided bone regeneration.¹⁹¹ A Ta coating was applied to electrospun PLA membranes through the deposition of sputtered Ta ions around the PLA fibres. This Ta-PLA coating greatly enhanced the attachment, proliferation, and differentiation of preosteoblasts on the membranes. *In vivo* studies demonstrated that within 6 weeks, a majority of calvarial defects treated with Ta-PLA membranes were completely covered with newly formed bone, while the defects treated with bare PLA membranes showed

minimal bone coverage.¹⁹² In recent years, porous Ta has been extensively investigated for its regulatory effects on BMSCs. It plays a crucial role in regulating the proliferation, migration, and differentiation of BMSCs, making it a widely used material for bone defect repair.^{193–195}

P

P is a vital element in the human body, comprising approximately 1% of total body weight as a constituent of bones.¹⁹⁶ Culturing human tonsil-derived MSCs in osteogenic medium containing incremental concentrations of P (a mixture of Na_2HPO_4 and NaH_2PO_4) for 14 days increased their ability to undergo osteogenic differentiation.¹⁹⁷ Black phosphorus exhibits the capability to regulate oxidation and degradation, resulting in the non-toxic byproduct PO_4^{3-} . This PO_4^{3-} acts as a mineralisation resource, promoting in the formation of calcium phosphate (CaP) deposits that facilitate bone repair.^{198, 199} Introduction of graphene oxide nanosheets enhances initial cell attachment and wraps around black phosphorus, enabling continuous release of PO_4^{3-} . This stimulation of cell osteogenesis promotes the formation of new bone.²⁰⁰ Numerous studies have demonstrated that P-rich materials can stimulate mineralisation and promote bone regeneration.²⁰¹

Bioactive elements, ranging from trace metals to rare earths, play a foundational role in bone metabolism and regeneration (Figure 6). Elements like Ag, Cu, and Zn actively influence osteogenesis, angiogenesis, and osteoblast proliferation. Ga and Si, traditionally known for antibacterial and bone mineralisation effects respectively, showcase potential in bone turnover and osteoclast modulation. Mn, F, and Co, though dose-dependent, exhibit promising osteogenic differentiation impacts. Li, Mg, and Ca ions enhance bone cell proliferation, differentiation, and overall bone tissue regeneration. Rarer elements like Rb, Sr, Sc, La, Ce, Gd, and Hf, when doped in biomaterials, activate specific pathways fostering bone cell proliferation, differentiation, and osteogenic gene expression. These elements, in synergy, offer avenues for innovative bone regeneration therapies.

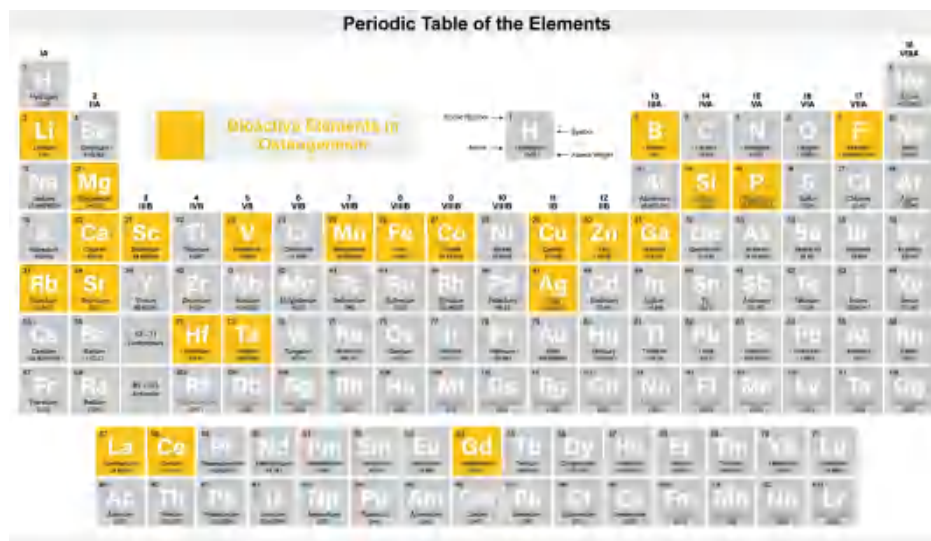


Figure 6. The role of bioactive elements in osteogenesis. Created with BioRender.com.

Challenges and Perspectives

This review comprehensively explores the role and mechanisms of bioactive elements such as Zn, Mg, and Si in bone regeneration. Initially, the review underlines the complex biological attributes and regeneration process of bone tissue, involving multiple stages like osteoimmunomodulation, neuroregulation, angiogenesis, and osteogenesis. Traditional bone regeneration strategies, although effective, are fraught with limitations such as stability, immunogenicity, and cost-effectiveness, often relying on growth factors and pharmaceuticals. Bioactive elements not only offer therapeutic efficacy but also superior stability and reduced biotic risks. These elements are frequently integrated into biomaterials, serving as multifaceted bioactive components that facilitate bone regeneration through controllable release mechanisms. In summary, this review establishes bioactive elements as a robust and clinically viable strategy for advanced bone regeneration, contributing to the advancement of bone tissue engineering.

The exploration of diverse elements in bone regeneration reveals promising prospects, showcasing a preference for employing a mixture of multiple elements in contemporary research endeavors. The myriad combinations, encompassing considerations of concentration and proportion among other parameters, necessitate rigorous experimental validations and iterative optimisations, thereby representing a time and resource-intensive endeavor. The integration of machine learning (ML) emerges as a potential solution to mitigate this impasse. ML, representing a facet of artificial intelligence, flourishes owing to its ability to evolve through data comprehension over time. It holds the promise to significantly expedite the screening and optimisation of elemental combinations for therapeutic efficacy, adeptly understanding the high-dimensional parameter space, and pinpointing potent combinations with minimal empirical trials.

Transitioning to the emerging realm of organoids, it unveils a fertile domain for clinical translational research, albeit the field of bone organoids remains nascent, with its construction strategies yet to reach maturation. The architectural complexities of bone organoids frequently necessitate the incorporation of a spectrum of growth factors to stimulate stem cell differentiation, yet the prohibitive cost of these factors presents a substantial impediment. The prospective benefits of bioactive elements in bone organoid construction herald a paradigm shift. The venture into multi-element incorporation could outline an economical and efficacious avenue, harboring the potential to revolutionize the bone organoid research paradigm. The envisaged synergistic interactions among these bioactive elements could not merely mimic the complex biochemical cues indispensable for bone development but also potentially unveil novel mechanisms underpinning bone regeneration, thereby augmenting the therapeutic and scientific horizons in bone tissue engineering and regenerative medicine.

Author contributions

JCS conceived the idea, LB handled the design, writing, and revision of the paper, and PR Song contributed to the writing and revision of this work. All authors approved the final version of the manuscript.

Financial support

This work was financially supported by National Natural Science Foundation of China (Nos. 82230071, 82172098), and Laboratory Animal Research Project of Shanghai Committee of Science and Technology (No. 23141900600).

Acknowledgement

None.

Conflicts of interest statement

There are no conflicts of interest.

Editor note: Jiacan Su is an Editorial Board member of *Biomaterials Translational*. He was blinded from reviewing or making decisions on the manuscript. The article was subject to the journal's standard procedures, with peer review handled independently of this Editorial Board member and his research group.

Open access statement

This is an open access journal, and articles are distributed under the terms of the Creative Commons Attribution-NonCommercial-ShareAlike 4.0 License, which allows others to remix, tweak, and build upon the work non-commercially, as long as appropriate credit is given and the new creations are licensed under the identical terms.

1. Koushik, T. M.; Miller, C. M.; Antunes, E. Bone tissue engineering scaffolds: function of multi-material hierarchically structured scaffolds. *Adv Healthc Mater.* **2023**, *12*, e2202766.
2. Stahl, A.; Yang, Y. P. Regenerative approaches for the treatment of large bone defects. *Tissue Eng Part B Rev.* **2021**, *27*, 539-547.
3. Fernandes, T. A. P.; Gonçalves, L. M. L.; Brito, J. A. A. Relationships between bone turnover and energy metabolism. *J Diabetes Res.* **2017**, *2017*, 9021314.
4. Yuan, J.; Maturavongsadit, P.; Metavarayuth, K.; Luckanagul, J. A.; Wang, Q. Enhanced bone defect repair by polymeric substitute fillers of multiarm polyethylene glycol-crosslinked hyaluronic acid hydrogels. *Macromol Biosci.* **2019**, *19*, e1900021.
5. Gyulay, K. K.; Karászi, P.; Rédei, M.; Sólymos, P.; Schandl, K.; Lacza, Z.; Horváthy, D. B. Evaluation of serum albumin-coated bone allograft for bone regeneration: a seven-year follow-up study of 26 cases. *Int J Mol Sci.* **2023**, *24*, 9232.
6. Ferraz, M. P. Bone grafts in dental medicine: an overview of autografts, allografts and synthetic materials. *Materials (Basel).* **2023**, *16*, 4117.
7. Bai, L.; Du, Z.; Du, J.; Yao, W.; Zhang, J.; Weng, Z.; Liu, S.; Zhao, Y.; Liu, Y.; Zhang, X.; Huang, X.; Yao, X.; Crawford, R.; Hang, R.; Huang, D.; Tang, B.; Xiao, Y. A multifaceted coating on titanium dictates osteoimmunomodulation and osteo/angio-genesis towards ameliorative osseointegration. *Biomaterials.* **2018**, *162*, 154-169.
8. Bosch-Ru  ,  .; D  ez-Tercero, L.; Buitrago, J. O.; Castro, E.; P  rez, R. A. Angiogenic and immunomodulation role of ions for initial stages of bone tissue regeneration. *Acta Biomater.* **2023**, *166*, 14-41.
9. Janmohammadi, M.; Nazemi, Z.; Salehi, A. O. M.; Seyfoori, A.; John, J. V.; Nourbakhsh, M. S.; Akbari, M. Cellulose-based composite scaffolds for bone tissue engineering and localized drug delivery. *Bioact Mater.* **2023**, *20*, 137-163.
10. Wu, J.; Cheng, X.; Wu, J.; Chen, J.; Pei, X. The development of magnesium-based biomaterials in bone tissue engineering: A review. *J Biomed Mater Res B Appl Biomater.* **2023**. doi: 10.1002/jbm.b.35326.
11. Wang, H.; Yu, R.; Wang, M.; Wang, S.; Ouyang, X.; Yan, Z.; Chen, S.; Wang, W.; Wu, F.; Fan, C. Insulin-like growth factor binding protein 4 loaded electrospun membrane ameliorating tendon injury by promoting retention of IGF-1. *J Control Release.* **2023**, *356*, 162-174.
12. Youssef, A.; Aboalola, D.; Han, V. K. The roles of insulin-like growth factors in mesenchymal stem cell niche. *Stem Cells Int.* **2017**, *2017*, 9453108.

13. Singh, S. K. Impact of product-related factors on immunogenicity of biotherapeutics. *J Pharm Sci.* **2011**, *100*, 354-387.
14. Jiskoot, W.; Randolph, T. W.; Volkin, D. B.; Middaugh, C. R.; Schöneich, C.; Winter, G.; Friess, W.; Crommelin, D. J.; Carpenter, J. F. Protein instability and immunogenicity: roadblocks to clinical application of injectable protein delivery systems for sustained release. *J Pharm Sci.* **2012**, *101*, 946-954.
15. Mitchell, A. C.; Briquez, P. S.; Hubbell, J. A.; Cochran, J. R. Engineering growth factors for regenerative medicine applications. *Acta Biomater.* **2016**, *30*, 1-12.
16. Apostolopoulos, V.; Bojarska, J.; Chai, T. T.; Elnagdy, S.; Kaczmarek, K.; Matsoukas, J.; New, R.; Parang, K.; Lopez, O. P.; Parhiz, H.; Perera, C. O.; Pickholz, M.; Remko, M.; Saviano, M.; Skwarczynski, M.; Tang, Y.; Wolf, W. M.; Yoshiya, T.; Zabrocki, J.; Zielenkiewicz, P.; AlKhazindar, M.; Barriga, V.; Kelaidonis, K.; Sarasia, E. M.; Toth, I. A global review on short peptides: frontiers and perspectives. *Molecules.* **2021**, *26*, 430.
17. Hamley, I. W. Small bioactive peptides for biomaterials design and therapeutics. *Chem Rev.* **2017**, *117*, 14015-14041.
18. Zou, P.; Chen, W. T.; Sun, T.; Gao, Y.; Li, L. L.; Wang, H. Recent advances: peptides and self-assembled peptide-nanosystems for antimicrobial therapy and diagnosis. *Biomater Sci.* **2020**, *8*, 4975-4996.
19. Chen, Z.; Klein, T.; Murray, R. Z.; Crawford, R.; Chang, J.; Wu, C.; Xiao, Y. Osteoimmunomodulation for the development of advanced bone biomaterials. *Mater Today.* **2016**, *19*, 304-321.
20. Chai, Y. C.; Mendes, L. F.; van Gastel, N.; Carmeliet, G.; Luyten, F. P. Fine-tuning pro-angiogenic effects of cobalt for simultaneous enhancement of vascular endothelial growth factor secretion and implant neovascularization. *Acta Biomater.* **2018**, *72*, 447-460.
21. Kong, N.; Lin, K.; Li, H.; Chang, J. Synergy effects of copper and silicon ions on stimulation of vascularization by copper-doped calcium silicate. *J Mater Chem B.* **2014**, *2*, 1100-1110.
22. De la Fuente, B.; Vázquez, M.; Rocha, R. A.; Devesa, V.; Vélez, D. Effects of sodium fluoride on immune response in murine macrophages. *Toxicol In Vitro.* **2016**, *34*, 81-87.
23. Liu, L.; Liu, Y.; Feng, C.; Chang, J.; Fu, R.; Wu, T.; Yu, F.; Wang, X.; Xia, L.; Wu, C.; Fang, B. Lithium-containing biomaterials stimulate bone marrow stromal cell-derived exosomal miR-130a secretion to promote angiogenesis. *Biomaterials.* **2019**, *192*, 523-536.
24. Shen, J.; Chen, B.; Zhai, X.; Qiao, W.; Wu, S.; Liu, X.; Zhao, Y.; Ruan, C.; Pan, H.; Chu, P. K.; Cheung, K. M. C.; Yeung, K. W. K. Stepwise 3D-spatio-temporal magnesium cationic niche: nanocomposite scaffold mediated microenvironment for modulating intramembranous ossification. *Bioact Mater.* **2021**, *6*, 503-519.
25. Bai, L.; Wu, R.; Wang, Y.; Wang, X.; Zhang, X.; Huang, X.; Qin, L.; Hang, R.; Zhao, L.; Tang, B. Osteogenic and angiogenic activities of silicon-incorporated TiO₂ nanotube arrays. *J Mater Chem B.* **2016**, *4*, 5548-5559.
26. Bai, L.; Hang, R.; Gao, A.; Zhang, X.; Huang, X.; Wang, Y.; Tang, B.; Zhao, L.; Chu, P. K. Nanostructured titanium-silver coatings with good antibacterial activity and cytocompatibility fabricated by one-step magnetron sputtering. *Appl Surf Sci.* **2015**, *355*, 32-44.
27. Yan, R.; Li, J.; Wu, Q.; Zhang, X.; Hu, L.; Deng, Y.; Jiang, R.; Wen, J.; Jiang, X. Trace element-augmented titanium implant with targeted angiogenesis and enhanced osseointegration in osteoporotic rats. *Front Chem.* **2022**, *10*, 839062.
28. Qiao, W.; Pan, D.; Zheng, Y.; Wu, S.; Liu, X.; Chen, Z.; Wan, M.; Feng, S.; Cheung, K. M. C.; Yeung, K. W. K.; Cao, X. Divalent metal cations stimulate skeleton interoception for new bone formation in mouse injury models. *Nat Commun.* **2022**, *13*, 535.
29. Bai, L.; Liu, Y.; Du, Z.; Weng, Z.; Yao, W.; Zhang, X.; Huang, X.; Yao, X.; Crawford, R.; Hang, R.; Huang, D.; Tang, B.; Xiao, Y. Differential effect of hydroxyapatite nano-particle versus nano-rod decorated titanium micro-surface on osseointegration. *Acta Biomater.* **2018**, *76*, 344-358.
30. Bai, L.; Chen, P.; Zhao, Y.; Hang, R.; Yao, X.; Tang, B.; Liu, C.; Xiao, Y.; Hang, R. A micro/nano-biomimetic coating on titanium orchestrates osteo/angio-genesis and osteoimmunomodulation for advanced osseointegration. *Biomaterials.* **2021**, *278*, 121162.
31. Kusumbe, A. P.; Ramasamy, S. K.; Adams, R. H. Coupling of angiogenesis and osteogenesis by a specific vessel subtype in bone. *Nature.* **2014**, *507*, 323-328.
32. Xie, Y.; Hu, C.; Feng, Y.; Li, D.; Ai, T.; Huang, Y.; Chen, X.; Huang, L.; Tan, J. Osteoimmunomodulatory effects of biomaterial modification strategies on macrophage polarization and bone regeneration. *Regen Biomater.* **2020**, *7*, 233-245.
33. Zhong, Z.; Wu, X.; Wang, Y.; Li, M.; Li, Y.; Liu, X.; Zhang, X.; Lan, Z.; Wang, J.; Du, Y.; Zhang, S. Zn/Sr dual ions-collagen co-assembly hydroxyapatite enhances bone regeneration through procedural osteoimmunomodulation and osteogenesis. *Bioact Mater.* **2022**, *10*, 195-206.
34. Wang, Y.; Wang, J.; Gao, R.; Liu, X.; Feng, Z.; Zhang, C.; Huang, P.; Dong, A.; Kong, D.; Wang, W. Biomimetic glycopeptide hydrogel coated PCL/nHA scaffold for enhanced cranial bone regeneration via macrophage M2 polarization-induced osteo-immunomodulation. *Biomaterials.* **2022**, *285*, 121538.
35. Schlundt, C.; Fischer, H.; Bucher, C. H.; Rendenbach, C.; Duda, G. N.; Schmidt-Bleek, K. The multifaceted roles of macrophages in bone regeneration: A story of polarization, activation and time. *Acta Biomater.* **2021**, *133*, 46-57.
36. Bai, X.; Liu, W.; Xu, L.; Ye, Q.; Zhou, H.; Berg, C.; Yuan, H.; Li, J.; Xia, W. Sequential macrophage transition facilitates endogenous bone regeneration induced by Zn-doped porous microcrystalline bioactive glass. *J Mater Chem B.* **2021**, *9*, 2885-2898.
37. Lee, J.; Byun, H.; Madhurakkat Perikamana, S. K.; Lee, S.; Shin, H. Current advances in immunomodulatory biomaterials for bone regeneration. *Adv Healthc Mater.* **2019**, *8*, e1801106.
38. Wang, Y.; Lin, Q.; Zhang, H.; Wang, S.; Cui, J.; Hu, Y.; Liu, J.; Li, M.; Zhang, K.; Zhou, F.; Jing, Y.; Geng, Z.; Su, J. M2 macrophage-derived exosomes promote diabetic fracture healing by acting as an immunomodulator. *Bioact Mater.* **2023**, *28*, 273-283.
39. Kushioka, J.; Chow, S. K.; Toya, M.; Tsubosaka, M.; Shen, H.; Gao, Q.; Li, X.; Zhang, N.; Goodman, S. B. Bone regeneration in inflammation with aging and cell-based immunomodulatory therapy. *Inflamm Regen.* **2023**, *43*, 29.
40. Xiang, X.; Pathak, J. L.; Wu, W.; Li, J.; Huang, W.; Wu, Q.; Xin, M.; Wu, Y.; Huang, Y.; Ge, L.; Zeng, S. Human serum-derived exosomes modulate macrophage inflammation to promote VCAM1-mediated angiogenesis and bone regeneration. *J Cell Mol Med.* **2023**, *27*, 1131-1143.
41. Lv, X.; Gao, F.; Cao, X. Skeletal interoception in bone homeostasis and pain. *Cell Metab.* **2022**, *34*, 1914-1931.
42. Tao, R.; Mi, B.; Hu, Y.; Lin, S.; Xiong, Y.; Lu, X.; Panayi, A. C.; Li, G.; Liu, G. Hallmarks of peripheral nerve function in bone regeneration. *Bone Res.* **2023**, *11*, 6.
43. Li, L.; Li, A.; Zhu, L.; Gan, L.; Zuo, L. Roxadustat promotes osteoblast differentiation and prevents estrogen deficiency-induced bone loss by

- stabilizing HIF-1 α and activating the Wnt/ β -catenin signaling pathway. *J Orthop Surg Res.* **2022**, *17*, 286.
44. Nencini, S.; Ringuet, M.; Kim, D. H.; Chen, Y. J.; Greenhill, C.; Ivanusic, J. J. Mechanisms of nerve growth factor signaling in bone nociceptors and in an animal model of inflammatory bone pain. *Mol Pain.* **2017**, *13*, 1744806917697011.
 45. Lai, Y.; Li, Y.; Cao, H.; Long, J.; Wang, X.; Li, L.; Li, C.; Jia, Q.; Teng, B.; Tang, T.; Peng, J.; Eglin, D.; Alini, M.; Grijpma, D. W.; Richards, G.; Qin, L. Osteogenic magnesium incorporated into PLGA/TCP porous scaffold by 3D printing for repairing challenging bone defect. *Biomaterials.* **2019**, *197*, 207-219.
 46. Yan, Y.; Wang, L.; Ge, L.; Pathak, J. L. Osteocyte-mediated translation of mechanical stimuli to cellular signaling and its role in bone and non-bone-related clinical complications. *Curr Osteoporos Rep.* **2020**, *18*, 67-80.
 47. Testa, U.; Castelli, G.; Pelosi, E. Role of endothelial progenitor cells in vascular development, homeostatic maintenance of blood vessels and in injury-mediated reparative response. *Stem Cell Investig.* **2020**, *7*, 7.
 48. Zhang, Y.; Zhang, Y. Y.; Pan, Z. W.; Li, Q. Q.; Sun, L. H.; Li, X.; Gong, M. Y.; Yang, X. W.; Wang, Y. Y.; Li, H. D.; Xuan, L. N.; Shao, Y. C.; Li, M. M.; Zhang, M. Y.; Yu, Q.; Li, Z.; Zhang, X. F.; Liu, D. H.; Zhu, Y. M.; Tan, Z. Y.; Zhang, Y. Y.; Liu, Y. Q.; Zhang, Y.; Jiao, L.; Yang, B. F. GDF11 promotes wound healing in diabetic mice via stimulating HIF-1 α -VEGF/SDF-1 α -mediated endothelial progenitor cell mobilization and neovascularization. *Acta Pharmacol Sin.* **2023**, *44*, 999-1013.
 49. Akatsu, Y.; Takahashi, N.; Yoshimatsu, Y.; Kimuro, S.; Muramatsu, T.; Katsura, A.; Maishi, N.; Suzuki, H. I.; Inazawa, J.; Hida, K.; Miyazono, K.; Watabe, T. Fibroblast growth factor signals regulate transforming growth factor- β -induced endothelial-to-myofibroblast transition of tumor endothelial cells via Elk1. *Mol Oncol.* **2019**, *13*, 1706-1724.
 50. Wang, Y.; Li, J. Current progress in growth factors and extracellular vesicles in tendon healing. *Int Wound J.* **2023**, *20*, 3871-3883.
 51. Miron, R. J.; Bosshardt, D. D. OsteoMacs: Key players around bone biomaterials. *Biomaterials.* **2016**, *82*, 1-19.
 52. Zhang, Q.; Liu, Y.; Li, J.; Wang, J.; Liu, C. Recapitulation of growth factor-enriched microenvironment via BMP receptor activating hydrogel. *Bioact Mater.* **2023**, *20*, 638-650.
 53. Rahman, M. S.; Akhtar, N.; Jamil, H. M.; Banik, R. S.; Asaduzzaman, S. M. TGF- β /BMP signaling and other molecular events: regulation of osteoblastogenesis and bone formation. *Bone Res.* **2015**, *3*, 15005.
 54. Hao, Z.; Ren, L.; Zhang, Z.; Yang, Z.; Wu, S.; Liu, G.; Cheng, B.; Wu, J.; Xia, J. A multifunctional neuromodulation platform utilizing Schwann cell-derived exosomes orchestrates bone microenvironment via immunomodulation, angiogenesis and osteogenesis. *Bioact Mater.* **2023**, *23*, 206-222.
 55. Hu, K.; Shang, Z.; Yang, X.; Zhang, Y.; Cao, L. Macrophage polarization and the regulation of bone immunity in bone homeostasis. *J Inflamm Res.* **2023**, *16*, 3563-3580.
 56. Veis, D. J.; O'Brien, C. A. Osteoclasts, Master Sculptors of Bone. *Annu Rev Pathol.* **2023**, *18*, 257-281.
 57. Yang, N.; Liu, Y. The role of the immune microenvironment in bone regeneration. *Int J Med Sci.* **2021**, *18*, 3697-3707.
 58. Cao, W.; Helder, M. N.; Bravenboer, N.; Wu, G.; Jin, J.; Ten Bruggenkate, C. M.; Klein-Nulend, J.; Schulten, E. Is there a governing role of osteocytes in bone tissue regeneration? *Curr Osteoporos Rep.* **2020**, *18*, 541-550.
 59. Chen, Y.; Guan, M.; Ren, R.; Gao, C.; Cheng, H.; Li, Y.; Gao, B.; Wei, Y.; Fu, J.; Sun, J.; Xiong, W. Improved immunoregulation of ultra-low-dose silver nanoparticle-loaded TiO(2) nanotubes via M2 macrophage polarization by regulating GLUT1 and autophagy. *Int J Nanomedicine.* **2020**, *15*, 2011-2026.
 60. Routray, I.; Ali, S. Boron induces lymphocyte proliferation and modulates the priming effects of lipopolysaccharide on macrophages. *PLoS One.* **2016**, *11*, e0150607.
 61. Lu, X.; Li, K.; Xie, Y.; Qi, S.; Shen, Q.; Yu, J.; Huang, L.; Zheng, X. Improved osteogenesis of boron incorporated calcium silicate coatings via immunomodulatory effects. *J Biomed Mater Res A.* **2019**, *107*, 12-24.
 62. Zhang, J.; Wu, Q.; Yin, C.; Jia, X.; Zhao, Z.; Zhang, X.; Yuan, G.; Hu, H.; Zhao, Q. Sustained calcium ion release from bioceramics promotes CaSR-mediated M2 macrophage polarization for osteoinduction. *J Leukoc Biol.* **2021**, *110*, 485-496.
 63. Yang, Y.; Ye, Y. C.; Chen, Y.; Zhao, J. L.; Gao, C. C.; Han, H.; Liu, W. C.; Qin, H. Y. Crosstalk between hepatic tumor cells and macrophages via Wnt/ β -catenin signaling promotes M2-like macrophage polarization and reinforces tumor malignant behaviors. *Cell Death Dis.* **2018**, *9*, 793.
 64. Balsano, C.; Porcu, C.; Sideri, S. Is copper a new target to counteract the progression of chronic diseases? *Metallomics.* **2018**, *10*, 1712-1722.
 65. Gaetke, L. M.; Chow-Johnson, H. S.; Chow, C. K. Copper: toxicological relevance and mechanisms. *Arch Toxicol.* **2014**, *88*, 1929-1938.
 66. Wu, P.; Dong, J.; Cheng, N.; Yang, R.; Han, Y.; Han, Y. Inflammatory cytokines expression in Wilson's disease. *Neurol Sci.* **2019**, *40*, 1059-1066.
 67. Chen, J.; Jiang, Y.; Shi, H.; Peng, Y.; Fan, X.; Li, C. The molecular mechanisms of copper metabolism and its roles in human diseases. *Pflugers Arch.* **2020**, *472*, 1415-1429.
 68. Huang, Q.; Li, X.; Elkhooly, T. A.; Liu, X.; Zhang, R.; Wu, H.; Feng, Q.; Liu, Y. The Cu-containing TiO(2) coatings with modulatory effects on macrophage polarization and bactericidal capacity prepared by micro-arc oxidation on titanium substrates. *Colloids Surf B Biointerfaces.* **2018**, *170*, 242-250.
 69. Wang, L.; Ren, L.; Tang, T.; Dai, K.; Yang, K.; Hao, Y. A novel nano-copper-bearing stainless steel with reduced Cu(2+) release only inducing transient foreign body reaction via affecting the activity of NF- κ B and Caspase 3. *Int J Nanomedicine.* **2015**, *10*, 6725-6739.
 70. Wu, S.; Xia, B.; Mai, S.; Feng, Z.; Wang, X.; Liu, Y.; Liu, R.; Li, Z.; Xiao, Y.; Chen, Z.; Chen, Z. Sodium fluoride under dose range of 2.4-24 μ M, a promising osteoimmunomodulatory agent for vascularized bone formation. *ACS Biomater Sci Eng.* **2019**, *5*, 817-830.
 71. Lee, M. J.; Chen, Y.; Huang, Y. P.; Hsu, Y. C.; Chiang, L. H.; Chen, T. Y.; Wang, G. J. Exogenous polyamines promote osteogenic differentiation by reciprocally regulating osteogenic and adipogenic gene expression. *J Cell Biochem.* **2013**, *114*, 2718-2728.
 72. Lee, M.; Arikawa, K.; Nagahama, F. Micromolar levels of sodium fluoride promote osteoblast differentiation through Runx2 signaling. *Biol Trace Elem Res.* **2017**, *178*, 283-291.
 73. Zhao, P. P.; Ge, Y. W.; Liu, X. L.; Ke, Q. F.; Zhang, J. W.; Zhu, Z. A.; Guo, Y. P. Ordered arrangement of hydrated GdPO4 nanorods in magnetic chitosan matrix promotes tumor photothermal therapy and bone regeneration against breast cancer bone metastases. *Chem Eng J.* **2020**, *381*, 122694.
 74. Seweryn, A.; Alicka, M.; Fal, A.; Kornicka-Garbowska, K.; Lawniczak-Jablonska, K.; Ozga, M.; Kuzmiuk, P.; Godlewski, M.; Marycz, K. Hafnium (IV) oxide obtained by atomic layer deposition (ALD) technology promotes early osteogenesis via activation of Runx2-OPN-mir21A axis while inhibits osteoclasts activity. *J Nanobiotechnology.* **2020**, *18*, 132.
 75. Bartnikowski, M.; Moon, H. J.; Ivanovski, S. Release of lithium from

- 3D printed polycaprolactone scaffolds regulates macrophage and osteoclast response. *Biomed Mater.* **2018**, *13*, 065003.
76. Fiorentini, D.; Cappadone, C.; Farruggia, G.; Prata, C. Magnesium: biochemistry, nutrition, detection, and social impact of diseases linked to its deficiency. *Nutrients.* **2021**, *13*, 1136.
 77. Wolf, F. I.; Cittadini, A. Chemistry and biochemistry of magnesium. *Mol Aspects Med.* **2003**, *24*, 3-9.
 78. Nielsen, F. H. Magnesium deficiency and increased inflammation: current perspectives. *J Inflamm Res.* **2018**, *11*, 25-34.
 79. Van Orden, R.; Eggett, D. L.; Franz, K. B. Influence of graded magnesium deficiencies on white blood cell counts and lymphocyte subpopulations in rats. *Magnes Res.* **2006**, *19*, 93-101.
 80. Qiao, W.; Wong, K. H. M.; Shen, J.; Wang, W.; Wu, J.; Li, J.; Lin, Z.; Chen, Z.; Matinlinna, J. P.; Zheng, Y.; Wu, S.; Liu, X.; Lai, K. P.; Chen, Z.; Lam, Y. W.; Cheung, K. M. C.; Yeung, K. W. K. TRPM7 kinase-mediated immunomodulation in macrophage plays a central role in magnesium ion-induced bone regeneration. *Nat Commun.* **2021**, *12*, 2885.
 81. Chen, Z.; Han, S.; Shi, M.; Liu, G.; Chen, Z.; Chang, J.; Wu, C.; Xiao, Y. Immunomodulatory effects of mesoporous silica nanoparticles on osteogenesis: From nanoimmunotoxicity to nanoimmunotherapy. *Appl Mater Today.* **2018**, *10*, 184-193.
 82. Huang, Y.; Wu, C.; Zhang, X.; Chang, J.; Dai, K. Regulation of immune response by bioactive ions released from silicate bioceramics for bone regeneration. *Acta Biomater.* **2018**, *66*, 81-92.
 83. Bai, L.; Liu, Y.; Zhang, X.; Huang, X.; Yao, X.; Hang, R.; Tang, B.; Xiao, Y. Favorable manipulation of macrophage/endothelial cell functionality and their cross-talk on silicon-doped titania nanotube arrays. *Nanoscale.* **2019**, *11*, 5920-5931.
 84. Rithidech, K. N.; Reungpatthanaphong, P.; Tungjai, M.; Jangiam, W.; Honikel, L.; Whorton, E. B. Persistent depletion of plasma gelsolin (pGSN) after exposure of mice to heavy silicon ions. *Life Sci Space Res (Amst).* **2018**, *17*, 83-90.
 85. Brown, D. M.; Beswick, P. H.; Donaldson, K. Induction of nuclear translocation of NF-kappaB in epithelial cells by respirable mineral fibres. *J Pathol.* **1999**, *189*, 258-264.
 86. Zhao, D. W.; Liu, C.; Zuo, K. Q.; Su, P.; Li, L. B.; Xiao, G. Y.; Cheng, L. Strontium-zinc phosphate chemical conversion coating improves the osseointegration of titanium implants by regulating macrophage polarization. *Chem Eng J.* **2021**, *408*, 127362.
 87. Yu, D.; Guo, S.; Yu, M.; Liu, W.; Li, X.; Chen, D.; Li, B.; Guo, Z.; Han, Y. Immunomodulation and osseointegration activities of Na(2)TiO(3) nanorods-arrayed coatings doped with different Sr content. *Bioact Mater.* **2022**, *10*, 323-334.
 88. Zhao, D. W.; Zuo, K. Q.; Wang, K.; Sun, Z. Y.; Lu, Y. P.; Cheng, L.; Xiao, G. Y.; Liu, C. Interleukin-4 assisted calcium-strontium-zinc-phosphate coating induces controllable macrophage polarization and promotes osseointegration on titanium implant. *Mater Sci Eng C Mater Biol Appl.* **2021**, *118*, 111512.
 89. Russell, K. C.; Phinney, D. G.; Lacey, M. R.; Barrilleaux, B. L.; Meyertholen, K. E.; O'Connor, K. C. In vitro high-capacity assay to quantify the clonal heterogeneity in trilineage potential of mesenchymal stem cells reveals a complex hierarchy of lineage commitment. *Stem Cells.* **2010**, *28*, 788-798.
 90. Luo, X.; Barbieri, D.; Davison, N.; Yan, Y.; de Bruijn, J. D.; Yuan, H. Zinc in calcium phosphate mediates bone induction: in vitro and in vivo model. *Acta Biomater.* **2014**, *10*, 477-485.
 91. Xu, Y.; Xu, C.; Yang, K.; Ma, L.; Li, G.; Shi, Y.; Feng, X.; Tan, L.; Duan, D.; Luo, Z.; Yang, C. Copper ion-modified germanium phosphorus nanosheets integrated with an electroactive and biodegradable hydrogel for neuro-vascularized bone regeneration. *Adv Healthc Mater.* **2023**, *12*, e2301151.
 92. Jing, X.; Xu, C.; Su, W.; Ding, Q.; Ye, B.; Su, Y.; Yu, K.; Zeng, L.; Yang, X.; Qu, Y.; Chen, K.; Sun, T.; Luo, Z.; Guo, X. Photosensitive and conductive hydrogel induced innervated bone regeneration for infected bone defect repair. *Adv Healthc Mater.* **2023**, *12*, e2201349.
 93. Zhang, Y.; Xu, J.; Ruan, Y. C.; Yu, M. K.; O'Laughlin, M.; Wise, H.; Chen, D.; Tian, L.; Shi, D.; Wang, J.; Chen, S.; Feng, J. Q.; Chow, D. H.; Xie, X.; Zheng, L.; Huang, L.; Huang, S.; Leung, K.; Lu, N.; Zhao, L.; Li, H.; Zhao, D.; Guo, X.; Chan, K.; Witte, F.; Chan, H. C.; Zheng, Y.; Qin, L. Implant-derived magnesium induces local neuronal production of CGRP to improve bone-fracture healing in rats. *Nat Med.* **2016**, *22*, 1160-1169.
 94. Jeanmonod, P.; Laschke, M. W.; Gola, N.; von Heesen, M.; Glanemann, M.; Dold, S.; Menger, M. D.; Moussavian, M. R. Silver acetate coating promotes early vascularization of Dacron vascular grafts without inducing host tissue inflammation. *J Vasc Surg.* **2013**, *58*, 1637-1643.
 95. Glenske, K.; Donkiewicz, P.; Köwitsch, A.; Milosevic-Oljaca, N.; Rider, P.; Rofall, S.; Franke, J.; Jung, O.; Smeets, R.; Schnettler, R.; Wenisch, S.; Barbeck, M. Applications of metals for bone regeneration. *Int J Mol Sci.* **2018**, *19*, 826.
 96. Kang, K.; Lim, D. H.; Choi, I. H.; Kang, T.; Lee, K.; Moon, E. Y.; Yang, Y.; Lee, M. S.; Lim, J. S. Vascular tube formation and angiogenesis induced by polyvinylpyrrolidone-coated silver nanoparticles. *Toxicol Lett.* **2011**, *205*, 227-234.
 97. Xia, L.; Ma, W.; Zhou, Y.; Gui, Z.; Yao, A.; Wang, D.; Takemura, A.; Uemura, M.; Lin, K.; Xu, Y. Stimulatory effects of boron containing bioactive glass on osteogenesis and angiogenesis of polycaprolactone: in vitro study. *Biomed Res Int.* **2019**, *2019*, 8961409.
 98. Haro Durand, L. A.; Góngora, A.; Porto López, J. M.; Boccaccini, A. R.; Zago, M. P.; Baldi, A.; Gorustovich, A. In vitro endothelial cell response to ionic dissolution products from boron-doped bioactive glass in the SiO(2)-CaO-P(2)O(5)-Na(2)O system. *J Mater Chem B.* **2014**, *2*, 7620-7630.
 99. Li, K.; Lu, X.; Liu, S.; Wu, X.; Xie, Y.; Zheng, X. Boron-incorporated micro/nano-topographical calcium silicate coating dictates osteo/angiogenesis and inflammatory response toward enhanced osseointegration. *Biol Trace Elem Res.* **2021**, *199*, 3801-3816.
 100. Chen, S.; Yang, Q.; Brow, R. K.; Liu, K.; Brow, K. A.; Ma, Y.; Shi, H. In vitro stimulation of vascular endothelial growth factor by borate-based glass fibers under dynamic flow conditions. *Mater Sci Eng C Mater Biol Appl.* **2017**, *73*, 447-455.
 101. Jacobs, A.; Renaudin, G.; Forestier, C.; Nedelec, J. M.; Descamps, S. Biological properties of copper-doped biomaterials for orthopedic applications: A review of antibacterial, angiogenic and osteogenic aspects. *Acta Biomater.* **2020**, *117*, 21-39.
 102. Wang, Y.; Zhang, W.; Yao, Q. Copper-based biomaterials for bone and cartilage tissue engineering. *J Orthop Translat.* **2021**, *29*, 60-71.
 103. Xiang, J.; Li, J.; He, J.; Tang, X.; Dou, C.; Cao, Z.; Yu, B.; Zhao, C.; Kang, F.; Yang, L.; Dong, S.; Yang, X. Cerium oxide nanoparticle modified scaffold interface enhances vascularization of bone grafts by activating calcium channel of mesenchymal stem cells. *ACS Appl Mater Interfaces.* **2016**, *8*, 4489-4499.
 104. Zheng, Y.; Yang, Y.; Deng, Y. Dual therapeutic cobalt-incorporated bioceramics accelerate bone tissue regeneration. *Mater Sci Eng C Mater Biol Appl.* **2019**, *99*, 770-782.

105. Fani, N.; Farokhi, M.; Azami, M.; Kamali, A.; Bakhshaiesh, N. L.; Ebrahimi-Barough, S.; Ai, J.; Eslaminejad, M. B. Endothelial and osteoblast differentiation of adipose-derived mesenchymal stem cells using a cobalt-doped cap/silk fibroin scaffold. *ACS Biomater Sci Eng.* **2019**, *5*, 2134-2146.
106. Delafontaine, P.; Bernstein, K. E.; Alexander, R. W. Insulin-like growth factor I gene expression in vascular cells. *Hypertension.* **1991**, *17*, 693-699.
107. Shi, H.; Yang, S.; Zeng, S.; Liu, X.; Zhang, J.; Zhang, J.; Wu, T.; Ye, X.; Yu, T.; Zhou, C.; Ye, J. Enhanced angiogenesis of biodegradable iron-doped octacalcium phosphate/poly(lactic-co-glycolic acid) scaffold for potential cancerous bone regeneration. *Appl Mater Today.* **2019**, *15*, 100-114.
108. Lin, S.; Yang, G.; Jiang, F.; Zhou, M.; Yin, S.; Tang, Y.; Tang, T.; Zhang, Z.; Zhang, W.; Jiang, X. A magnesium-enriched 3D culture system that mimics the bone development microenvironment for vascularized bone regeneration. *Adv Sci (Weinh).* **2019**, *6*, 1900209.
109. Ye, L.; Xu, J.; Mi, J.; He, X.; Pan, Q.; Zheng, L.; Zu, H.; Chen, Z.; Dai, B.; Li, X.; Pang, Q.; Zou, L.; Zhou, L.; Huang, L.; Tong, W.; Li, G.; Qin, L. Biodegradable magnesium combined with distraction osteogenesis synergistically stimulates bone tissue regeneration via CGRP-FAK-VEGF signaling axis. *Biomaterials.* **2021**, *275*, 120984.
110. Gu, Z.; Xie, H.; Huang, C.; Peng, H.; Tan, H.; Li, L.; Yu, X. Effects of strontium-doped calcium polyphosphate on angiogenic growth factors expression of co-culturing system in vitro and of host cell in vivo. *RSC Adv.* **2014**, *4*, 2783-2792.
111. Zhao, F.; Lei, B.; Li, X.; Mo, Y.; Wang, R.; Chen, D.; Chen, X. Promoting in vivo early angiogenesis with sub-micrometer strontium-contained bioactive microspheres through modulating macrophage phenotypes. *Biomaterials.* **2018**, *178*, 36-47.
112. Srinath, P.; Abdul Azeem, P.; Venugopal Reddy, K. Review on calcium silicate-based bioceramics in bone tissue engineering. *Int J Appl Ceram Technol.* **2020**, *17*, 2450-2464.
113. Li, H.; Chang, J. Stimulation of proangiogenesis by calcium silicate bioactive ceramic. *Acta Biomater.* **2013**, *9*, 5379-5389.
114. Zhai, W.; Lu, H.; Chen, L.; Lin, X.; Huang, Y.; Dai, K.; Naoki, K.; Chen, G.; Chang, J. Silicate bioceramics induce angiogenesis during bone regeneration. *Acta Biomater.* **2012**, *8*, 341-349.
115. Mao, L.; Xia, L.; Chang, J.; Liu, J.; Jiang, L.; Wu, C.; Fang, B. The synergistic effects of Sr and Si bioactive ions on osteogenesis, osteoclastogenesis and angiogenesis for osteoporotic bone regeneration. *Acta Biomater.* **2017**, *61*, 217-232.
116. Tang, Y. Q.; Wang, Q. Y.; Ke, Q. F.; Zhang, C. Q.; Guan, J. J.; Guo, Y. P. Mineralization of ytterbium-doped hydroxyapatite nanorod arrays in magnetic chitosan scaffolds improves osteogenic and angiogenic abilities for bone defect healing. *Chem Eng J.* **2020**, *387*, 124166.
117. Zhu, D.; Su, Y.; Zheng, Y.; Fu, B.; Tang, L.; Qin, Y. X. Zinc regulates vascular endothelial cell activity through zinc-sensing receptor ZnR/GPR39. *Am J Physiol Cell Physiol.* **2018**, *314*, C404-C414.
118. Ma, J.; Zhao, N.; Zhu, D. Endothelial cellular responses to biodegradable metal zinc. *ACS Biomater Sci Eng.* **2015**, *1*, 1174-1182.
119. Zhang, J.; Park, Y. D.; Bae, W. J.; El-Fiqi, A.; Shin, S. H.; Lee, E. J.; Kim, H. W.; Kim, E. C. Effects of bioactive cements incorporating zinc-bioglass nanoparticles on odontogenic and angiogenic potential of human dental pulp cells. *J Biomater Appl.* **2015**, *29*, 954-964.
120. Hassan, A.; Elebeedy, D.; Matar, E. R.; Fahmy Mohamed Elsayed, A.; Abd El Maksoud, A. I. Investigation of angiogenesis and wound healing potential mechanisms of zinc oxide nanorods. *Front Pharmacol.* **2021**, *12*, 661217.
121. Bosch-Ru e, E.; Diez-Tercero, L.; Giordano-Kelhoff, B.; Delgado, L. M.; Bosch, B. M.; Hoyos-Nogu es, M.; Mateos-Timoneda, M. A.; Tran, P. A.; Gil, F. J.; Perez, R. A. Biological roles and delivery strategies for ions to promote osteogenic induction. *Front Cell Dev Biol.* **2020**, *8*, 614545.
122. Santos, C. J.; Ferreira Soares, D. C.; Ferreira, C. A.; de Barros, A. L. B.; Silva Cunha Junior, A. D.; Filho, F. M. Antiangiogenic evaluation of ZnWO(4) nanoparticles synthesised through microwave-assisted hydrothermal method. *J Drug Target.* **2018**, *26*, 806-817.
123. Song, Y.; Wu, H.; Gao, Y.; Li, J.; Lin, K.; Liu, B.; Lei, X.; Cheng, P.; Zhang, S.; Wang, Y.; Sun, J.; Bi, L.; Pei, G. Zinc silicate/nanohydroxyapatite/collagen scaffolds promote angiogenesis and bone regeneration via the p38 MAPK pathway in activated monocytes. *ACS Appl Mater Interfaces.* **2020**, *12*, 16058-16075.
124. Qing, T.; Mahmood, M.; Zheng, Y.; Biris, A. S.; Shi, L.; Casciano, D. A. A genomic characterization of the influence of silver nanoparticles on bone differentiation in MC3T3-E1 cells. *J Appl Toxicol.* **2018**, *38*, 172-179.
125. Wu, Y.; Cheng, Z.; Hu, W.; Tang, S.; Zhou, X.; Dong, S. Biosynthesized silver nanoparticles inhibit osteoclastogenesis by suppressing NF- B signaling pathways. *Adv Biol (Weinh).* **2023**, e2300355.
126. Liu, X.; Lee, P. Y.; Ho, C. M.; Lui, V. C.; Chen, Y.; Che, C. M.; Tam, P. K.; Wong, K. K. Silver nanoparticles mediate differential responses in keratinocytes and fibroblasts during skin wound healing. *ChemMedChem.* **2010**, *5*, 468-475.
127. Nielsen, F. H. The emergence of boron as nutritionally important throughout the life cycle. *Nutrition.* **2000**, *16*, 512-514.
128. Dessordi, R.; Spirlandeli, A. L.; Zamarioli, A.; Volpon, J. B.; Navarro, A. M. Boron supplementation improves bone health of non-obese diabetic mice. *J Trace Elem Med Biol.* **2017**, *39*, 169-175.
129. Yin, C.; Jia, X.; Zhao, Q.; Zhao, Z.; Wang, J.; Zhang, Y.; Li, Z.; Sun, H.; Li, Z. Transcription factor 7-like 2 promotes osteogenic differentiation and boron-induced bone repair via lipocalin 2. *Mater Sci Eng C Mater Biol Appl.* **2020**, *110*, 110671.
130. Li, X.; Wang, X.; Jiang, X.; Yamaguchi, M.; Ito, A.; Bando, Y.; Golberg, D. Boron nitride nanotube-enhanced osteogenic differentiation of mesenchymal stem cells. *J Biomed Mater Res B Appl Biomater.* **2016**, *104*, 323-329.
131. Yin, C.; Jia, X.; Miron, R. J.; Long, Q.; Xu, H.; Wei, Y.; Wu, M.; Zhang, Y.; Li, Z. Setd7 and its contribution to Boron-induced bone regeneration in Boron-mesoporous bioactive glass scaffolds. *Acta Biomater.* **2018**, *73*, 522-530.
132. Ying, D.; Ouyang, Z.; Liu, T.; Liu, X.; Huang, Q. Boron-containing micro/nano-structured TiO2/bioceramics coatings with modulatory effects on SaOS-2 cell response. *Mater Lett.* **2018**, *228*, 29-32.
133. Cai, B.; Tan, P.; Jiang, N.; Guo, Z.; Ay, B.; Li, S.; Hou, Y.; Li, Y.; You, Y.; Zhang, L.; Zhu, S. Bioinspired fabrication of calcium-doped TiP coating with nanofibrous microstructure to accelerate osseointegration. *Bioconjug Chem.* **2020**, *31*, 1641-1650.
134. Peacock, M. Calcium metabolism in health and disease. *Clin J Am Soc Nephrol.* **2010**, *5 Suppl 1*, S23-30.
135. Foreman, M. A.; Gu, Y.; Howl, J. D.; Jones, S.; Publicover, S. J. Group III metabotropic glutamate receptor activation inhibits Ca²⁺ influx and nitric oxide synthase activity in bone marrow stromal cells. *J Cell Physiol.* **2005**, *204*, 704-713.
136. Riddle, R. C.; Taylor, A. F.; Genetos, D. C.; Donahue, H. J. MAP kinase and calcium signaling mediate fluid flow-induced human mesenchymal stem cell proliferation. *Am J Physiol Cell Physiol.* **2006**, *290*, C776-784.

137. Liu, D.; Genetos, D. C.; Shao, Y.; Geist, D. J.; Li, J.; Ke, H. Z.; Turner, C. H.; Duncan, R. L. Activation of extracellular-signal regulated kinase (ERK1/2) by fluid shear is Ca(2+)- and ATP-dependent in MC3T3-E1 osteoblasts. *Bone*. **2008**, *42*, 644-652.
138. Danciu, T. E.; Adam, R. M.; Naruse, K.; Freeman, M. R.; Hauschka, P. V. Calcium regulates the PI3K-Akt pathway in stretched osteoblasts. *FEBS Lett.* **2003**, *536*, 193-197.
139. Lee, M. N.; Hwang, H. S.; Oh, S. H.; Roshanzadeh, A.; Kim, J. W.; Song, J. H.; Kim, E. S.; Koh, J. T. Elevated extracellular calcium ions promote proliferation and migration of mesenchymal stem cells via increasing osteopontin expression. *Exp Mol Med*. **2018**, *50*, 1-16.
140. Gaharwar, A. K.; Mihaila, S. M.; Swami, A.; Patel, A.; Sant, S.; Reis, R. L.; Marques, A. P.; Gomes, M. E.; Khademhosseini, A. Bioactive silicate nanoplatelets for osteogenic differentiation of human mesenchymal stem cells. *Adv Mater*. **2013**, *25*, 3329-3336.
141. Westhauser, F.; Rehder, F.; Decker, S.; Kunisch, E.; Moghaddam, A.; Zheng, K.; Boccaccini, A. R. Ionic dissolution products of Cerium-doped bioactive glass nanoparticles promote cellular osteogenic differentiation and extracellular matrix formation of human bone marrow derived mesenchymal stromal cells. *Biomed Mater*. **2021**, *16*, 035028.
142. Hsu, S. H.; Chen, C. T.; Wei, Y. H. Inhibitory effects of hypoxia on metabolic switch and osteogenic differentiation of human mesenchymal stem cells. *Stem Cells*. **2013**, *31*, 2779-2788.
143. Yoo, H. I.; Moon, Y. H.; Kim, M. S. Effects of CoCl₂ on multi-lineage differentiation of C3H/10T1/2 mesenchymal stem cells. *Korean J Physiol Pharmacol*. **2016**, *20*, 53-62.
144. Burghardt, I.; Lüthen, F.; Prinz, C.; Kreikemeyer, B.; Zietz, C.; Neumann, H. G.; Rychly, J. A dual function of copper in designing regenerative implants. *Biomaterials*. **2015**, *44*, 36-44.
145. Lin, Z.; Cao, Y.; Zou, J.; Zhu, F.; Gao, Y.; Zheng, X.; Wang, H.; Zhang, T.; Wu, T. Improved osteogenesis and angiogenesis of a novel copper ions doped calcium phosphate cement. *Mater Sci Eng C Mater Biol Appl*. **2020**, *114*, 111032.
146. Zhang, J.; Wu, H.; He, F.; Wu, T.; Zhou, L.; Ye, J. Concentration-dependent osteogenic and angiogenic biological performances of calcium phosphate cement modified with copper ions. *Mater Sci Eng C Mater Biol Appl*. **2019**, *99*, 1199-1212.
147. Chen, M.; Wang, X. Q.; Zhang, E. L.; Wan, Y. Z.; Hu, J. Antibacterial ability and biocompatibility of fluorinated titanium by plasma-based surface modification. *Rare Met*. **2022**, *41*, 689-699.
148. Chen, L.; Song, W.; Markel, D. C.; Shi, T.; Muzik, O.; Matthew, H.; Ren, W. Flow perfusion culture of MC3T3-E1 osteogenic cells on gradient calcium polyphosphate scaffolds with different pore sizes. *J Biomater Appl*. **2016**, *30*, 908-918.
149. Qu, W. J.; Zhong, D. B.; Wu, P. F.; Wang, J. F.; Han, B. Sodium fluoride modulates caprine osteoblast proliferation and differentiation. *J Bone Miner Metab*. **2008**, *26*, 328-334.
150. Pan, X.; Huang, J.; Zhang, K.; Pei, Z.; Ding, Z.; Liang, Y.; Gu, Z.; Li, G.; Xie, H. Iron-doped brushite bone cement scaffold with enhanced osteoconductivity and antimicrobial properties for jaw regeneration. *Ceram Int*. **2021**, *47*, 25810-25820.
151. Strazic Geljic, I.; Melis, N.; Boukhechba, F.; Schaub, S.; Mellier, C.; Janvier, P.; Laugier, J. P.; Bouler, J. M.; Verron, E.; Scimeca, J. C. Gallium enhances reconstructive properties of a calcium phosphate bone biomaterial. *J Tissue Eng Regen Med*. **2018**, *12*, e854-e866.
152. Liao, F.; Peng, X. Y.; Yang, F.; Ke, Q. F.; Zhu, Z. H.; Guo, Y. P. Gadolinium-doped mesoporous calcium silicate/chitosan scaffolds enhanced bone regeneration ability. *Mater Sci Eng C Mater Biol Appl*. **2019**, *104*, 109999.
153. Zhao, P. P.; Hu, H. R.; Liu, J. Y.; Ke, Q. F.; Peng, X. Y.; Ding, H.; Guo, Y. P. Gadolinium phosphate/chitosan scaffolds promote new bone regeneration via Smad/Runx2 pathway. *Chem Eng J*. **2019**, *359*, 1120-1129.
154. Zhu, D. Y.; Lu, B.; Yin, J. H.; Ke, Q. F.; Xu, H.; Zhang, C. Q.; Guo, Y. P.; Gao, Y. S. Gadolinium-doped bioglass scaffolds promote osteogenic differentiation of hBMSC via the Akt/GSK3 β pathway and facilitate bone repair in vivo. *Int J Nanomedicine*. **2019**, *14*, 1085-1100.
155. Chu, M.; Sun, Z.; Fan, Z.; Yu, D.; Mao, Y.; Guo, Y. Bi-directional regulation functions of lanthanum-substituted layered double hydroxide nanohybrid scaffolds via activating osteogenesis and inhibiting osteoclastogenesis for osteoporotic bone regeneration. *Theranostics*. **2021**, *11*, 6717-6734.
156. Cheng, H.; Guo, Q.; Zhao, H.; Liu, K.; Kang, H.; Gao, F.; Guo, J.; Yuan, X.; Hu, S.; Li, F.; Yang, Q.; Fang, Z. An injectable hydrogel scaffold loaded with dual-drug/sustained-release PLGA microspheres for the regulation of macrophage polarization in the treatment of intervertebral disc degeneration. *Int J Mol Sci*. **2022**, *24*, 390.
157. Zhang, J.; Cai, L.; Tang, L.; Zhang, X.; Yang, L.; Zheng, K.; He, A.; Boccaccini, A. R.; Wei, J.; Zhao, J. Highly dispersed lithium doped mesoporous silica nanospheres regulating adhesion, proliferation, morphology, ALP activity and osteogenesis related gene expressions of BMSCs. *Colloids Surf B Biointerfaces*. **2018**, *170*, 563-571.
158. Mo, F.; Jiang, K.; Zhao, D.; Wang, Y.; Song, J.; Tan, W. DNA hydrogel-based gene editing and drug delivery systems. *Adv Drug Deliv Rev*. **2021**, *168*, 79-98.
159. Tan, Z.; Zhou, B.; Zheng, J.; Huang, Y.; Zeng, H.; Xue, L.; Wang, D. Lithium and copper induce the osteogenesis-angiogenesis coupling of bone marrow mesenchymal stem cells via crosstalk between canonical Wnt and HIF-1 α signaling pathways. *Stem Cells Int*. **2021**, *2021*, 6662164.
160. Huang, T. B.; Li, Y. Z.; Yu, K.; Yu, Z.; Wang, Y.; Jiang, Z. W.; Wang, H. M.; Yang, G. L. Effect of the Wnt signal-RANKL/OPG axis on the enhanced osteogenic integration of a lithium incorporated surface. *Biomater Sci*. **2019**, *7*, 1101-1116.
161. Wang, J.; Ma, X. Y.; Feng, Y. F.; Ma, Z. S.; Ma, T. C.; Zhang, Y.; Li, X.; Wang, L.; Lei, W. Magnesium ions promote the biological behaviour of rat calvarial osteoblasts by activating the PI3K/Akt signalling pathway. *Biol Trace Elem Res*. **2017**, *179*, 284-293.
162. Pantulap, U.; Arango-Ospina, M.; Boccaccini, A. R. Bioactive glasses incorporating less-common ions to improve biological and physical properties. *J Mater Sci Mater Med*. **2021**, *33*, 3.
163. Barrioni, B. R.; Norris, E.; Li, S.; Naruphontjirakul, P.; Jones, J. R.; Pereira, M. M. Osteogenic potential of sol-gel bioactive glasses containing manganese. *J Mater Sci Mater Med*. **2019**, *30*, 86.
164. Wu, T.; Shi, H.; Liang, Y.; Lu, T.; Lin, Z.; Ye, J. Improving osteogenesis of calcium phosphate bone cement by incorporating with manganese doped β -tricalcium phosphate. *Mater Sci Eng C Mater Biol Appl*. **2020**, *109*, 110481.
165. Su, Y.; Chen, L. J.; He, J. R.; Yuan, X. J.; Cen, Y. L.; Su, F. X.; Tang, L. Y.; Zhang, A. H.; Chen, W. Q.; Lin, Y.; Wang, S. M.; Ren, Z. F. Rubidium in breast cancers. *Clin Chim Acta*. **2011**, *412*, 2305-2309.
166. Ouyang, S.; Zheng, K.; Huang, Q.; Liu, Y.; Boccaccini, A. R. Synthesis and characterization of rubidium-containing bioactive glass nanoparticles. *Mater Lett*. **2020**, *273*, 127920.
167. Chen, M.; Wu, S.; Tan, Y.; Li, R.; Liu, Y.; Huang, Q. Rubidium-doped titanium surfaces with modulatory effects on MC3T3-E1 cell response

- and antibacterial capacity against *Staphylococcus aureus*. *Biomed Mater.* **2019**, *14*, 045016.
168. Tan, Y. N.; Chen, W. J.; Wei, W.; Huang, Q. L.; He, X. Rubidium-modified bioactive glass-ceramics with hydroxyapatite crystals for bone regeneration. *Trans Nonferrous Met Soc China.* **2021**, *31*, 521-532.
 169. Ren, N.; Yu, X.; Wang, A.; Liang, N.; Feng, Z.; Sun, C. Effects of scandium chloride on osteogenic and adipogenic differentiation of mesenchymal stem cells. *J Rare Earths.* **2022**, *40*, 161-168.
 170. Millucci, L.; Minetti, M.; Orlandini, M.; Braconi, D.; Schiavone, M. L.; Galderisi, S.; Marzocchi, B.; Spiga, O.; Rappuoli, R.; Spreafico, A.; Perretti, G.; Bernardini, G.; Santucci, A. Beer promotes differentiation and mineralization of human osteoblastic cells: Role of silicon. *J Funct Foods.* **2019**, *54*, 109-118.
 171. Reffitt, D. M.; Ogston, N.; Jugdaohsingh, R.; Cheung, H. F.; Evans, B. A.; Thompson, R. P.; Powell, J. J.; Hampson, G. N. Orthosilicic acid stimulates collagen type 1 synthesis and osteoblastic differentiation in human osteoblast-like cells in vitro. *Bone.* **2003**, *32*, 127-135.
 172. Dong, M.; Jiao, G.; Liu, H.; Wu, W.; Li, S.; Wang, Q.; Xu, D.; Li, X.; Liu, H.; Chen, Y. Biological silicon stimulates collagen type 1 and osteocalcin synthesis in human osteoblast-like cells through the BMP-2/Smad/RUNX2 signaling pathway. *Biol Trace Elem Res.* **2016**, *173*, 306-315.
 173. Zhou, H.; Jiao, G.; Dong, M.; Chi, H.; Wang, H.; Wu, W.; Liu, H.; Ren, S.; Kong, M.; Li, C.; Zhang, L.; Chen, Y. Orthosilicic acid accelerates bone formation in human osteoblast-like cells through the PI3K-Akt-mTOR pathway. *Biol Trace Elem Res.* **2019**, *190*, 327-335.
 174. Zhou, X.; Moussa, F. M.; Mankoci, S.; Ustiyana, P.; Zhang, N.; Abdelmagid, S.; Molenda, J.; Murphy, W. L.; Safadi, F. F.; Sahai, N. Orthosilicic acid, Si(OH)₄, stimulates osteoblast differentiation in vitro by upregulating miR-146a to antagonize NF- κ B activation. *Acta Biomater.* **2016**, *39*, 192-202.
 175. Ma, W.; Wang, F.; You, Y.; Wu, W.; Chi, H.; Jiao, G.; Zhang, L.; Zhou, H.; Wang, H.; Chen, Y. Ortho-silicic acid inhibits RANKL-induced osteoclastogenesis and reverses ovariectomy-induced bone loss in vivo. *Biol Trace Elem Res.* **2021**, *199*, 1864-1876.
 176. You, Y.; Ma, W.; Wang, F.; Jiao, G.; Zhang, L.; Zhou, H.; Wu, W.; Wang, H.; Chen, Y. Ortho-silicic acid enhances osteogenesis of osteoblasts through the upregulation of miR-130b which directly targets PTEN. *Life Sci.* **2021**, *264*, 118680.
 177. Liangjiao, C.; Ping, Z.; Ruoyu, L.; Yanli, Z.; Ting, S.; Yanjun, L.; Longquan, S. Potential proinflammatory and osteogenic effects of dicalcium silicate particles in vitro. *J Mech Behav Biomed Mater.* **2015**, *44*, 10-22.
 178. Geng, Z.; Sang, S.; Wang, S.; Meng, F.; Li, Z.; Zhu, S.; Cui, Z.; Jing, Y.; Wang, C.; Su, J. Optimizing the strontium content to achieve an ideal osseointegration through balancing apatite-forming ability and osteogenic activity. *Biomater Adv.* **2022**, *133*, 112647.
 179. Li, Y.; Yue, J.; Liu, Y.; Wu, J.; Guan, M.; Chen, D.; Pan, H.; Zhao, X.; Lu, W. W. Strontium regulates stem cell fate during osteogenic differentiation through asymmetric cell division. *Acta Biomater.* **2021**, *119*, 432-443.
 180. Stefanic, M.; Peroglio, M.; Stancic, A. M.; Machado, G. C.; Campbell, I.; Krz̄manc, M. M.; Alini, M.; Zhang, X. The influence of strontium release rate from bioactive phosphate glasses on osteogenic differentiation of human mesenchymal stem cells. *J Eur Ceram Soc.* **2018**, *38*, 887-897.
 181. Montagna, G.; Cristofaro, F.; Fassina, L.; Bruni, G.; Cucca, L.; Kochen, A.; Divieti Pajevic, P.; Bragdon, B.; Visai, L.; Gerstenfeld, L. An in vivo comparison study between strontium nanoparticles and rhBMP2. *Front Bioeng Biotechnol.* **2020**, *8*, 499.
 182. Huang, D.; Zhao, F.; Gao, W.; Chen, X.; Guo, Z.; Zhang, W. Strontium-substituted sub-micron bioactive glasses inhibit osteoclastogenesis through suppression of RANKL-induced signaling pathway. *Regen Biomater.* **2020**, *7*, 303-311.
 183. Barrio, D. A.; Etcheverry, S. B. Vanadium and bone development: putative signaling pathways. *Can J Physiol Pharmacol.* **2006**, *84*, 677-686.
 184. Cortizo, A. M.; Molinuevo, M. S.; Barrio, D. A.; Bruzzone, L. Osteogenic activity of vanadyl(IV)-ascorbate complex: evaluation of its mechanism of action. *Int J Biochem Cell Biol.* **2006**, *38*, 1171-1180.
 185. Jin, G.; Cao, H.; Qiao, Y.; Meng, F.; Zhu, H.; Liu, X. Osteogenic activity and antibacterial effect of zinc ion implanted titanium. *Colloids Surf B Biointerfaces.* **2014**, *117*, 158-165.
 186. Kwun, I. S.; Cho, Y. E.; Lomeda, R. A.; Shin, H. I.; Choi, J. Y.; Kang, Y. H.; Beattie, J. H. Zinc deficiency suppresses matrix mineralization and retards osteogenesis transiently with catch-up possibly through Runx 2 modulation. *Bone.* **2010**, *46*, 732-741.
 187. Moonga, B. S.; Dempster, D. W. Zinc is a potent inhibitor of osteoclastic bone resorption in vitro. *J Bone Miner Res.* **1995**, *10*, 453-457.
 188. Guo, B.; Yang, M.; Liang, D.; Yang, L.; Cao, J.; Zhang, L. Cell apoptosis induced by zinc deficiency in osteoblastic MC3T3-E1 cells via a mitochondrial-mediated pathway. *Mol Cell Biochem.* **2012**, *361*, 209-216.
 189. Hadley, K. B.; Newman, S. M.; Hunt, J. R. Dietary zinc reduces osteoclast resorption activities and increases markers of osteoblast differentiation, matrix maturation, and mineralization in the long bones of growing rats. *J Nutr Biochem.* **2010**, *21*, 297-303.
 190. O'Connor, J. P.; Kanjilal, D.; Teitelbaum, M.; Lin, S. S.; Cottrell, J. A. Zinc as a therapeutic agent in bone regeneration. *Materials (Basel).* **2020**, *13*, 2211.
 191. Hu, G.; Zhu, Y.; Xu, F.; Ye, J.; Guan, J.; Jiang, Y.; Di, M.; Li, Z.; Guan, H.; Yao, X. Comparison of surface properties, cell behaviors, bone regeneration and osseointegration between nano tantalum/PEEK composite and nano silicon nitride/PEEK composite. *J Biomater Sci Polym Ed.* **2022**, *33*, 35-56.
 192. Hwang, C.; Park, S.; Kang, I. G.; Kim, H. E.; Han, C. M. Tantalum-coated polylactic acid fibrous membranes for guided bone regeneration. *Mater Sci Eng C Mater Biol Appl.* **2020**, *115*, 111112.
 193. Zhou, Z.; Liu, D. Mesenchymal stem cell-seeded porous tantalum-based biomaterial: a promising choice for promoting bone regeneration. *Colloids Surf B Biointerfaces.* **2022**, *215*, 112491.
 194. Mas-Moruno, C.; Garrido, B.; Rodriguez, D.; Ruperez, E.; Gil, F. J. Biofunctionalization strategies on tantalum-based materials for osseointegrative applications. *J Mater Sci Mater Med.* **2015**, *26*, 109.
 195. Shi, L. Y.; Wang, A.; Zang, F. Z.; Wang, J. X.; Pan, X. W.; Chen, H. J. Tantalum-coated pedicle screws enhance implant integration. *Colloids Surf B Biointerfaces.* **2017**, *160*, 22-32.
 196. Qing, Y.; Li, R.; Li, S.; Li, Y.; Wang, X.; Qin, Y. Advanced black phosphorus nanomaterials for bone regeneration. *Int J Nanomedicine.* **2020**, *15*, 2045-2058.
 197. Kim, H. D.; Jang, H. L.; Ahn, H. Y.; Lee, H. K.; Park, J.; Lee, E. S.; Lee, E. A.; Jeong, Y. H.; Kim, D. G.; Nam, K. T.; Hwang, N. S. Biomimetic whitlockite inorganic nanoparticles-mediated in situ remodeling and rapid bone regeneration. *Biomaterials.* **2017**, *112*, 31-43.
 198. Eckart, R. E.; Shry, E. A.; Burke, A. P.; McNear, J. A.; Appel, D. A.; Castillo-Rojas, L. M.; Avedissian, L.; Pearse, L. A.; Potter, R. N.; Tremaine, L.; Gentlesk, P. J.; Huffer, L.; Reich, S. S.; Stevenson, W. G.; Department of Defense Cardiovascular Death Registry Group.

Biomaterials contain bioactive elements for bone repair

- Sudden death in young adults: an autopsy-based series of a population undergoing active surveillance. *J Am Coll Cardiol.* **2011**, *58*, 1254-1261.
199. Goretti Penido, M.; Alon, U. S. Phosphate homeostasis and its role in bone health. *Pediatr Nephrol.* **2012**, *27*, 2039-2048.
200. Liu, X.; Miller, A. L., 2nd; Park, S.; George, M. N.; Waletzki, B. E.; Xu, H.; Terzic, A.; Lu, L. Two-dimensional black phosphorus and graphene oxide nanosheets synergistically enhance cell proliferation and osteogenesis on 3D printed scaffolds. *ACS Appl Mater Interfaces.* **2019**, *11*, 23558-23572.
201. Avgoulas, E. I.; Sutcliffe, M. P. F.; Linderman, S. W.; Birman, V.; Thomopoulos, S.; Genin, G. M. Adhesive-based tendon-to-bone repair: failure modelling and materials selection. *J R Soc Interface.* **2019**, *16*, 20180838.

Received: November 1, 2023

Revised: November 21, 2023

Accepted: December 8, 2023

Available online: December 28, 2023

Harvest of functional mesenchymal stem cells derived from *in vivo* osteo-organoids

Shunshu Deng^{1,2,3}, Fuwei Zhu^{1,2,3}, Kai Dai^{1,2,3,4,*}, Jing Wang^{1,3,4,*}, Changsheng Liu^{2,3,4,5,*}

Key Words:

anti-replicative senescence; *in vivo* osteo-organoid; mesenchymal stem cell; recombinant human bone morphogenetic protein 2; stem cell therapy

From the Contents

Introduction	270
Methods	271
Results	273
Discussion	276

ABSTRACT

Bone marrow-derived mesenchymal stem cells (BM-MSCs) play a crucial role in stem cell therapy and are extensively used in regenerative medicine research. However, current methods for harvesting BM-MSCs present challenges, including a low yield of primary cells, long time of *in vitro* expansion, and diminished differentiation capability after passaging. Meanwhile mesenchymal stem cells (MSCs) recovered from cell banks also face issues like toxic effects of cryopreservation media. In this study, we provide a detailed protocol for the isolation and evaluation of MSCs derived from *in vivo* osteo-organoids, presenting an alternative to autologous MSCs. We used recombinant human bone morphogenetic protein 2-loaded gelatin sponge scaffolds to construct *in vivo* osteo-organoids, which were stable sources of MSCs with large quantity, high purity, and strong stemness. Compared with protocols using bone marrow, our protocol can obtain large numbers of high-purity MSCs in a shorter time (6 days vs. 12 days for obtaining passage 1 MSCs) while maintaining higher stemness. Notably, we found that the *in vivo* osteo-organoid-derived MSCs exhibited stronger anti-replicative senescence capacity during passage and amplification, compared to BM-MSCs. The use of osteo-organoid-derived MSCs addresses the conflict between the limitations of autologous cells and the risks associated with allogeneic sources in stem cell transplantation. Consequently, our protocol emerges as a superior alternative for both stem cell research and tissue engineering.

<http://doi.org/10.12336/biomatertransl.2023.04.006>

How to cite this article:
Deng, S.; Zhu, F.; Dai, K.; Wang, J.; Liu, C.
Harvest of functional mesenchymal stem cells derived from *in vivo* osteo-organoids. *Biomater Transl.* 2023, 4(4), 270-279.



Introduction

Mesenchymal stem cells (MSCs) are kinds of stem cells that widely exist in various tissues and organs of the adult body.¹⁻³ They have the potential for multi-lineage differentiation, such as osteogenic, adipogenic, myogenetic, chondrogenic, and neurogenic differentiation.^{2,4,5} This makes MSCs a popular choice for research on cancer, ageing-related topics,^{6,7} and stem cell engineering.^{8,9} Because the MSCs still display strong proliferation and differentiation performance *in vitro*,^{1,10} coupled with cytokine secretion and immune function,¹¹⁻¹⁴ they are often used in tissue engineering. This includes, but not limited to, research on coronavirus disease 2019 (COVID-19),¹⁵ spinal cord injury,¹⁶ femoral

head necrosis,¹⁷ systemic lupus erythematosus,¹⁸ and colitis.¹⁹ Research models related to MSCs primarily use bone marrow,²⁰ compact bone,^{1,21} peripheral blood,²² adipose tissue,²³ urine^{24,25} and joint synovium.³ MSCs from various sources exhibit different characteristics because they tend to be different subtypes of stem cells. For adult humans, compared with other methods, isolation from bone marrow is a more established method for autologous stem cell extraction.^{26,27} Bone marrow-derived MSCs (BM-MSCs) possess superior three-lineage differentiation capability compared with other adult tissue-derived MSCs. However, their lower yield, lower purity, and longer expansion cycle than allogeneic MSCs limit the clinical applications.

Rapid obtaining strategy of massive MSCs

Recently, the concept of *in vivo* tissue engineering^{5, 14, 23} co-constructed by cells and materials^{28, 29} has emerged as a feasible solution for obtaining autologous stem cells. In previous work, we found that the gelatin sponge loaded with recombinant human bone morphogenetic protein 2 (rhBMP-2) formed periosteum-like tissues³⁰ rich in functional stem cells after being implanted in mice for several days. The periosteum-like tissue gradually developed into mature osteo-organoids with a bone marrow-like structure.³¹ In previous experiments, we isolated stem cells from these osteo-organoids,³² thus defining these cells as osteo-organoid-derived MSCs (odMSCs). Interestingly, based on the implantation site³³ and the cell phenotype,³⁴ it was speculated that these cells are related to myoideum, making osteo-organoids a stable source of this new subtype of BM-MSCs.

In this study, to better emphasise the advantages of odMSCs, we constructed osteo-organoids in the mouse hindlimb muscles, using the femur and tibia as controls. After isolation and culture, the MSCs were further evaluated, including the colony forming unit-fibroblast (CFU-F) experiment conducted before the primary cells were washed. The purified MSCs at passage 2 (P2) were used for flow cytometry, tri-lineage differentiation and proliferation assays. The odMSCs could be obtained in sufficient quantities in half the time compared with BM-MSCs. Besides, odMSCs showed better stemness and activity, even after multiple passages. Given the aforementioned advantages, we can conclude that this protocol for obtaining MSCs holds significant research value and broad application prospects.

Methods

Animals

We selected the C57BL/6J mouse strain (8 weeks, male, with an average weight of approximately 25 g) for our protocol. All mice were purchased from and housed in Shanghai Shengchang Biotechnology Co., Ltd. (Shanghai, China; license No. SCXK (Hu) 2021-0002) and housed at 22–23°C on a 12-hour light/dark cycle with free access to water and food, as indicated. All experimental procedures were approved by the Animal Care and Use Committee of the East China University of Science and Technology (approval No. ECUST-2022-053) on March 9, 2022. All efforts were made to minimise animal suffering.

Preparation and implantation of rhBMP-2 loaded gelatin scaffolds

For implant preparation, 10 µL of rhBMP-2 (1 mg/mL in phosphate-buffered saline; Rebone Biomaterials Co., Shanghai, China) was absorbed by a gelatin scaffold (5 mm × 5 mm × 5 mm; Xiang'en Medical Technology Development Co., Nanchang, Jiangxi, China). The procedure was conducted under sterile conditions, then the scaffold was frozen at –20°C

for 4 hours and lyophilised for 8 hours. The rhBMP-2-loaded gelatin scaffolds were stored at –20°C.

To mitigate the potential interference of location differences *in vivo*, the source of MSCs was selected in hindlimbs. For osteo-organoid generation, mice were anaesthetised (ZS-MV-IV; Hetian Scientific Instruments Co., Shanghai, China; isoflurane, 0.5% of the maximal flow, inhalation). Subsequently, two scaffolds were implanted in the muscle of both hindlimbs, respectively. Once revived on a warming station, the mice were allowed to eat and drink *ad libitum* as usual.

Isolation of MSCs from osteo-organoids

A buffer for cell suspension was prepared using 2% fetal bovine serum (Gibco, Grand Island, NY, USA) in Hank's balanced salt solution (with Ca²⁺/Mg²⁺; Gibco). After 5 days of feeding, the mice were anaesthetised with isoflurane inhalation, and then terminated by cervical dislocation. They were placed in a beaker where the whole body was immersed in 75% (v/v) ethanol for 3 minutes, and then the body was transferred to biosafety cabinet. To prevent contamination of the countertop, sterile gauze was placed in advance (**Figure 1A**). Skin and muscle between hindlimbs and trunk were removed by ophthalmic scissors with little or no bleeding. Subsequently, the feet and the entire skin on the hindlimbs were removed. After that, the trochanter major was cut off (**Figure 1B**) allowing for the entire leg. Typically, the osteo-organoids could be found in the hamstrings (**Figure 1C**). Once isolated from the muscle, the osteo-organoids were immersed in a 60-mm cell culture dish (Corning Incorporated, Corning, NY, USA) containing 3 mL of the cell suspension buffer (**Figure 1D**). Osteo-organoids were first cut and then shredded in different shear directions by curved blade ophthalmic scissors (**Figure 1E and F**). Finally, all osteo-organoid fragments, including the buffer, were transferred to a sterile 15-mL Falcon tube. In addition, native bone marrows from femora and tibia were flushed out by syringe as a traditional method.²⁰

The tubes containing bone marrow or osteo-organoid fragments were centrifuged at 300 × g for 10 minutes to remove the supernatant. Meanwhile the digestive enzyme mixture was prepared. Each 1 mL of this mixture contained: stock of collagenase type I (Worthington, Lakewood, NJ, USA) 100 µL, neutral protease (Roche, Basel, Switzerland) 100 µL and DNase (Mkbio, Shanghai, China) 20 µL in 800 µL Hanks' balanced salt solution (containing Ca²⁺/Mg²⁺).³⁵ This mixture was then added to the tubes containing the tissue pellets from bone marrow or osteo-organoid fragments. Then the tissue pellets were kept static for digestion at 37°C for 15 minutes. The tissue pellets were then left undisturbed for digestion at 37°C for 15 minutes. The tissue pellets were

1 State Key Laboratory of Bioreactor Engineering, East China University of Science and Technology, Shanghai, China; 2 Key Laboratory for Ultrafine Materials of the Ministry of Education, East China University of Science and Technology, Shanghai, China; 3 Engineering Research Center for Biomedical Materials of the Ministry of Education, East China University of Science and Technology, Shanghai, China; 4 Frontiers Science Center for Materiobiology and Dynamic Chemistry, East China University of Science and Technology, Shanghai, China; 5 Shanghai University, Shanghai, China

*Corresponding authors:

Kai Dai, daikai233@foxmail.com; Jing Wang, biomatwj@163.com; Changsheng Liu, liucs@ecust.edu.cn.

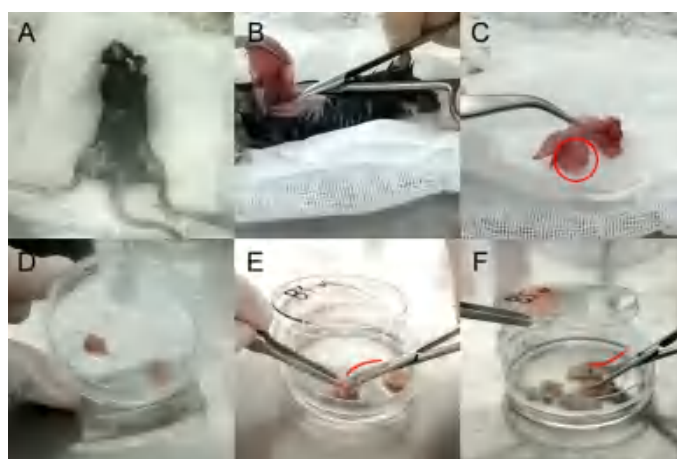


Figure 1. Illustrations of osteo-organoid cell separation procedures. (A) The mouse body soaked in 75% (v/v) ethanol was placed in biosafety cabinet. (B) After removing skin and muscle, a hindlimb was completely cut off, so that the femur and tibia could be used for extraction of bone marrow-derived mesenchymal stem cells (BM-MSCs). (C) The osteo-organoid was hidden in the swollen part of the muscle (red circle) between femur and calf. (D) Osteo-organoids covered with periosteum-like tissue were separated in a 60-mm cell culture dish. (E) The surface of the blade was convex (red curve) to cut the osteo-organoids. (F) The surface of the blade was concave (red curve) to shred the osteo-organoids.

resuspended using a vortex mixer and subsequently deposited on ice for 1 minute. The cell suspension extracted by digestion was then added to 10 mL of digestive enzyme neutraliser (0.4% ethylenediaminetetraacetic acid (0.5 M; Gibco) and 2% fetal bovine serum in Hanks' balanced salt solution (containing $\text{Ca}^{2+}/\text{Mg}^{2+}$)), followed by centrifugation at $300 \times g$ for 10 minutes to remove the supernatant. To yield more cells, the digested tissue pellets could undergo another round of digestion and the subsequent operations were repeated.

Culture and purification of MSCs from osteo-organoids

The collected cells were resuspended in 1 mL of the cell

suspension buffer using trimmed pipette tips to minimise cell damage. The cell suspension was then filtered through a 70- μm filter mesh to remove any fragments or cell clumps. When the complete medium (minimal essential medium α (nucleosides; Gibco) supplemented with 20% fetal bovine serum, 1% penicillin-streptomycin (10,000 U/mL; Gibco), 1% sodium pyruvate (100 mM; Gibco) and 0.1% Rho-associated kinase inhibitor (Y-27632 dihydrochloride; 1 mL in dimethyl sulfoxide (10 mM); MedChemExpress, Monmouth Junction, NJ, USA)) had been warmed up in cell incubator, the cell suspension was seeded in 6-well plates or 100-mm cell culture dish (**Table 1**) containing the medium.

Table 1. Details of cell culture in different experiments

Experiment	Culture vessel	Volume of medium	Seeding density	Other suggestions
Colony forming unit-fibroblast	6-well plate	2 mL per well	5×10^5 cells per well	Replace α -MEM with DMEM to prepare the complete medium
Purification	100-mm dish	15 mL per dish	1×10^7 cells per dish	Culture under the condition of 5% O_2 atmosphere
Differentiation	6-well plate	2 mL per well	2×10^5 cells per well	Use α -MEM containing 10% fetal bovine serum and 1% penicillin-streptomycin as the medium before differentiation assays
Proliferation	60-mm dish	5 mL per dish	2×10^5 cells per well	Incubate the MSC for 2 hours in a medium containing 50 μM EdU

Note: DMEM: Dulbecco's modified Eagle medium; EdU: 5-ethynyl-2'-deoxyuridine; MSC: mesenchymal stem cell; α -MEM: minimal essential medium α .

Once evenly dispersed, the cells were cultured in a cell incubator at 37°C under normal oxygen conditions. The culture medium was refreshed the following morning and every 3 days thereafter. Adherent cells were washed with Dulbecco's phosphate-buffered saline before adding fresh medium, thus purifying the MSCs. The primary cells were referred to passage 0 (P0) cells.

When MSCs reached 70–90% confluence, they could be passaged. That is, cells were washed twice with Dulbecco's

phosphate-buffered saline and then digested using 600 μL (per 100-mm dish) of 0.25% trypsin (with phenol red; Gibco) at 37°C , for no longer than 2 minutes. This medium was used to wash the cells until the MSCs were completely detached from the bottom of the dish. The medium was used to wash cells until the MSCs were completely detached from the bottom of the dish. For passaging at a split ratio of 1:3, 2 mL of the cell suspension per dish was transferred to a new dish with the complete medium. The above procedures were based on the characteristics of MSCs (**Table 2**).

Table 2. Purification operations are based on the characteristics of MSCs

Characteristics	Operations
Adhesion of MSCs are earlier than other cells from marrow	Wash cells using Dulbecco's phosphate-buffered saline after seeding overnight
MSCs are easy to be digested and suspended	Time of digestion during the cell passage is not recommended to exceed 2 minutes
Low oxygen pressure increases the proliferation and reduces spontaneous differentiation of MSCs	Expand cells under the hypoxic condition (5% O ₂)

Note: MSCs: mesenchymal stem cells.

***In vitro* multilineage differentiation and cell proliferation assays**

MSCs were cultured in 6-well plates (or in a 15-mL Falcon tube for chondrogenic differentiation) in preparation for differentiation and proliferation experiments (Table 1). The operations of osteogenic, adipogenic, and chondrogenic differentiation were respectively performed according to the manual of OriCell™ Mesenchymal Stem Cell Osteogenic/Adipogenic/Chondrogenic Differentiation Medium (Cyagen Biosciences, Santa Clara, CA, USA). Cell proliferation was measured by 5-ethynyl-2'-deoxyuridine (EdU) assay, and the operations were performed according to the manual of BeyoClick™ EdU Cell Proliferation Kit (Beyotime, Shanghai, China).

CFU-F assay and flow cytometry

For CFU-F assay, MSCs extracted from osteo-organoids were directly cultured in 6-well plates for 5 days (Table 1). After washed using Dulbecco's phosphate-buffered saline, the MSCs were fixed using 4% (w/v) paraformaldehyde for 30 minutes and then stained using toluidine blue (0.1%; Yuanye Biotechnology Co., Shanghai, China). After being washed using ddH₂O, the colony formation could be observed under an optical microscope (DMI8; Leica, Hessia, Wetzlar, Germany).

For flow cytometry, purified MSCs were cultured until they reached 80–90% confluence. After washed using Dulbecco's phosphate-buffered saline and digested, MSCs they were stained using fluorescent antibodies in flow tubes and then analysed by flow cytometry. The cell aliquots were incubated: fluorescein isothiocyanate-conjugated CD45 or phycoerythrin-conjugated CD44, CD29 and CD31 or Alexa Fluor 700-conjugated stem cell antigen-1 and CD11b or Allophycocyanin-conjugated CD105 and CD140a (BD Biosciences, San Jose, CA, USA). The incubation was carried out at 4°C for 30 minutes in the dark. The cells were resuspended in 300 µL cell staining buffer (BD Biosciences) after washing. The flow cytometric analysis, including the test of EdU assay cell proliferation, was operated on CytoFLEX LX flow cytometer (Beckman Coulter, Brea, CA, USA). The data were analysed using FlowJo X (Three Star, San Carlos, CA, USA).

β-Galactosidase assay

MSCs were cultured in 6-well plates before cells reached 100% confluence, with other culture conditions referring to the operations for purification (Table 1). The procedure was

carried out in accordance with the manual of the senescence β-galactosidase staining kit (Beyotime). This kit allows for the assessment of the degree of cell ageing, as it measures the up-regulated activity level of senescence-associated β-galactosidase, a known marker of cellular senescence.³⁵

Statistical analysis

At least three sets of independent experiments were performed for each assay. All quantitative data were analysed by using GraphPad Prism (version 8.0.2 for Windows, GraphPad Software, Boston, MA, USA, www.graphpad.com). Significance of difference between groups was calculated by Student's *t*-test or two-way analysis of variance followed by Bonferroni's multiple comparison test.

Results

Morphology of osteo-organoid-derived mesenchymal stem cells

Cells isolated from osteo-organoids were cultured under hypoxic conditions (5% O₂ and 5% CO₂), and were purified either by medium refreshment or cell passage (Figure 2A). Specifically, spindle-shaped cells were observed among non-adherent cells before the first medium refresh. Adherent spindle-shaped cells were retained, while most non-adherent cells were washed away. These adherent, spindle-shaped cells were identified as MSCs.^{4, 20} When cell confluence reached 70–90%, the cells were observed to be predominantly spindle-shaped, because MSCs proliferate more rapidly than other cells.

Proliferation of osteo-organoid-derived mesenchymal stem cells

The CFU-F assay was utilised to investigate the proportion of MSCs in cells isolated from osteo-organoids, and compared with that from native bone marrow.²⁰ After a 5-day culture period under normal conditions (21% O₂ and 5% CO₂), cells stained with toluidine blue were observed under an optical microscope. The control groups, i.e., cells isolated from native bone (Figure 2B), showed a few colonies with a spindle shape, small size and low cell density. In contrast, cells isolated from osteo-organoids formed a significantly larger number of colonies (Figure 2B), which exhibited a slender spindle shape, large scale and high cell density. This phenomenon also suggested that odMSCs had rapid proliferation rates or high abundance at P0.

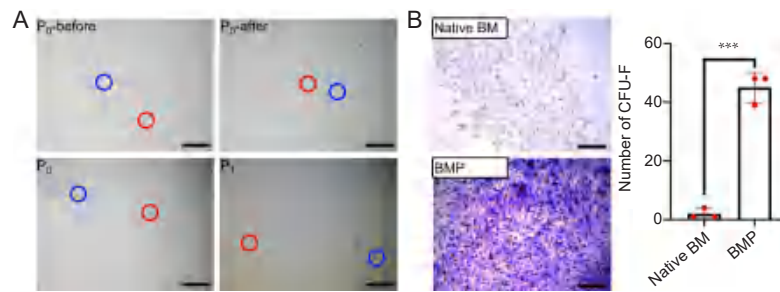


Figure 2. Morphology of MSCs and CFU-F assay. (A) Primary cells before (P0-before) and after (P0-after) the first refreshing of the medium, and MSCs at 80% confluence at P0 and P1. Red and blue circles indicate spindle-shaped and round cells. (B) Left: Primary cells from osteo-organoids (constructed with recombinant human bone morphogenetic protein 2-loaded gelatin sponge scaffolds) formed larger colonies than that from bone marrow (native BM). Scale bars: 200 μm . Right: The number of colonies in each well of a standard 6-well plate. Data are expressed as mean \pm SD ($n = 3$). *** $P < 0.001$ (Student's t -test). CFU-F: colony forming unit-fibroblast; MSCs: mesenchymal stem cells; P: passage.

Cell surface phenotype and multilineage differentiation of osteo-organoid-derived mesenchymal stem cells

When 80% confluence at P2, the MSCs cultured in plates were digested and then analysed by flow cytometry. Results showed that the cells from both BM-MSC and odMSC were largely negative for haematopoietic marker CD45, endothelial cell marker CD31, and myeloid cell marker CD11b (Figure 3A). In contrast, the MSC markers (stem cell antigen-1, CD29, CD105, CD44 and CD140a) were strongly positive, and especially the positive rates of stem cell antigen-1 and CD140a of odMSCs were more obvious than those from native BM (Figure 3A). The above result displayed that the cells isolated from osteo-organoids were determinately identified as MSCs, suggesting the successful acquisition of a new stem cell subtype.

To assess the multipotency of the MSCs at P2 (Figure 3B), cells that had reached the appropriate confluence were cultured in various types of differentiation induction media. Alizarin red staining (Figure 3B) and oil red O staining (Figure 3B) demonstrated the primary cells from osteo-organoids (constructed with recombinant human bone morphogenetic protein 2-loaded gelatin sponge scaffolds) showed distinctly more calcified nodules and mature adipocytes than cells from bone marrow did, suggesting that odMSCs had greater osteogenic and adipogenic differentiation capabilities than BM-MSCs did. Concurrently, alcian blue staining of the cartilage revealed that MSCs from both sources had similar chondrogenic differentiation capabilities.

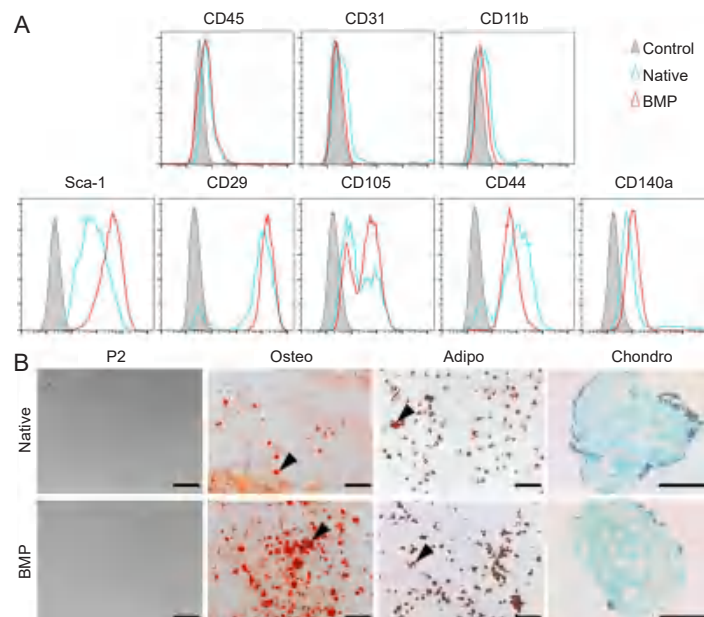


Figure 3. Cell surface phenotype and multilineage differentiation of MSCs at P2. (A) Flow cytometry of odMSCs (constructed with recombinant human bone morphogenetic protein 2-loaded gelatin sponge scaffolds; BMP) and bone marrow (native). (B) Alizarin red, oil red O or Alcian blue staining after differentiation under the osteogenic, adipogenic or chondrogenic induction. The osteogenic and adipogenic differentiation of odMSCs were more obvious than that of BM-MSCs. Black triangles indicate calcified nodules and mature adipocytes. Scale bars: 200 μm . BM-MSCs: bone marrow-derived mesenchymal stem cells; MSCs: mesenchymal stem cells; odMSCs: osteo-organoid-derived mesenchymal stem cells; P2: passage 2; Sca-1: stem cell antigen-1.

Ageing process of osteo-organoid-derived mesenchymal stem cells

In order to assess the ageing process of odMSCs during *in vitro* passage, a senescence-associated β -galactosidase assay was used to evaluate the senescence level of cells from P0 to P2 (Figure 4). From the staining images, it was obvious that native BM-MSCs (native group) had few senescence-associated β -galactosidase positive cells at P0. However, as the passage times increased, the cells gradually aged, and thus showed

noticeable senescence-associated β -galactosidase expression. In contrast, for the odMSCs, light-colored products of β -galactosidase were observed at the P0. Despite this, the ratio of cells expressing β -galactosidase and the depth of blue in odMSCs did not change significantly throughout the passages. From these observations, it can be concluded that unlike BM-MSCs, odMSCs did not exhibit significant ageing during the passage from P0 to P2.

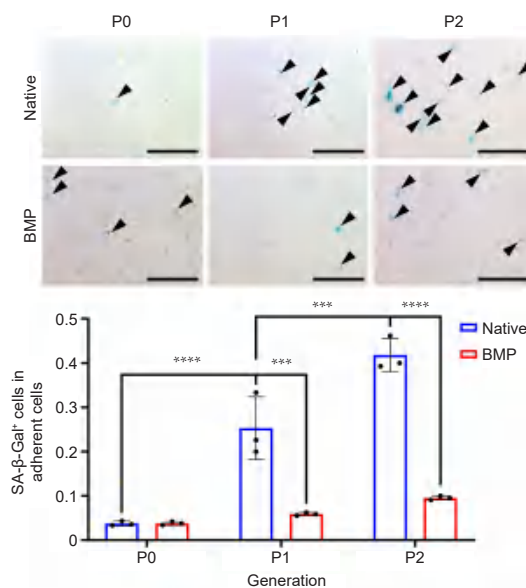


Figure 4. Upper: Ageing process for MSCs from P0 to P2. Black triangles indicate SA- β -Gal positive cells. Scale bars: 200 μ m. Lower: The proportions of SA- β -Gal positive cells. The proportion of cell senescence in the native BM-MSCs group (native) increased with passage, while it remained basically unchanged in the odMSCs (constructed with recombinant human bone morphogenetic protein 2-loaded gelatin sponge scaffolds; BMP). Data are expressed as mean \pm SD ($n = 3$). **** $P < 0.0001$, *** $P < 0.001$ (two-way analysis of variance followed by Bonferroni's multiple comparison test). BM-MSCs: bone marrow-derived mesenchymal stem cells; odMSCs: osteo-organoid-derived mesenchymal stem cells; P: passage; SA- β -Gal: senescence-associated β -galactosidase.

Cell growth of osteo-organoid-derived mesenchymal stem cells

The odMSCs reached 80% confluence in a shorter time than the BM-MSCs when cultured under hypoxic conditions (Table 3). However, the difference at P0 was greater than at P1. In order to define whether the cell proliferation of odMSCs was still faster than that of BM-MSC after passage, MSCs from both sources at P2 were seeded in 60-mm dish in equal numbers. The MSCs were used for an EdU assay when cell confluence reached 80%, but no more than 100%. The flow

cytometric scatter plots for both groups exhibited a similar horseshoe shape (Figure 5A). Statistical analysis indicated the no significant difference between the proportions of EdU⁺ cells in both groups (Figure 5B). The proportion of EdU⁺ cells for the BMP group was higher than that of the native group. This was further confirmed by fluorescence images (Figure 5C and D). That is, the total number of cells in odMSCs was higher than that in BM-MSCs, but the proportion of EdU⁺ cells in the former was not significantly higher than that in the latter.

Table 3. Time of mesenchymal stem cell passage from the osteo-organoid vs. native bone marrow

Source	P0	P1	Total
Osteo-organoid	3 days	3 days	6 days
Native bone marrow	8 days	4 days	12 days

Note: P0: mesenchymal stem cells isolated from an osteo-organoid, or a tibia and a femur; P1: mesenchymal stem cells passaged at a split ratio of 1:3 from P0.

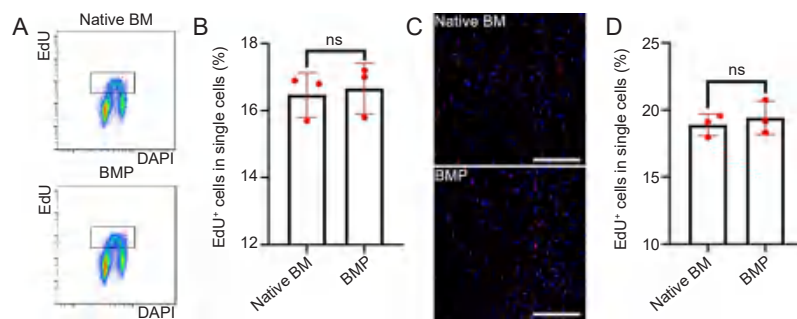


Figure 5. Cell proliferation of MSCs at P2. (A, B) Scatter diagrams (A) and content of EdU⁺ cells (B) by flow cytometric analysis. (C, D) Fluorescence confocal image (blue: DAPI; red: EdU; C) and statistical analysis (D). Scale bars: 200 μ m. Data are expressed as mean \pm SD ($n = 3$), and were analyzed by Student's *t*-test. BM: native bone marrow-derived mesenchymal stem cells; BMP: osteo-organoid-derived mesenchymal stem cells (constructed with recombinant human bone morphogenetic protein 2-loaded gelatin sponge scaffolds); DAPI: 4',6-diamidino-2-phenylindole; EdU: 5-ethynyl-2'-deoxyuridine; MSCs: mesenchymal stem cells; ns: not significant; P2: passage 2.

The above results illustrated that the primary cells played a more important role in proliferation than the cells passed for generations did. In other words, as the native BM group becomes purified, the macroscopic proliferation duration of these MSCs tends to align with that of odMSCs. Last but not least, based on the above results, we could infer that the growth rate of BM-MSCs at P0 was not lower than that of odMSCs, because the former aged faster³⁶ (Figure 4), while both cell types proliferated at the same rate at P2 (Figure 5). Furthermore, it could be considered that the abundance of odMSCs at P0 was significantly higher than that of BM-MSCs (Figure 2B).

Discussion

The above results indicate that the MSCs obtained using this method exhibit superior differentiation (Figure 3B) and sufficient proliferation (Figure 5) levels compared with those obtained using traditional methods. Moreover, the osteo-organoid assay yields a higher quantity of MSCs compared with BM-MSCs, since the proportion of primary MSCs to total cells greatly surpasses that of native bone marrow isolated in the same manner (Figure 2B). The number of cells isolated from a tibia and a femur is generally three to four times higher than the cells from osteo-organoids, whereas the latter achieves the same number of MSCs in only half the total time of the former (Table 3). At P2, the proliferation of MSCs from both sources is essentially the same. It was likely because the purity of MSCs with high proliferative activity increases following passage, leading to consistent cell growth rates. BM-MSCs often experience replicative senescence during expansion,³⁷ which results in a decline in stemness (mainly including capabilities of differentiation, regeneration, proliferation and migration).³⁸ In contrast, the method described in this paper can reduce the time of *in vitro* expansion to delay the ageing process (Figure 4). The low level of senescence is one reason for the strong differentiation capability of odMSCs at P2. Based on our previous researches, we found that osteo-organoids, after about 1 week of development, exhibit a youthful state and tissue repair activity.³⁰⁻³² BM-MSCs are located in the more developed native bone marrow, hence the younger odMSCs

have a high abundance and the ability of anti-replicative senescence.

Compared with the traditional medium, the complete medium used in this protocol was added with Rho-associated kinase inhibitor, as a differentiation inhibitor, and sodium pyruvate and a higher proportion (20%) of fetal bovine serum were used to promote cell growth. The aim is to prevent the loss of stemness due to premature differentiation when MSCs are cultured *in vitro*. Besides, The method eventually purifies stem cells isolated from osteo-organoids, which exhibit a phenotype akin to BM-MSCs (Figure 3A), leading us to classify them as MSCs. However, MSCs from these two sources exhibit some differences in morphology, and the expression levels of cell markers^{21,39} are not entirely consistent. Notably, CD140a, also known as platelet-derived growth factor alpha, is an important marker of myofibroblasts^{10,21,39,40} and is highly expressed in odMSCs. The thinner and longer cell morphology of these cells is similar to the classic shape of C2C12 myoblasts cells cultured *in vitro*, which can also respond to bone morphogenetic protein-2 in osteogenesis-related biochemical processes.^{34,40} Therefore, we infer that odMSCs are essentially myogenic MSCs, and they differ from BM-MSCs in terms of cytokine secretion, immunological performance^{10,40} and tissue repair activity.^{39,41} Moreover, the form, structure, composition, and properties of the selected materials are highly customizable, and the implantation time³² can be selected. In theory, stem cells from different sources or ageing systems can be obtained. For example, we used a gelatin sponge added with chondroitin sulfate and then loaded with rhBMP-2 as a material, and implanted it on the back to create a periosteum-like tissue,³⁰ enhanced the regenerative capacity of the MSCs. Another example is that we used sulfonated gelatin hydrogel⁴² instead of the gelatin sponge to build growth factor-enriched niche, which accelerated bone regeneration. Hence osteo-organoids can be considered an efficient and highly flexible model for studying stem cells such as MSCs.

In the current clinical autologous transplantation methods,^{26,27} the quantity of extracted bone marrow is limited, but patients who need to use MSCs for treatment often have stem cells

Rapid obtaining strategy of massive MSCs

with insufficient activity. Due to these limitations, MSCs from autologous bone marrow are usually not recommended for stem cell therapy. Even so, compared with allogeneic tissue, autologous tissue is more acceptable to patients due to factors such as higher safety, a simpler application process, better autonomy, and less psychological burden. Although transplantation matching is not required for MSCs usage, non-cryopreserved allogeneic stem cells used for treatments carry some risk from donors.⁴³ Fresh cells have a limited usage window, thus the transportation efficiency directly impacts the success rate of the operation; the viability and activity of MSCs decrease under cryopreservation conditions,⁴⁴ and cell cryopreservation reagents can cause some adverse reactions *in vivo*.⁴⁵ Additionally, umbilical cord or adipose-tissue derived MSCs, which are commonly used in stem cell banks, do not exhibit high anti-inflammatory properties as well as BM-MSCs, especially in hypoxic environments.⁴⁶ Contrarily, the stem cells obtained through this novel protocol consider the benefits of autologous sources and provide high stem cell quantity and quality, which can be a competitive method for stem cell therapy.

There were still limitations in our study. The odMSCs may come from mixed sources. It is not completely clear the subtype composition and specific of odMSCs. In theory, BM-MSCs should be the main type of odMSCs given that osteo-organoids ultimately form complete bone structures.⁴⁷ But in fact, our research has found that odMSCs are likely to be myogenic MSCs. Despite this, the proportion of various MSCs has not been well distinguished. For application, it takes 5 days for osteo-organoids to develop, and not everyone is willing to undergo two surgeries in such a short period of time. Therefore, relevant minimally invasive surgical techniques urgently need to be developed in order to broaden the acceptance of clinical applications.

In conclusion, we constructed osteo-organoids that can generate MSCs in large quantities, high purity, and high quality by means of *in vivo* tissue engineering. The odMSCs can be used in the *in vitro* study of stem cells through simple purification, and odMSCs maintain youthful states during short-term *in vitro* expansion, which will contribute to research and applications on reversing senescence. On this basis, more researches, such as the myoideum source characterisation, bone marrow ablation models, and scaffold materials modification, are underway. Furthermore, for clinical application, this method is a fast way to harvest high density of stem cells. Therefore, this study provides an alternative protocol for obtaining large quantities of and high quality MSCs and is expected to be a novel solution for stem cell therapy.

Author contributions

SD: investigation, experiments, analysis, validation, writing and editing; FZ: experiments; KD: investigation, experiments, validation and writing; JW: funding acquisition, resources, supervision, review, and editing; CL: funding acquisition, resources, supervision, review, and editing. All authors discussed the results, commented on the manuscript, and approved the final version of the manuscript.

Financial support

This study was supported by the Basic Science Center Program of National Natural Science Foundation of China, No. T2288102, the Key Program of the National Natural Science Foundation of China, No. 32230059, the Foundation

of Frontiers Science Center for Materiobiology and Dynamic Chemistry, No. JKVD1211002, the Wego Project of Chinese Academy of Sciences, No. (2020) 005, the National Natural Science Foundation of China, No. 32301123, the China Postdoctoral Science Foundation, No. 2022M721147, and the Project of National Facility for Translational Medicine (Shanghai), No. TMSK-2021-134.

Acknowledgement

We thank Professor Rui Yue's research group at Tongji University for their careful guidance of isolation cells from bone marrow and epiphysis using digestive enzyme mixture.

Conflicts of interest statement

There are no conflicts to declare.

Editor note: Changsheng Liu is an Editorial Board member of *Biomaterials Translational*. He was blinded from reviewing or making decisions on the manuscript. The article was subject to the journal's standard procedures, with peer review handled independently of this Editorial Board member and his research group.

Open access statement

This is an open access journal, and articles are distributed under the terms of the Creative Commons Attribution-NonCommercial-ShareAlike 4.0 License, which allows others to remix, tweak, and build upon the work non-commercially, as long as appropriate credit is given and the new creations are licensed under the identical terms.

- Zhu, H.; Guo, Z. K.; Jiang, X. X.; Li, H.; Wang, X. Y.; Yao, H. Y.; Zhang, Y.; Mao, N. A protocol for isolation and culture of mesenchymal stem cells from mouse compact bone. *Nat Protoc.* **2010**, *5*, 550-560.
- Li, W. Y.; Choi, Y. J.; Lee, P. H.; Huh, K.; Kang, Y. M.; Kim, H. S.; Ahn, Y. H.; Lee, G.; Bang, O. Y. Mesenchymal stem cells for ischemic stroke: changes in effects after ex vivo culturing. *Cell Transplant.* **2008**, *17*, 1045-1059.
- Kurth, T. B.; Dell'accio, F.; Crouch, V.; Augello, A.; Sharpe, P. T.; De Bari, C. Functional mesenchymal stem cell niches in adult mouse knee joint synovium in vivo. *Arthritis Rheum.* **2011**, *63*, 1289-1300.
- Huang, S.; Xu, L.; Sun, Y.; Wu, T.; Wang, K.; Li, G. An improved protocol for isolation and culture of mesenchymal stem cells from mouse bone marrow. *J Orthop Translat.* **2015**, *3*, 26-33.
- Rossi, C. A.; Flaibani, M.; Blaauw, B.; Pozzobon, M.; Figallo, E.; Reggiani, C.; Vitiello, L.; Elvassore, N.; De Coppi, P. In vivo tissue engineering of functional skeletal muscle by freshly isolated satellite cells embedded in a photopolymerizable hydrogel. *FASEB J.* **2011**, *25*, 2296-2304.
- Zhai, W.; Yong, D.; El-Jawhari, J. J.; Cuthbert, R.; McGonagle, D.; Win Naing, M.; Jones, E. Identification of senescent cells in multipotent mesenchymal stromal cell cultures: current methods and future directions. *Cytotherapy.* **2019**, *21*, 803-819.
- Karnoub, A. E.; Dash, A. B.; Vo, A. P.; Sullivan, A.; Brooks, M. W.; Bell, G. W.; Richardson, A. L.; Polyak, K.; Tubo, R.; Weinberg, R. A. Mesenchymal stem cells within tumour stroma promote breast cancer metastasis. *Nature.* **2007**, *449*, 557-563.
- Salazar-Noratto, G. E.; Luo, G.; Denoed, C.; Padrona, M.; Moya, A.; Bensidhoum, M.; Bizios, R.; Potier, E.; Logeart-Avramoglou, D.; Petite, H. Understanding and leveraging cell metabolism to enhance mesenchymal stem cell transplantation survival in tissue engineering and regenerative medicine applications. *Stem Cells.* **2020**, *38*, 22-33.
- Wang, Y.; Zhang, W.; Yao, Q. Copper-based biomaterials for bone and cartilage tissue engineering. *J Orthop Translat.* **2021**, *29*, 60-71.
- Uezumi, A.; Fukada, S.; Yamamoto, N.; Takeda, S.; Tsuchida, K. Mesenchymal progenitors distinct from satellite cells contribute to ectopic fat cell formation in skeletal muscle. *Nat Cell Biol.* **2010**, *12*, 143-152.

11. Tidu, F.; De Zuani, M.; Jose, S. S.; Bendíčková, K.; Kubala, L.; Caruso, F.; Cavalieri, F.; Forte, G.; Frič, J. NFAT signaling in human mesenchymal stromal cells affects extracellular matrix remodeling and antifungal immune responses. *iScience*. **2021**, *24*, 102683.
12. Wang, G.; Cao, K.; Liu, K.; Xue, Y.; Roberts, A. I.; Li, F.; Han, Y.; Rabson, A. B.; Wang, Y.; Shi, Y. Kynurenic acid, an IDO metabolite, controls TSG-6-mediated immunosuppression of human mesenchymal stem cells. *Cell Death Differ*. **2018**, *25*, 1209-1223.
13. Kfoury, Y.; Scadden, D. T. Mesenchymal cell contributions to the stem cell niche. *Cell Stem Cell*. **2015**, *16*, 239-253.
14. McCullen, S. D.; Chow, A. G.; Stevens, M. M. In vivo tissue engineering of musculoskeletal tissues. *Curr Opin Biotechnol*. **2011**, *22*, 715-720.
15. Li, Z.; Niu, S.; Guo, B.; Gao, T.; Wang, L.; Wang, Y.; Wang, L.; Tan, Y.; Wu, J.; Hao, J. Stem cell therapy for COVID-19, ARDS and pulmonary fibrosis. *Cell Prolif*. **2020**, *53*, e12939.
16. Hejcl, A.; Sedý, J.; Kapcalová, M.; Toro, D. A.; Amemori, T.; Lesný, P.; Likavcanová-Mašínová, K.; Krumbholcová, E.; Prádný, M.; Michálek, J.; Burian, M.; Hájek, M.; Jendelová, P.; Syková, E. HPMA-RGD hydrogels seeded with mesenchymal stem cells improve functional outcome in chronic spinal cord injury. *Stem Cells Dev*. **2010**, *19*, 1535-1546.
17. Maruyama, M.; Pan, C. C.; Moeinzadeh, S.; Storaci, H. W.; Guzman, R. A.; Lui, E.; Ueno, M.; Utsunomiya, T.; Zhang, N.; Rhee, C.; Yao, Z.; Takagi, M.; Goodman, S. B.; Yang, Y. P. Effect of porosity of a functionally-graded scaffold for the treatment of corticosteroid-associated osteonecrosis of the femoral head in rabbits. *J Orthop Translat*. **2021**, *28*, 90-99.
18. Sun, L.; Akiyama, K.; Zhang, H.; Yamaza, T.; Hou, Y.; Zhao, S.; Xu, T.; Le, A.; Shi, S. Mesenchymal stem cell transplantation reverses multiorgan dysfunction in systemic lupus erythematosus mice and humans. *Stem Cells*. **2009**, *27*, 1421-1432.
19. Cao, X.; Duan, L.; Hou, H.; Liu, Y.; Chen, S.; Zhang, S.; Liu, Y.; Wang, C.; Qi, X.; Liu, N.; Han, Z.; Zhang, D.; Han, Z. C.; Guo, Z.; Zhao, Q.; Li, Z. IGF-1C hydrogel improves the therapeutic effects of MSCs on colitis in mice through PGE(2)-mediated M2 macrophage polarization. *Theranostics*. **2020**, *10*, 7697-7709.
20. Soleimani, M.; Nadri, S. A protocol for isolation and culture of mesenchymal stem cells from mouse bone marrow. *Nat Protoc*. **2009**, *4*, 102-106.
21. Houlihan, D. D.; Mabuchi, Y.; Morikawa, S.; Niibe, K.; Araki, D.; Suzuki, S.; Okano, H.; Matsuzaki, Y. Isolation of mouse mesenchymal stem cells on the basis of expression of Sca-1 and PDGFR- α . *Nat Protoc*. **2012**, *7*, 2103-2111.
22. Lin, W.; Xu, L.; Lin, S.; Shi, L.; Wang, B.; Pan, Q.; Lee, W. Y. W.; Li, G. Characterisation of multipotent stem cells from human peripheral blood using an improved protocol. *J Orthop Translat*. **2019**, *19*, 18-28.
23. Matsuda, K.; Falkenberg, K. J.; Woods, A. A.; Choi, Y. S.; Morrison, W. A.; Dilley, R. J. Adipose-derived stem cells promote angiogenesis and tissue formation for in vivo tissue engineering. *Tissue Eng Part A*. **2013**, *19*, 1327-1335.
24. Lin, W.; Xu, L.; Li, G. A novel protocol for isolation and culture of multipotent progenitor cells from human urine. *J Orthop Translat*. **2019**, *19*, 12-17.
25. Xu, Y.; Zhang, T.; Chen, Y.; Shi, Q.; Li, M.; Qin, T.; Hu, J.; Lu, H.; Liu, J.; Chen, C. Isolation and characterization of multipotent canine urine-derived stem cells. *Stem Cells Int*. **2020**, *2020*, 8894449.
26. Huang, R. L.; Kobayashi, E.; Liu, K.; Li, Q. Bone graft prefabrication following the in vivo bioreactor principle. *EBioMedicine*. **2016**, *12*, 43-54.
27. Yin, J. Q.; Zhu, J.; Ankrum, J. A. Manufacturing of primed mesenchymal stromal cells for therapy. *Nat Biomed Eng*. **2019**, *3*, 90-104.
28. Mauney, J. R.; Nguyen, T.; Gillen, K.; Kirker-Head, C.; Gimple, J. M.; Kaplan, D. L. Engineering adipose-like tissue in vitro and in vivo utilizing human bone marrow and adipose-derived mesenchymal stem cells with silk fibroin 3D scaffolds. *Biomaterials*. **2007**, *28*, 5280-5290.
29. Cui, L.; Xiang, S.; Chen, D.; Fu, R.; Zhang, X.; Chen, J.; Wang, X. A novel tissue-engineered bone graft composed of silicon-substituted calcium phosphate, autogenous fine particulate bone powder and BMSCs promotes posterolateral spinal fusion in rabbits. *J Orthop Translat*. **2021**, *26*, 151-161.
30. Dai, K.; Deng, S.; Yu, Y.; Zhu, F.; Wang, J.; Liu, C. Construction of developmentally inspired periosteum-like tissue for bone regeneration. *Bone Res*. **2022**, *10*, 1.
31. Dai, K.; Shen, T.; Yu, Y.; Deng, S.; Mao, L.; Wang, J.; Liu, C. Generation of rhBMP-2-induced juvenile ossicles in aged mice. *Biomaterials*. **2020**, *258*, 120284.
32. Dai, K.; Zhang, Q.; Deng, S.; Yu, Y.; Zhu, F.; Zhang, S.; Pan, Y.; Long, D.; Wang, J.; Liu, C. A BMP-2-triggered in vivo osteo-organoid for cell therapy. *Sci Adv*. **2023**, *9*, eadd1541.
33. Dey, D.; Bagarova, J.; Hatsell, S. J.; Armstrong, K. A.; Huang, L.; Ermann, J.; Vonner, A. J.; Shen, Y.; Mohedas, A. H.; Lee, A.; Eekhoff, E. M.; van Schie, A.; Demay, M. B.; Keller, C.; Wagers, A. J.; Economides, A. N.; Yu, P. B. Two tissue-resident progenitor lineages drive distinct phenotypes of heterotopic ossification. *Sci Transl Med*. **2016**, *8*, 366ra163.
34. Smith, E.; Yang, J.; McGann, L.; Sebald, W.; Uludag, H. RGD-grafted thermoreversible polymers to facilitate attachment of BMP-2 responsive C2C12 cells. *Biomaterials*. **2005**, *26*, 7329-7338.
35. Zhou, B. O.; Yue, R.; Murphy, M. M.; Peyer, J. G.; Morrison, S. J. Leptin-receptor-expressing mesenchymal stromal cells represent the main source of bone formed by adult bone marrow. *Cell Stem Cell*. **2014**, *15*, 154-168.
36. Leong, D. J.; Sun, H. B. Mesenchymal stem cells in tendon repair and regeneration: basic understanding and translational challenges. *Ann N Y Acad Sci*. **2016**, *1383*, 88-96.
37. Wagner, W.; Horn, P.; Castoldi, M.; Diehlmann, A.; Bork, S.; Saffrich, R.; Benes, V.; Blake, J.; Pfister, S.; Eckstein, V.; Ho, A. D. Replicative senescence of mesenchymal stem cells: a continuous and organized process. *PLoS One*. **2008**, *3*, e2213.
38. Dimri, G. P.; Lee, X.; Basile, G.; Acosta, M.; Scott, G.; Roskelley, C.; Medrano, E. E.; Linskens, M.; Rubelj, I.; Pereira-Smith, O.; et al. A biomarker that identifies senescent human cells in culture and in aging skin in vivo. *Proc Natl Acad Sci U S A*. **1995**, *92*, 9363-9367.
39. Julien, A.; Kanagalingam, A.; Martínez-Sarrà, E.; Megret, J.; Luka, M.; Ménager, M.; Relaix, F.; Colnot, C. Direct contribution of skeletal muscle mesenchymal progenitors to bone repair. *Nat Commun*. **2021**, *12*, 2860.
40. Wang, X.; Matthews, B. G.; Yu, J.; Novak, S.; Grcevic, D.; Sanjay, A.; Kalajzic, I. PDGF modulates BMP2-induced osteogenesis in periosteal progenitor cells. *JBMR Plus*. **2019**, *3*, e10127.
41. Lees-Shepard, J. B.; Yamamoto, M.; Biswas, A. A.; Stoessel, S. J.; Nicholas, S. E.; Cogswell, C. A.; Devarakonda, P. M.; Schneider, M. J., Jr.; Cummins, S. M.; Legendre, N. P.; Yamamoto, S.; Kaartinen, V.; Hunter, J. W.; Goldhamer, D. J. Activin-dependent signaling in fibro/adipogenic progenitors causes fibrodysplasia ossificans progressiva. *Nat Commun*. **2018**, *9*, 471.
42. Zhang, Q.; Liu, Y.; Li, J.; Wang, J.; Liu, C. Recapitulation of growth

Rapid obtaining strategy of massive MSCs

- factor-enriched microenvironment via BMP receptor activating hydrogel. *Bioact Mater.* **2023**, *20*, 638-650.
43. Fernández-Santos, M. E.; García-Arranz, M.; Andreu, E. J.; García-Hernández, A. M.; López-Parra, M.; Villarón, E.; Sepúlveda, P.; Fernández-Avilés, F.; García-Olmo, D.; Prosper, F.; Sánchez-Guijo, F.; Moraleda, J. M.; Zapata, A. G. Optimization of mesenchymal stromal cell (MSC) manufacturing processes for a better therapeutic outcome. *Front Immunol.* **2022**, *13*, 918565.
 44. Saha, D.; Hofmann, N.; Mueller, T.; Niemann, H.; Glasmacher, B. C-2014: Investigation of genetic and epigenetic changes of cryopreserved mesenchymal stem cells. *Cryobiology.* **2014**, *69*, 519.
 45. Shu, Z.; Heimfeld, S.; Gao, D. Hematopoietic SCT with cryopreserved grafts: adverse reactions after transplantation and cryoprotectant removal before infusion. *Bone Marrow Transplant.* **2014**, *49*, 469-476.
 46. Lagonda, C. A.; Tjahjadi, F. B.; Fauza, D.; Kusnadi, Y. Hypoxia increases vegf secretion in multiple sources of mesenchymal stem cell. *Cytotherapy.* **2018**, *20*, S44-S45.
 47. Wang, X.; Li, F.; Xie, L.; Crane, J.; Zhen, G.; Mishina, Y.; Deng, R.; Gao, B.; Chen, H.; Liu, S.; Yang, P.; Gao, M.; Tu, M.; Wang, Y.; Wan, M.; Fan, C.; Cao, X. Inhibition of overactive TGF- β attenuates progression of heterotopic ossification in mice. *Nat Commun.* **2018**, *9*, 551.

Received: September 21, 2023

Revised: November 14, 2023

Accepted: November 30, 2023

Available online: December 28, 2023

Fabrication of magnesium-doped porous polylactic acid microsphere for bone regeneration

Ziwei Tao^{1,#}, Ziyang Yuan^{2,#}, Dong Zhou^{3,#}, Lang Qin¹, Lan Xiao⁴, Shihao Zhang¹, Changsheng Liu^{1,*}, Jinzhong Zhao^{2,*}, Yulin Li^{1,5,*}

Key Words:

magnesium ion; osteogenesis; polylactic acid; porous microspheres

From the Contents

Introduction	280
Methods	281
Results	283
Discussion	287

ABSTRACT

Biodegradable polymer microspheres that can be used as drug carriers are of great importance in biomedical applications, however, there are still challenges in controllable preparation of microsphere surface morphology and improvement of bioactivity. In this paper, firstly, poly(L-lactic acid) (PLLA) was synthesised by ring-opening polymerisation under anhydrous anaerobic conditions and further combined with the emulsion method, biodegradable PLLA microspheres (PM) with sizes ranging from 60–100 μm and with good sphericity were prepared. In addition, to further improve the surface morphology of PLLA microspheres and enhance their bioactivity, functionalised porous PLLA microspheres loaded with magnesium oxide (MgO)/magnesium carbonate (MgCO_3) (PMg) were also prepared by the emulsion method. The results showed that the loading of MgO/ MgCO_3 resulted in the formation of a porous structure on the surface of the microspheres (PMg) and the dissolved Mg^{2+} could be released slowly during the degradation of microspheres. In vitro cellular experiments demonstrated the good biocompatibility of PM and PMg, while the released Mg^{2+} further enhanced the anti-inflammatory effect and osteogenic activity of PMg. Functionalised PMg not only show promise for controlled preparation of drug carriers, but also have translational potential for bone regeneration.

<http://doi.org/10.12336/biomatertransl.2023.04.007>

How to cite this article:

Tao, Z.; Yuan, Z.; Zhou, D.; Qin, L.; Xiao, L.; Zhang, S.; Liu, C.; Zhao, J.; Li, Y. Fabrication of magnesium-doped porous polylactic acid microsphere for bone regeneration. *Biomater Transl.* 2023, 4(4), 280-290.



Introduction

Biodegradable polymer microspheres have many advantages, such as good biocompatibility, low dosage and few side effects, and therefore have a wide range of applications in medical fields such as medical aesthetic fillers,¹⁻³ drug delivery^{4, 5} and tissue engineering,^{6, 7} whereas the preparation of microsphere with controlled morphological diversity remains a significant challenge.⁸⁻¹⁰ Polylactic acid (PLA) is a biodegradable polymer approved by the U.S. Food and Drug Administration with good biocompatibility and can be absorbed by the human body after implantation,^{11, 12} and is now widely used in biomedical applications as drug delivery microspheres, resorbable membranes for bone defect repair, and surgical treatment

sutures.¹³⁻¹⁷ However, the poor biological activity of PLA and the acidic degradation environment can easily cause tissue inflammation, which has significantly hindered the further application of PLA.¹⁸⁻²¹

Mg^{2+} is an important trace element in the human body and an important component of bones and teeth. It can regulate cell behaviour, such as improving cell adhesion and stimulating cell differentiation, and stimulate local bone formation and healing by promoting angiogenesis, thereby promoting bone regeneration. Studies found that the controlled release of Mg^{2+} promoted angiogenesis, thereby synergistically promoting *in situ* bone regeneration by developing a new magnesium

Magnesium-doped microsphere for bone regeneration

doped double crosslinked hydrogel.²²⁻²⁶ Magnesium oxide (MgO) and magnesium carbonate (MgCO_3) are bioactive materials with good biocompatibility,²⁷⁻²⁹ and have different rates of Mg^{2+} dissolution.^{30,31} MgO and MgCO_3 are alkaline and can neutralise the acidic environment caused by the degradation of PLA, thus maintaining a stable pH environment,^{7, 32, 33} and the loading of MgO and MgCO_3 changes the surface morphology of the microspheres.³⁴ However, when different mass ratios of MgO and MgCO_3 were added, the release rate of Mg^{2+} and the surface morphology of the microspheres changed accordingly,³⁴ therefore, an appropriate MgO/ MgCO_3 mass ratio can effectively enhance the bioactivity of microspheres, which has a crucial impact on osteogenic transition.³⁵

As shown in **Figure 1A**, poly(L-lactic acid) (PLLA) was successfully synthesised by ring-opening polymerisation,

and the microspheres (PMg) loaded with MgO/ MgCO_3 with uniform particle size and controlled morphology were prepared by the emulsion method. The loading of MgO/ MgCO_3 led to the appearance of porous structure on the surface of the microspheres, which facilitated the interactions with the cells compared with the conventional solid PLLA.^{6, 36, 37} The MgO and MgCO_3 could further neutralise the acidic environment generated during the degradation process of the PMg. In addition, the Mg^{2+} rich microenvironment and porous structure of PMg facilitate the migration, proliferation and differentiation of tendon-derived stem cells (TDSCs)³⁸ (**Figure 1B**). Therefore, this study provides an advanced strategy to synthesise microspheres with controlled morphology and bioactive properties for bone healing.

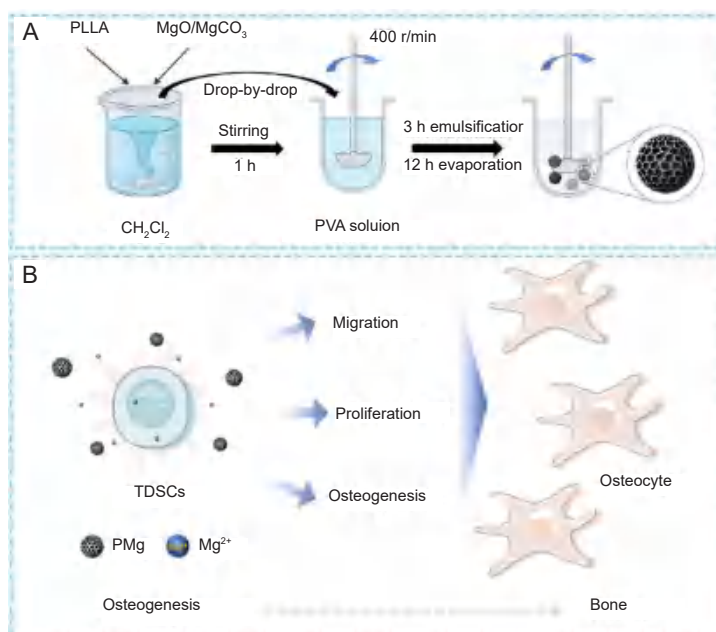


Figure 1. Schematic preparation of poly(L-lactic acid) microsphere loaded with magnesium oxide (MgO)/magnesium carbonate (MgCO_3) microspheres (PMg) and influence of PMg on tendon-derived stem cells (TDSCs). (A) PMg microspheres were obtained in the form of oil in water, dichloromethane (CH_2Cl_2) is the oil phase, and polyvinyl alcohol (PVA) is the water phase, the oil phase and the water phase are incompatible, so an oil-in-water system is formed, and during stirring, CH_2Cl_2 gradually evaporates, and poly(L-lactic acid) microsphere (PM) and PMg are formed. (B) PMg microspheres can maintain the continuing release of Mg^{2+} to promote the TDSC migration, proliferation, osteogenesis. Created with BioRender.com.

Methods

Synthesis of PLLA

In our previous work, we have successfully synthesised PLLA.³⁹ PLLA was synthesised by anhydrous and anaerobic ring-

opening polymerisation, briefly, a certain amount of L-lactide (Jinan Daigang Biomaterials Co., Ltd., Jinan, China) was mixed with 0.1% $\text{Sn}(\text{Oct})_2$ (Titan Technology Co., Ltd., Shanghai, China) in the dry flask, the temperature was raised into 140°C,

1 Engineering Research Centre for Biomedical Materials of Ministry of Education, Key Laboratory for Ultrafine Materials of Ministry of Education, School of Materials Science and Engineering, East China University of Science and Technology, Shanghai, China; 2 Department of Sports Medicine, Shanghai Sixth People's Hospital Affiliated to Shanghai Jiao Tong University School of Medicine, Shanghai, China; 3 School of Chemistry and Chemical Engineering, Nanchang University, Nanchang, Jiangxi Province, China; 4 School of Mechanical, Medical and Process Engineering, Center of Biomedical Technology, Queensland University of Technology, Brisbane, Australia; 5 Wenzhou Institute of Shanghai University, Wenzhou, Zhejiang Province, China

*Corresponding authors:

Yulin Li, yulinli@ecust.edu.cn; Changsheng Liu, liucs@ecust.edu.cn; Jinzhong Zhao, jzzhao@sjtu.edu.cn.

#Author equally.

and the reaction was maintained in an inert atmosphere, 7 hours later, the crude products were dissolved with dichloromethane (Anhui Chemical Technology Co., Ltd., Nantong, China), followed by precipitation in ethanol (Anhui Chemical Technology Co., Ltd.), and then lyophilised.

Micro-structural analysis of PLLA

The microstructure of PLLA was detected by Fourier transformed infrared spectrophotometer (Thermo Scientific, Franklin, MA, USA) in the wavelength range of 500–4000 cm^{-1} . The chemical structure of PLLA was examined by nuclear magnetic resonance spectroscopy (Bruker, Karlsruhe, UK).

Preparation of microspheres

PLLA microspheres were prepared using a previously reported method.⁴⁰ To obtain microspheres, 200 mg of PLLA was dissolved in dichloromethane and mixed with MgO/MgCO_3 (Shanghai Nai Cheng Biotechnology Co., Ltd., Shanghai, China), 1 hour later, the mixture was dropped into the 1% polyvinyl alcohol (Shanghai Macklin Biochemical Co., Ltd., Shanghai, China), emulsified for 3 hours, and kept stirred for overnight at room temperature to remove the dichloromethane. Finally, the collected microspheres were then washed by centrifugation three times and freeze-dried, designated as PMg. The above steps were repeated without the addition of MgO/MgCO_3 to obtain microspheres and named as PM.

Characterisation of microspheres

The surface morphology of microspheres was observed with a scanning electron microscope (S-3400N, Hitachi, Tokyo, Japan), and the particle size and pore size were calculated by ImageJ software (1.52t, National Institutes of Health, Bethesda, MD, USA).⁴¹ The water contact angle of microsphere samples PM and PMg was measured using a contact angle meter (Shanghai Zhongchen Digital Technology Equipment Co., Ltd., Shanghai, China) by spreading a 1 $\text{cm} \times 1 \text{ cm}$ piece of double-sided adhesive flat on a slide, then weighing the same mass of microsphere samples and spreading the microspheres uniformly and densely on the surface of the double-sided adhesive.¹⁰ Three parallel samples were tested in each group and three different points on each parallel sample were taken for measurement.

In vitro degradability of microspheres

The mass and pH value changes of the microspheres were measured to assess the degradation of microspheres in phosphate buffer saline (PBS) (Shanghai Sehan Co., Ltd., Shanghai, China). Briefly, 10 mg PM and 10 mg PMg were dispersed in 10 mL of PBS solution, stored in an incubator at 37°C and rotated at 80 r/min. The microspheres were separated from PBS at different time points (1, 3, 5, 7, 15, and 30 days), followed by determining the pH of the degradation solution of microspheres by using a pH meter (MTD, Zurich, Switzerland) and the number average molecular weight of microspheres by gel permeation chromatography. While polystyrene was used as the standard sample, and tetrahydrofuran (chromatographic grade) was used as the solvent and eluent at a flow rate of 1.0

mL/min. Finally, scanning electron microscopy was used to observe the morphological changes of the microspheres during the degradation process.

In vitro Mg^{2+} release from microspheres

10 mg of PMg was immersed in 10 mL of PBS and incubated at $37 \pm 1^\circ\text{C}$ for 30 days. On days 1, 3, 5, 7, 15, and 30, 1 mL of sample liquid was removed and diluted to 10 mL with PBS (three parallel samples were tested at each time point), and then analysed by high-performance liquid chromatography-inductively coupled plasma mass spectrometer (NexION 2000 – (A – 10), PerkinElmer, Waltham, MA, USA).

In vitro cytocompatibility

Preparation of leachate

Firstly, 10 mg of each microsphere was accurately weighed and immersed in 75% ethanol for overnight sterilisation, followed by washing the microsphere three times with PBS and twice with serum-free Dulbecco's modified Eagle medium (Gibco Life Technologies, Grand Island, NY, USA) medium, respectively. The microspheres were immersed in serum-free Dulbecco's modified Eagle medium (10 mg of microspheres:1 mL of Dulbecco's modified Eagle medium), and then placed in a thermostatic shaker (Taicang Hualida Co., Ltd., Taicang, China) at 37°C and 30 r/min for 24 hours. The leachate was collected and filtered with a 0.22- μm biofilter filtration, then 10% fetal bovine serum, 1% penicillin/streptomycin were added to prepare culture medium containing material extracts for cells.

Evaluation of cytotoxicity

All animal experiments were approved by the Ethics Committee of Shanghai Sixth People's Hospital affiliated with Shanghai Jiaotong University School of Medicine (approval No. DWSY2023-0115) on August 22, 2023. Tendon-derived stem cells (TDSCs) were isolated from the achilles tendon of 3–4-week-old male Sprague-Dawley rats (Shanghai Bikewing Biotechnology Co., Ltd., Shanghai, China) according to a previous protocol,⁴² and the isolated cells were inoculated in Dulbecco's modified Eagle medium containing 10% fetal bovine serum, 1% triple antibiotic, and cultured at 37°C, 5% CO_2 environment. The medium was replaced every 2 days. The cells were passaged when they reached 80–90% confluence, and the experiments were conducted using passages 3–5 cells in this study. After 2×10^3 TDSCs/mL were seeded in 96-well plates, the cells were treated with the corresponding leachate for 24, 48, or 72 hours. The cells were incubated with 10 μL of CCK-8 (Beyotime, Shanghai, China) for 2 hours. The absorbance peak at 450 nm in each well was measured by a microplate reader (Molecular Device, Sunnyvale, CA, USA) to obtain the optical density (OD), and the cell viability was calculated as follows: Cell viability (%) = $100 \times \frac{\text{OD}_{\text{experimental}}}{\text{OD}_{\text{Control}}}$, where $\text{OD}_{\text{experimental}}$ and $\text{OD}_{\text{control}}$ are the optical densities for the experimental and control groups, respectively.

Live-dead staining

The cytocompatibility was evaluated by live-dead cell staining assay (Beyotime). Briefly, 5×10^3 TDSCs/mL were seeded in

Magnesium-doped microsphere for bone regeneration

24-well plates and placed in a 37°C, 5% CO₂ incubator for 8 hours. After the cells were adhered to the wall, the leachate of the corresponding material groups was used to treat cells for 24, 48, or 72 hours. After washing with PBS, cells were stained with calcein yellow chlorophyll and propidium iodide for 30 minutes at 37°C at 24, 48, and 72 hours. The result was observed by using confocal laser scanning microscope (Air, Tokyo, Japan).

In vitro osteogenic capacity evaluation

Alkaline phosphatase staining assay

TDSCs were seeded in 24-well plates and material-extract medium was then mixed with osteogenic medium (Beyotime) at a ratio of 1:10. After 7 days of incubation, the cells were fixed with 4% paraformaldehyde for 15 minutes, stained with alkaline phosphatase (ALP; Beyotime), stained at 37°C for 1 hour, washed twice with PBS, and photographed for observation using confocal laser scanning microscope.

Polymerase chain reaction assay

Quantitative polymerase chain reaction was tested to study the gene expression of *Arg-1* (anti-inflammatory),

Runx2 (osteogenic differentiation gene) and *Ocn* (osteogenic differentiation gene) in TDSCs. TDSCs were seeded in 6-well plates and treated with the osteogenic medium containing material leachate (1:10) for 14 days. RAW264.7 cells (Cell Bank, Chinese Academy of Science, CSTR:19375.09.3101MOUTCM13) were pretreated with 10 ng/mL lipopolysaccharides (Beyotime) for 24 hours to mimic inflammation and then incubated with extracts from each group of microspheres for 48 hours. Total RNA was isolated using the EZ pressRNA Purification kit (EZBioscience, Roseville, MN, USA) and reverse transcribed into complementary DNA using the ColorReverseTranscription kit (EZBioscience). A 10 µL reaction system was prepared using 2× SYBRGreenqPCRMasterMix (EZBioscience) and complementary DNA from each group, and quantitative polymerase chain reaction was performed on the ABI7500 polymerase chain reaction instrument (Thermo Fisher Scientific) (95°C for 30 seconds, 1 cycle; 95°C for 5 seconds; 60°C for 30 seconds, 40 cycles). The primer sequences were shown in **Table 1**. Expression levels' normalization was based on glyceraldehyde-3-phosphate dehydrogenase (*GAPDH*) expression. The gene expression level was analysed and calculated by the 2^{-ΔΔCt} method.⁴³

Table 1. The primer sequence for polymerase chain reaction

Gene	Primer sequence (5'-3')
<i>Arg-1</i>	Forward: ATC AAC ACT CCG CTG ACA ACC
	Reverse: ATC TCG CAA GCC GAT GTA CAC
<i>Runx-2</i>	Forward: CGA ACA GAG CAA CAT CTC C
	Reverse: GTC AGT GCC TTC CTT GG
OCN	Forward: ACA AGT CCC ACA CAG CAA C
	Reverse: CCA GGT CAG AGA GGC AGA
<i>GAPDH</i>	Forward: CAA GAA GGT GGT GAA GCA G
	Reverse: CAA AGG TGG AAG AAT GGG

Note: Arg-1: arginase-1; GAPDH: glyceraldehyde-3-phosphate dehydrogenase; OCN: osteocalcin.

Statistical analysis

Student's unpaired *t*-test and one-way analysis of variance followed by Dunnett's multiple comparisons test were performed using GraphPad Prism (version 8.0.2 for Windows, GraphPad Software, San Diego, CA, USA, www.graphpad.com). Differences with *P* values of less than 0.05 indicated significance.

Results

Characterisation of PLLA structure

Nuclear magnetic resonance spectroscopy and Fourier transform infrared spectroscopy were used to analyse the chemical composition of PLLA. The nuclear magnetic resonance spectroscopy spectrum is depicted in **Figure 2A**, PLLA has two typical chemical shifts at 1.57 ppm and 5.17 ppm,⁴⁴ corresponding to the typical (-CH₃) and (-CH) of PLA. A typical Fourier transformed infrared spectrophotometer spectrum of PLLA is shown in **Figure 2B**, where the absorption peak at 2996 cm⁻¹ corresponds to the stretching vibration of

-CH in PLLA, and the absorption peaks at 1456 and 1361 cm⁻¹ correspond to the bending vibration of -CH, the absorption peak at 2881 cm⁻¹ corresponds to the stretching vibration of -CH₃ in PLLA; the absorption peaks at 1760 and 1187 cm⁻¹ correspond to the stretching vibration of -C=O and C-O-C.^{45,46} All these results indicate that PLLA has been successfully synthesised.

Characterisation of microspheres

Figure 3A and **B** depict the morphology and particle size distribution of PM and PMg under the influence of mechanical stirring, and it can be observed from scanning electron microscope images that the PM was well sphericalised, whereas the sphericalisation of PMg was slightly decreased after the addition of MgO/MgCO₃. Both PM and PMg showed a uniform particle size distribution (**Figure 3C** and **D**). The results suggest that there is a tendency for the particle size of the microspheres to decrease after the addition of MgO/MgCO₃. The particle size distribution of microspheres is shown in **Figure 3E**, and was

in the range of 60–100 μm : the particle size of PM was $82.2 \pm 15.3 \mu\text{m}$, and the particle size of PMg was $80.4 \pm 14.6 \mu\text{m}$. Infrared analysis may also be used to examine the structure of PM and PMg, and the results showed that the structure did

not change considerably when compared to the raw material during the creation of microspheres (Figure 3F). The addition of MgO/MgCO_3 did not destroy the crystal structure of PLLA but further increased its crystallinity (Additional Figure 1).

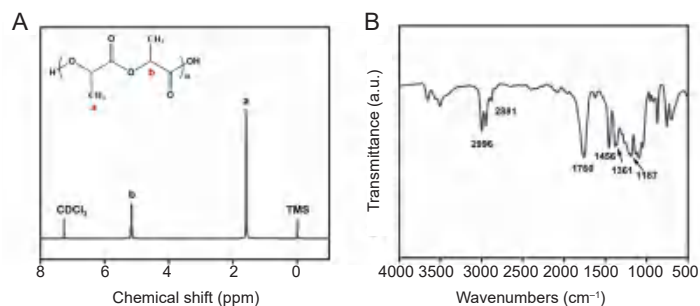


Figure 2. Chemical structure and microstructure analysis of poly(L-lactic acid) (PLLA). (A) Nuclear magnetic resonance spectroscopy, PLLA is a typical structure of polylactide, and the chemical structure of the polymer can be clearly analysed by measuring the chemical shift value of hydrogen. (B) Fourier transformed infrared spectrophotometer, the infrared visible light spectrum can clearly reflect the characteristic functional group structure in the polymer, and the polymer can be detected by the characteristic absorption peak. a.u.: arbitrary unit.

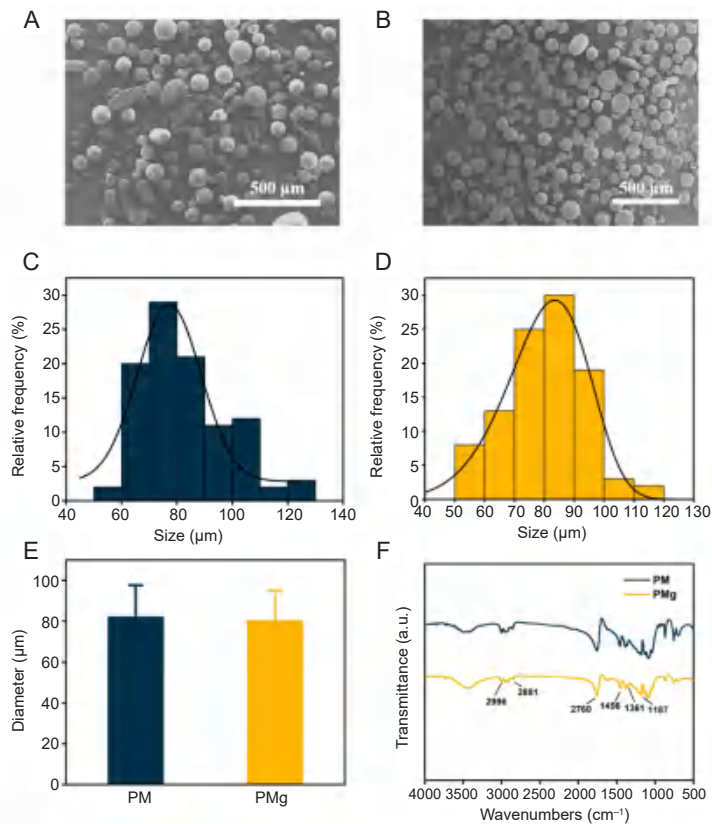


Figure 3. Characterisation of poly(L-lactic acid) microsphere (PM) and poly(L-lactic acid) microsphere loaded with magnesium oxide (MgO)/magnesium carbonate (MgCO_3) (PMg). (A, B) Scanning electron micrograph image of PM (A) and PMg (B). (C, D) Particle size distribution of PM (C) and PMg (D). (E) Particle size of PM and PMg. Data are expressed as mean \pm SD. (F) Fourier transformed infrared spectrophotometer spectra of PM and PMg. a.u.: arbitrary unit.

Figure 4A–D display enlarged electron micrographs of PM and PMg, and the details of PM and PMg, respectively. Although the surface of PM was comparatively smooth, the addition of MgO/MgCO_3 resulted in the formation of

numerous holes on the surface of PMg, which may have been brought on by the CO_2 production from MgCO_3 during the manufacturing of the microspheres. As shown statistically in Figure 4E, the surface of PMg produced many pore structures

with pore diameters in the range of 1–10 μm . The contact angle was measured according to previously reported work.¹⁰ The contact angles of PM and PMg were 112.7° and 113.3° at first second, respectively. After 10 seconds of stationary, the contact angles changed to 110.2° and 103.8°, respectively.

The corresponding contact angles decreased by 2.5° and 9.5°, respectively, and the decrease in the contact angle of PMg (which has a porous structure) was more obvious. This decrease may be caused by that the porous microspheres absorbed more water (Figure 4F).

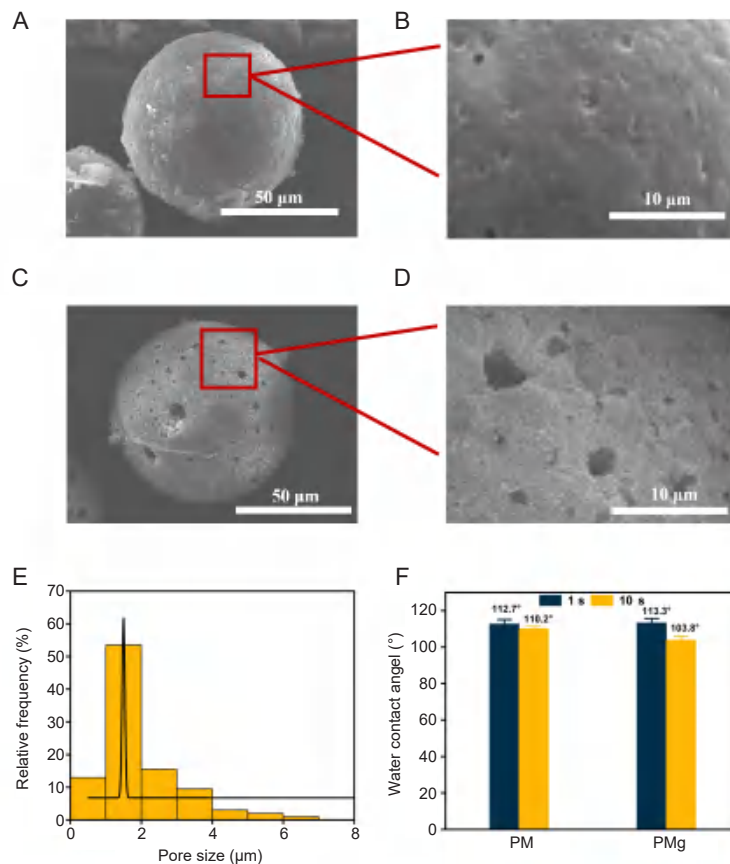


Figure 4. Enlarged microscopic images of poly(L-lactic acid) microsphere (PM) and poly(L-lactic acid) microsphere loaded with magnesium oxide (MgO)/magnesium carbonate (MgCO_3) (PMg). (A–D) PM surface is smooth and without porous structure, and pores appeared on the surface of PMg, which was attributed to the generation of CO_2 from MgCO_3 . Scale bars: 50 μm (A, C), 10 μm (B, D). (E) The distribution of pore size on the surface of PMg. (F) The contact angle test of PM and PMg. PMg is more hydrophilic and absorbent compared to PM. Data are expressed as mean \pm SD.

As indicated in Figure 5A, the number average molecular weight of PM and PMg decreased during the 30-day degradation cycle by 27.8 and 66.3 kDa, respectively, while the number average molecular weight degradation rates were 33.7% and 60.1%, respectively. These results imply that the addition of MgO and MgCO_3 significantly accelerates the molecular weight degradation of microspheres. As shown in Figure 5B, the pH of the degradation solution of PM and PMg changed from the initial 7.30 to 7.17 and 7.33, respectively, compared to PM, the pH of PMg was stabilised in the range of 7.20–7.40 during degradation, which would not interfere with the body's typical acidic and alkaline environments. As shown in Figure 5C, during the 30-day degradation cycle, the release of Mg^{2+} was slightly faster during the first 7 days, and the release of Mg^{2+} continued to be slow from days 7–30, and there was no burst release throughout the degradation. Figure 5D and G are scanning electron microscope images of microspheres before degradation, when degradation

continued for 30 days, numbers of the “crater” structure on the PM surface increased obviously (Figure 5E and F), and the small pores on the surface of PMg gradually grew larger (Figure 5H and I).

In vitro cytocompatibility

The *in vitro* biocompatibility evaluation of the microspheres was further performed using CCK-8. As indicated in Figure 6, the cell survival rate was over 80% after co-cultivating the materials with TDSCs for 24, 48, and 72 hours (Figure 6A). The number of cells gradually increased with the increasing culture time. At 72 hours, the PMg group had the highest number of cells, indicating that the synthesised materials had no obvious inhibitory effects on cell proliferation. The live-dead staining examination revealed that the number of live cells (green) grew steadily while the number of dead cells (red) was zero, demonstrating the biocompatibility of PM and PMg (Figure 6B).

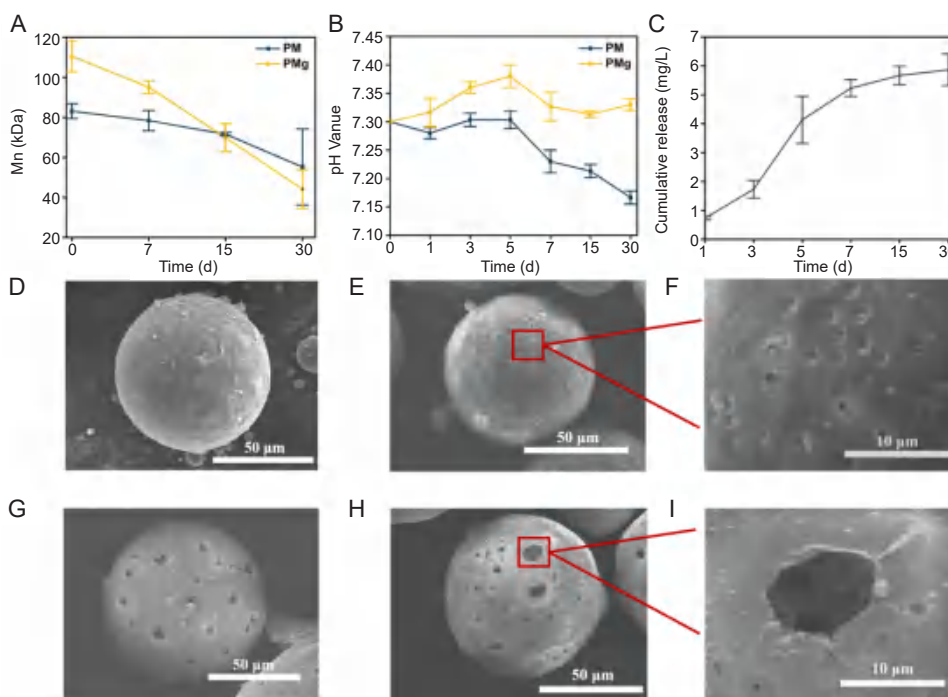


Figure 5. *In vitro* degradation behaviours of poly(L-lactic acid) microsphere (PM) and poly(L-lactic acid) microsphere loaded with magnesium oxide (MgO)/magnesium carbonate (MgCO₃) (PMg). (A) Accelerated degradation of PMg compared to PM, shows that MgO and MgCO₃ accelerate the rate of molecular weight degradation of microspheres. (B) The degradation environment pH of PMg is stable in the neutral range and does not interfere with the body's typical acidic and alkaline environment. (C) No sudden release of Mg²⁺ occurred during the 30-day degradation cycle. Data are expressed as mean ± SD, and were analysed by Student's unpaired *t*-test. (D) The scanning electron micrograph images of PM before degradation. (E) On the 30th day of degradation, scanning electron micrograph image showed that there was a significant increase in the number of "craters" on the surface of PM. (F) Enlarged scanning electron micrograph images at 30 days of PM degradation (G) The scanning electron micrograph images of PMg before degradation. (H) At 30 days of degradation, the electron micrographs showed that the pores on the surface of PMg were significantly enlarged due to corrosion. (I) Enlarged scanning electron micrograph images at 30 days of PMg degradation. Scale bars: 50 μm (D, E, G, H), 10 μm (F, I).

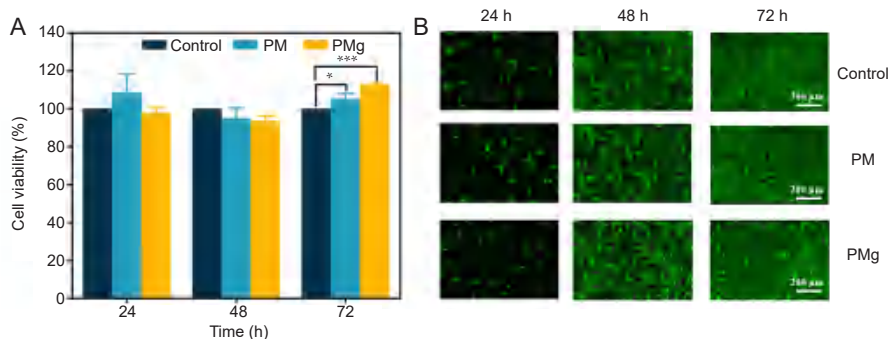


Figure 6. Cytocompatibility evaluation and live-dead staining of poly(L-lactic acid) microsphere (PM) and poly(L-lactic acid) microsphere loaded with magnesium oxide (MgO)/magnesium carbonate (MgCO₃) (PMg). (A) More than 80% of cell viability of tendon-derived stem cells (TDSCs) on PM and PMg, which were normalised by control group. Data are expressed as the mean ± SD (*n* = 3). **P* < 0.05, ****P* < 0.001 (one-way analysis of variance followed by Dunnett's multiple comparisons test). (B) Cytocompatibility of TDSCs on PM and PMg. The live/dead staining assay demonstrated that PM and PMg exhibits no cytotoxicity to cells. TDSCs cultured with osteogenic medium were used as control. Scale bars: 200 μm.

Osteogenic capacity of PM and PMg

Osteoconductive capacity is the ability of a material to support the growth of bone cells on its surface. It is an important property for bone grafts and implants, as it facilitates the

integration of the material with the host bone tissue. ALP is an important biomarker of osteoblast activity. Currently, ALP activity has been used to study bone mineralisation mechanisms and bone-active biomaterials, among others.²³

To demonstrate the osteoconductive ability of the materials, we performed a co-culture of TDSCs with the material-extract medium and evaluated ALP activity and osteogenic gene expression levels. As shown in **Figure 7A**, PM showed a stronger osteogenic capacity as indicated by the significantly higher ALP activities compared with the control, and the PMg with added MgO/MgCO₃ had the strongest osteogenic capacity. The above results suggest that the PLLA material had a certain osteogenic capacity,³⁵ and Mg²⁺ as well as the porous structure of microspheres play a more significant role in promoting the osteogenic differentiation and proliferation of TDSCs.⁴⁷ To examine the potential effect of microsphere degradation on local immune response, the expression of anti-

inflammatory gene (*Arg-1*) was examined in RAW264.7 cells treated with PM and PMg, and the results showed that PMg increased the expression of *Arg-1* compared with PM (**Figure 7B**), which indicated that Mg²⁺ released from microspheres could effectively inhibit inflammation. The effects of PM and PMg on osteogenic differentiation of rat TDSCs continued to be detected by polymerase chain reaction, after 14 days of co-cultivation with the material, there was an increase in the expression of *Runx2* and *Ocn* in PM and PMg compared to the control group, whereas the gene expression in the PMg group was the highest (**Figure 7C and D**), which indicated that the Mg²⁺ produced by PMg group significantly enhanced the osteogenic differentiation of TDSCs.

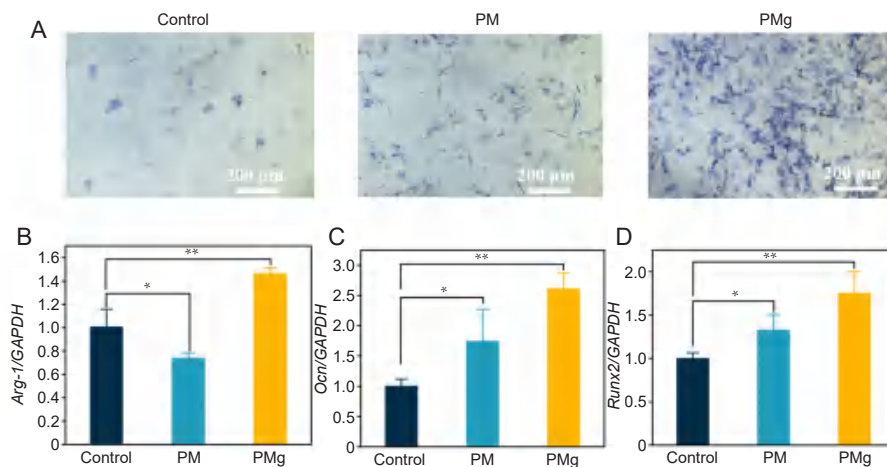


Figure 7. Osteogenic capacity evaluation of poly(L-lactic acid) microsphere (PM) and poly(L-lactic acid) (PLLA) microsphere loaded with magnesium oxide (MgO)/magnesium carbonate (MgCO₃) (PMg). (A) The level of alkaline phosphatase (ALP) was more obvious in PMg compared to PM. PMg has more osteogenic properties compared to PM, while PLLA material has some osteogenic properties compared to the control. (B) The expression of anti-inflammatory gene (arginase-1, *Arg-1*) was more obvious in PMg compared to PM. (C, D) The expression of osteogenic differentiation gene (osteocalcin, *Ocn*) and (*Runx2*) was more obvious in PMg compared to PM, while PLLA material can promote osteogenic differentiation of tendon-derived stem cells (TDSCs) compared to the control. RAW264.7 cells were induced with lipopolysaccharides as controls in B and TDSCs cultured with osteogenic medium were as controls in C and D. Data (normalised by control group) are expressed as the mean \pm SD ($n = 3$). * $P < 0.05$, ** $P < 0.01$ (one-way analysis of variance followed by Dunnett's multiple comparisons test). *GAPDH*: glyceraldehyde-3-phosphate dehydrogenase.

Discussion

PLLA was a promising U.S. Food and Drug Administration-approved biomaterial with excellent biocompatibility and degradability properties.⁴⁸ Therefore, the synthesis and application of PLLA become important, but it was a challenge to use a simple and efficient method to synthesise the PLLA and apply it to biomedical applications.^{49,50} In addition, PLLA can be prepared into different shapes and structure, and employed for biomedical applications, such as, antibacterial,⁵¹ bone regeneration,⁵² anti-inflammatory,⁵³ anti-tumor.⁵⁴ Among them, bioabsorbable microspheres have been widely used for drug delivery⁵⁵ and translational bone regeneration.⁵⁶

Herein, we prepared biodegradable PLLA with good biocompatibility by a simple and green synthesis method, and porous PLLA microspheres (PMg) loaded with MgO/MgCO₃ have a controllable range of particle sizes using the

double-emulsion method. Compared with conventional smooth microspheres, PMg has a rougher surface morphology, which facilitates cell adhesion and proliferation and increases material-cell interactions. In addition, the freeing of hydroxide ions (OH⁻) by PMg degradation not only neutralised the acidity of the PLLA, but also the controlled release of Mg²⁺ promoted the osteogenic differentiation of TDSCs.

Through the results of a large number of literature studies, it was found that when the microspheres were loaded with the same mass of MgO and MgCO₃, the optimal Mg²⁺ release rate of the microspheres was achieved,³⁴ therefore, this study only explored the effect of the same mass of MgO/MgCO₃ on the surface topography of the microspheres and the release of Mg²⁺ and did not further investigate the effect of the different mass ratios of MgO/MgCO₃ on the topography of the microspheres and the Mg²⁺ release rate.

In this study, we successfully prepared porous magnesium-containing microspheres with uniform particle size, combination of large and small pores, and good biocompatibility using solvent evaporation method. The average particle size of the microspheres was 60–100 μm , and the average pore size was 1–10 μm . The generation of pore structure made the surface morphology of the microspheres more controllable, which was more favorable for cell adhesion and proliferation. In addition, the slow release of Mg^{2+} during the microsphere degradation maintains a suitable concentration of Mg^{2+} at the treatment site, which inhibits inflammation and promotes the proliferation and osteogenic differentiation of osteoblasts. Therefore, this study provided an advanced strategy to prepare functionalised microspheres for bone regeneration.

Author contributions

Conceptualization, methodology, project administration and funding acquisition: CL, YL, JZ; study design, and data generation, collection, investigation, and validation: ZT, ZY; manuscript review and editing: ZT, DZ, LQ, LX, SZ. All authors approved the final version of this manuscript.

Financial support

The study was supported by National Key R&D Program of China, Nos. 2018YFE0201500, 2022YFC2405802 and National Natural Science Foundation of China, No. 51973060.

Acknowledgement

None.

Conflicts of interest statement

The authors declare no conflict of interest.

Editor note: Changsheng Liu is an Editorial Board member of *Biomaterials Translational*. He was blinded from reviewing or making decisions on the manuscript. The article was subject to the journal's standard procedures, with peer review handled independently of this Editorial Board member and his research group.

Open access statement

This is an open access journal, and articles are distributed under the terms of the Creative Commons Attribution-NonCommercial-ShareAlike 4.0 License, which allows others to remix, tweak, and build upon the work non-commercially, as long as appropriate credit is given and the new creations are licensed under the identical terms.

Additional file

Additional Figure 1: The X-ray powder diffraction XRD analysis of PM and PMg.

- Cho, E. R.; Kang, S. W.; Kim, B. S. Poly(lactic-co-glycolic acid) microspheres as a potential bulking agent for urological injection therapy: preliminary results. *J Biomed Mater Res B Appl Biomater.* **2005**, *72*, 166-172.
- Gao, Q.; Duan, L.; Feng, X.; Xu, W. Superiority of poly(l-lactic acid) microspheres as dermal fillers. *Chin Chem Lett.* **2021**, *32*, 577-582.
- Kang, S. W.; Cho, E. R.; Jeon, O.; Kim, B. S. The effect of microsphere degradation rate on the efficacy of polymeric microspheres as bulking agents: an 18-month follow-up study. *J Biomed Mater Res B Appl Biomater.* **2007**, *80*, 253-259.
- Zhang, M.; Tang, Y.; Zhu, Z.; Zhao, H.; Yao, J.; Sun, D. Paclitaxel and etoposide-loaded Poly(lactic-co-glycolic acid) microspheres fabricated by coaxial electrospinning for dual drug delivery. *J Biomater Sci Polym Ed.* **2018**, *29*, 1949-1963.
- Yu, C.; Zhu, W.; He, Z.; Xu, J.; Fang, F.; Gao, Z.; Ding, W.; Wang, Y.; Wang, J.; Wang, J.; Huang, A.; Cheng, A.; Wei, Y.; Ai, S. ATP-triggered drug release system based on ZIF-90 loaded porous poly(lactic-co-glycolic acid) microspheres. *Colloids Surf Physicochem Eng Aspects.* **2021**, *615*, 126255.
- Shi, X. D.; Sun, P. J.; Gan, Z.H. Preparation of porous polylactide microspheres and their application in tissue engineering. *Chin J Polym Sci.* **2018**, *36*, 712-719.
- Seyyed Nasrollah, S. A.; Karimi-Soflou, R.; Karkhaneh, A. Photo-click crosslinked hydrogel containing MgO_2 -loaded PLGA microsphere with concurrent magnesium and oxygen release for bone tissue engineering. *Mater Today Chem.* **2023**, *28*, 101389.
- Yuan, X.; Lin, S.; Zhao, K.; Han, Y. Emulsion-ultrasonic spray method to prepare polylactic acid microspheres. *Mater Lett.* **2022**, *309*, 131461.
- Zeng, Y.; Li, X.; Liu, X.; Yang, Y.; Zhou, Z.; Fan, J.; Jiang, H. PLLA porous microsphere-reinforced silk-based scaffolds for auricular cartilage regeneration. *ACS Omega.* **2021**, *6*, 3372-3383.
- Lin, A.; Liu, S.; Xiao, L.; Fu, Y.; Liu, C.; Li, Y. Controllable preparation of bioactive open porous microspheres for tissue engineering. *J Mater Chem B.* **2022**, *10*, 6464-6471.
- Ali, W.; Ali, H.; Gillani, S.; Zinck, P.; Souissi, S. Poly(lactic acid) synthesis, biodegradability, conversion to microplastics and toxicity: a review. *Environ Chem Lett.* **2023**, *21*, 1761-1786.
- Amiryaghoubi, N.; Fathi, M.; Barar, J.; Omidian, H.; Omid, Y. Hybrid polymer-grafted graphene scaffolds for microvascular tissue engineering and regeneration. *Eur Polym J.* **2023**, *193*, 112095.
- Polyák, P.; Nagy, K.; Vértessy, B.; Pukánszky, B. Self-regulating degradation technology for the biodegradation of poly(lactic acid). *Environ Technol Innov.* **2023**, *29*, 103000.
- Bee, S. L.; Hamid, Z. A. A.; Mariatti, M.; Yahaya, B. H.; Lim, K.; Bee, S. T.; Sin, L. T. Approaches to improve therapeutic efficacy of biodegradable PLA/PLGA microspheres: a review. *Polym Rev.* **2018**, *58*, 495-536.
- Sahini, M. G. Poly(lactic acid) (PLA)-based materials: a review on the synthesis and drug delivery applications. *Emergent Mater.* **2023**, *6*, 1461-1479.
- Dodda, J. M.; Azar, M. G.; Bělský, P.; Šlouf, M.; Gajdošová, V.; Kasi, P. B.; Anerillas, L. O.; Kovářik, T. Bioresorbable films of polycaprolactone blended with poly(lactic acid) or poly(lactic-co-glycolic acid). *Int J Biol Macromol.* **2023**, *248*, 126654.
- Bogdanova, A.; Pavlova, E.; Polyanskaya, A.; Volkova, M.; Biryukova, E.; Filkov, G.; Trofimenko, A.; Durymanov, M.; Klinov, D.; Bagrov, D. Acceleration of electrospun PLA degradation by addition of gelatin. *Int J Mol Sci.* **2023**, *24*, 3535.
- Chen, Y.; Geever, L. M.; Killion, J. A.; Lyons, J. G.; Higginbotham, C. L.; Devine, D. M. Review of multifarious applications of poly(lactic acid). *Polym Plast Technol Eng.* **2016**, *55*, 1057-1075.
- Swetha, T. A.; Ananthi, V.; Bora, A.; Sengottuvelan, N.; Ponnuchamy, K.; Muthusamy, G.; Arun, A. A review on biodegradable polylactic acid (PLA) production from fermentative food waste - Its applications and degradation. *Int J Biol Macromol.* **2023**, *234*, 123703.
- Brunšek, R.; Kopitar, D.; Schwarz, I.; Marasović, P. Biodegradation properties of cellulose fibers and PLA biopolymer. *Polymers (Basel).* **2023**, *15*, 3532.
- Shahdan, D.; Rosli, N. A.; Chen, R. S.; Ahmad, S.; Gan, S. Strategies for strengthening toughened poly(lactic acid) blend via natural reinforcement with enhanced biodegradability: A review. *Int J Biol Macromol.* **2023**, *251*, 126214.
- Niu, Y.; Stadler, F. J.; Fu, M. Biomimetic electrospun tubular PLLA/gelatin nanofiber scaffold promoting regeneration of sciatic nerve transection in SD rat. *Mater Sci Eng C Mater Biol Appl.* **2021**, *121*, 111858.
- Hou, Y.; Zhang, R.; Cheng, H.; Wang, Y.; Zhang, Q.; Zhang, L.; Wang, L.; Li, R.; Wu, X.; Li, B. Mg^{2+} -doped carbon dots synthesized based

- on Lycium ruthenicum in cell imaging and promoting osteogenic differentiation in vitro. *Colloids Surf Physicochem Eng Aspects*. **2023**, *656*, 130264.
24. Zhu, S.; Dai, Q.; Yao, L.; Wang, Z.; He, Z.; Li, M.; Wang, H.; Li, Q.; Gao, H.; Cao, X. Engineered multifunctional nanocomposite hydrogel dressing to promote vascularization and anti-inflammation by sustained releasing of Mg²⁺ for diabetic wounds. *Compos B Eng*. **2022**, *231*, 109569.
 25. Zhang, X.; Huang, P.; Jiang, G.; Zhang, M.; Yu, F.; Dong, X.; Wang, L.; Chen, Y.; Zhang, W.; Qi, Y.; Li, W.; Zeng, H. A novel magnesium ion-incorporating dual-crosslinked hydrogel to improve bone scaffold-mediated osteogenesis and angiogenesis. *Mater Sci Eng C Mater Biol Appl*. **2021**, *121*, 111868.
 26. Zhu, Y.; Zhao, S.; Cheng, L.; Lin, Z.; Zeng, M.; Ruan, Z.; Sun, B.; Luo, Z.; Tang, Y.; Long, H. Mg²⁺-mediated autophagy-dependent polarization of macrophages mediates the osteogenesis of bone marrow stromal stem cells by interfering with macrophage-derived exosomes containing miR-381. *J Orthop Res*. **2022**, *40*, 1563-1576.
 27. Faisal, S.; Abdullah, Jan, H.; Shah, S. A.; Shah, S.; Rizwan, M.; Zaman, N.; Hussain, Z.; Uddin, M. N.; Bibi, N.; Khattak, A.; Khan, W.; Iqbal, A.; Idrees, M.; Masood, R. Bio-catalytic activity of novel mentha arvensis intervened biocompatible magnesium oxide nanomaterials. *Catalysts*. **2021**, *11*, 780.
 28. Li, J.; Khalid, A.; Verma, R.; Abraham, A.; Qazi, F.; Dong, X.; Liang, G.; Tomljenovic-Hanic, S. Silk fibroin coated magnesium oxide nanospheres: a biocompatible and biodegradable tool for noninvasive bioimaging applications. *Nanomaterials (Basel)*. **2021**, *11*, 695.
 29. Welch, K.; Latifzada, M. A.; Frykstrand, S.; Strømme, M. Investigation of the antibacterial effect of mesoporous magnesium carbonate. *ACS Omega*. **2016**, *1*, 907-914.
 30. Palominos, N.; Castillo, A.; Guerrero, L.; Borja, R.; Huiliñir, C. Coupling of anaerobic digestion and struvite precipitation in the same reactor: effect of zeolite and bischofite as Mg²⁺ source. *Front Environ Sci*. **2021**, *9*, 706730.
 31. Hornak, J. Synthesis, properties, and selected technical applications of magnesium oxide nanoparticles: a review. *Int J Mol Sci*. **2021**, *22*, 12752.
 32. Lin, Z.; Shen, D.; Zhou, W.; Zheng, Y.; Kong, T.; Liu, X.; Wu, S.; Chu, P. K.; Zhao, Y.; Wu, J.; Cheung, K. M. C.; Yeung, K. W. K. Regulation of extracellular bioactive cations in bone tissue microenvironment induces favorable osteoimmune conditions to accelerate in situ bone regeneration. *Bioact Mater*. **2021**, *6*, 2315-2330.
 33. Fan, D.; De Rosa, E.; Murphy, M. B.; Peng, Y.; Smid, C. A.; Chiappini, C.; Liu, X.; Simmons, P.; Weiner, B. K.; Ferrari, M.; Tasciotti, E. Mesoporous silicon-PLGA composite microspheres for the double controlled release of biomolecules for orthopedic tissue engineering. *Adv Funct Mater*. **2012**, *22*, 282-293.
 34. Yuan, Z.; Wei, P.; Huang, Y.; Zhang, W.; Chen, F.; Zhang, X.; Mao, J.; Chen, D.; Cai, Q.; Yang, X. Injectable PLGA microspheres with tunable magnesium ion release for promoting bone regeneration. *Acta Biomater*. **2019**, *85*, 294-309.
 35. Wang, L.; Li, Y.; Jiang, S.; Zhang, Z.; Zhao, S.; Song, Y.; Liu, J.; Tan, F. Alginate hydrogels containing different concentrations of magnesium-containing poly(lactic-co-glycolic acid) microspheres for bone tissue engineering. *Biomed Mater*. **2023**, *18*, 055022.
 36. Yuan, X.; Yang, W.; Fu, Y.; Tao, Z.; Xiao, L.; Zheng, Q.; Wu, D.; Zhang, M.; Li, L.; Lu, Z.; Wu, Y.; Gao, J.; Li, Y. Four-arm polymer-guided formation of curcumin-loaded flower-like porous microspheres as injectable cell carriers for diabetic wound healing. *Adv Healthc Mater*. **2023**, e2301486.
 37. Hong, Y.; Gao, C.; Shi, Y.; Shen, J. Preparation of porous polylactide microspheres by emulsion-solvent evaporation based on solution induced phase separation. *Polym Adv Technol*. **2005**, *16*, 622-627.
 38. Lee, H.; Nguyen, T. T.; Kim, M.; Jeong, J. H.; Park, J. B. The effects of biodegradable poly(lactic-co-glycolic acid)-based microspheres loaded with quercetin on stemness, viability and osteogenic differentiation potential of stem cell spheroids. *J Periodontol Res*. **2018**, *53*, 801-815.
 39. Yang, S.; Liu, H.; Huang, H.; Zhang, Z. Fabrication of superparamagnetic magnetite/poly(styrene-co-12-acryloxy-9-octadecenoic acid) nanocomposite microspheres with controllable structure. *J Colloid Interface Sci*. **2009**, *338*, 584-590.
 40. Pan, X.; Gao, M.; Wang, Y.; He, Y.; Si, T.; Sun, Y. Poly(lactic acid)-aspirin microspheres prepared via the traditional and improved solvent evaporation methods and its application performances. *Chin J Chem Eng*. **2023**, *60*, 194-204.
 41. Schneider, C. A.; Rasband, W. S.; Eliceiri, K. W. NIH image to ImageJ: 25 years of image analysis. *Nat Methods*. **2012**, *9*, 671-675.
 42. Rui, Y. F.; Lui, P. P.; Li, G.; Fu, S. C.; Lee, Y. W.; Chan, K. M. Isolation and characterization of multipotent rat tendon-derived stem cells. *Tissue Eng Part A*. **2010**, *16*, 1549-1558.
 43. Livak, K. J.; Schmittgen, T. D. Analysis of relative gene expression data using real-time quantitative PCR and the 2(-Delta Delta C(T)) Method. *Methods*. **2001**, *25*, 402-408.
 44. Liu, S.; Chen, W.; Xiao, L.; Zhao, Z.; Liu, F.; Lu, S.; Chen, C.; Luo, W.; Jiang, L.; Li, Y. Robust osteoconductive β -tricalcium phosphate/L-poly(lactic acid) membrane via orientation-strengthening technology. *ACS Biomater Sci Eng*. **2023**, *9*, 5293-5303.
 45. Yuan, X.; Yang, W.; Fu, Y.; Tao, Z.; Xiao, L.; Zheng, Q.; Wu, D.; Zhang, M.; Li, L.; Lu, Z.; Wu, Y.; Gao, J.; Li, Y. Four-arm polymer-guided formation of curcumin-loaded flower-like porous microspheres as injectable cell carriers for diabetic wound healing. *Adv Healthc Mater*. **2023**, *12*, e2301486.
 46. Lai, X. L.; Yang, W.; Wang, Z.; Shi, D. W.; Liu, Z. Y.; Yang, M. B. Enhancing crystallization rate and melt strength of PLLA with four-arm PLLA grafted silica: the effect of molecular weight of the grafting PLLA chains. *J Appl Polym Sci*. **2018**, *135*, 45675.
 47. Lee, J. Y.; Kim, S. E.; Yun, Y. P.; Choi, S. W.; Jeon, D. I.; Kim, H. J.; Park, K.; Song, H. R. Osteogenesis and new bone formation of alendronate-immobilized porous PLGA microspheres in a rat calvarial defect model. *J Ind Eng Chem*. **2017**, *52*, 277-286.
 48. Capuana, E.; Lopresti, F.; Ceraulo, M.; La Carrubba, V. Poly-L-lactic acid (PLLA)-based biomaterials for regenerative medicine: a review on processing and applications. *Polymers (Basel)*. **2022**, *14*, 1153.
 49. Zan, J.; Qian, G.; Deng, F.; Zhang, J.; Zeng, Z.; Peng, S.; Shuai, C. Dilemma and breakthrough of biodegradable poly-L-lactic acid in bone tissue repair. *J Mater Res Technol*. **2022**, *17*, 2369-2387.
 50. Feng, P.; Shen, S.; Shuai, Y.; Peng, S.; Shuai, C.; Chen, S. PLLA grafting draws GO from PGA phase to the interface in PLLA/PGA bone scaffold owing enhanced interfacial interaction. *Sustain Mater Technol*. **2023**, *35*, e00566.
 51. Yao, H.; Wang, J.; Deng, Y.; Li, Z.; Wei, J. Osteogenic and antibacterial PLLA membrane for bone tissue engineering. *Int J Biol Macromol*. **2023**, *247*, 125671.
 52. Han, X.; Zhou, X.; Qiu, K.; Feng, W.; Mo, H.; Wang, M.; Wang, J.; He, C. Strontium-incorporated mineralized PLLA nanofibrous membranes for promoting bone defect repair. *Colloids Surf B Biointerfaces*. **2019**, *179*, 363-373.
 53. Baek, S. W.; Kim, D. S.; Song, D. H.; Lee, S.; Lee, J. K.; Park, S. Y.; Kim,

- J. H.; Kim, T. H.; Park, C. G.; Han, D. K. PLLA composites combined with delivery system of bioactive agents for anti-inflammation and re-endothelialization. *Pharmaceutics*. **2022**, *14*, 2661.
54. Shuai, Y. A tumor-microenvironment-activated nanoplatform of modified SnFe₂O₄ nanozyme in scaffold for enhanced PTT/PDT tumor therapy. *Heliyon*. **2023**, *9*, e18019.
55. Li, B.; Yang, H.; Cheng, K.; Song, H.; Zou, J.; Li, C.; Xiao, W.; Liu, Z.; Liao, X. Development of magnetic poly(L-lactic Acid) nanofibrous microspheres for transporting and delivering targeted cells. *Colloids Surf B Biointerfaces*. **2023**, *223*, 113175.
56. Wang, Y.; Zhao, L.; Zhou, L.; Chen, C.; Chen, G. Sequential release of vascular endothelial growth factor-A and bone morphogenetic protein-2 from osteogenic scaffolds assembled by PLGA microcapsules: A preliminary study in vitro. *Int J Biol Macromol*. **2023**, *232*, 123330.

Received: October 20, 2023

Revised: November 14, 2023

Accepted: November 25, 2023

Available online: December 28, 2023

AI accelerated discovery of self-assembling peptides

Yejiao Shi^{1,*}, Honggang Hu^{2,*}

Self-assembly is a process capitalized by nature for converting chemically simple building blocks into hierarchically ordered structures and materials to function in living systems cooperatively.¹ Among all the building blocks, proteins are the most commonly utilized and form diverse structures ranging from oligomers and nanospheres to tubes and hierarchical architectures.² These structures with unique physical properties play crucial roles in vast biological functions, for instance, structural support, cargo transport, and microbial defence.³ The formation of these structures is predominantly driven and governed by non-covalent interactions, conferring the dynamism and flexibility of these structures. By studying the fundamental principles that control the self-assembly processes of native proteins, functional materials can be replicated in a bottom-up approach, whereby synthetic building blocks are designed for assembling into desired architectures with specific properties.⁴ In this context, biomimetic peptides with comparatively shorter sequences than proteins emerge as ideal building blocks.⁵ They provide a versatile approach for mimicking complex structures and materials with structural and functional diversity in a more tractable but less expensive approach.

The self-assembly behaviours of peptides depend strongly on their amino acid sequences.⁶ To date, the design of self-assembling peptides still relies on the examination of natural amino acid sequences, professional expertise in the peptide field, or laboratory discoveries by serendipity. However, these inefficient approaches fail to meet the growing demands for functional peptide materials since the design range of self-assembling peptides can be extremely broad. The amount of possible amino acid combinations for a peptide can reach up to 20^n , where 20 is the number of commonly available amino acids and n is the amino acid number in the peptide.⁷ For instance, tripeptides ($n = 3$) containing 8000 combinations are intractable for any rigorous experimental study. Even though a brute-

force computational search based on coarse-gained molecular dynamic (MD) simulations has been proposed by Ulijn's team to overcome the search bias and has successfully identified several self-assembling tripeptides.⁸ Due to the high computational costs, it is impossible to extend it to longer sequence lengths ($n > 3$). Accurate prediction of the assembling processes and discovery of the assembling peptides remain challenging.

Artificial intelligence (AI) is an emerging interdisciplinary that integrates computer science, mathematics, and psychology among others to emulate human cognitive functions for tasks requiring intelligence, such as language understanding and decision making.⁹ It holds great potential to navigate through the vast search space among amino acid combinations and present a subset displaying the most promising possibilities. Recently, writing in Nature Chemistry, Sankaranarayanan's team introduced an "AI expert" that combined the Monte Carlo tree search (MCTS) algorithm with coarse-gained MD simulations for identifying self-assembling peptides that exhibit high aggregation propensities in aqueous solution.¹⁰

Performing in an autonomous way, the AI expert first utilized MCTS to generate peptide sequences before utilising MD simulations to estimate the aggregation propensity of the generated sequences and provide feedback to improve the quality of MCTS and guide future searches (Figure 1). Notably, an innovative concept of uniqueness function within the MCTS objective function, together with a random forest based surrogate model were included to boost the performance of the MCST algorithm. Compared to MCTS without the random forest model, random search, and brute-force search, the AI expert enabled by MCTS and random forest scheme was demonstrated to be the most efficient in identifying tripeptide with the highest-scoring.

1 Institute of Translational Medicine, Shanghai University, Shanghai, China;
2 School of Medicine, Shanghai University, Shanghai, China

***Corresponding authors:**

Yejiao Shi,
sh10yj@shu.edu.cn;
Honggang Hu,
hhu66@shu.edu.cn.

<http://doi.org/10.12336/biomatertransl.2023.04.008>

How to cite this article:
Shi, Y.; Hu, H. AI accelerated discovery of self-assembling peptides. *Biomater Transl.* 2023, 4(4), 291-293.



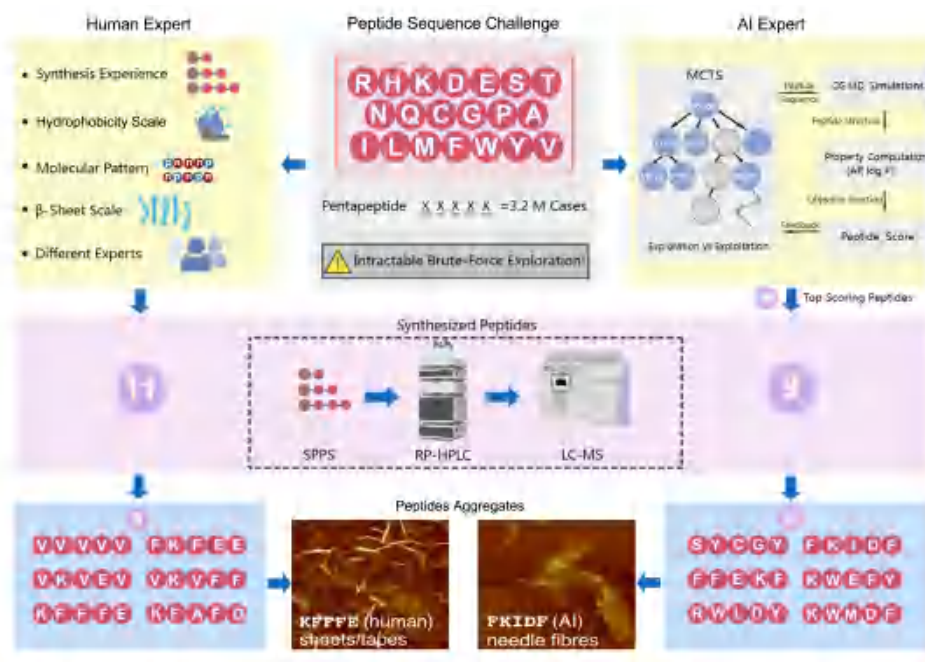


Figure 1. Comparison of the workflow using the input of self-assembling pentapeptides from AI expert and human expert. The search range for peptides increases dramatically due to the multiple combinations of 20 amino acids, and 3.2 million pentapeptides are unmanageable to be calculated with the brute-force method. Human expert adopted rationally design methods such as hydrophobic scales, molecular patterns (nprnp), and personal experience. Six of the eleven pentapeptides proposed by six human experts were synthesised and observed to be clustered together. In contrast, AI expert developed a combination of MCTS. Six of the nine pentapeptides proposed by the AI expert were synthesised and found to be clustered. AI expert has also proposed novel sequences involving multiple amino acids to recover some intuitive sequences, reflecting its advantages in overcoming human bias. Atomic force microscope images of some promising pentapeptides from both groups are shown. Created with MedPeer (www.medpeer.cn). AI: artificial intelligence; AP: aggregation propensity; CG: coarse-grained; LC-MS: liquid chromatography-mass spectrometry; MCTS: Monte Carlo tree searches; MD: molecular dynamic; n: non-polar; p: polarity; RP-HPLC: reverse phase high performance liquid chromatography; SPPS: solid phase peptide synthesis.

Having validated the efficiency of AI experts, Sankaranarayanan and colleagues went on using it to discover self-assembling pentapeptides. Among the 3.2 million (20^5) pentapeptide permutations, the AI expert first evaluated approximately 6600 cases based on MD simulations and then selected the top 100 candidates for further MD simulations using more rigorous parameters and longer timescales to improve the estimates of aggregation propensity. Nine candidates with top scores were filtered out and six of them were observed to aggregate according to experimental dynamic light scattering and atomic force microscope measurements. Comparatively, six out of eleven pentapeptides proposed by human experts were found to aggregate. By analysing the sequence similarity of identified peptides, the AI expert was found could not only recover known sequences similar to the human experts but also discover unknown sequences that deviate notably from the existing ones, indicating its potential to overcome the bias from humans and accelerate the discovery of peptides.

Integrated with coarse-grained MD, machine learning, and experiments, the AI expert was demonstrated to be an efficient “human-in-the-loop” framework for the discovery of self-assembling peptides. Future efforts were anticipated to be made to connect the developed AI expert to a robotic platform that

can synthesise and characterise innovative peptides. As such experimental feedback could be digested by AI expert directly, supporting the search to progress in an iterative manner. Additional information obtained from the simulations, for instance, the aspect ratio and number of the peptides, their morphologies, and their moments of inertia were expected to be included to improve the MCTS scoring function. Similar AI strategies could also be developed for screening and discovering more functional peptides and peptide assemblies, providing great potential for further innovations in peptide-based novel therapeutics and functional materials.

Author contributions

YJS conceived and wrote the draft, HGH reviewed and edited the draft. Both authors approved the final version of the manuscript.

Financial support

The work was supported by the Shanghai Pujiang Program (No. 21PJ1404100).

Acknowledgement

None.

Conflicts of interest statement

The authors declare no conflicts of interest.

Open access statement

This is an open access journal, and articles are distributed under the terms of the Creative Commons Attribution-NonCommercial-ShareAlike 4.0 License, which allows others to remix, tweak, and build upon the work noncommercially, as long as appropriate credit is given and the new creations are licensed under the identical terms.

- Whitesides, G. M.; Grzybowski, B. Self-assembly at all scales. *Science*. **2002**, *295*, 2418-2421.
- Luo, Q.; Hou, C.; Bai, Y.; Wang, R.; Liu, J. Protein assembly: versatile approaches to construct highly ordered nanostructures. *Chem Rev*. **2016**, *116*, 13571-13632.
- Desai, M. S.; Lee, S. W. Protein-based functional nanomaterial design for bioengineering applications. *Wiley Interdiscip Rev Nanomed Nanobiotechnol*. **2015**, *7*, 69-97.
- Zhang, S. Fabrication of novel biomaterials through molecular self-assembly. *Nat Biotechnol*. **2003**, *21*, 1171-1178.
- Pearce, A. K.; Wilks, T. R.; Arno, M. C.; O'Reilly, R. K. Synthesis and applications of anisotropic nanoparticles with precisely defined dimensions. *Nat Rev Chem*. **2021**, *5*, 21-45.
- Mendes, A. C.; Baran, E. T.; Reis, R. L.; Azevedo, H. S. Self-assembly in nature: using the principles of nature to create complex nanobiomaterials. *Wiley Interdiscip Rev Nanomed Nanobiotechnol*. **2013**, *5*, 582-612.
- Ulijn, R. V.; Smith, A. M. Designing peptide based nanomaterials. *Chem Soc Rev*. **2008**, *37*, 664-675.
- Frederix, P. W.; Scott, G. G.; Abul-Haija, Y. M.; Kalafatovic, D.; Pappas, C. G.; Javid, N.; Hunt, N. T.; Ulijn, R. V.; Tuttle, T. Exploring the sequence space for (tri-)peptide self-assembly to design and discover new hydrogels. *Nat Chem*. **2015**, *7*, 30-37.
- Hamet, P.; Tremblay, J. Artificial intelligence in medicine. *Metabolism*. **2017**, *69s*, S36-S40.
- Batra, R.; Loeffler, T. D.; Chan, H.; Srinivasan, S.; Cui, H.; Korendovych, I. V.; Nanda, V.; Palmer, L. C.; Solomon, L. A.; Fry, H. C.; Sankaranarayanan, S. Machine learning overcomes human bias in the discovery of self-assembling peptides. *Nat Chem*. **2022**, *14*, 1427-1435.

Received: November 12, 2023

Revised: November 29, 2023

Accepted: December 2, 2023

Available online: December 28, 2023

Early immunomodulation by magnesium ion: catalyst for superior osteogenesis

Bo Li*

The bioactive ion, magnesium ion (Mg^{2+}), serving as a vital factor in promoting osteogenesis, has received a decade-long of attention and research.^{1, 2} Over the past decades, numerous works have revealed the positive effects of Mg^{2+} on osteogenesis, and the underlying mechanisms were also investigated in detail. For instance, numerous researchers attribute the positive effects of Mg^{2+} on osteogenesis to its immunomodulatory property, which hastens the transition of pro-inflammatory M1 phenotype to the anti-inflammatory M2 phenotype of macrophages, consequently enhancing osteogenesis.^{3, 4} Additionally, Zheng et al.⁵ discovered alternative mechanisms through which Mg^{2+} promotes osteogenesis. They elucidated that Mg^{2+} elevates neuronal calcitonin gene-related polypeptide- α levels in the femoral peripheral cortex and the ipsilateral dorsal root ganglia, which, in turn, leads to calcitonin receptor-like receptor- and receptor activity-modifying protein 1-dependent activation of cyclic adenosine monophosphate-responsive element binding protein 1 and osterix, ultimately enhancing the osteo-differentiation of isolated rat stem cells. This work offers valuable insights into the effect of Mg^{2+} in accelerating calcitonin gene-related polypeptide- α -mediated osteo-differentiation, shedding light on the therapeutic potential of Mg^{2+} in bone injury, especially in addressing special pathologic conditions like osteoporosis. Nevertheless, detrimental effects on osteogenesis of Mg^{2+} released upon degradation of Mg-based implants also have been detected.^{6, 7} These contradictory outcomes may stem from an imprecise understanding of the multifaceted roles of Mg^{2+} in the intricate biological process of bone healing, suggesting the possibility that different types of cells engaged in various phases of bone formation may respond to Mg^{2+} in distinct ways. Reporting in *Nature Communications*, Qiao et al.⁸ provide a detailed investigation into the effects and the underlying biological mechanism of

Mg^{2+} on immunomodulatory osteogenesis, with a special focus on its dose- and time-dependent behaviour. Transient exposure to Mg^{2+} during the first week at an artificial defect in the distal end of rat femora results in significant increases in trabecular bone fraction, trabecular number, bone mineral density and trabecular thickness without compromising the mechanical properties of the new bone when compared to both the control group without Mg^{2+} exposure and the sham group. Meanwhile, in the Mg^{2+} exposure group, a decrease in the number of osteoclasts was observed on day 56. Conversely, the enhanced role of Mg^{2+} in osteogenesis is attenuated when exposure is delayed to the 2nd week, even at the same dose. Furthermore, continuous Mg^{2+} delivery over the initial 2 weeks post-injury shows no differences in bone formation between Mg^{2+} treatment group and the group without Mg^{2+} exposure. Based on these findings, it appears that Mg^{2+} boosts osteogenesis when administered during the beginning stage of bone formation, while extended treatment seems to have detrimental effects on bone formation.

The authors attribute the time-dependent modulatory effects of Mg^{2+} on osteogenesis to its modulation of macrophages. Concretely, extracellular Mg^{2+} significantly promotes the activities of monocytes and their maturation into macrophages, and the enhanced effects positively correlate to the concentration of extracellular Mg^{2+} . More importantly, extracellular Mg^{2+} facilitates the upregulation of genes encoding cytokines in monocytes-derived macrophages that favour osteogenesis, including C-C motif chemokine ligand 5, interleukin (IL)-1 receptor antagonist, IL-8, transforming growth factor- β 1, bone morphogenetic protein 2, vascular endothelial growth factor A, IL-10, and the downregulation of genes encoding cytokines that favour osteoclastogenesis, such as oncostatin M, IL-6, IL-1 β , tumour necrosis factor α . It is because that extracellular Mg^{2+} contributes to

State Key Laboratory for Mechanical Behavior of Materials, Xi'an Jiaotong University, Xi'an, Shaanxi Province, China

***Corresponding author:**

Bo Li,
libo1137@xjtu.edu.cn.

<http://doi.org/10.12336/biomatertransl.2023.04.009>

How to cite this article:

Li, B. Early immunomodulation by magnesium ion: catalyst for superior osteogenesis. *Biomater Transl.* 2023, 4(4), 294-296.



the elevated expression of the transient receptor potential cation channel member 7, and triggers a transient receptor potential cation channel member 7-dependent Mg^{2+} influx in macrophages. This process results in the cleavage and nuclear accumulation of transient receptor potential cation channel member 7-cleaved kinase fragments, which leads to the phosphorylation of Histone H3, giving rise to the transition of macrophage into a pro-osteogenic phenotype. Sequentially, IL-8 secreted by macrophages predominantly enhances the osteogenic effect when it appears within the first week of culture, while impairing the mineralisation process when present in the later stages of osteo-differentiation. Noticeably, the enhanced role of Mg^{2+} exposure in the osteogenic behaviours of mesenchymal stem cells is more pronounced when mediated by macrophages, compared to its direct effect on mesenchymal stem cells. In addition, prolonged exposure to Mg^{2+} (3 days or more) leads to elevated expression of inhibitory- κ B kinase- α and - β in macrophages to phosphorylate inhibitor of κ B and translocate p65 into nuclear, thereby over-activating the nuclear factor kappa B signalling pathway. This upregulation promotes osteoclastic differentiation of

macrophages, increasing the amount of tartrate resistant acid phosphatase positive cells, and hinders extracellular matrix calcification, ultimately compromising bone formation (**Figure 1A**). This work conducts an in-depth investigation into the effects of Mg^{2+} on immunomodulatory osteogenesis, unveiling an effective window for administrating Mg^{2+} to facilitate bone healing: emphasizing the greater significance of the initial inflammation stage over the subsequent active bone repair stage.

Progressively, in a follow-up study, the authors further discovered that divalent metal cations like Mg^{2+} , Zn^{2+} , and Cu^{2+} stimulate macrophages to secrete prostaglandin E2, which interacts with prostaglandin E2 receptor 4 in sensory nerves, promoting their sprouting and arborisation.⁹ This behaviour, regulated through cyclic adenosine monophosphate-response element binding protein signalling, leads to a downregulation of sympathetic tone, giving rise to promoted osteogenesis and downregulated osteoclastogenesis in the injured bone (**Figure 1B**). This work elucidates how Mg^{2+} mediates osteogenic effects through the interplay between immunomodulation and neuroregulation.

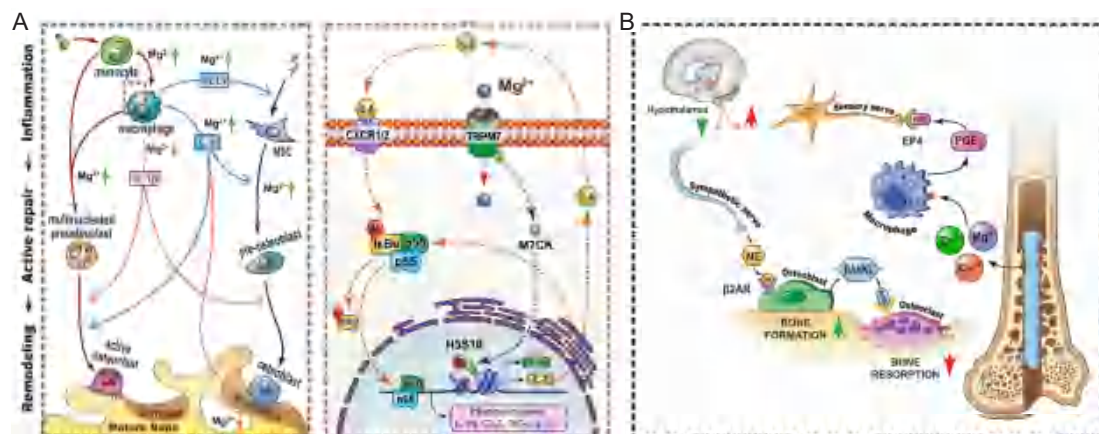


Figure 1. (A) Schematic illustration showing the mechanism by which Mg^{2+} regulates both macrophages and mesenchymal stem cells in the bone remodeling process. Reprinted from Qiao et al.⁸ (B) schematic illustration showing the interplay between Mg^{2+} induced immunomodulation and central neuroregulation. Reprinted from Qiao et al.⁹

More generally, Mg plays an enhanced role in osteogenesis; however, optimising the ideal administration window is crucial for maximising its effectiveness and achieve greater efficiency. Simultaneously, the enhanced osteogenetic mechanism of Mg^{2+} likely initiates through early immunomodulation, followed by a complex series of physiological processes, involving osteogenic differentiation of mesenchymal stem cells, osteoclastic differentiation of macrophages, central neuroregulation and more. These works provide great enlightening and guiding insights, reminding researchers to bear in mind the balance between the osteo-enhancing and -impairing effects of Mg^{2+} exposure when utilizing Mg-based orthopaedic implants. Crucially, delving into the cross-talk between inflammation responses triggered by divalent metal cations and the subsequent physiological processes can potentially spark

innovation in orthopaedic biomaterials infused with bioactive metal cations for advanced bone tissue engineering.

It is also needed to point out that recent works on the immunomodulatory osteogenic effects of Mg^{2+} have primarily concentrated on its regulation of innate immune responses, such as macrophage polarisation.^{3, 4, 8, 9} Nevertheless, the adaptive immune system, particularly T cells, also holds significant sway in maintaining bone homeostasis.^{10, 11} However, until now, the regulatory effects and underlying mechanism of Mg^{2+} on the adaptive immune system, as well as its subsequent cross-talk with osteogenesis-related cells have not been explored. Hence, it is expected that the upcoming studies will unveil these associated effects and mechanisms, further maximising the osteogenic effects of orthopaedic implants through the controlled release of bioactive ions.

Author contributions

BL: Conceptualization, investigation, and writing-review & editing. The author read and approved the final version of the manuscript.

Financial support

None.

Acknowledgement

The work was supported by the Shaanxi Province Natural Science Research Program, Nos. 2023YBSF194, 2023LLQY44; State Key Laboratory of Solidification Processing in NWP, No. SKLSP202313; and Sichuan Science and Technology Program, No. 2022NSFSC1966.

Conflicts of interest statement

None.

Open access statement

This is an open access journal, and articles are distributed under the terms of the Creative Commons Attribution-NonCommercial-ShareAlike 4.0 License, which allows others to remix, tweak, and build upon the work noncommercially, as long as appropriate credit is given and the new creations are licensed under the identical terms.

1. Wang, J. L.; Xu, J. K.; Hopkins, C.; Chow, D. H.; Qin, L. Biodegradable magnesium-based implants in orthopedics-a general review and perspectives. *Adv Sci (Weinh)*. **2020**, *7*, 1902443.
2. Staiger, M. P.; Pietak, A. M.; Huadmai, J.; Dias, G. Magnesium and its alloys as orthopedic biomaterials: a review. *Biomaterials*. **2006**, *27*, 1728-1734.
3. Yu, D.; Li, B.; Yu, M.; Guo, S.; Guo, Z.; Han, Y. Cubic multi-ions-doped Na(2)TiO(3) nanorod-like coatings: Structure-stable, highly efficient platform for ions-exchanged release to immunomodulatory promotion on vascularized bone apposition. *Bioact Mater*. **2022**, *18*, 72-90.
4. Lin, Z.; Shen, D.; Zhou, W.; Zheng, Y.; Kong, T.; Liu, X.; Wu, S.; Chu, P. K.; Zhao, Y.; Wu, J.; Cheung, K. M. C.; Yeung, K. W. K. Regulation of extracellular bioactive cations in bone tissue microenvironment induces favorable osteoimmune conditions to accelerate in situ bone regeneration. *Bioact Mater*. **2021**, *6*, 2315-2330.
5. Zhang, Y.; Xu, J.; Ruan, Y. C.; Yu, M. K.; O'Laughlin, M.; Wise, H.; Chen, D.; Tian, L.; Shi, D.; Wang, J.; Chen, S.; Feng, J. Q.; Chow, D. H.; Xie, X.; Zheng, L.; Huang, L.; Huang, S.; Leung, K.; Lu, N.; Zhao, L.; Li, H.; Zhao, D.; Guo, X.; Chan, K.; Witte, F.; Chan, H. C.; Zheng, Y.; Qin, L. Implant-derived magnesium induces local neuronal production of CGRP to improve bone-fracture healing in rats. *Nat Med*. **2016**, *22*, 1160-1169.
6. Luthringer, B. J.; Willumeit-Römer, R. Effects of magnesium degradation products on mesenchymal stem cell fate and osteoblastogenesis. *Gene*. **2016**, *575*, 9-20.
7. Lawrence, T.; Natoli, G. Transcriptional regulation of macrophage polarization: enabling diversity with identity. *Nat Rev Immunol*. **2011**, *11*, 750-761.
8. Qiao, W.; Wong, K. H. M.; Shen, J.; Wang, W.; Wu, J.; Li, J.; Lin, Z.; Chen, Z.; Matinlinna, J. P.; Zheng, Y.; Wu, S.; Liu, X.; Lai, K. P.; Chen, Z.; Lam, Y. W.; Cheung, K. M. C.; Yeung, K. W. K. TRPM7 kinase-mediated immunomodulation in macrophage plays a central role in magnesium ion-induced bone regeneration. *Nat Commun*. **2021**, *12*, 2885.
9. Qiao, W.; Pan, D.; Zheng, Y.; Wu, S.; Liu, X.; Chen, Z.; Wan, M.; Feng, S.; Cheung, K. M. C.; Yeung, K. W. K.; Cao, X. Divalent metal cations stimulate skeleton interoception for new bone formation in mouse injury models. *Nat Commun*. **2022**, *13*, 535.
10. Takayanagi, H. Osteoimmunology in 2014: Two-faced immunology-from osteogenesis to bone resorption. *Nat Rev Rheumatol*. **2015**, *11*, 74-76.
11. Yu, F.; Lian, R.; Liu, L.; Liu, T.; Bi, C.; Hong, K.; Zhang, S.; Ren, J.; Wang, H.; Ouyang, N.; Du, L. J.; Liu, Y.; Zhou, L.; Liu, Y.; Fang, B.; Li, Y.; Duan, S. Z.; Xia, L. Biomimetic hydroxyapatite nanorods promote bone regeneration via accelerating osteogenesis of BMSCs through T cell-derived IL-22. *ACS Nano*. **2022**, *16*, 755-770.

Received: November 20, 2023

Revised: November 28, 2023

Accepted: December 5, 2023

Available online: December 28, 2023

Comments on Innovative design of minimal invasive biodegradable poly(glycerol-dodecanoate) nucleus pulposus scaffold with function regeneration

Hao Zhou, Aimin Wu*

Department of Orthopaedics, Key Laboratory of Orthopaedics of Zhejiang Province, The Second Affiliated Hospital and Yuying Children's Hospital of Wenzhou Medical University, Wenzhou, Zhejiang Province, China

*Corresponding author: Aimin Wu, aiminwu@wmu.edu.cn.

<http://doi.org/10.12336/biomatertransl.2023.04.010>

How to cite this article: Zhou, H.; Wu, A. Comments on Innovative design of minimal invasive biodegradable poly(glycerol-dodecanoate) nucleus pulposus scaffold with function regeneration. *Biomater Transl.* 2023, 4(4), 297-298.



This study sought to be inspired by the spreading shape of cucumber vines to design and prepare a disc nucleus pulposus scaffold with regenerative capabilities to address the serious problems associated with disc degeneration.¹ Intervertebral disc degeneration is a common health problem that usually leads to back pain and nerve compression, significantly affecting patients' quality of life.² For the treatment of disc degeneration, traditional methods include surgical interventions and medications, but there are limitations and risks. As a result, researchers have begun to explore more innovative treatment modalities for more effective intervertebral disc repair and regeneration.³

In this study, the researchers used poly(glycerol-dodecanoate) (PGD) to prepare an implantable disc nucleus pulposus scaffold that can be implanted *in vivo*, and the regenerative function of the scaffold was achieved by specifically linking the chemokine stromal cell-derived factor-1 α (SDF-1 α) to PGD. These scaffolds possessed key properties such as shape memory, mechanical support and degradation rate, which could be optimised by adjusting the synthesis parameters of PGD to ensure compatibility with the native disc nucleus pulposus (Figure 1).

The first concerns the use of the chemokine SDF-1 α . The researchers chose SDF-1 α as an induction factor for the disc nucleus pulposus scaffold because SDF-1 α has strong biological activity in inducing cell migration and chemoattraction. By linking SDF-1 α to PGD, the researchers realised that the scaffold releases SDF-1 α *in vivo*, which attracts autologous stem cells to migrate to the region of the disc nucleus pulposus and promotes the regeneration of the degenerated nucleus pulposus. This approach can be used as an innovative biological therapy that provides new ideas for treating disc degeneration.⁴ The second is about the shape memory property of the scaffold. This property refers to the ability of a scaffold to remember its original shape and to regain that shape under some stimulus

conditions. In this study, the PGD scaffold was able to spontaneously undergo shape changes to adapt to the cavity of the nucleus pulposus of the intervertebral disc, which means that the scaffold is better able to adapt to different disc morphologies, improving the success rate of the surgery and patient outcomes. In addition, the scaffold degraded at a moderate rate compared to conventional implants, without being too fast or too slow, which allowed for the slow release of SDF-1 α and the provision of needed regulatory factors for stem cells, which could reduce the deleterious effects on patients.^{5,6}

In the experiment, the researchers first delivered PGD rods with smaller diameters into the disc nucleus pulposus cavity of New Zealand white rabbits through hollow needles and observed that stimulated by body temperature, the PGD scaffolds would spontaneously undergo shape changes to fit into the disc nucleus pulposus cavity and to avoid extruding out of the puncture holes in the annulus fibrosus when compressed.

Encouragingly, the experimental results showed that the PGD intervertebral disc nucleus pulposus scaffold not only maintains the height of the intervertebral disc, but also has the ability to stimulate autologous stem cells to migrate and regenerate the degenerated nucleus pulposus in a relatively short period of time through the released SDF-1 α . This novel minimally invasive nucleus pulposus regeneration treatment has great potential for clinical application.

Overall, this study designed and prepared for the first time a regenerative disc nucleus pulposus scaffold with regenerative function inspired by the morphology of a plant vine, which successfully realised the properties of form the memory, physiological assistance, and the rate of degradation, and was able to suit with autologous nucleus pulposus, and achieved satisfactory results in the experiments. This innovative treatment provides new ideas for the treatment of intervertebral disc degeneration and brings new hope to patients.

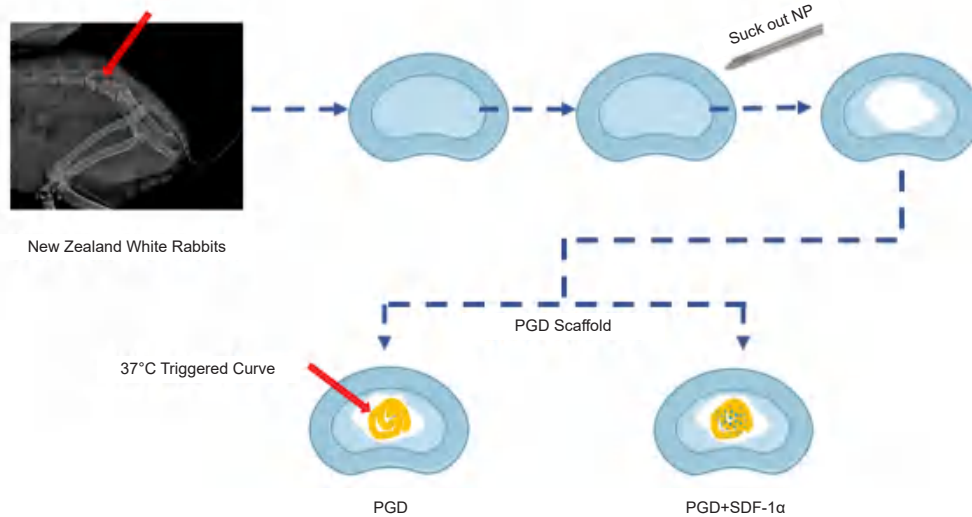


Figure 1. The surgical procedure for nucleus pulposus scaffold implantation in the L5–L6 intervertebral disc of rabbits involves the use of a C-arm machine. A hollow needle with a diameter of 1.2 mm is inserted into the nucleus pulposus of the L5–L6 intervertebral disc. During the operation, a platinum ring is fixed onto the nucleus pulposus scaffold, and the position of the scaffold is observed using X-ray imaging. The nucleus pulposus scaffold group is divided into the implant PGD group and the PGD + SDF-1 α scaffold group. Created with BioRender.com. PGD: poly(glycerol-dodecanoate); SDF-1 α : stromal cell-derived factor-1 α .

However, I still have some concerns. Firstly, this research is still in the laboratory stage and has not been widely validated in clinical practice. Although the experimental results have shown promising effectiveness, further clinical trials are necessary to assess the efficacy, safety, and long-term tolerance of the scaffold. Only after sufficient validation can its feasibility and effectiveness in clinical applications be determined. Additionally, the study needs to further consider the long-term effects and stability of the scaffold. Intervertebral disc degeneration is a chronic process, and the treatment approach requires long-lasting effects. Issues such as the degradation rate of the scaffold, the persistence of cell migration, and the long-term stability of regenerating nucleus pulposus need to be further researched and evaluated. Finally, treating intervertebral disc degeneration is just one application direction in the field of medicine. The potential application of the scaffold in other diseases still needs further research and exploration. Different diseases may have different treatment needs and mechanisms, hence further research is needed to determine the feasibility and effectiveness of the scaffold in other diseases.

Author contributions

HZ: Data curation, investigation, methodology, software, writing – original draft; AW: conceptualization, project administration, resources, supervision, writing – review & editing. Both authors approved the final version of the manuscript.

Financial support

The work was supported by the Wenzhou Major Scientific and Technological Innovation Project, No. ZY2022010, and the National Natural Science Foundation of China, No. 82272555 (both to AW).

Acknowledgement

None.

Conflicts of interest statement

The authors declare that they have no known competing financial interests or personal relationships that could have appeared to influence the work reported in this manuscript.

Open access statement

This is an open access journal, and articles are distributed under the terms of the Creative Commons Attribution-NonCommercial-ShareAlike 4.0 License, which allows others to remix, tweak, and build upon the work

noncommercially, as long as appropriate credit is given and the new creations are licensed under the identical terms.

1. Wang, L.; Jin, K.; Li, N.; Xu, P.; Yuan, H.; Ramaraju, H.; Hollister, S. J.; Fan, Y. Innovative design of minimal invasive biodegradable poly(glycerol-dodecanoate) nucleus pulposus scaffold with function regeneration. *Nat Commun.* **2023**, *14*, 3865.
2. Zhou, H.; Qian, Q.; Chen, Q.; Chen, T.; Wu, C.; Chen, L.; Zhang, Z.; Wu, O.; Jin, Y.; Wang, X.; Guo, Z.; Sun, J.; Zhang, J.; Shen, S.; Wang, X.; Jones, M.; Khan, M. A.; Makvandi, P.; Zhou, Y.; Wu, A. Enhanced mitochondrial targeting and inhibition of pyroptosis with multifunctional metallopolyphenol nanoparticles in intervertebral disc degeneration. *Small.* **2023**, e2308167.
3. Zhang, H.; Yu, S.; Zhao, X.; Mao, Z.; Gao, C. Stromal cell-derived factor-1 α -encapsulated albumin/heparin nanoparticles for induced stem cell migration and intervertebral disc regeneration in vivo. *Acta Biomater.* **2018**, *72*, 217–227.
4. Migneco, F.; Huang, Y. C.; Birla, R. K.; Hollister, S. J. Poly(glycerol-dodecanoate), a biodegradable polyester for medical devices and tissue engineering scaffolds. *Biomaterials.* **2009**, *30*, 6479–6484.
5. Pereira, C. L.; Gonçalves, R. M.; Peroglio, M.; Pattappa, G.; D’Este, M.; Eglin, D.; Barbosa, M. A.; Alini, M.; Grad, S. The effect of hyaluronan-based delivery of stromal cell-derived factor-1 on the recruitment of MSCs in degenerating intervertebral discs. *Biomaterials.* **2014**, *35*, 8144–8153.
6. Solorio, L. D.; Bocks, M. L.; Hollister, S. J. Tailoring the physicochemical and shape memory properties of the biodegradable polymer poly(glycerol dodecanoate) via curing conditions. *J Biomed Mater Res A.* **2017**, *105*, 1618–1623.

Received: November 21, 2023

Revised: November 27, 2023

Accepted: December 4, 2023

Available online: December 28, 2023